The University of Oxford

The Role of the Lysosome in Innate Immune Function

A thesis submitted for the degree of Doctor of Philosophy Medical Sciences Division, University of Oxford

Stephanie Koosje Newman *BSc., MSc.*
Linacre College

Supervised by: Prof. Fran Platt & Dr. Nick Platt
Department of Pharmacology



Abstract

Niemann-Pick disease type C (NPC) is a rare autosomal recessive neurodegenerative lysosomal storage disease caused by a mutation in the *NPC1* or *NPC2* genes. The functions of the proteins these genes encode are not fully understood, but are thought to be involved in cholesterol egress from the acidic compartment. The pathogenic cascade in proposed to begin with sphingosine accumulation followed by reduction of acidic store calcium levels. This results in impairing intracellular trafficking and storage of multiple lipid substrates in the late endosome/lysosomal compartment including cholesterol and multiple sphingolipids.

Although clinically characterized by progressive neurodegeneration, there is also evidence of altered innate immune responses, such as neuroinflammation, that promotes disease progression. In this thesis, we initiated an investigation into whether phagocytosis, an important innate immune activity and the process by which particles are ingested by professional phagocytes, is defective in NPC. Our results indicate a global defect in phagocytosis that is not particle or size specific. We further found evidence of altered phagocytosis *in vitro* and *in vivo* that is likely contributing to NPC disease pathology and disease progression and may contribute to iron deficiency and Crohn's disease susceptibility in NPC patients.

We next analysed lipid content on the plasma membrane. We found evidence to support the hypothesis that intracellular accumulation of lipids (e.g.

glycosphingolipids) in NPC directly contributes to abnormal actin dynamics at the plasma membrane, leading to defective formation of phagocytic cups. When we reintroduced certain glycosphingolipids exogenously to the cells we were able to partially rescue the phagocytic defect suggesting that GM1 ganglioside may be a regulator of actin: plasma membrane contact sites. Lastly, we present evidence showing that some current NPC therapeutics partially correct the phagocytic defect.

Taken together, this thesis provides insights into a novel aspect of NPC pathogenesis (innate immune dysfunction) and provides new knowledge of underlying immune defects in NPC, that in the future may act as novel targets for treatments.

Acknowledgements

First and foremost, I would like to express my sincere gratitude to my supervisor Dr. Nick Platt for the continuous support of my DPhil research, for his patience, dedication, encouragement and immense subject knowledge. His guidance has helped me in all stages of research and writing of this thesis. I will be forever grateful. I would also like to thank my co-supervisor Prof. Fran Platt for her support, guidance, and mentorship along the way and for introducing me to the field of rare disease research.

Many thanks to all members of the Platt lab for making the past 3 years such a memorable experience. To Dave (the mouse whisperer) and Lauren for helping me face my fear of mice and always being there to assist me with all things mouse related (and also for always listening to stories about my dog). To Oscar for helping me start this project. To Danielle for being able to answer any question about ordering, flow cytometry, paper work, and parenting etc. To Kerri for always being friendly to chat with both personally and professionally and for making cider and elderflower champagne. To James for helping me with PCR, microscopy, statistics, friendly advice, etc. To Ralu for always encouraging me to do more. To Doris for your friendship and advice. To Paul for answering all questions, always lending a helping hand and most memorably for showing me where to find distilled water. To David for being the friendliest person, always giving compliments and sharing lipids with me. To Mylene for your friendship all of your assistance with HPLC. To Allie for always being a friend, before and after work, where we could share DPhil student difficulties, and have way too much fun at Christmas parties. To Rizwana for

being the sweetest person in the world, always smiling, always keeping in touch. To Ecem for being friendly and fun to talk with. To Giulia for helping me with ELISAs and showing me gorgeous photos of Italy on dreary days. Finally, to Gokhan for becoming such a close friend and confidant, for ordering things for me, and helping with me many last minute experiments and of course having coffee breaks way too often. I absolutely will remember all of you fondly forever.

Thank you to Lianne Davis and Ant Morgan for allowing me to borrow your confocal microscope and to Esther Garcia for assisting me with microscopy at the WIMM.

Thank you to all of my friends for their continued support for the past 3 years. Particularly to Anne and Francesca for all of the dinner nights and baked cakes, to Rachel and Pete for babysitting Poppy. To Tim, Amanda, Maddie and Pippa for the fun weekend adventures. To Harpreet for coming to visit me all the way from London. To Marie and Sara for caring for Poppy whilst I was working on this project.

Thank you to my parents (Gary and Nancy), brother and sister for their continued moral support, excessive encouragement, always keeping in touch, coming to visit, and making sure I was home for Christmas. To Christine for being my best friend and other half. To my extended family, particularly my Aunt Leslie and Uncle David who have supported me and gave me the opportunity to study at Oxford. To the Bak family for your continued support, particularly to Jeff for proof reading yet another thesis.

And last, but certainly not least I wish to thank Mike and Poppy. Mike you have always believed I can achieve anything I set my mind to, and have supported me all the way to England. Thank you for helping create such a great life over the past 4 years that has been filled with travel, happiness, and fun memories. And of course, thank you to Poppy St. Clare-you are my greatest accomplishment.

Contents

Abstract i
Acknowledgements iii
List of Figures xi
Abbreviations xiv
Chapter 1: Introduction. 1
1.1 The Lysosome. 1
1.1 Lysosomal storage disorders. 4
1.2 Niemann-Pick Disease Type C. 5
1.2.1 Clinical features and diagnostic markers of NPC. 7
1.3 Biochemistry and lipid accumulation in NPC. 8
1.4 Pathological cascades in NPC. 10
1.5 Animal models of NPC. 12
1.6 Evidence of immune dysfunction in NPC. 13
1.7 The innate immune system. 15
1.8 Phagocytosis – general principles. 16
1.9.1 Receptors involved in phagocytosis. 16
1.8.1.1 Fc Receptors. 18
1.8.1.2 Complement Receptors. 19
1.8.2 The process of phagocytosis. 20
1.8.3 Particle recognition. 20
1.8.4 Existence of discrete phagocytic mechanisms. 21
1.8.4.1 Actin polymerisation and changes to the cytoskeleton during phagocytosis. 24
1.8.4.2 Signal transduction and information processing during phagocytosis. 25
1.9 Diseases associated with defective phagocytosis. 26
1.10 Thesis objectives. 28
Chapter 2. Analysis of Phagocytosis in Pharmacological Models of NPC. 29
2.1 Introduction. 29
2.2 Materials and Methods. 31
2.2.1 Chemicals and reagents. 31
2.2.2 Cell lines. 31
2.2.3 U18666A induction of NPC phenotype. 31
2.2.4 Lysotracker™ staining. 31
2.2.5 Localisation of cellular cholesterol by filipin staining. 32
2.2.6 Preparation of CellTracker™ green labelled sheep red blood cells. 32

2.2.7 Preparation of Ox-sRBC. 33
2.2.8 Preparation of pHrodo® green *E. coli* Bio particles and 33
pHrodo® green zymosan Bio particles. 33
2.2.9 Preparation of polystyrene beads. 33
2.2.9.1 IgG-opsonized polystyrene beads. 33
2.2.9.2 Preparation of non-opsonized polystyrene beads. 34
2.2.10 Preparation of coverslips. 34
2.2.11 Measurement of phagocytosis by fluorescence 34
microscopy. 34
2.2.12 Immunofluorescent staining and microscopy. 35
2.2.13 Measurement of phagocytosis by FACS. 35
2.2.14 Statistical analysis 36
2.3 Results. 37
2.3.1 Treatment with U18666A induces an NPC storage 37
phenotype. 37
2.3.2 U18666A-treated RAW 264.7 MΦ accumulate cholesterol 40
2.3.3 Analysis of phagocytosis. 40
2.3.3.1 U18666A-treated J774A.1 MΦ display impaired 41
phagocytosis of IgG-sRBC. 41
2.3.3.2 NPC RAW 264.7 MΦ display impaired phagocytosis 43
of IgG-sRBC; Analysis by microscopy and FACS 43
..... 47
2.3.3.3 NPC RAW 264.7 MΦ display impaired phagocytosis of 48
sRBC opsonized with complement; Analysis by microscopy 48
and FACS 48
2.3.3.4 NPC RAW 264.7 MΦ display impaired phagocytosis of 52
Ox-sRBC; Analysis by microscopy and FACS 52
2.3.3.5 NPC RAW 264.7 cells display impaired phagocytosis of 56
***Escherichia coli*; Analysis by microscopy and FACS. 56**
2.3.3.6 NPC RAW 264.7 MΦ show an insignificant decrease in 60
phagocytosis of zymosan Bio particles; Analysis by 60
microscopy and FACS 60
2.3.4 Phagocytic defect in NPC J774A.1 and RAW 264.7 MΦ is 64
independent of particle size. 64
2.3.5 Receptors expression is not altered by treatment with 71
U18666A. 71
2.4 Discussion. 73
Chapter 3. Defective Phagocytosis in NPC 79
Primary Macrophages. 79
3.1 Introduction. 79
3.1.1 NPC Mouse Model. 80
3.2 Materials and Methods. 82
3.2.1 Reagents. 82
3.2.2 Mice 82
3.2.3 Genotyping of Mice. 83
3.2.3.1 *Npc1*$^{-/-}$ mice. 83
3.2.3.2 Sandhoff disease (*hexb*$^{-/-}$) mice 83
3.2.4 Isolation of peritoneal MΦ 84
3.2.4.1 Isolation of resident peritoneal MΦ (RPMΦ). 84
3.2.4.2 Isolation of elicited inflammatory peritoneal MΦ 84

(EPMΦ) **84**
3.2.5 Isolation of thymocytes and induction of apoptosis. **85**
3.2.6 *In vitro* phagocytosis assay. **85**
3.2.6.1 LysoTracker™ staining. **85**
3.2.6.1 Fluorescent microscopy. **85**
3.2.6.2 FACS staining and analysis. **85**
3.2.7 Isolation of blood monocytes from Gaucher Disease **86**
patients and MΦ differentiation. **86**
3.2.8 Preparation of coverslips. **86**
3.2.9 Enzyme-linked immunoassay (ELIS(A) supernatant **86**
cytokines. **86**
3.2.10 Measurement of reactive oxygen species (ROS) **86**
production. **86**
3.2.11 Statistics. **87**
3.3 Results. 87
3.3.1 Lysotracker™ Staining and phenotyping of RPMΦ and **87**
EPMΦ. **87**
..... **89**
3.3.2. *Npc1*$^{-/-}$ RPMΦ display reduced phagocytosis of IgG- **91**
sRBC in comparison to *Npc1*$^{+/+}$ RPMΦ. **91**
3.3.3. *Npc1*$^{-/-}$ EPMΦ display reduced phagocytosis of IgG- **93**
sRBC; Analysis by microscopy and FACS **93**
3.3.3.1 Phagocytic efficiency is impaired in *Npc1*$^{-/-}$ EPMΦ **97**
3.3.3.2 *Npc1*$^{-/-}$ EPMΦ display reduced phagocytosis of sRBC **98**
opsonised with complement; Analysis by microscopy and **98**
FACS **98**
3.3.3.3 *Npc1*$^{-/-}$ EPMΦ display reduced phagocytosis of **103**
Ox-sRBC; Analysis by microscopy and FACS **103**
3.3.3.4 *Npc1*$^{-/-}$ EPMΦ display reduced phagocytosis of *E. coli*; **107**
Analysis by microscopy and FACS **107**
3.3.3.5 *Npc1*$^{-/-}$ EPMΦ display reduced phagocytosis of **111**
zymosan Bio particles; Analysis by microscopy and FACS **111**
3.3.3.6 *Npc1*$^{-/-}$ EPMΦ show impaired phagocytosis of apoptotic **115**
thymocytes **115**
3.3.4 Expression of specific receptors is apparently normal in **117**
***Npc1*$^{-/-}$ EPMΦ** **117**
3.3.5 *Npc1*$^{-/-}$ EPMΦ produce lower levels of pro-inflammatory **119**
cytokines after incubation with IgG-sRBC. **119**
3.3.6 Decreased production of ROS by *Npc1*$^{-/-}$ EPMΦ after co- **121**
incubation with IgG-sRBC or *E. coli* Bio particles. **121**
3.3.7 Phagocytic activities of MΦ with phenotypes of other **122**
LSDs **122**
3.3.7.1 EPMΦ from Sandhoff disease (*hexb*$^{-/-}$) mice do not **122**
display-impaired phagocytosis of IgG-sRBC **122**
3.3.7.2 Monocyte-derived MΦ from Gaucher Disease patients **124**
do not display impaired phagocytosis of IgG-sRBC or **124**
polystyrene beads. **124**
3.4 Discussion 128
Chapter 4. The Actin Cytoskeleton, GSLs **139**
and Phagocytosis. **139**

4.1. Introduction. 139
4.2. Materials and Methods. 140
4.2.1. Cells. 140
4.2.2.1. Visualisation of actin by microscopy. 141
4.2.2.2. Nuclear Staining. 141
4.2.3. Particle binding assay. 141
4.2.4. Assay of phagocytic cup formation. 142
4.2.5. Preparation of opsonised polystyrene particles. 143
4.2.6. Phagocytosis assay. 143
Phagocytosis assay is described in Section 2.2.11. 143
4.2.7 Live cell imaging of phagocytosis. 143
4.2.8. Measuring phasosomal/ lysosomal fusion. 143
4.2.9. Intracellular distribution of lipid species. 144
4.2.9.1. Localisation of GM1 with cholera toxin B (CtxB). 144
4.2.10. GSL analysis. 144
4.2.10.1. Extraction and purification of GSLs. 144
4.2.10.2. Ceramide glycanase digestion. 145
4.2.10.3. 2-Anthranilic acid (2AA) labeling. 145
4.2.11. Normal Phase High-Performance Liquid 146
Chromatography (NP-HPLC). 146
4.2.12. Measurement of protein concentration. 146
4.2.13. Addition of exogenous lipids to EPMΦ in culture. 147
4.2.14. Statistics. 147
4.3. Results. 147
4.3.1. Reduced binding of IgG-sRBC and IgG opsonised 147
polystyrene beads by U18666A-treated RAW 264.7 and *Npc1*$^{-/-}$ 147
EPMΦ. 147
4.3.2 Formation of phagocytic cups by *Npc1*$^{-/-}$ EPMΦ and 151
U18666A-treated RAW 264.7 MΦ is impaired 151
4.3.4 Live cell microscopy confirms altered F-actin dynamics 153
during phagocytic cup formation in NPC MΦ. 153
4.3.5 Accumulation of GSLs and defective lipid trafficking in 155
***Npc1*$^{-/-}$ EPMΦ 155**
4.3.6 Abnormal phagosome/ lysosome fusion allows for GM1 156
accumulation in the endolysosome thus depleting GM1 from 156
the plasma membrane of *Npc1*$^{-/-}$ EPMΦ 156
4.3.7 Exogenous GM1 ganglioside increases the level of 158
plasma membrane-associated GM1 in *Npc1*$^{-/-}$ EPMΦ 158
4.3.8 Addition of exogenous GM1 partially corrects 159
phagocytic activities in *Npc1*$^{-/-}$ EPMΦ 159
4.3.9 Impact of exogenous additions of GSLs on phagocytosis 162
4.3.9.1 Exogenous GM1, but not GA1 or a cocktail of GM3, ... 162
GD1a and GD1b, partially restores phagocytic activity in 162
***Npc1*$^{-/-}$ EPMΦ. 162**
4.3.9.2 GM1 and GA1, but not a cocktail of GM3, GD1a and 164
GD1b increase binding of IgG opsonized particles by *Npc1*$^{-/-}$ 164
EPMΦ. 164
4.3.9.3. Exogenous Lac-Cer, Glc-Cer and GM3 partially restore 166
phagocytic activity in *Npc1*$^{-/-}$ EPMΦ. 166
4.3.9.4 Exogenous Glc-Cer is rapidly metabolized to GM1 in 167

***Npc1*$^{-/-}$ EPMΦ. 167**
4.4 Discussion 168
Chapter 5. Impact of NPC Therapies on Phagocytosis 175
5.1 Introduction. 175
5.1.1 Miglustat. 175
5.1.2 2-hydroxypropyl-β-cyclodextrin (HPβCD). 177
5.1.3 Curcumin. 178
5.2 Methods. 180
5.2.1 Reagents. 180
5.2.2 Cells. 180
5.2.3 Drug treatment and cholesterol storage measurment 180
5.2.4 Correction of phagocytic defects in *Npc1*$^{-/-}$ EPMΦ by 181
NPC therapies. 181
5.2.5 FACS assays to assess effectiveness of NPC therapies 181
on phagocytosis. 181
5.2.6 Enzyme-linked immunoassay (ELISA) analysis of 181
supernatant cytokines. 181
5.3 Results. 182
5.3.1 NPC Therapies correct U18666A-induced cholesterol 182
storage. 182
5.3.2 Miglustat and curcumin correct phagocytic defects in 184
***Npc1*$^{-/-}$ EPMΦ; HPβCD has no significant on phagocytosis by 184**
***Npc1*$^{-/-}$ EPMΦ 184**
Discussion. 192
Chapter 6: Defective Phagocytosis *In Vivo.* 195
6.1 Introduction. 195
6.2 Materials and Methods 195
6.2.1 Mice 195
6.2.2 Preparation of IgG beads. 196
6.2.3 In vivo phagocytosis of IgG-opsonised beads. 196
6.2.4 Histology. 196
6.2.5 Statistics. 196
6.3 Results. 197
6.3.1 *Npc1*$^{-/-}$ EPMΦ display reduced phagocytosis of 197
3μm polystyrene beads in vivo 197
6.3.2 Abnormal accumulation of RBC in liver of NPC mouse, ... 198
that is improved with miglustat treatment. 198
6.3.3 Treatment with miglustat reduces the accumulation of 201
RBCs in liver of *Npc1*$^{-/-}$ mice 201
..... 202
6.4 Discussion. 203
Chapter 7 Conclusions. 205
Appendix 222

List of Figures

Figure 1.1 The Lysosome 3
Figure 1.2 Structures of NPC1 and NPC2 proteins 6
Figure 1.3 Structure of NPC storage lipids. 10
Figure 1.4 Proposed pathological cascade in NPC cells. 12
Figure 1.5 The phagocytic cup. 23
Figure 1.6 The cytoskeleton during phagocytosis 25
Figure 2.1. U18666A-treated J774A.1 MΦ show a significant increase in LysoTracker staining in comparison to vehicle-treated J774A.1 MΦ 38
Figure 2.2. U18666A-treated RAW 264.7 MΦ show a significant increase in LysoTrackerstaining in comparison to vehicle-treated RAW 264.6 MΦ 39
Figure 2.3. Effect of U18666A on Cholesterol Distribution in RAW 264.7 MΦ after 48h treatment with U18666A 40
Figure 2.4 J774A.1 MΦ treated with U18666A display decreased phagocytosis of IgG-sRBC: 42
Figure 2.5. RAW 264.7 MΦ treated with U18666A display decreased phagocytosis of IgG-sRBC: 44
Figure 2.6. U18666A-treated J774A.1 MΦ display impaired phagocytosis of IgG-sRBC. 46
Figure 2.7. U18666A-treated RAW 264.7 MΦ display impaired phagocytosis of IgG-sRBC 47
Figure 2.8. RAW 264.7 MΦ treated with U18666A show a significant defect in phagocytosis of CR-sRBC 49
Figure 2.9. U18666A-treated RAW 264.7 MΦ display impaired phagocytosis of CR-sRBC 51
Figure 2.10. RAW 264.7 MΦ treated with U18666A show significantly reduced phagocytosis of Ox-sRBC. 53
Figure 2.11. U18666A-treated RAW 264.7 MΦ display reduced phagocytosis of Ox-sRBC 55
Figure 2.12. RAW 264.7 MΦ treated with U18666A show a significant reduction in phagocytosis of E. coli Bio particles 57
Figure 2.13. U18666A-treated RAW 264.7 MΦ display significantly reduced phagocytosis of E. coli Bio particles: 59
Figure 2.15. RAW 264.7 MΦ display defective phagocytosis of zymosan Bio particles as quantified by FACS 63
Figure 2.16. U18666A-treated J774A.1 MΦ display significantly reduced phagocytosis of IgG-opsonised polystyrene beads 65
Figure 2.17. U18666A-treated RAW 264.7 MΦ display significantly reduced phagocytosis of IgG-opsonised polystyrene beads independent of their size 67
Figure 2.18. U18666A-treated RAW 264.7 MΦ display significantly reduced phagocytosis of different sized non-opsonised polystyrene beads 71
Figure 2.19. RAW 264.7 MΦ treated with U18666A show unaltered expression of specific receptors 72
Figure 3.1. RPMΦ show NPC phenotype as determined by increased Lysotracker™ fluorescence measured by FACS: 89
Figure 3.2. EPMΦ show NPC phenotype as determined by increased Lysotracker™ fluorescence measured by FACS 90

Figure 3.3. RPMΦ from *Npc1*$^{-/-}$ mice display impaired phagocytosis of IgG –sRBC 92
Figure 3.4. EPMΦ display defective phagocytosis of sRBC by FcyR mediated pathway....94
Figure 3.5. *Npc1*$^{-/-}$ EPMΦ display decreased frequency of fluorescence as quantified by FACS MOI 20:1....96
Figure 3.6. Phagocytic efficiency is impaired in NPC....98
Figure 3.7. *Npc1*$^{-/-}$ EPMΦ display defective phagocytosis of complement-sRBC 100
Figure 3.8. *Npc1*$^{-/-}$ EPMΦ display decreased frequency of fluorescence as quantified by FACS MOI 20:1....102
Figure 3.9. *Npc1*$^{-/-}$ EPMΦ display defective phagocytosis of Ox-sRBC....104
Figure 3.10. *Npc1*$^{-/-}$ EPMΦ display defective phagocytosis of Ox-sRBC as quantified by FACS....106
Figure 3.13. *Npc1*$^{-/-}$ EPMΦ display defective phagocytosis of zymosan bio particles 112
Figure 3.14 *Npc1*$^{-/-}$ EPMΦ display defective phagocytosis of zymosan Bio particles as quantified by FACS....114
Figure 3.15 *Npc1*$^{-/-}$ EPMΦ display decreased phagocytosis of apoptotic thymocytes 117
Figure 3.16. *Npc1*$^{-/-}$ EPMΦ show unaltered expression of specific phagocytic receptors....118
Figure 3.18 *Npc1*$^{-/-}$ EPMΦ show reduced ROS production in response to phagocytosis of IgG-sRBC....121
Figure 3.19. EPMΦ from Sandhoff mice display normal phagocytic activity....124
Figure 3.21. Gaucher Disease patient monocyte derived MΦ show normal phagocytosis of 3 μm polystyrene beads....127
Figure 4.1 U18666A-treated RAW 264.7 MΦ show reduced formation of IgG-sRBC rosettes:....148
Figure 4.2 Fewer IgG-sRBC rosettes are formed with *Npc1*$^{-/-}$ EPMΦ than with *Npc1*$^{+/+}$ EPMΦ....149
Figure 4.3 *Npc1*$^{-/-}$ EPMΦ display decreased binding of IgG opsonised polystyrene beads....150
Figure 4.4 Abnormal phagocytic cup formation in U18666A-treated RAW 264.7 MΦ: 152
Figure 4.6 Compilation of Live Cell Microscopy....154
Figure 4.8 Hydrazide trafficking appears delayed in *Npc1*$^{-/-}$ EPMΦ:....157
Figure 4.9 Plasma membrane associated GM1 is reduced in NPC....158
Figure 4.10 Exogenous GM1 partially restores plasma membrane- associated GM1 in *Npc1*$^{-/-}$ EPMΦ:....159
Figure 4.11 Extracellular addition of GM1 partially restores phagocytic activity in *Npc1*$^{-/-}$ EPMΦ....161
Figure 4.12 Related GSLs have no significant impact on phagocytosis: 164
Figure 4.13 GM1 and GA1 increase *Npc1*$^{-/-}$ MΦ target recognition efficacy....165
Figure 4.13 GM1, GM3, Lac-Cer and Glc-Cer improve phagocytosis 166
Figure 4.14 Glc-Cer is metabolized to GM1 in *Npc1*$^{-/-}$ EPMΦ:....168
Figure 5.1. Miglustat and the metabolism of Glc-Cer and related sphingolipids 177
Figure 5.2. Schematic representation of the effect of curcumin on compensating for reduced acidic compartment calcium release in NPC1 cells....179

Figure 5.3 U18666A induces cholesterol accumulation in LE/ Lys of RAW 264.7 MΦ which can be corrected with miglustat, HPβCD or curcumin.....183
Figure 5.4 Miglustat and curcumin treatment improve the phagocytic activity of *Npc1*$^{-/-}$ EPMΦ whereas HPβCD has no significant effect: (A) 188
Figure 5.6. Miglustat but not HPβCD treatment increases the secretion of pro-inflammatory cytokines by *Npc1*$^{-/-}$ EPMΦ after co-incubation with IgG beads191
Figure 6.1 *Npc1*$^{-/-}$ EPMΦ.....198
Figure 6.2 Increased splenic and liver weight in *Npc1*$^{-/-}$ mouse.....199
Figure 6.4 Treatment with miglustat decreases accumulation of RBC in *Npc1*$^{-/-}$ liver 202

Abbreviations

μL	microliter
2-AA	2-Anthranilic acid
3-MA	3- Methyladenine
3x	3 times (unit of measurement)
AF	Alexa Fluor®
BSA	Bovine serum albumin (Fraction V)
Ca^{2+}	Free, unbound calcium
C:M	Chloroform:methanol
CMFDA	5-chloromethylfluorescein diacetate, Celltracker Green
CNS	Central nervous system
CO_2	Carbon Dioxide
CR	Complement receptor
CR–sRBC	Sheep red blood cells (in Alsvier) opsonised with IgM antibody and complement 5 deficient serum to investigate complement mediated phagocytosis
CtxB	Cholera toxin subunit B
DAMP	Damage-associated molecular patterns
DAPI	4'-6-diamidino-phenylindoe
DCFDA	Cellular Reactive Oxygen Species Detection Assay Kit
DMSO	Dimethyl sulfoxide
E. coli	Escherichia coli
EE	Early endosome
EPMϕ	Elicited peritoneal macrophage

ER	Endoplasmic Reticulum
FACS	Fluorescence-activated cell sorting
FcR	Fc receptor
Fcγ R	High-affinity Fc receptor I for IgG (also known as CD64)
FCS	Fetal calf serum
FITC	Fluorescein isothiocyanate
FL1	Fluorescent parameter 1
Glc-Cer	GlucosylCeramide
GM1	Monosialoganglioside GM1(Galβ3GalNAcβ4(Neu5Acα3)Galβ4GlcCer)
GM1a	Monosilaoganglioside GM1a (Galβ3GalNAcβ4(Neu5Acα3)Galβ4GlcCer) ☒
GM1b	Monosilaoganglioside GM1b (Neu5Acα3Galβ3GalNAcβ4Galβ4GlcCer) ☒
GM2	Monosialoganglioside GM2 (GalNAcβ4(Neu5Acα3)Galβ4GlcCer) ☒
GM3	Monosialoganglioside GM3 (Neu5Acα3Galβ4GlcCer)
Golgi	Golgi Apparatus
GSL	Glycosphingolipid
h	Hour (s)
HBSS	Hank's balances salt solution
H&E	Haematoxylin and eosin
hexb$^{+/+}$	Murine model of Sandhoff disease with no HexB mutation used as control
hexb$^{-/-}$	Murine model of Sandhoff disease that has a HexB mutation causing deletion of the HexB gene

HPβCD	Hydroxypropyl-β-cyclodextrin
HPLC	High performance liquid chromatography
IgG	Immunoglobulin G
IgG-sRBC	Sheep red blood cells (in Alsvier) opsonized with IgG antibody for investigation of FcyR mediated phagocytosis
IgM	Immunoglobulin M
IL-1β	Interleukin 1 beta
IL-6	Interleukin 6
LAMP	Lysosome associated membrane protein
Lac-Cer	Lactosylceramide
LE/Lys	Late endosome/lysosome
LSD	Lysosomal Storage Disease
MΦ	Macrophage
M-CSF	Macrophage colony stimulating factor
MEFL	Mean equivalents of fluorescence
min	Minute
mL	Milliliter
MOI	Multiplicity of infection
NB-DGJ	N-buytldexoygalactonojirimycin
NB-DNJ	N-butyl-deoxynojirimycin
NPD	Niemann Pick Disease
NPC	Niemann Pick Disease type C (Niemann Pick Disease type C1)
NPC1	Niemann Pick C protein 1

Npc1$^{+/+}$	Niemann Pick Disease type C mouse model used as control
Npc1$^{-/-}$	Niemann Pick Disease type C genetic mutant mouse
NPC2	Niemann Pick C protein 2
NK	Natural Killer (cells)
Ox-sRBC	Oxidized sheep red blood cells
PBS	Dulbecco's Phosphate-Buffered Saline
PE	Phycoerythrin
PFA	Paraformaldehyde
PM	Plasma Membrane
PRR	Pattern recognition receptor
P/S	Penicillin/streptomycin
R10	Complete cell medium (containing 10% FBS +supplements)
RBC	Red blood cell
ROS	Reactive oxygen species
RPMΦ	Resident peritoneal macrophage
RT	Room temperature
S1P	Sphingosine-1-phosphate
SD	Standard Deviation (statistical analysis)
SEM	Standard error of mean
sRBC	Sheep red blood cell
SRT	Substrate reduction therapy
TLC	Thin layer chromatography
TNFα	Tumor necrosis factor alpha

TRP	Transient receptor potential channel
TRPML1	Transient receptor potential channel mucolipin-1
WT	Wild type

Chapter 1: Introduction.

1.1 The Lysosome.

The lysosome is now recognized as a multi-functional organelle that is the terminal compartment of the endolysosomal system (Saftig, 2006). It is essential for the removal of cellular components, destruction of unwanted or damaged organelles and maintenance of metabolic homeostasis and cellular health in general (Saftig, 2006; Saftig and Klumperman, 2009). (**Fig.1.1**). Historically, the best understood lysosomal functions are catabolism and recycling (Luzio et al., 2007). Material reaches the lysosome from both extracellular and intracellular sources where it is catabolized by the plethora of hydrolytic enzymes that break down proteins, lipids, carbohydrates, nucleic acids and other macromolecules into constituents that are then made available via recycling to biosynthetic pathways (Saftig and Klumperman, 2009).

Originally identified by de Duve (Appelmans et al., 1955), the lysosome (so called “suicide bag”) is membrane-bound and has an acidic internal pH that is typically in the range 4.5-5.5 (Saftig, 2006; Saftig and Klumperman, 2009; Appelqvist et al., 2013). Although identifiable within the cell by immunostaining for lysosome-specific markers (e.g. lysosome-associated membrane glycoprotein 1 – LAMP1 (Eskelinen, 2006) and at the ultrastructural level by electron microscopy (Essner and Novikoff, 1961), lysosomes display heterogeneity in form and appearance (Essner and Novikoff, 1961; Saftig and Klumperman, 2009). The unique environment of the lumen is sustained through the combined activities of specific proteins in the limiting lysosomal membrane

such as ion channels, pumps, transporters and permeases (Saftig and Klumperman, 2009). The low pH and ionic composition of the lysosome provides optimal conditions for the hydrolases and thus ensures efficient degradation of substrates.

More recently, our appreciation of lysosome biology has advanced significantly with recognition of other important activities that include it being a signaling hub, a calcium (Ca^{2+}) store, part of a signaling pathway that communicates with the nucleus and also a nutrient sensor. It is also the organelle that can fuse with the plasma membrane to mediate plasma membrane repair (Luzio et al., 2007). Taken together, this places the lysosome at the center of the regulation of cell metabolism (Sardiello et al., 2009; Settembre et al., 2013). We are also now aware that the lysosome makes significant contributions to multiple common diseases, including neurodegeneration, cancer, obesity and infection (Ballabio, 2016).

Multiple endocytic pathways, including phagocytosis, macropinocytosis and clathrin-dependent and independent endocytosis are responsible for importing extracellular molecules and particles and these cargoes are delivered by a succession of compartmental fusion and maturation events that converge on the lysosome where they are degraded (Saftig, 2006; Saftig and Klumperman, 2009). For example, phagocytosis is responsible for internalization of particles or microbes into a phagosome, which in turn undergoes fusion with the lysosome (phagolysosome) to deliver the contents into an environment that facilitates destruction and recycling. In addition, cytosolic complexes, misfolded proteins and dysfunctional organelles are isolated by a double membrane (a process known as autophagy) and are delivered via a separate fusion pathway,

to the lysosome (Yeung and Grinstein, 2007; Erwig and Henson, 2008; Settembre et al., 2013; Poon et al., 2014).

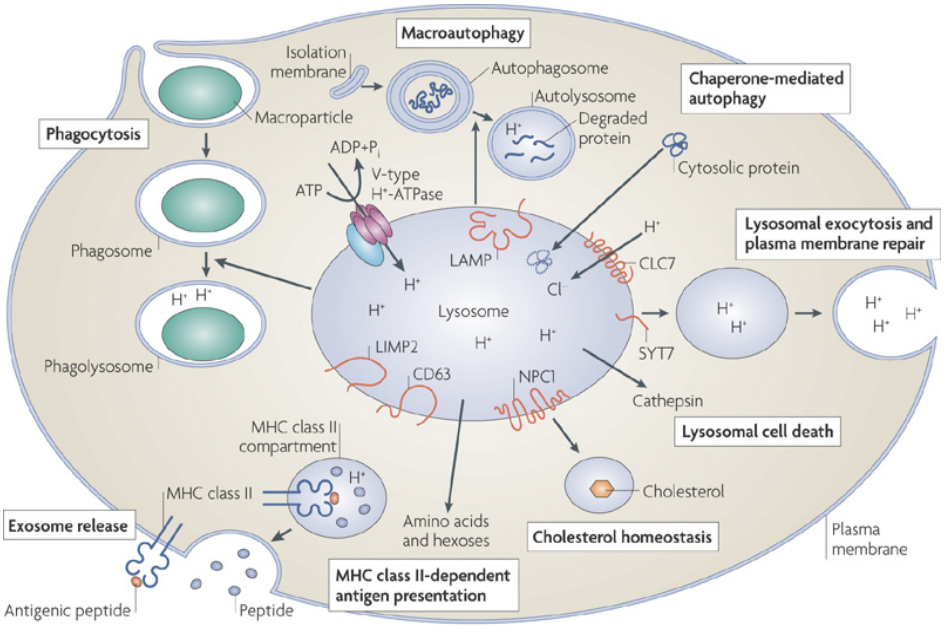


Figure 1.1 The Lysosome. Lysosomes are involved in the degradation and recycling of macromolecules and invading viruses, particles, and microbes. They are able to fuse with phagosomes and late endosomes to assist in degradation. The process of lysosomal-mediated breakdown involves various products that together can be used to generate new cellular components responsible for energy production when required. Lysosomes are partially responsible for intracellular Ca^{2+} homeostasis by regulation of exocytosis to secrete their contents into intracellular space and repair damage to the plasma membrane. During plasma membrane injury, the lysosome can rapidly migrate to the damaged site and fuse with the plasma membrane to allow for efficient repair. More recently, the lysosome has been identified as a signaling organelle that can sense changes in nutrient requirements that are required to activate a lysosome-nucleus signaling pathway that regulates the cell starvation response and energy metabolism. Taken from Saftig et al.

1.1 Lysosomal storage disorders.

The importance of the lysosome to the overall well-being of the cell and organism as a whole is best illustrated by the severe consequences that result from its dysfunction (Futerman and van Meer, 2004; Vellodi, 2005; Vitner et al., 2010; Platt et al., 2012). Lysosomal storage diseases (LSDs) are a subgroup of inborn errors of metabolism that are caused by inheritance of mutations in lysosomal proteins or in some cases non-lysosomal proteins (Platt et al., 2012). LSDs, of which greater than 70 discrete disorders have been described, are monogenic disorders that are individually rare, but have an estimated combined frequency of 1 in 5000 live births (Vitner et al., 2010; Platt et al., 2012) and are the most common cause of childhood neurodegeneration. Although affected proteins are frequently lysosomal hydrolases, for example glucocerebrosidase which is mutated in Gaucher disease (Karageorgos et al., 2011), they can also be membrane proteins and non-enzymatic soluble proteins (Vitner et al., 2010; Platt et al., 2012).

LSDs are characterized by accumulation (storage) of undegraded macromolecules within the endo-lysosomal system that leads to an increase in acidic compartment volume (Vanier, 2010). Clinically, LSDs are usually devastating for health and pathologically can affect both the central nervous system (CNS) and peripheral organs (Vitner et al., 2010). Despite the variation in the chemical nature of the storage material, LSDs frequently share common pathologies, which suggest convergence of pathological mechanisms (Vitner et al., 2010). However, understanding of these pathological processes remains poor. This is complicated further by the spectrum of phenotypes that patients afflicted with a particular disorder can display – which is a reflection of not only

the specific mutation in the affected gene and therefore how much residual activity may remain, but also the effects of genetic and epigenetic modifiers, along with environmental influences (so called genotype-phenotype variability) (Argmann et al., 2016). Together, these significantly influence the age of clinical onset and rate of disease progression. With a small number of exceptions LSDs are currently untreated and there is an urgent need for the development of new therapies.

1.2 Niemann-Pick Disease Type C.

Niemann-Pick disease type C (NPC) is an autosomal recessive LSD that is unusual because it can be caused by mutations in two independent genes, *NPC1* or *NPC2* (Vanier, 2010). Mutations in the *NPC1* gene are responsible for about 95% of clinical cases (Vanier, 2010). It is an integral protein of the limiting lysosomal membrane (Lloyd-Evans et al., 2008) with the gene located on chromosome 18 (**Fig. 1.2 (A)**, whereas NPC2 is a soluble lysosomal cholesterol-binding protein (previously known as HE1) and was first described in 2007 (**Fig. 1.2 B**) (Vanier, 2010). Mutations in *NPC1* and *NPC2* cause indistinguishable clinical phenotypes and it is believed they act in the same cellular pathway (Platt et al., 2012). The function of NPC1 remains contentious (Garver and Heidenreich, 2002; Ioannou, 2005; Louwette et al., 2013). The generally prevailing view is that NPC1 mediates the movement of cholesterol out of the lysosome (hence the cholesterol accumulation when it is inactivated) (Vanier, 2010), but experimental data are not fully compatible with this hypothesis (Ioannou, 2005; Lloyd-Evans and Platt, 2010). An alternative proposal is that NPC1 acts as a sphingosine transporter to move this lipid out of the lysosome. Lloyd-Evans and colleagues(Lloyd-Evans et al., 2008)

demonstrated that when NPC1 is inactivated, sphingosine is the first lipid to accumulate, which results in altered lysosome Ca^{2+} homeostasis and secondary storage of sphingolipids and cholesterol (see Section 1.5). Recently, researchers have proposed that the luminal C domain of NPC1 acts as an essential endosomal receptor for the Ebola virus (Carette et al., 2011).

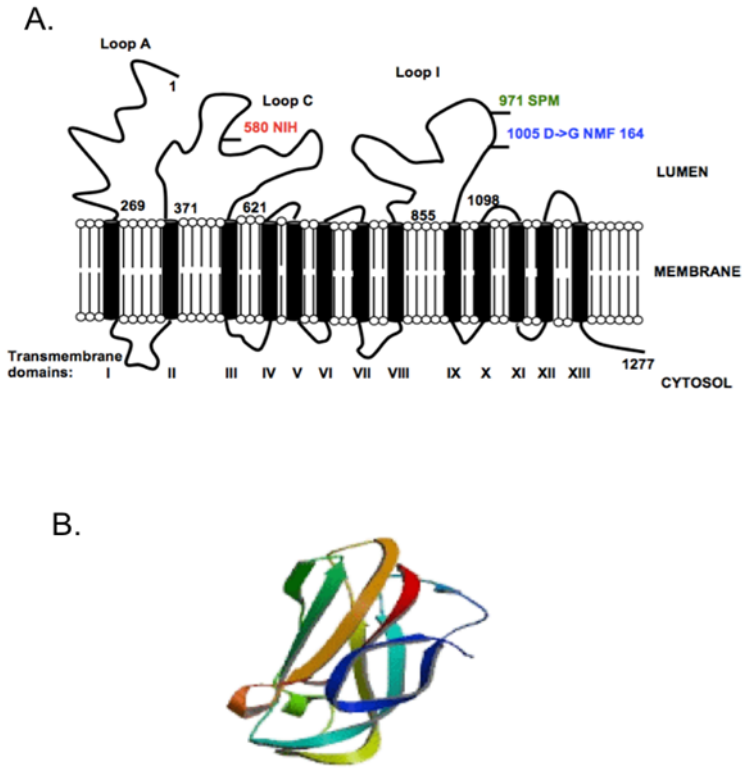


Figure 1.2 Structures of NPC1 and NPC2 proteins. (A) The predicted topology of NPC1 showing the 13 transmembrane protein domains (I to XIII) that span along the LE/Lys, three hydrophilic loops (where NTD (N-terminal domain) and SSD (sterol sensing domain) reside and multiple small loops facing out of the cytosol. Figure taken from(Lloyd-Evans et al., 2008). It is thought to function be mediating intracellular cholesterol trafficking in mammals. **(B)** A ribbon representation of NPC2 taken from (Friedland et al., 2003). NPC2 is a protein containing lipid recognition domain. The encoded protein is thought to function together with NPC1 in cholesterol trafficking. It is suggested that NPC2 is responsible for the transport of cholesterol through the LE/Lys system.

1.2.1 Clinical features and diagnostic markers of NPC.

Clinically, individuals afflicted with classical infantile or juvenile forms of the disease are typically diagnosed in childhood, but adult onset variants have also been described (Vanier, 2010) and evidence strongly suggests NPC is under diagnosed (Wassif et al., 2016). The disease can also present more dramatically in neonates where progression is rapid and fatal due to hepatic failure (Vanier, 2010). Patients are often diagnosed clinically by filipin staining of cultured fibroblasts, which can be problematic when dealing with mild phenotypes (Vanier, 2010). Indeed, because greater than three hundred different mutations in NPC1 have been identified (Vanier, 2010), genetic analysis is typically not an initial method of diagnosis. There has recently been an appreciable effort to validate biomarkers for NPC and the realization of specific oxysterol species (Fan et al., 2013), sphingomelin-509 (Giese et al., 2015) and changes in bile acids (Jiang and Ory, 2016; Mazzacuva et al., 2016) have the potential to simplify and speed up diagnosis. Furthermore, the use of LysoTracker™ staining to measure the relative volume of the acidic compartment of patient B lymphocytes has been documented in a long-term prospective multicenter collaborative study and was able to quantify responses to treatment and generate age adjusted disease sensitivity scores (Te Vruchte et al., 2015). The clinical course of disease is dominated by progressive neurodegeneration and neurological deterioration, which present as ataxia, dysphagia, dystonia, dementia and cognitive impairment. Histologically, characteristic features include neurofibrillary tangles and meganeurite formation, extensive ectopic dendrite growth, and neuroaxonal dystrophy (Walkley and Suzuki, 2004). Affected children often display neurological

features that are normally associated with adult-onset Alzheimer's disease (Mengel et al., 2013). Premature death typically occurs in late teenage years or early adulthood, with patients succumbing to aspiration pneumonia (Patterson et al., 2012). Peripheral symptoms frequently include splenomegaly and liver disease (Vanier, 2010).

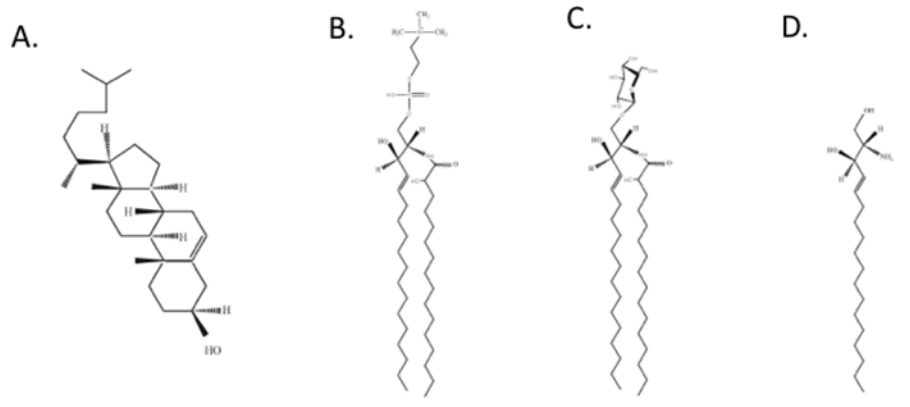
1.3 Biochemistry and lipid accumulation in NPC.

At the cellular level, the most obvious feature that results from mutations in *NPC1* or *NPC2* is the accumulation of cholesterol in the late endosome/ lysosome, but a range of other lipid species are stored (Vanier, 1999) including glycosphingolipids (GSLs), sphingosine and sphingomelin (which is also stored in the related diseases, Niemann-Pick Types A and B (Desnick et al., 2010; Schuchman and Wasserstein, 2015). In the CNS of NPC patients there is not a significant accumulation of cholesterol and sphingomyelin, but there is storage of GSLs (particularly GM2 and GM3 gangliosides). Gangliosides are a group of sialylated GSLs that are found in greatest concentration in the grey matter of the CNS and are essential for neural development and function (Schengrund, 2015). Glucosylceramide, a precursor of GSLs and lactosylceramide, a bioactive sphingolipid containing a lactose group are also increased in the CNS of NPC patients. Significant storage of sphingosine, an amino alcohol that forms the backbone of sphingolipids is unique to NPC and is generated as a result of lysosomal catabolism of ceramide derived from GSLs and sphingomeyelin (te Vruchte et al., 2004; Lloyd-Evans and Platt, 2010). However, it should be remembered that the overall abundance of any lipid species is also influenced by the amount that is lost as a consequence of processes such as neurodegeneration, which may have a selective impact on

biochemical profiles. All of the lipid species mentioned are elevated in the liver and spleen of NPC patients (**Fig. 1.3E**).

There is more comprehensive lipid data available for a mouse model of NPC (*Npc1*$^{-/-}$) (Loftus et al., 1997). Broadly, the tissue distribution and relative increases in lipids measured in the murine model replicate those available for human samples. In the CNS of *Npc1*$^{-/-}$ *mice*, cholesterol and sphingomyelin are not significantly elevated but are redistributed to the endosomal system as compared to *Npc1*$^{+/+}$ animals, but GSLs and sphingosine are increased 3 and 4 fold respectively, whereas for the liver, both cholesterol and sphingomyelin are 4 times higher, GSLs 2-fold and sphingosine greater than 12-fold (Lloyd-Evans and Platt, 2010).

The other significant cell biological defect in NPC is a block in trafficking and fusion events in the endolysosomal system (Ko et al., 2001; Lloyd-Evans and Platt, 2010). This has consequences not only for the failure to catabolise cargoes that enter the pathway and which accumulate because they are prevented from reaching the terminal lysosomal compartment, but also for the distribution of lipids that are normally re-distributed via dynamic membrane trafficking (Samie and Xu 2014).



E.

	Cholesterol	Sphingomyelin	Glucosylceramide (GSLs)	Sphingosine
Brain	0X	0X	3X	4X
Liver	4X	4X	2X	12X

Figure 1.3 Structure of NPC storage lipids. A subset of 4 storage lipids that are known to accumulate in NPC cells; **(A)** Cholesterol **(B)** Sphingomyelin **(C)** Glucosylceramide **(D)** Sphingosine. Images taken from (Lloyd-Evans and Platt, 2010). **(E)** An accumulation of these lipids has been shown in both the liver and spleen of NPC patients.

1.4 Pathological cascades in NPC.

The sequence of pathological events that result in NPC and the precise contribution(s) of the mutated proteins, NPC1 and NPC2 remain controversial. In particular, the most widely accepted model, which is based off the accumulation of cholesterol resulting from loss of ability to transport the lipid out of the lysosome does not easily account for all of the cell biological and biochemical hallmarks observed in patients and authentic animal models (Lloyd-Evans and Platt, 2010). In an experimental approach aimed at defining the early sequence of biological steps that characterize the disorder, Lloyd-Evans and colleagues (Lloyd-Evans et al., 2008) treated a murine macrophage (MΦ) cell line, RAW 264.7 with U18666A, an amphiphilic amino steroid whose

effects mimics those of the loss of Npc1 activity (Cenedella, 2009). The authors confirmed that sphingosine was the first species to accumulate in drug-treated cells, with its levels being significantly raised within 30 min following addition of the drug. This was followed by a rapid and significant fall in lysosomal Ca^{2+} content (at 30 – 60 min), whereas detectable storage of GSLs and cholesterol did not occur until 4h and 8h respectively. The hypothesis that sphingosine is an initiator of disease was strengthened further with the demonstration that exogenous addition of the lipid, but not related sphinganine, was able to induce NPC phenotypes in normal cells (Lloyd-Evans et al., 2008). Mechanistically, sphingosine has been shown independently to inhibit calcium mobilization (Betto et al., 1992), which is compatible with the lysosomal Ca^{2+} phenotype. More recently, research by Hoglinger *et al* (Hoglinger et al., 2015) used caged sphingosine to show that sphingosine acts as a signal to trigger the release of Ca^{2+} ions from lysosomes. In summary, inactivation of *Npc1* first causes sphingosine build up in the lysosome because it cannot be effluxed out, which inhibits the filling of the organelle and/or promotes Ca^{2+} leak perhaps via TPC1(Hoglinger et al., 2015) that means insufficient Ca^{2+} is released when triggered, thereby causing a block in endolysosomal trafficking and fusion events and secondary storage of GSLs and cholesterol **(Fig.1.4)**.

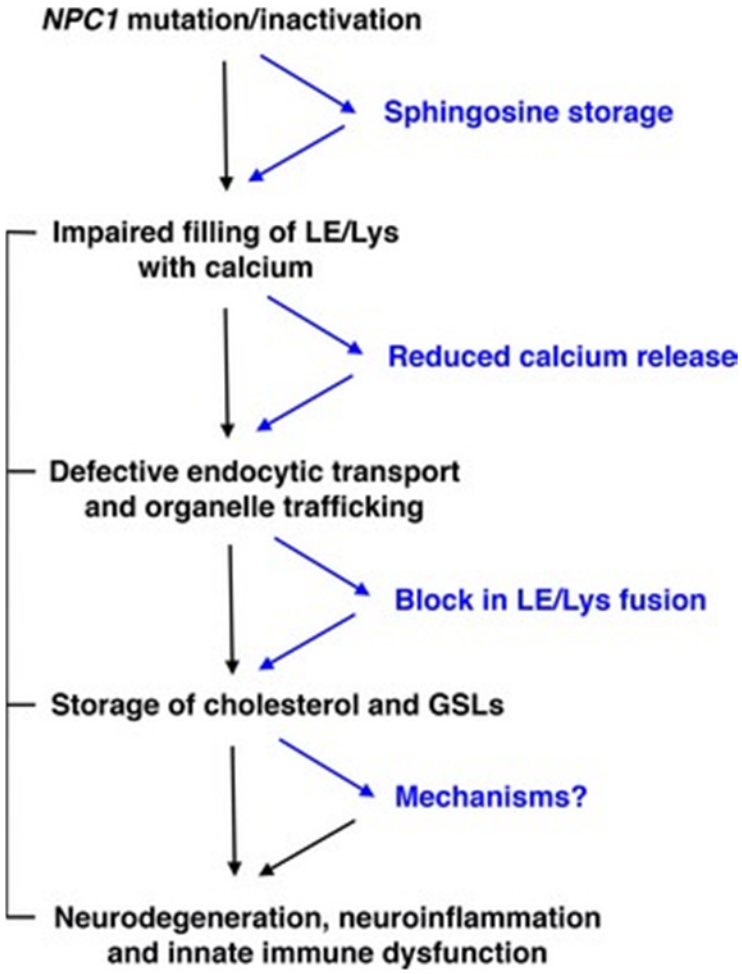


Figure 1.4 Proposed pathological cascade in NPC cells. A cartoon representation of the proposed pathological processes that underlie NPC cellular phenotypes as described above and results in neurodegeneration, neuroinflammation and the dysregulation of innate immune response. Image obtained from (Platt et al., 2016).

1.5 Animal models of NPC.

A number of different animal models of NPC have been described, which span yeast and *Drosophila* through to the cat (Lowenthal et al., 1990; Brown et al., 1994; Loftus et al., 1997; Huang et al., 2005; Fluegel et al., 2006). Their availability and use have been major factors in the increasing understanding of the processes that contribute to disease, the identification of biomarkers that

facilitate measurement of progression of the disorder and the trialing of potential treatments. In this thesis we take advantage of a mutant mouse strain (*Npc1*$^{-/-}$) that arose spontaneously at the NIH in the 1980's and when analysed was found to encode a severely truncated Npc1 protein and displays all of the human disease phenotypes (Loftus et al., 1997). The model displays a pre-symptomatic period from birth-6 weeks of age then a progressive neurodegenerative clinical course to a humane end point at 12 weeks (Williams et al., 2014).

1.6 Evidence of immune dysfunction in NPC.

Although NPC is clinically diagnosed as a neurodegenerative disease there is published evidence of altered innate immune responses occurring in this disorder. In common with other LSDs with CNS involvement, neuroinflammation is a notable characteristic (Vitner et al., 2010). There is abundant microglial activation in NPC disease. Microglia are myeloid cells of the CNS that behave as sentinels, detecting and responding to changes in the microenvironment within the brain (Ginhoux et al., 2013). Activated microglia are detectable early on (post-natal d14) in the brain of *Npc1*$^{-/-}$ mice, before neurodegeneration is detectable (Smith et al., 2009). Comprehensive CNS gene expression analysis of *Npc1*$^{-/-}$ mice has confirmed existence of a pro-inflammatory profile (Cluzeau et al., 2012). Importantly, beneficial effects have been seen with anti-inflammatory drugs in the NPC mouse model. Non-steroidal drugs, aspirin and ibuprofen extended lifespan and delayed disease onset, confirming neuroinflammation actively promotes the progression of the disease (Smith et al., 2009). In fact even LSDs that display disease entirely within peripheral tissues, (e.g. type 1 Gaucher disease) also have abnormal

inflammation in affected organs, suggesting that inflammation is a feature of all LSDs (Mizukami et al., 2002; Vitner et al., 2010). However, it remains unclear why or how lysosomal dysfunction triggers inappropriate pro-inflammatory responses (Bosch and Kielian, 2015).

Changes to innate immune cell populations and their activities are not restricted to the CNS. Gadola *et al.* (Gadola et al., 2006) showed loss of invariant natural killer T cells, an innate immune cell population that contributes to lipid recognition by the immune system and amplifies immune responses, in several murine LSDs with GSL involvement, including NPC, but a subsequent study of NPC patients confirmed the presence of normal cell frequencies (Speak et al., 2012).

Perhaps the most detailed study so far reported of immune dysfunction in NPC looked at the frequencies, phenotypes and activities of natural killer cells (NK cells) (Speak et al., 2014). NK cells are an important innate immune cell population that play roles in the detection and killing of virally infected and transformed cells (Vivier et al., 2011). Sphingosine, the first lipid to accumulate in NPC (Lloyd-Evans et al., 2008) is generated in the lysosome by acid ceramidase and is then transported out of the lysosome (potentially by Npc1) and then phosphorylated by two kinases to yield sphingosine-1-phosphate (S1P), a lipid that has multiple biological functions (Maceyka and Spiegel, 2014), including acting as a chemo-attractant to affect specific immune cell trafficking. In NPC, the accumulation of sphingosine in the lysosome results in reduced generation of S1P (Lloyd-Evans et al., 2008). Speak *et al* (Speak et al., 2014) confirmed alteration in the normal gradient of the lipid between tissues (lymph node) and circulation (blood and lymph) in *Npc1*$^{-/-}$ mice, which

resulted in abnormal distribution of NK cells between these compartments. Isolated NK cells from *Npc1*$^{-/-}$ mice were found to have an immature phenotype and were impaired in killing activities because of failure to degranulate cytotoxic granules (lysosome related organelles). Importantly, comparable deficiencies were also measured in blood from NPC patients and interestingly, heterozygous patients also showed a deficit in age-related expansion of NK cell frequencies, perhaps suggesting possible biological consequences for carrier genotypes.

In this thesis we will describe a series of investigations of whether important innate immune mechanisms (in particular phagocytosis) and cell populations (MΦ) are also affected in NPC. We will now provide a brief description of aspects of innate immunity that are relevant to understanding of the experimental data.

1.7 The innate immune system.

The innate immune system functions to maintain tissue homeostasis, acts as a first line of host defense against pathogens and instructs the nature of the acquired immune response (Janeway and Medzhitov, 2002; Akira et al., 2006; Mogensen, 2009; Kumar et al., 2011). It is composed of distinct cell types, including MΦ, neutrophils, NK cells, dendritic cells and a number of other leukocyte populations (Janeway and Medzhitov, 2002; Akira et al., 2006). It is able to mediate the identification, destruction, and clearance of infectious agents and unwanted materials of host origin by using a combination of activities. These include production of soluble factors such as complement, secretion of bioactive molecules such as specific cytokines and the generation

of reactive molecular species such as nitric oxide for killing (Janeway and Medzhitov, 2002).

1.8 Phagocytosis – general principles.

One of the most significant protective immune mechanisms is phagocytosis, a process that requires re-organisation of the cytoskeleton to enable ingestion of particles (>0.5 μm in size), such as microbes and dying host cells (Janeway and Medzhitov, 2002). Requirement for changes to the cytoskeleton distinguishes it from other mechanisms that allow sampling of the extracellular environment, such as endocytosis and micropinocytosis (Mulcahy et al., 2014). Phagocytosis is an evolutionary ancient process, and has been shown to be important in relatively simple animals such as *C. elegans* and *Drosophila (Stuart and Ezekowitz, 2005)*. In such organisms there may not be specialised populations of phagocytes but even in mammals it seems all cells can perform phagocytosis, at least to a limited extent. However, MΦ in particular and neutrophils are uniquely efficient and are for this reason referred to as "professional phagocytes". Internalised material is delivered via maturation and fusion of the phagosome with the lysosome for destruction (Flannagan et al., 2012).

1.9.1 Receptors involved in phagocytosis.

Phagocytosis is dependent upon the expression of phagocytic receptors. Phagocytic receptors are defined as ones containing specific elements or amino acid sequences in their cytoplasmic domain(s) that are able to engage signalling pathways or adaptor molecules that result in actin polymerisation that is required for membrane extension around the particle, its internalisation and formation of a phagosome (Sarantis and Grinstein, 2012). The property of such

a domain within a cytoplasmic region can be demonstrated most easily by creation of a chimeric receptor, which includes the cytoplasmic domain fused to the extracellular region of a molecule that can normally only exhibit particle binding, but not internalisation. Phagocytic activity can be confirmed with the demonstration that when transfected into non-phagocytic cells, the chimeric receptor can alone mediate internalisation of specific particles (e.g. (Mitchell et al., 1994). Importantly, whilst some of the germ-line encoded receptors, known as pattern recognition receptors (PRRs), which can discriminate microbial ligands and are vital for the functioning of the innate immune system (Akira et al., 2006; Mogensen, 2009; Kumar et al., 2011) have also been shown, according to these criteria, to mediate phagocytosis (such as specific scavenger receptors, Dectin 1 etc.), many PRRs have not been implicated in the phagocytic process(Underhill and Goodridge, 2012). In addition, there are phagocytic receptors such as Fc receptors that are not PRRs. However, the situation is more complex because of evidence that specific receptors (e.g. certain Toll-like receptors) may be able to tether particles and affect signalling pathways that result in co-operation with additional phagocytic receptors, which in turn can bring about successful particle internalisation (West et al., 2004). Table 1.1 lists examples of receptors and their ligands for which there is evidence of contributions to phagocytosis. That there are multiple receptors known to be associated with phagocytosis is very likely a reflection not only of the wide variety of targets that phagocytes can recognise but also an indication of the multifaceted cell responses that can result.

Particle	Phagocytic receptor/ligand	Reference
RBC	Fc receptor, complement	(Cannon and Swanson, 1992)
Senescent RBC (oxidised, $CD47^{-/-}$)	OxRBC receptor, scavenger receptors,	(Olsson and Oldenborg, 2008)
Apoptotic cell	PS receptor, scavenger receptor, complement, integrins, TIM receptors etc.	(Reddy et al., 2002)
Bacteria (Gram + and Gram – ve)	Opsonised, Fc, complement	(Costa et al., 2005)
Yeast (zymosan)	CR3, β-glucan receptor, mannose receptor	(Maekawa et al., 1993)
Latex beads (unmodified and opsonised)	Various receptors	(Akira et al., 2006)

Table 1.1 Particles tested for phagocytosis and descriptions of receptors and ligands associated with each particle.

1.8.1.1 Fc Receptors.

A major pathway of phagocytosis is one initiated by Fc receptors (FcRs) that can bind to Fc regions of immunoglobulin G (IgG). As a consequence of the deposition or coating (opsonisation) of a particle with IgG via the antigen-binding domains, the Fc tail is available for binding by FcR in the plasma membrane. The latter triggers FcR-mediated signal transduction that initiates phagocytosis (Diakonova et al., 2002; Swanson and Hoppe, 2004). The signalling complexes activate proteins that regulate cytoskeletal elements (such as actin and myosin), membrane fusion and specify the generation of appropriate effector responses, such as reactive oxygen intermediates. In mammalian species, there are four defined classes of Fc receptors: FcγRI (CD64), FcγRIIA (CD32(A), FcγRIIB (CD32b) FcγRIII (CD16) and FcγRIV (Ravetch and Bolland, 2001). All are single chain polypeptides, which contain an extracellular Fc binding domain, a transmembrane domain and a

cytoplasmic tail that includes specific signalling regions (ITAM motifs that contain the YXXL sequence of amino acids) responsible for tyrosine activation. Activating FcγRs recruit an ITAM-containing γ chain to transduce activating signals via src-family kinases that in turn activate Syk kinases, to bring about actin assembly, other necessary cytoskeletal changes and subsequent effector responses (Swanson and Hoppe, 2004; Tohyama and Yamamura, 2006; Lowell, 2011). On the other hand, specific FcRs, such as FcγIIb (CD32b) are inhibitory and contain an ITIM domain that recruits phosphatases to inhibit activation signals (Rankin et al., 2006). The expression of different FcγRs are individually regulated and dynamic, meaning the phagocytic capacity of MΦ can be carefully tailored to meet demand.

1.8.1.2 Complement Receptors.

A phagocytic mechanism distinct from that involving FcRs is one mediated by complement receptors (CRs). The third component of the classical pathway of complement activation, C3 is processed to C3b, which can bind to cell surfaces via hydroxyl and amino groups (Rus et al., 2005). It is subsequently rapidly cleaved to yield inactive iC3b. These proteins can be bound by receptors specific for C3b (CR1) or iC3b (CR3 – CD18/ CD11b and CR4 – CD18/ CD11c) (Bajic et al., 2013) or a receptor that can recognise both (CRIg) (Helmy et al., 2006). CR3 and CR4 are heterodimer integrins, composed of α chains (α_M for CR3 and α_x for CR4) and a shared β chain (β2). Importantly, CRs of resident MΦ are not constitutively active for phagocytosis (particles are bound but not internalised) and require additional stimuli to induce uptake (Underhill and Ozinsky, 2002). An additional difference between FcR and CR-mediated phagocytosis is that the latter does not trigger the release of inflammatory

mediators such as reactive oxygen species and arachidonic acid metabolites (Aderem and Underhill, 1999).

1.8.2 The process of phagocytosis.

As is the case for many other processes, with increasing numbers of studies has come the realisation of a greater complexity to phagocytosis than was originally anticipated (Stuart and Ezekowitz, 2005; Underhill and Goodridge, 2012). Experimental evidence has been obtained from a wide range of detailed investigations that, for example, have extended from reports of specific receptor mechanisms, particularly FcR (Crowley et al., 1997) and CRs (Allen and Aderem, 1996) through to studies focused on broader issues, such as why the biological consequences of uptake of apoptotic cells differ so significantly from those that result from bacterial ingestion (Poon et al., 2014). A comprehensive review of all the published literature on phagocytosis is therefore beyond the scope of this introductory chapter so we will restrict discussion to topics that are most pertinent to our own studies. What is clear is that phagocytosis is important for the health and survival of the organism, because its impairment significantly increases susceptibility to pathogens (Alberts, 2002; Flannagan et al., 2009) and the induction of damaging inflammatory and autoimmune responses when removal of unwanted host cells is compromised (Lekstrom-Himes and Gallin, 2000).

1.8.3 Particle recognition.

The initial step of phagocytosis requires detection of the particle by the phagocyte, involving surface recognition. Phagocytes can discriminate not only between types of particle (such as distinguishing between microbes and dying host cells) through the detection of specific ligands (such as pathogen-

associated molecular patterns – PAMPs and danger-associated molecular patterns – DAMPs (Janeway and Medzhitov, 2002) but also physical properties such as size and shape (Champion and Mitragotri, 2006; Doshi and Mitragotri, 2010). Receptors can be classified into two distinct groups. Non-opsonic phagocytosis involves receptors that recognise ligands inherent to the particle itself, (such as Dectin 1 binding of β-glucan on fungi; (Brown et al., 2007), whereas opsonic phagocytosis targets uptake by specific receptors through the deposition of host proteins on the particle (opsonisation), such as IgG for FcR directed uptake (Ravetch and Bolland, 2001). However, particles often engage a number of different receptors, of which only one or more may be actually required for uptake but the others may contribute important signals that impact upon internalisation and subsequent downstream events (Mogensen, 2009).

1.8.4 Existence of discrete phagocytic mechanisms.

As we have outlined, engulfment of targets is dependent upon recognition and binding by cell-surface receptors and engagement of adaptor and signalling molecules that are required for activation of the actin cytoskeleton and completion of internalisation. Distinct types of phagocytosis have been described. The two mechanisms that have been investigated in the greatest detail are “zippering” or “feeling” phagocytosis, illustrated by FcγR mediated ingestion and “sinking” phagocytosis, utilised by CR3 (integrin$\alpha_M\beta 2$) (Underhill and Goodridge, 2012). In the former, internalisation of IgG-opsonised particles is considered to involve three major steps – plasma membrane extension and ruffling and binding of opsonised particle to FcR, second, clustering of FcRs in the membrane beneath the particle, which causes induction of a signalling cascade that converges on the actin cytoskeleton and third, engulfment or

internalisation into a phagosome that is isolated from the plasma membrane by an actin-driven mechanism (Flannagan et al., 2012). One of the most prominent features of FcR phagocytosis is the rapid organization of the actin cytoskeleton to form a phagocytic cup (Hall et al., 2006). Following receptor ligation, an orderly progression of cellular changes leads to rearrangement of the actin cytoskeleton and membrane remodelling that together form a phagocytic cup (**Fig.1.5**) (Stuart and Ezekowitz, 2008). The formation of the phagocytic cup initiates envelopment of the particle, isolation from the extra-cellular space and transfer into the interior of the cell in the context of formation of the phagosome. In contrast, for phagocytosis mediated by CR3, iC3b opsonised particles are observed to sink into the plasma membrane without obvious pseudopod extension or protrusion (although this observation is perhaps now contentious; see (Hall et al., 2006). The two mechanisms of phagocytosis differ in the use of specific guanine nucleotide exchange factors (GTP-binding proteins) that signal to the cytoskeleton to affect F-actin polymerisation. FcRγ-mediated uptake is dependent upon the Rho family members, Rac and CDC42; in contrast CR3-mediated ingestion requires RhoA (Caron and Hall, 1998).

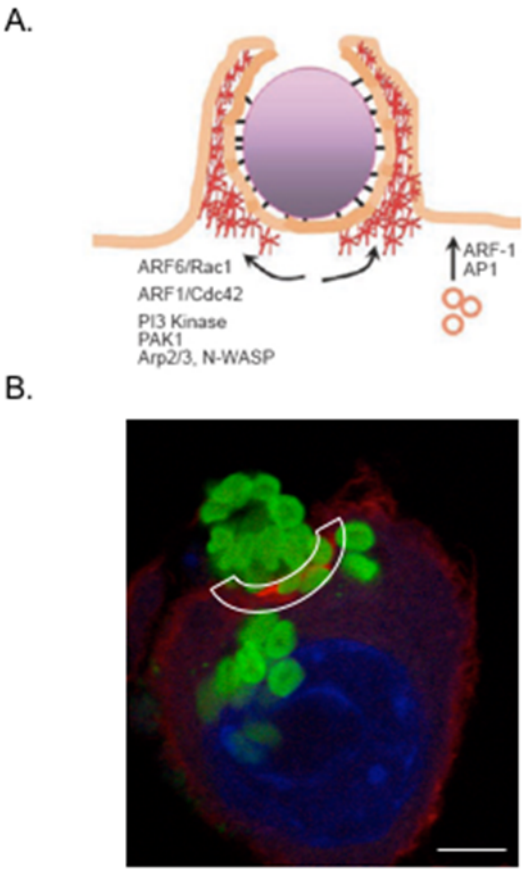


Figure 1.5 The phagocytic cup. Following activation of phagocytic receptors, the actin cytoskeleton is prompted to reorganize to form a cup surrounding the target particle. **(A)** A schematic diagram showing an actin rich phagocytic cup surrounding an opsonised particle **(B)** A confocal microscopy image showing a MΦ (red) during phagocytosis of IgG opsonised sheep red blood cells (sRBC), green. The formed phagocytic cup is outlined in white. Scale bar represents 10μm. Panel A taken from Kumari et al., 2010.

1.8.4.1 Actin polymerisation and changes to the cytoskeleton during phagocytosis.

Remodelling of the actin cytoskeleton is essential for phagocytosis; when blocked internalisation is prevented (May and Machesky, 2001). In brief, deformation of the plasma membrane allows for release of F-actin monomers in the cortical cytoskeleton to permit lateral diffusion of receptors and associated adaptor molecules. Second, F-actin polymerisation, promoted by nucleators, such as Arp2/3 complex and WASp proteins involves formation of actin trimers, which is not favoured in the resting cytoskeleton, facilitates extension of pseudopods, formation of the phagocytic cup and ultimately closure of the phagosome (Freeman and Grinstein, 2014). The process is dependent therefore upon precise spatial and temporal controlled activation and inactivation of multiple proteins that regulate actin dynamics (**Fig. 1.6**). We have given here only a brief description of the cytoskeletal changes required for phagocytosis and the reader is directed to specific publications for substantially greater detail (Freeman and Grinstein, 2014).

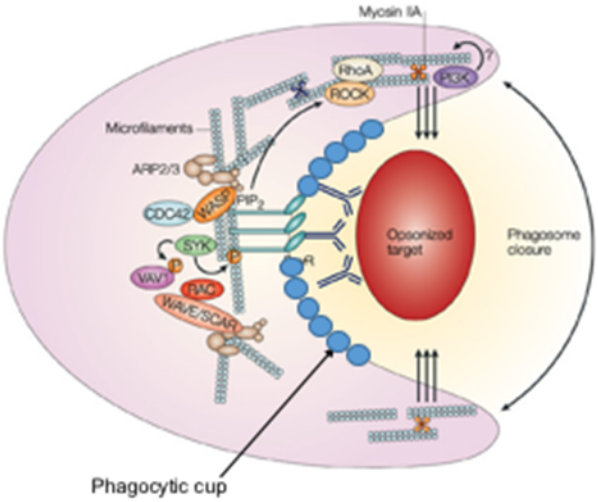


Figure 1.6 The cytoskeleton during phagocytosis. Signalling events associated with the activation of Fc receptors on phagocytic cells are shown. Briefly, early kinase signalling mediated by SYK allows for the formation of the phagocytic cup (involving interactions with WAVE/SCAR, SYK, WASP, CDC42) in co-operation with PIP2 are involved in actin dependant membrane protrusions and particle engulfment. Other signalling kinases (PIK2, RhoA, ROCK) are involved in particle-phagosome maturation and closure of the phagocytic cup. Image adapted from(Vicente-Manzanares and Sanchez-Madrid, 2004).

1.8.4.2 Signal transduction and information processing during phagocytosis.

Complex signal transduction pathways are engaged when receptors bind to specific particles that initiate the cellular events required to instruct and complete phagocytosis. Equally as important as the triggering of the process of engulfment is the conveying of information about the nature of the particle that impacts upon the nature of the effector response(s). It is critical that the effector response is appropriate to the precise biological situation. For example, phagocytosis of microbes results in the induction of anti-microbial activities

such as generation of free radicals, pro-inflammatory cytokines, chemokines etc., which are important for control of infection (Ponnappan and Ponnappan, 2011). In contrast, removal of unwanted host cells that die as a result of apoptosis needs to happen in the absence of inflammation and is immunologically silent (Elliott and Ravichandran, 2010; Hochreiter-Hufford and Ravichandran, 2013). What has become apparent is that whilst the involvement of specific receptors in the phagocytosis of specific particles goes a long way to delineating the response, information is gathered at multiple other points in the phagocytic process (for example during phagosome maturation and target degradation) and is integrated to shape the immune response (Underhill and Goodridge, 2012)

1.9 Diseases associated with defective phagocytosis.

Defects in phagocytosis can have considerable consequences for health and is associated with various diseases such as systemic lupus erythematosus, chronic obstructive pulmonary disease, HIV, and chronic granulomatous disease (Pollock et al., 1995; Kedzierska et al., 2003; Taylor et al., 2010; Debaisieux et al., 2015). Patients may be more susceptible to bacterial infection (immune-compromised) or can suffer from auto-immunity. A list of various disorders connected with phagocytic defects is provided in Table 1.2.

Disease	Molecular or Genetic Defect	Pathogenesis and Sites Affected	Clinical Presentation
Severe congenital neutropenia			
i) Cyclic neutropenia	ELA2 encoding neutrophil elastase	Episodic bacterial infections, ulcers, gingivitis, cellulitis.	Extended fluctuations in neutrophil, monocyte, platelet and lymphocyte counts.
ii)Congenital neutropenia	Unknown	*S.aeurus*, peritoneal abscess, meningitis	Arrested development of bone marrow myeloid cells, increased risk of acute myelogenous leukemia.
Schwann Diamond Syndrome	Unknown	Infections in lung, bone, skin and urinary tract.	Cyclic neutropenia; associated skeletal abnormalities; insufficient pancreatic function; Recurrent infection of sinus, bone, lung, skin and urinary tract; increased risk of aplasia and leukemia
Leukocyte Adhesion Deficiency			
i)Type 1	CD18	Gram negative enteric bacteria, S. aeurus, candida species, aspergillus	Recurrent infection of skin, soft tissue, respiratory tract and gastrointestinal tract, periodontal disease, delayed separation of umbilical cord.
ii) Type 2	Carbohydrate fucosalation	Gram negative enteric bacteria, S. aeurus, candida species, aspergillus species	Same as Type1, with addition of growth retardation, dysmorphic features, and neurological defects.
Rac 2 Deficiency	Deficiency of Rac 2	Not reported	Recurrent peritoneal abscess; Poor wound healing; Absence of pus at site of infection; leukocytosis; neutrophilia
Interferon-y and Interferon-12 defects	Interferon-y receptor ligand binding chain, interferon-y receptor signaling chain, interleukin-12-receptor y ß1 chain, Interleukin-12 P40 deficiency	Bacille Calmette-Guerin; Mycobacterium arium complex, *M smegmatis,* salmonella species.	Infection with intracellular microorganisms with severe *mycrobacterial* disease; Onset in infancy; Dissemination and failure to form granulomas.
Chronic Granulomatous	gp91^{phex}	Chronic positive microorganisms, *S.aeurus*, aspergillus species, nocardia species	Abscess formation in the lungs, liver, brain, soft tissue infection; Gastrointestinal and urogenital obstruction from granulomas
Chediak-Higashi Syndrome	Mutation in the LYST encoding a cytoplasmic protein involved in protein transport	*S. aeurus*, beta hemolytic streptococcus	Partial ocular and cutaneous albinism; Peripheral neuropathy; Recurrent bacterial infection; Easily bruised; Mild mental retardation; Severe periodontal disease
Chronic Obstructive Pulmonary Disease (COPD)	Not reported	*Streptococcus pneumoniae* and *Haemophilus influenzae*	Decreased pulmonary reserve; dyspnea; cognitive decline in late stage

Table 1.2 Diseases associated with defective phagocytosis, adapted from (Lekstrom-Himes and Gallin, 2000).

1.10 Thesis objectives.

The studies described in this thesis were undertaken with the objectives investigating potential phagocytic defects in NPC, exploring the mechanisms that may underlie such defects and the implication of altered phagocytic activity for the pathology and clinical management of patients.

The thesis is organized as follows:

Chapter 2. Defective phagocytosis in a drug-induced model of NPC.

Chapter 3. Defective phagocytosis in *Npc1*$^{-/-}$ MΦ.

Chapter 4. The actin cytoskeleton, glycosphingolipids and phagocytosis.

Chapter 5. Effect of NPC therapies on phagocytosis.

Chapter 6. Phagocytosis in *Npc1*$^{-/-}$ mice *in vivo.*

Chapter 7. Final conclusions and future objectives

Chapter 2. Analysis of Phagocytosis in Pharmacological Models of NPC.

2.1 Introduction.

In Chapter 1 we discussed the published evidence of innate immune dysfunction in NPC and the importance of phagocytosis as a protective mechanism. In this chapter we will describe investigations made using a pharmacological model of NPC to examine for changes to phagocytic activity in NPC cells.

Murine models of NPC have been very successfully exploited for study (and experiments using cells isolated from *Npc1*$^{-/-}$ mice will be described in Chapter 3) but only relatively limited numbers of cells can be easily obtained from individual animals. This issue is compounded because production of mutant mice is not straightforward (they are generated by mating of heterozygous animals) and deficient offspring are born at a sub-Mendelian frequency (Pentchev et al., 1984). Drug-induced NPC cells permit studies that demand significantly larger amounts of biological material.

The hydrophobic amine 3-β-[2-(diethylamino)ethoxy]androst-5-en-17-one (U18666A) has been shown to pharmacologically-induce all the NPC phenotypes characteristic of the disease (Mohammadi et al., 2001; Cenedella, 2009; Iftakhar et al., 2009; Liu et al., 2009; Poh et al., 2012). The use of U18666A has been insightful for elucidating disease-associated pathological processes. Firstly, U18666A can induce disease phenotypes in a very broad range of cell types (Mohammadi et al., 2001; Iftakhar et al., 2009) thus allowing examination for the consequences of inhibiting NPC1 on cell specific activities.

Secondly, the use of U18666A permitted the temporal sequence of the pathological cascade that follows inactivation of NPC1 to be defined (Lloyd-Evans et al., 2008).

Our objective was to undertake a broad investigation of whether phagocytic activity was perturbed or altered in NPC. To achieve this we treated immortalised MΦ cell lines with U18666A to induce the cellular characteristics of the disease. We then challenged cells with a range of particles that are ingested by a number of different phagocytic systems. We established two methods to analyse relative phagocytic activity *in vitro*. Fluorescent microscopy permitted visual inspection of MΦ for evidence of ingestion of fluorescently labelled particles, but with a relatively low experimental through put. Phagocytosis of fluorescent particles was also analysed by fluorescence-activated cell sorting (FACS). In this method the frequency and intensity of fluorescence of the phagocyte is a measure of how many cells have been able to ingest particles and the relative number of particles they have internalised.

Major objectives of this chapter.

- Investigate whether pharmacological induction of the NPC phenotype in MΦ affects phagocytosis.
- Through the use particles that are internalised by distinct phagocytic pathways determine whether phagocytic deficiency may be restricted to a particular uptake mechanism or is more generalised in nature.

2.2 Materials and Methods.

2.2.1 Chemicals and reagents.

U18666A was purchased from Merck (UK). Stock solutions were prepared at 10mg/mL in DMSO, stored at -20^{o}C and diluted to working concentration with cell culture medium as required. LysoTracker^{TM} Green DND 26 and CellTracker^{TM} green (5-chloromethylfluorescein diacetate; CMFDA) were from Invitrogen. Mowiol 4-88 was from Calbiochem. PBS was from Sigma-Aldrich (UK). CytoPainter F-actin Staining Kit - Red Fluorescence was from Abcam. Cytochalasin D from *Xygosporium mansonii* was from Sigma-Aldrich. Filipin was purchased from Sigma-Aldrich.

2.2.2 Cell lines.

J774A.1 and RAW 264.7 MΦ were obtained from the European Cell Culture Collection (Porton Down) and maintained in RPMI 1640 (Sigma-Aldrich) supplemented with 10% Fetal Calf Serum (FCS) (Bioser A), 1% penicillin/streptomycin and 1% glutamine (both Invitrogen) at 37^{o}C in 5% CO_2. Cells were routinely sub-cultured to maintain viability.

2.2.3 U18666A induction of NPC phenotype.

To induce an NPC cellular phenotype J774A.1 MΦ were treated with 2 μg/mL U18666A for 72h and RAW 264.7 MΦ were treated with 2 μg/mL U18666A for 48h. Control cells were incubated with 0.1% DMSO.

2.2.4 Lysotracker^{TM} staining.

Staining was performed according to te Vruchte *et al (Te Vruchte et al., 2015)*. In brief, cells were stained with 200nM LysoTracker^{TM} Green DND-26 for 10 min at RT in PBS, washed and immediately analysed by fluorescence-activated

cell sorting (FACS) on a Beckton Dickinson FACS Canto cytometer. Data were analysed using FlowJo software (FlowJo, LLC).

2.2.5 Localisation of cellular cholesterol by filipin staining.

Fixed cells were incubated with 1 mL filipin working solution (0.05 mg/mL in PBS with 0.2% Triton X100) for 1h at room temperature, followed by washing 3x with PBS.

2.2.6 Preparation of CellTracker^{TM} green labelled sheep red blood cells.

Sheep red blood cells (sRBC; in Alsever's buffer (saline liquid used to prevent coagulation of blood composed of 2.05% dextrose, 0.8% sodium citrate, 0.055% citric acid, and 0.42% sodium chloride)) were obtained from TCS Biosciences (Claydon, UK). For fluorescent labelling, sRBC were harvested by centrifugation (2000 rpm, 10 min) and washed three times with PBS. Cell concentration was adjusted to 1x10^6 cells/mL in Opti-Mem serum free medium (Invitrogen) and labelled with CellTracker^{TM} green at final concentration of 20 μM (determination of optimal labelling concentration is shown in Appendix Fig A1). sRBCs were pelleted by centrifugation (2000 rpm, 15 min); cells were washed three times with PBS before use.

For FcγR-mediated phagocytosis, CellTracker^{TM} labelled sRBC were opsonized by incubating 1x10^9 sRBC with rabbit anti-sheep red blood cell antibody, IgG fraction (1:50; Abcam, UK) for 30 min at 37^{o}C, then washed three times with PBS to remove excess antibody.

For CR-mediated phagocytosis, CMFDA-labelled sRBC were opsonized by incubating 1x10^9 sRBC with rabbit anti-sheep immunoglobulin M (IgM) fraction (1:500; Invitrogen) for 30 min at 37^{o}C, then washed 3x with PBS and re-

incubated at 37^{o}C with C5-deficient serum (1:1000; Invitrogen) for 60 min. Cells were washed 3x with PBS to remove excess antibody.

2.2.7 Preparation of Ox-sRBC.

Ox-sRBCs were prepared using a protocol adapted from Olsson and Oldenborg (Olsson and Oldenborg, 2008). sRBCs (in Alsvier's) were pelleted by centrifugation (2000 rpm, 10 min) and washed three times with PBS. sRBCs were re-suspended at a concentration of 1x10^{9} cells/mL in Hanks buffered salt solution (HBSS; Sigma-Aldrich), and incubated with 0.2 mM $CuSO_4$ and 5 mM ascorbic acid at 37^{o}C for 60 min. sRBCs were then washed twice with PBS and suspended at 10^{8}/cells/mL in serum-free medium. Ox-sRBC were then labelled with CellTracker^{TM} green as described above.

2.2.8 Preparation of pHrodo® green *E. coli* Bio particles and pHrodo® green zymosan Bio particles.

pHrodo® green *E.coli* and pHrodo® green zymosan Bio particles were obtained from Invitrogen. Bio particles were thawed, diluted in 2 mL of Opti-MEM. The vial was vortexed for 10-15 min, and re-suspended in Opti-MEM to concentrations of 1 mg/mL for pHrodo® *E.coli* and 0.5 mg/mL for pHrodo® zymosan Bio particles. Bio particles were then sonicated for 5 min (or until all fluorescent particles were homogenously dispersed). Phagocytosis assays were performed as described below by addition of 20 μL of Bio particles.

2.2.9 Preparation of polystyrene beads.

2.2.9.1 IgG-opsonized polystyrene beads.

2 μm, 3 μm, 6 μm and 10 μm green fluorescent beads (Polysciences Inc.) were diluted by addition of 40 μL of 10% suspension of beads to 500 μL of PBS.

Beads were centrifuged at 1500 rpm for 5 min, supernatant was discarded, and beads were re-suspended in 500 µL fresh PBS. This was repeated three times. Beads were opsonised by re-suspending in PBS with IgG anti-rabbit (50 mg/mL stock, diluted 1:100) for 60 min at room temperature, then washed 3x with PBS to remove excess antibody. Beads were then re-suspended in 500 µL of PBS.

2.2.9.2 Preparation of non-opsonized polystyrene beads.

Non-opsonised ("naked") polystyrene beads were also used as phagocytic targets. Particles of four different sizes (2 µm, 3 µm, 6 µm and 10 µm - Polysciences), were prepared by washing with PBS and blocked by incubation in PBS with 5% BSA (BSA Fraction B; Invitrogen). Phagocytosis assays were performed using the described protocol, in which beads were overlaid at an MOI of 20:1.

2.2.10 Preparation of coverslips.

Coverslips were washed in concentrated nitric acid for 2h, prior to extensive washing with MilliQ quality water. Water was decanted and coverslips stored in ethanol. Coverslips were air dried in a sterile environment prior to use.

2.2.11 Measurement of phagocytosis by fluorescence microscopy.

Opsonised, Celltracker ™ green labelled sRBC (or other particles) were washed three times with PBS and concentration adjusted to $2x10^6$ cells/mL. Labelled sRBC were overlain onto J774A.1 or RAW 264.7 murine MΦ monolayers on glass coverslips at an MOI of 20:1 sRBC: MΦ as determined by preliminary investigations shown in Appendix (**Fig. A1**), and co-cultured for various lengths of time at 37°C in 5% CO_2. Non-ingested sRBC were removed

by treatment with mouse RBC lysing buffer (Sigma-Aldrich, UK) for 10 min, followed by two washes with PBS. Cells were fixed with 4% (w/v) paraformaldehyde (PFA) (TAAB). Phagocytosis assays were performed as described above for each particle type using MOIs as indicated.

2.2.12 Immunofluorescent staining and microscopy.

Fixed and washed J774A.1 and RAW 264.7 MΦ were permeabilised and blocked with 0.2% Triton X-100 in PBS/ 10% heat inactivated goat serum for 1h at room temperature. After multiple washes with PBS, cells were counterstained with Rhodamine Phallodin (CytoPainter F-actin staining kit) according to manufacturer's instructions and DAPI (100 ng/mL, 4'-6-diamidino—phenylindoe; Sigma-Aldrich), mounted with anti-fade mounting medium (Invitrogen) and analysed by fluorescent microscopy. Images were viewed on a Zeiss 510 meta confocal microscope and data collected in the Multi-track mode. Excitation/emission (nm): green (488/505-530), red (543/>560). To quantify phagocytosis, MΦ that had internalized >1 CellTracker^{TM} labelled sRBC were scored as positive and their frequency determined as a percentage of total MΦ. A minimum of 200 cells for each treatment was counted in random fields. At least three independent experiments were made.

2.2.13 Measurement of phagocytosis by FACS.

RAW 264.7 MΦ were plated at 1x10^6 cells/mL in 6-well plates in complete culture media (composition described in section 2.2.2) and cultured overnight to ensure confluence. MΦ were overlaid with CMFA-sRBC at a multiplicity of infection (MOI; the ratio of agents (e.g. phage or more generally virus, bacteria) to infection targets (e.g. cell)) of 20:1 (**Fig. A2**). Phagocytosis was initiated by

briefly spinning cells at 1200rpm at 4^{o}C, and then warmed to 37^{o}C. Non-ingested sRBC were removed by lysis. Cells were scraped from 6-well dish and transferred to u-bottom 96-well plate in triplicates. Samples were spun and washed 3X with PBS. Samples were re-suspended in FACS buffer (500 μL PBS, 1% PBS, 1% Sodium Azide) and analysed using a FACS CANTO flow cytometer. MΦ that had not been co-incubated with sRBC and CellTracker^{TM} green labelled sRBC alone were used to set up gating parameters. Fluorescence from CellTrackerTM green labelled sRBC was detected in the FITC channel (excitation max 493nm, laser excitation line 488nm; emission detector 525) of the cytometer. MΦ that had not been co-incubated with labelled sRBC, were used to establish the gating criteria on the FITC channel and forward scatter on the x-axis. Data from experimental samples (samples incubated with labelled sRBC) were collected using the same parameter settings as were applied to negative control samples (MΦ not exposed to labeled sRBC).

The extent of phagocytosis was determined as the molecules of equivalent fluorochrome (MEFL; cells that are detected as positive in a select fluorescent channel) in the FITC channel with increasing signal indicative of greater internalization of CellTracker^{TM} labelled sRBC.

2.2.14 Statistical analysis.

Data are presented as the mean ± SD. Statistical analysis was performed using GraphPad Prism software (GraphPad Software). An unpaired 2-tailed Student's *t*-test with Welch's correction was used to determine significance. *p* values less than 0.05 were considered statistically significant.

2.3 Results.

2.3.1 Treatment with U18666A induces an NPC storage phenotype.

Increased volume of the acidic compartment is indicative of NPC1 dysfunction (te Vruchte et al., 2004; Lloyd-Evans et al., 2008). LysoTracker™ is a weakly basic amine that is protonated at low pH and accumulates in the acidic compartment of the cell (late endosome/ lysosome), (te Vruchte et al., 2004) where it emits a fluorescent signal, which can be measured by FACS. The intensity is proportional to the relative volume of the acidic compartment. Cells with a storage disease phenotype display more intense staining with LysoTracker green than healthy cells. Examples of FACS profiles for J774A.1 MΦ stained with LysoTracker green are shown in **Fig 2.1.** U18666A-treated J774A.1 MΦ showed 2-fold greater fluorescence in the FL1 channel (MEFL=36382±689) as compared to untreated J774A.1 cells (MEFL=19174±573), confirming the induction of a storage phenotype, consistent with NPC (**Fig. 2.1**). Similarly, histogram representation of FACS analysis of U18666A-treated RAW 264.7 MΦ cells showed 3-fold greater fluorescence, consistent with induction of an NPC phenotype (**Fig. 2.2**).

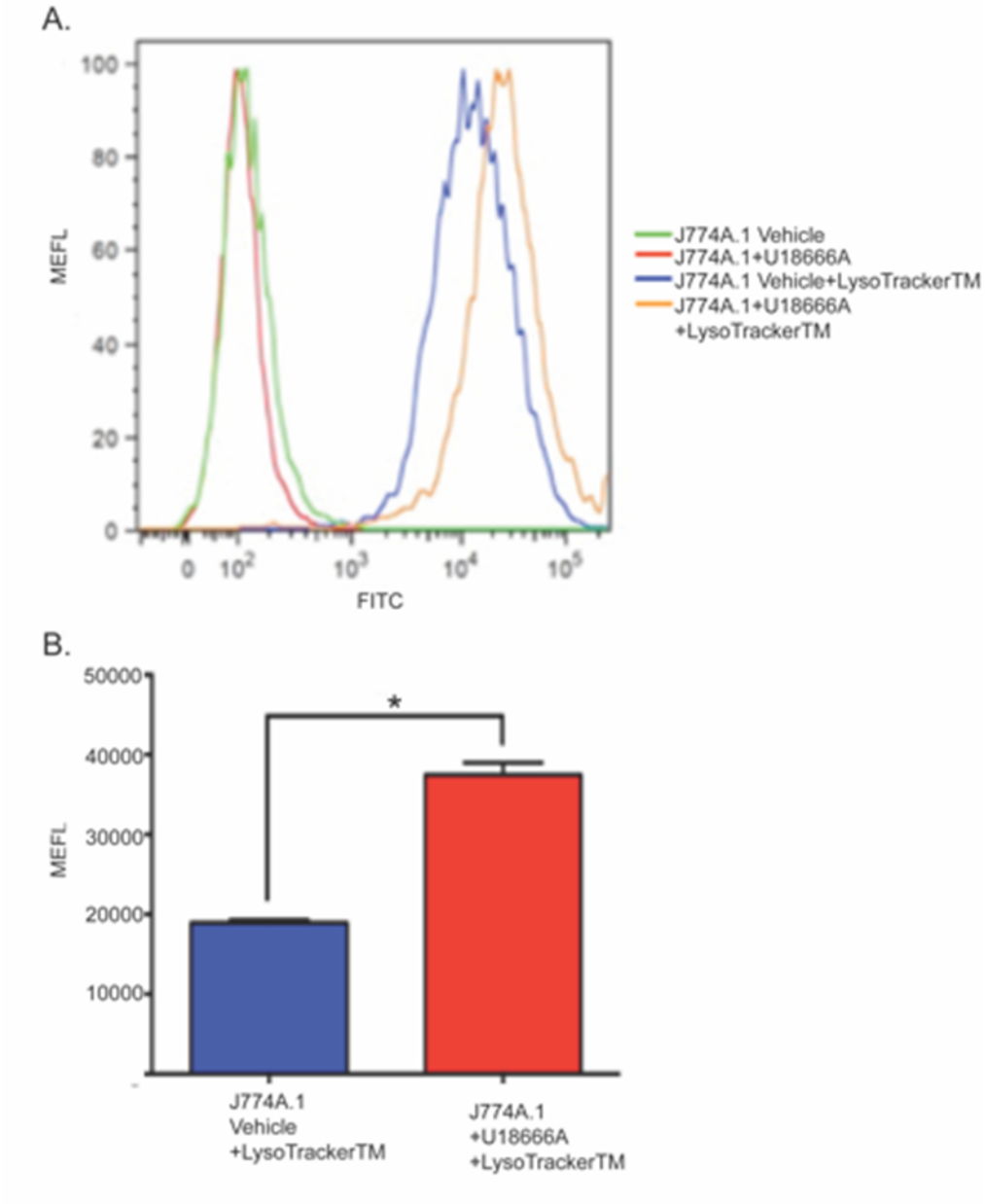


Figure 2.1. U18666A-treated J774A.1 MΦ show a significant increase in LysoTracker staining in comparison to vehicle-treated J774A.1 MΦ (A) FACS profiles of vehicle-treated J774A.1 and J774A.1+U18666A MΦ, unstained or stained with LysoTracker. **(B)** Histogram of MEFL of LysoTracker green stained vehicle-treated (blue column) and U18666A-treated (red column) J774A.1 MΦ. Mean ± SD. N = 4, **p*<0.05. (*t*-test with Welch's correction). Data representative of greater than 10 independent experiments.

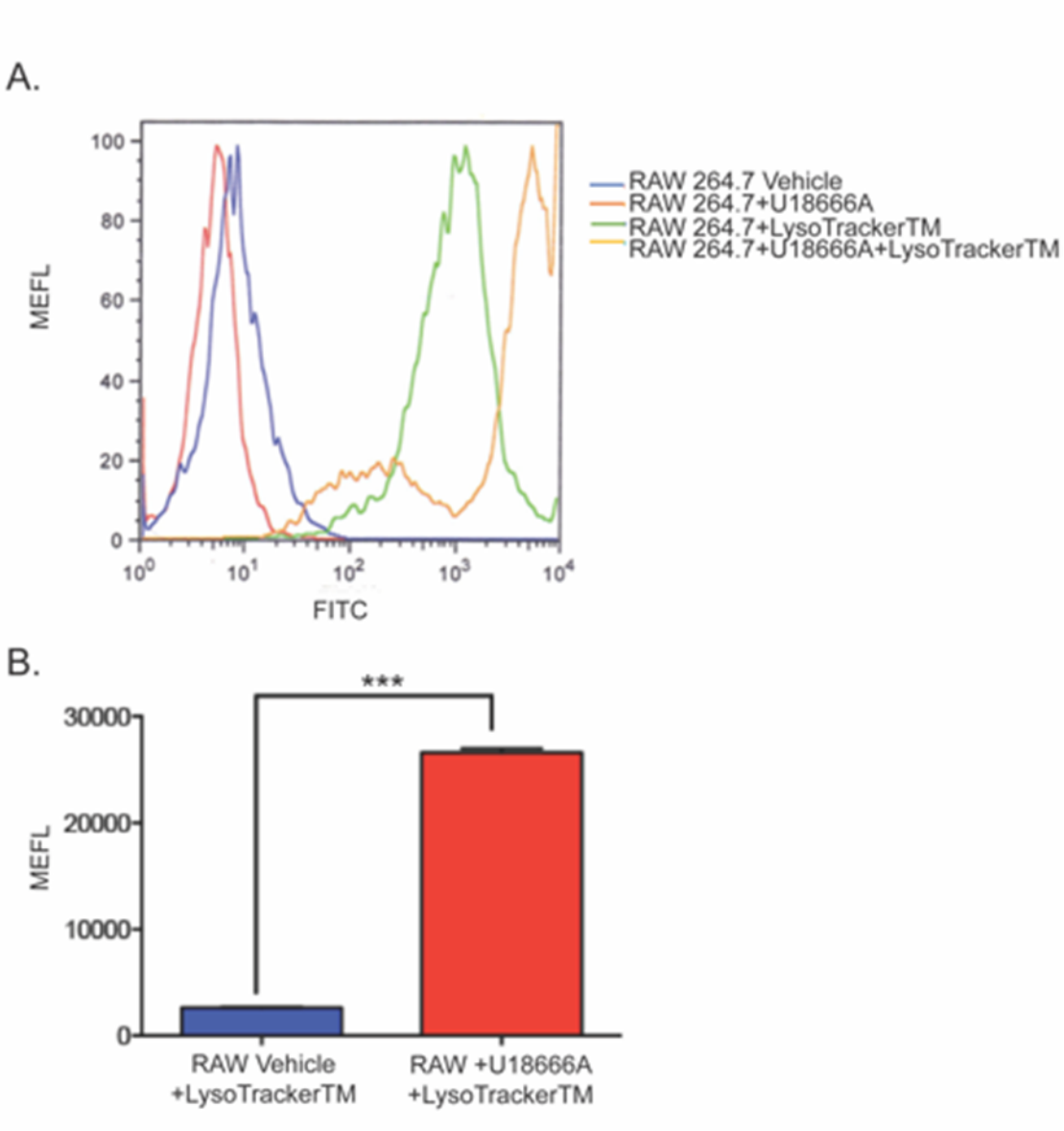


Figure 2.2. U18666A-treated RAW 264.7 MΦ show a significant increase in LysoTrackerstaining in comparison to vehicle-treated RAW 264.6 MΦ (A) FACS profiles of vehicle-treated RAW 264.7 and RAW 264.7 + U18666A MΦ, unstained or stained with LysoTracker. **(B)** Histogram of MEFL of LysoTracker green stained vehicle-treated (blue column) and U18666A-treated (red column) RAW 264.7 MΦ. Mean ± SD. N=4, ***p<0.001. (t-test with Welch's correction). Data is representative of greater than 10 independent experiments.

2.3.2 U18666A-treated RAW 264.7 MΦ accumulate cholesterol.

Filipin (a fluorescent probe for unesterified cholesterol (Vanier, 2010) staining was brighter and more punctate in cells treated with U18666A for 48h than vehicle- treated controls, indicative of lysosomal accumulation of free cholesterol (**Fig.2.3**).

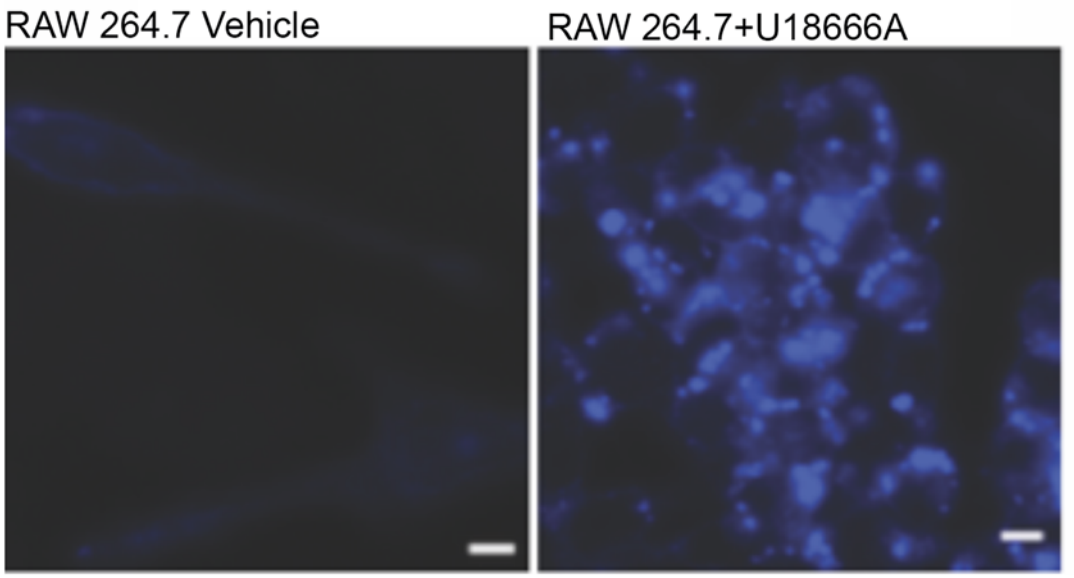


Figure 2.3. Effect of U18666A on Cholesterol Distribution in RAW 264.7 MΦ after 48h treatment with U18666A: Images shown are representative. Blue = filipin (cholesterol). Scale bar, 5 μm, 63x magnification.

2.3.3 Analysis of phagocytosis.

We established *in vitro* phagocytosis assays with the aim of measuring the phagocytic capacity of drug-induced NPC MΦ in comparison to control MΦ. The immortalized murine MΦ cell lines, J774A.1 and RAW 264.7 were treated with U18666A to induce NPC cellular phenotypes, overlaid with fluorescent particles, co-incubated for varying periods of time and then examined by fluorescent microscopy or FACS and the frequency of phagocytes that showed evidence of particle internalization determined.

2.3.3.1 U18666A-treated J774A.1 MΦ display impaired phagocytosis of IgG-sRBC.

To assess whether FcγR dependent phagocytosis is affected in NPC, *in vitro* assays were performed using fluorescently labelled IgG opsonised sRBC overlaid onto J774A.1 MΦ. Uptake by J774A.1 MΦ was determined at 30, 60, 90 and 120 min after addition of IgG-sRBC (**Fig. 2.4**). Inspection of representative fields by fluorescent microscopy revealed that at 30 min, 35.5% of U18666A-treated J774A.1 cells displayed evidence of internalisation (>1 IgG-sRBC per MΦ); at 60 min, 44.5%; at 90 min 52.5%; at 120 min 59% (**Fig. 2.4**), whereas for vehicle-treated J774A.1 cells, at 30 min 63.5% contained ingested IgG-sRBC; at 60 min, 85%; at 90 min 92.5%; at 120 min, 94.5%. The reduction in relative phagocytic activity in drug-treated MΦ was statistically significant at all time points (**Fig. 2.4B**).

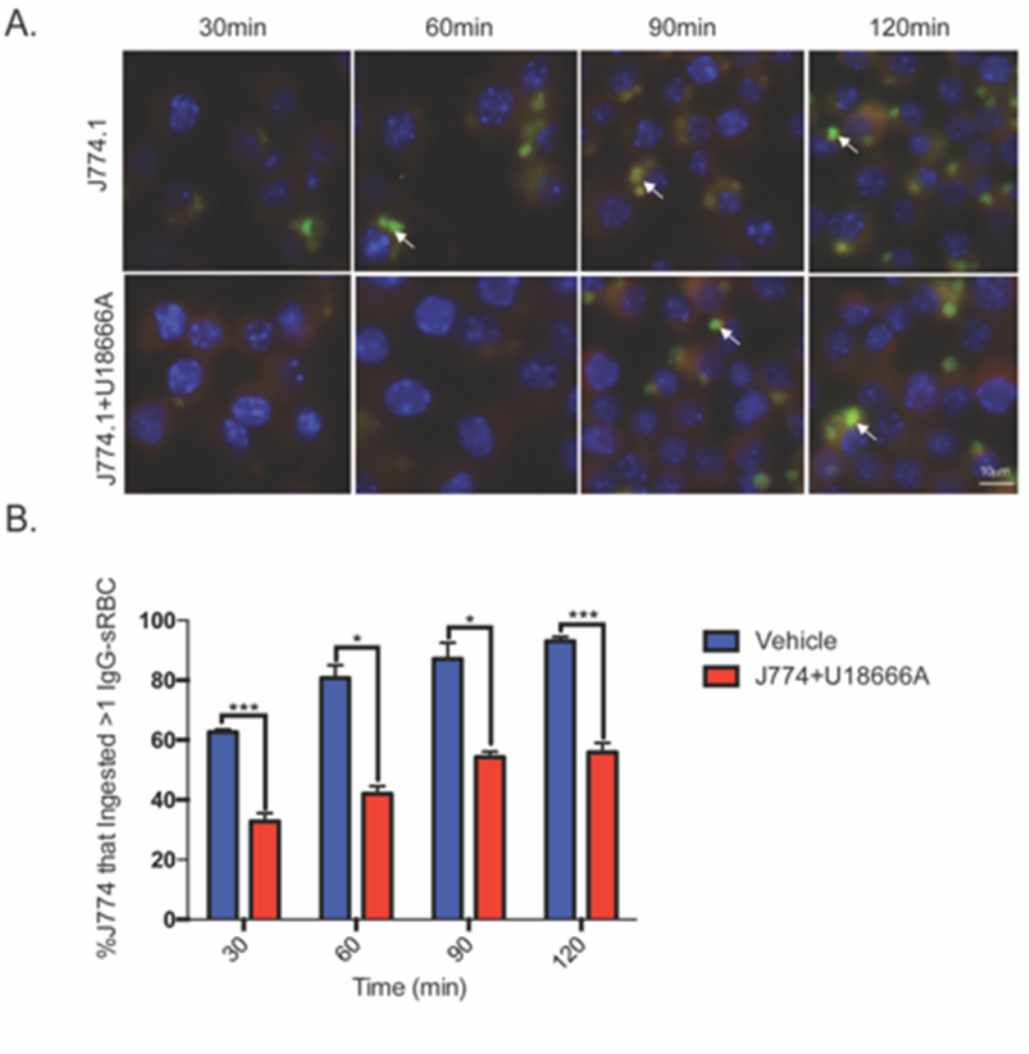


Figure 2.4 J774A.1 MΦ treated with U18666A display decreased phagocytosis of IgG-sRBC: (A) Representative fields of vehicle-treated (upper row) and U18666A-treated (lower row) J774A.1 co-incubated with IgG- sRBC (green) for 30, 60, 90 and 120 mins. Examples of ingested sRBC (green) are indicated by white arrows. Blue=DAPI **(B)** Quantification of relative phagocytic activities of vehicle-treated (blue columns) and U18666A-treated (red columns) J774A.1 MΦ**.** Mean ±SD. N=4, **p*>0.05, ****p*>0.001. Data is representative of three independent experiments. Scale bar = 10μm, 40x magnification.

2.3.3.2 NPC RAW 264.7 MΦ display impaired phagocytosis of IgG-sRBC; Analysis by microscopy and FACS

RAW 264.7 MΦ were analyzed using the same phagocytosis assay; however, incubation times were 5, 15, 30, 40, and 60 min. This allowed for assessment of whether phagocytic activity might be inhibited over the entire period of co-incubation or if it might be compromised only at early or late time points (**Fig. 2.5(A)**.

Inspection of representative fields revealed that at 5 min, 13.9% of U18666A-treated RAW 264.7 cells displayed evidence of internalisation (>1 IgG-sRBC per MΦ); 15 min, 32.5%; at 30 min 42.0%; at 40 min 54.3%; at 60min 59.6% (**Fig. 2.5**), whereas at 5 min for vehicle-treated RAW 264.7 cells, 34.5% contained ingested IgG-sRBC; at 15 min, 62.6%; at 30 min, 80.7%; at 40 min 87.1% and at 60 min 91.1% (**Fig. 2.5**). The reduction in relative phagocytic activity in drug-treated MΦ was statistically significant at all time points (**Fig 2.5).**

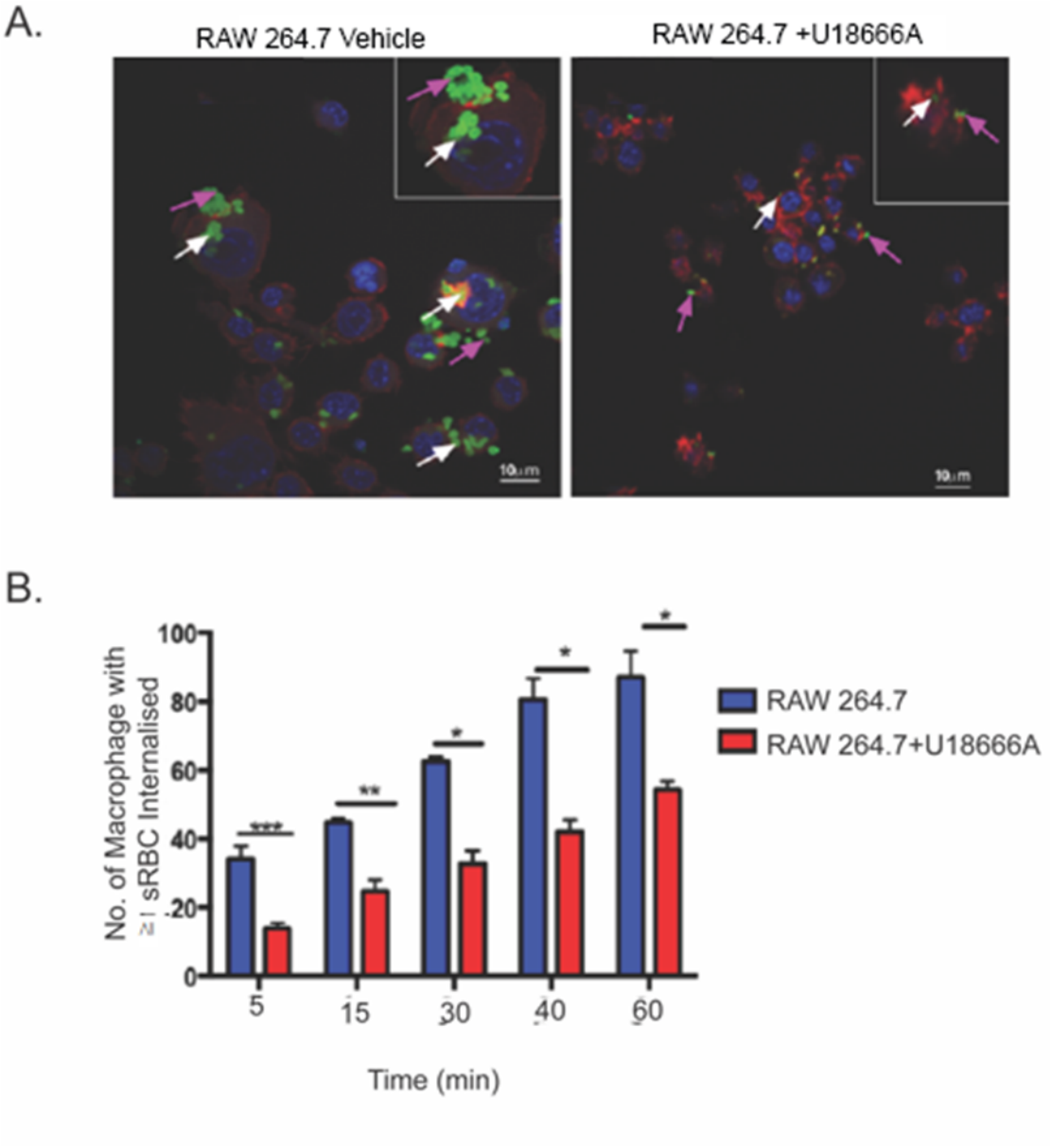


Figure 2.5. RAW 264.7 MΦ treated with U18666A display decreased phagocytosis of IgG-sRBC: **(A)**Representative confocal microscopy images of vehicle-treated RAW 264.7 MΦ (left panel) and RAW 264.7 MΦ treated with U18666A (right panel) stained with phalloidin (red) that have been co-incubated with IgG-sRBC (green) for the indicated times. Examples of ingested IgG-sRBC (white arrows) and bound but not internalized IgG-sRBC (magenta arrows) are indicated. Scale bar = 10μm, 63x. **(B**) RAW 264.7+U18666A show significantly decreased phagocytosis. Data presented as mean ± SD. N=5 *p<0.05, **p<0.01 ***p<0.001 (student's t-test with Welch's correction). Data is representative of three independent experiments.

We employed FACS to compare phagocytic activities of vehicle-treated and U18666A-treated phagocytes. FACS analysis enabled rapid quantification of internalization because the frequency and fluorescent intensity in the green (488 nm) channel would be a measure of the relative number of Cell Tracker^{TM} green labelled IgG-sRBC ingested. Representative FACS profiles for J774A.1 and RAW 264.7 cells (vehicle and U18666A-treated) are shown in **Fig. 2.6** and **Fig. 2.7**, respectively. Vehicle-treated J774A.1 MΦ showed an almost 2-fold greater fluorescence in the FL1 channel (MEFL= 8481 ± 98.3) as compared to J774A.1 treated with U18666A (MEFL= 5086 ± 22.5). Vehicle J774A.1 showed a fluorescent frequency of 48.3% compared to a fluorescent frequency of 12.6% of U18666A-treated J774A.1, indicating a higher incidence of internalisation by untreated J774A.1 MΦ. Histogram representation of MEFLs for control and U18666A-treated J774A.1 MΦ is shown in **Fig.2.6B**.

Representative FACS profiles for RAW 264.7 MΦ that were co-incubated with Cell Tracker^{TM} green labelled IgG-sRBC (for 0, 10 and 60 min) are shown in **Fig. 2.7**. RAW 264.7 MΦ (vehicle) showed an approximate 2-fold greater fluorescence in the FL1 channel (MEFL=4557) as compared to RAW 264.7 treated with U18666A (MEFL=1971). Vehicle RAW 264.7 MΦ showed a fluorescent frequency of 13.6% after 10 min and 57.1% after 60 min compared to 4.11% and 31.3% in U18666A-treated RAW 264.7 MΦ. Histogram representation of MEFLs for vehicle and U18666A-treated RAW 264.7 MΦ is shown in **Fig.2.7B**.

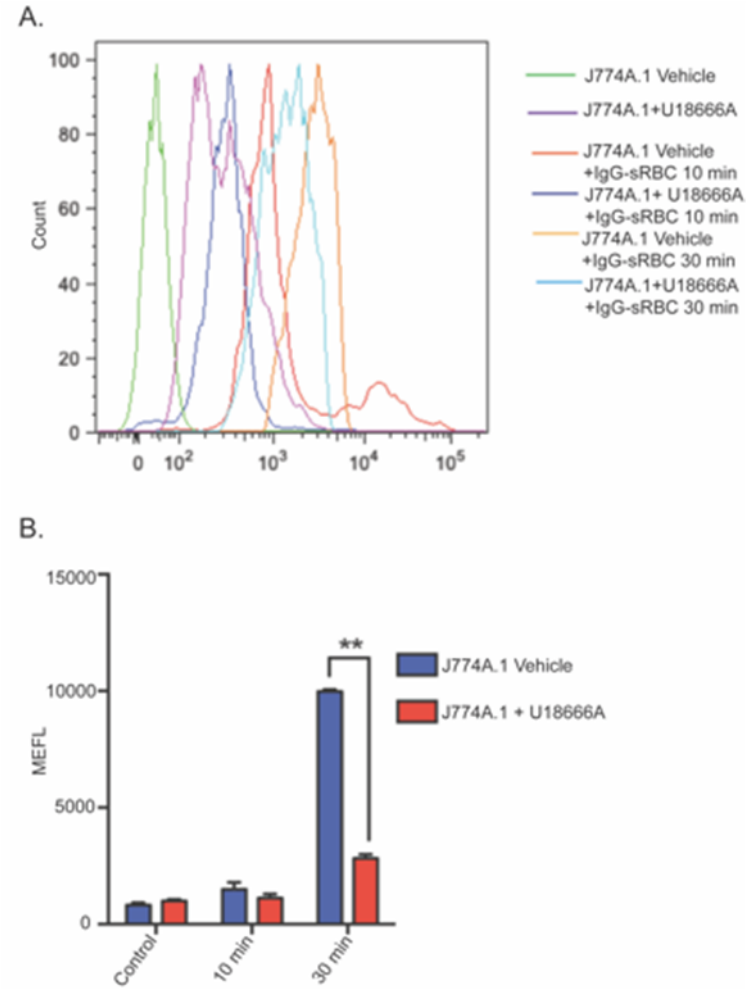


Figure 2.6. U18666A-treated J774A.1 MΦ display impaired phagocytosis of IgG-sRBC. (A) FACS profiles showing increased fluorescence of vehicle-treated J774A.1, indicating greater uptake of labelled IgG-sRBC as compared to U18666A-treated J774A.1 cells. **(B)** Histogram of relative fluorescence of vehicle treated (blue columns) and U18666A-treated (red columns) J774A.1 cells. Mean $\pm$ SD. N=3. $^{**}p<0.01$. (student *t*-test with Welch's correction). Data is representative of three independent experiments.

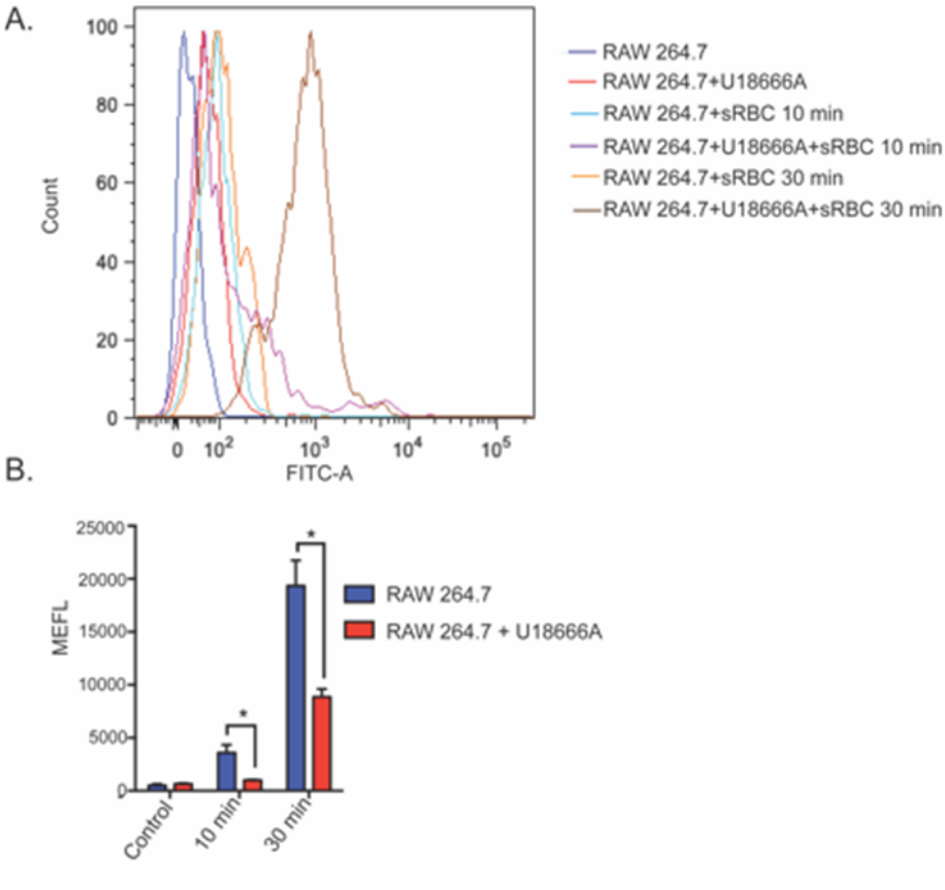


Figure 2.7. U18666A-treated RAW 264.7 MΦ display impaired phagocytosis of IgG-sRBC:
(A) FACS profiles showing increased fluorescence of vehicle-treated RAW 264.7, indicative of greater uptake of labelled IgG-sRBC relative to U18666A-treated RAW 264.7 cells. **(B)** Histogram of relative fluorescence of vehicle-treated (blue columns) and U18666A-treated (red columns) RAW 264.7 cells incubated with CellTracker™ green labelled IgG-sRBC. Mean ± SD. N=6, **p*<0.05 (*t*-test with Welch's correction). Data is representative of four independent experiments.

2.3.3.3 NPC RAW 264.7 MΦ display impaired phagocytosis of sRBC opsonized with complement; Analysis by microscopy and FACS

A second mechanistically distinct pathway of particle ingestion is complement receptor (CR) mediated uptake. Labelled sRBC opsonized for uptake via CR were prepared as described and co-incubated with RAW 264.7 MΦ at a MOI of RAW 264.7 MΦ**:** CR-sRBC of 1: 20. After 5 min of co-incubation, a mean of 7.1% of U18666A-treated RAW 264.7 MΦ displayed evidence of internalisation (>1 CR-sRBC per MΦ) as compared to a mean of 18.4% for control MΦ; after 10 min of co-incubation a mean of 16.1% of U18666A-treated RAW 264.7 MΦ displayed evidence of internalisation as compared to a mean of 34.6% for vehicle-treated; at 30 min, a mean of 25.3% of U18666A-treated RAW 264.7 MΦ displayed evidence of uptake as compared to a mean of 39.1% for control MΦ; at 40 min, 38.4% of U18666A-treated RAW 264.7 MΦ showed evidence of phagocytosis as compared to a mean of 51.2% for control MΦ; finally, by 60 min of co-incubation, 61.3% of U18666A-treated RAW 264.7 MΦ had internalization CR-sRBC compared to a mean of 80.4% of vehicle-treated MΦ. The reduction in relative phagocytic activity in drug-treated RAW 264.7 MΦ was statistically significant at all time points (**Fig.2.8)**.

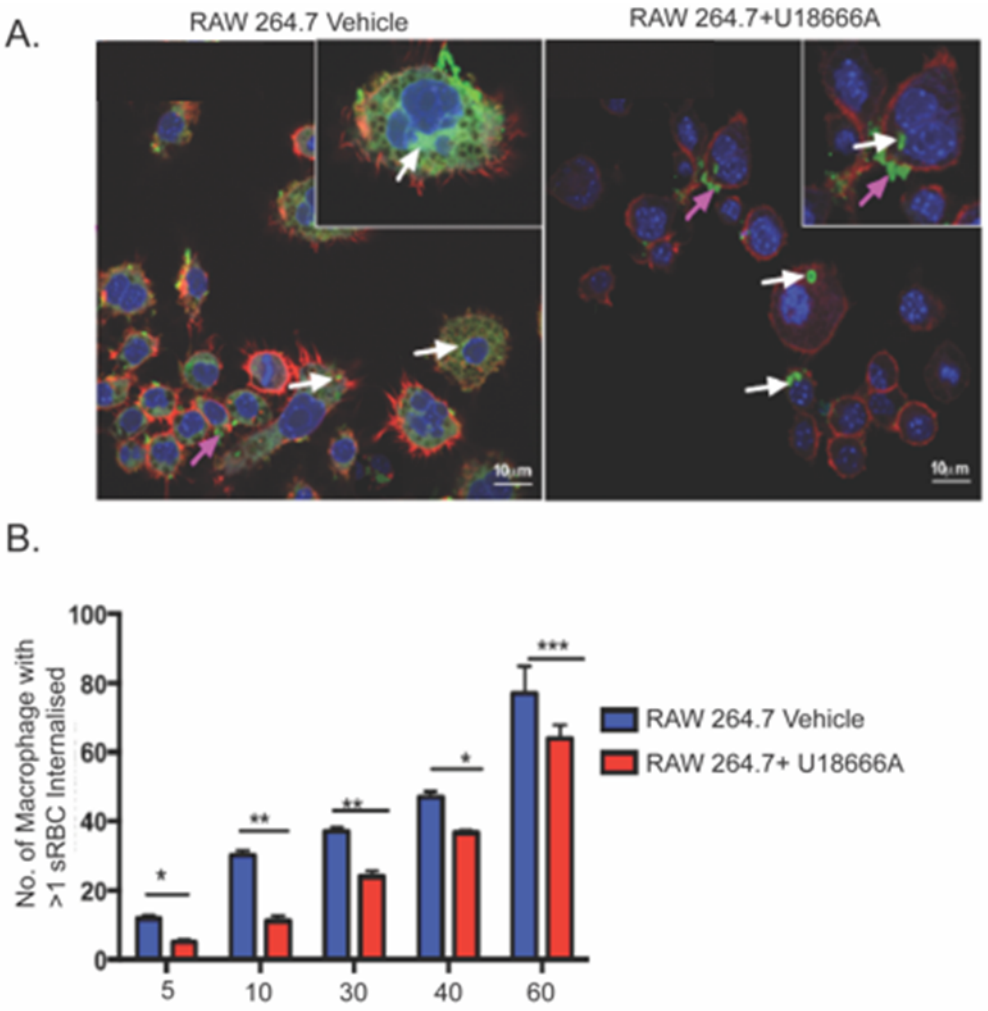


Figure 2.8. RAW 264.7 MΦ treated with U18666A show a significant defect in phagocytosis of CR-sRBC: (A) Representative confocal microscopy images of control RAW 264.7 MΦ (left panel) and RAW 264.7 MΦ treated with U18666A (right panel) stained with phalloidin (red) that have been co-incubated with CR-sRBC (green) for the indicated times. Examples of ingested CR-sRBC (white arrows) and bound, but not internalized IgG-sRBC (magenta arrows) are indicated**.** Scale bar=10μm, 63x **(B)** Quantification of phagocytic activity of RAW 264.7 + U18666A MΦ (red columns) as compared to vehicle-treated MΦ (blue columns). Mean ± SD. N=5 *p<0.05, **p <0.01, ***p<0.001 (student's t-test with Welch's correction). Data is representative of three independent experiments.

We employed FACS to compare the phagocytic activities of untreated and U18666A-treated phagocytes and to verify the data obtained by microscopy. Examples of FACS profiles of untreated and U18666A-treated RAW 264.7 MΦ co-incubated with CR-sRBC are shown in **Fig.2.9**. Vehicle-treated RAW 264.7 MΦ had a 2-fold greater fluorescence in the FL1 channel (10 min, MEFL=1754±19.42; 30 min, MEFL=4203±75.08) relative to RAW 264.7 MΦ treated with U18666A (10 min, MEFL=1153±29.1; 30 min, MEFL=2139±47.6). Vehicle RAW 264.7 MΦ showed a fluorescent frequency of 11.9% after 10 min and 43.1% after 30 min compared to 5.7% and 16.4% in U18666A-treated RAW 264.7 MΦ. Histograms of the relative fluorescence of vehicle-treated and U18666A-treated RAW 264.7 MΦ cells are shown in **Fig.2.9B.**

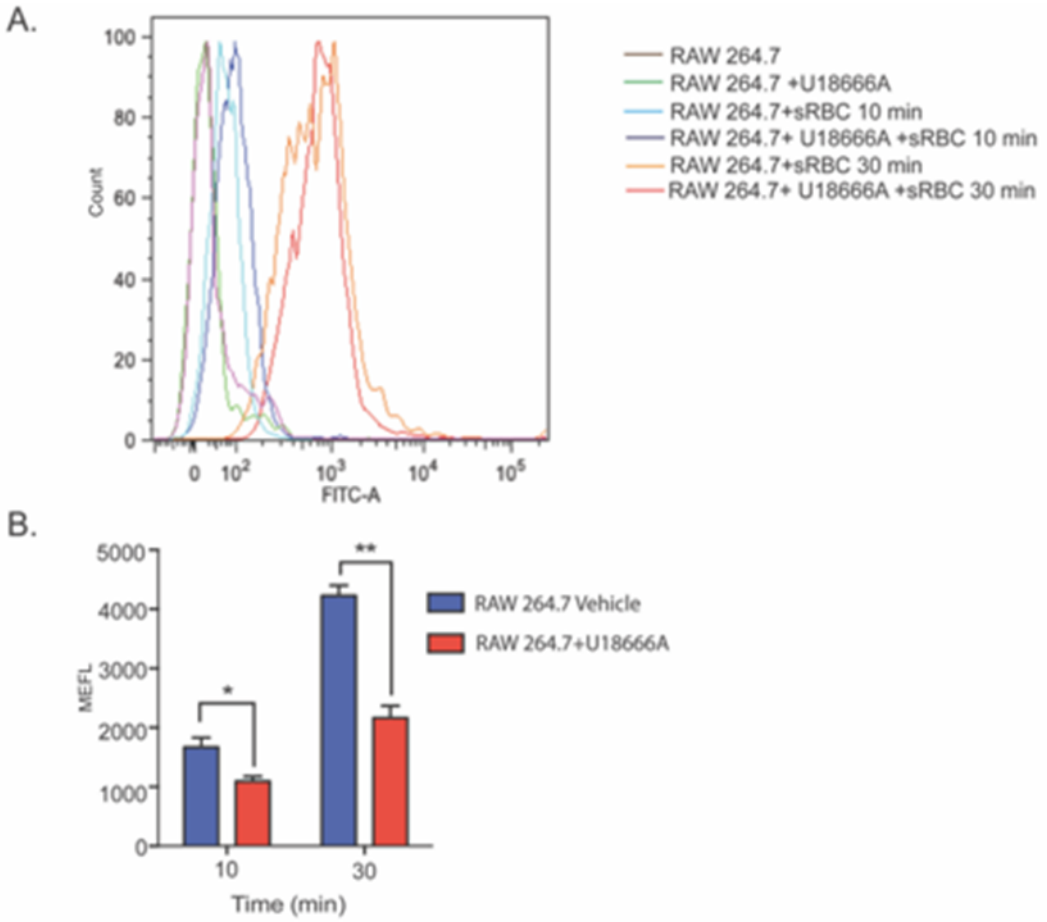


Figure 2.9. U18666A-treated RAW 264.7 MΦ display impaired phagocytosis of CR-sRBC: (A) FACS profiles showing increased fluorescence of vehicle-treated, as compared to U18666A-treated RAW 264.7 MΦ. **(B)** MEFL values for vehicle-treated (blue columns) and U18666A-treated (red columns) of RAW 264.7 MΦ co-incubated with labelled CR-sRBC for 10 min and 30 min. Mean ± SD. N=5. ****p*<0.001**.** Data is representative of three independent experiments.

2.3.3.4 NPC RAW 264.7 MΦ display impaired phagocytosis of Ox-sRBC; Analysis by microscopy and FACS.

We analyzed phagocytosis of Ox-sRBC by RAW 264.7 MΦ at a MOI of RAW 264.7 MΦ: Ox-sRBC of 1: 20. Prior treatment with cytochalasin D prevented essentially all Ox-sRBC uptake, confirming ingestion was by a mechanism dependent upon actin polymerization (i.e. phagocytosis)(images not show).

At a 10 min of co-incubation, 11.4% of U18666A-treated RAW 264.7 MΦ displayed evidence of ingestion (>1 Ox-sRBC per Mϕ) as compared to a mean of 23.6% for vehicle-treated cells; at 20 min of co-incubation a mean of 21.4% of U18666A-treated RAW 264.7 MΦ displayed evidence of internalisation as compared to 44.8% of vehicle-treated MΦ; at 30 min a mean of 29.4% of U18666A-treated RAW 264.7 MΦ had ingested a particle compared to a mean of 66.1% for vehicle-treated MΦ. By 40 min, 45.2% of U18666A-treated cells contained >1 Ox-sRBC as compared to a mean of 81.2% for vehicle-treated MΦ. The reduction in relative phagocytic activity in drug-treated MΦ was statistically significant at all four time points **(Fig. 2.10)**.

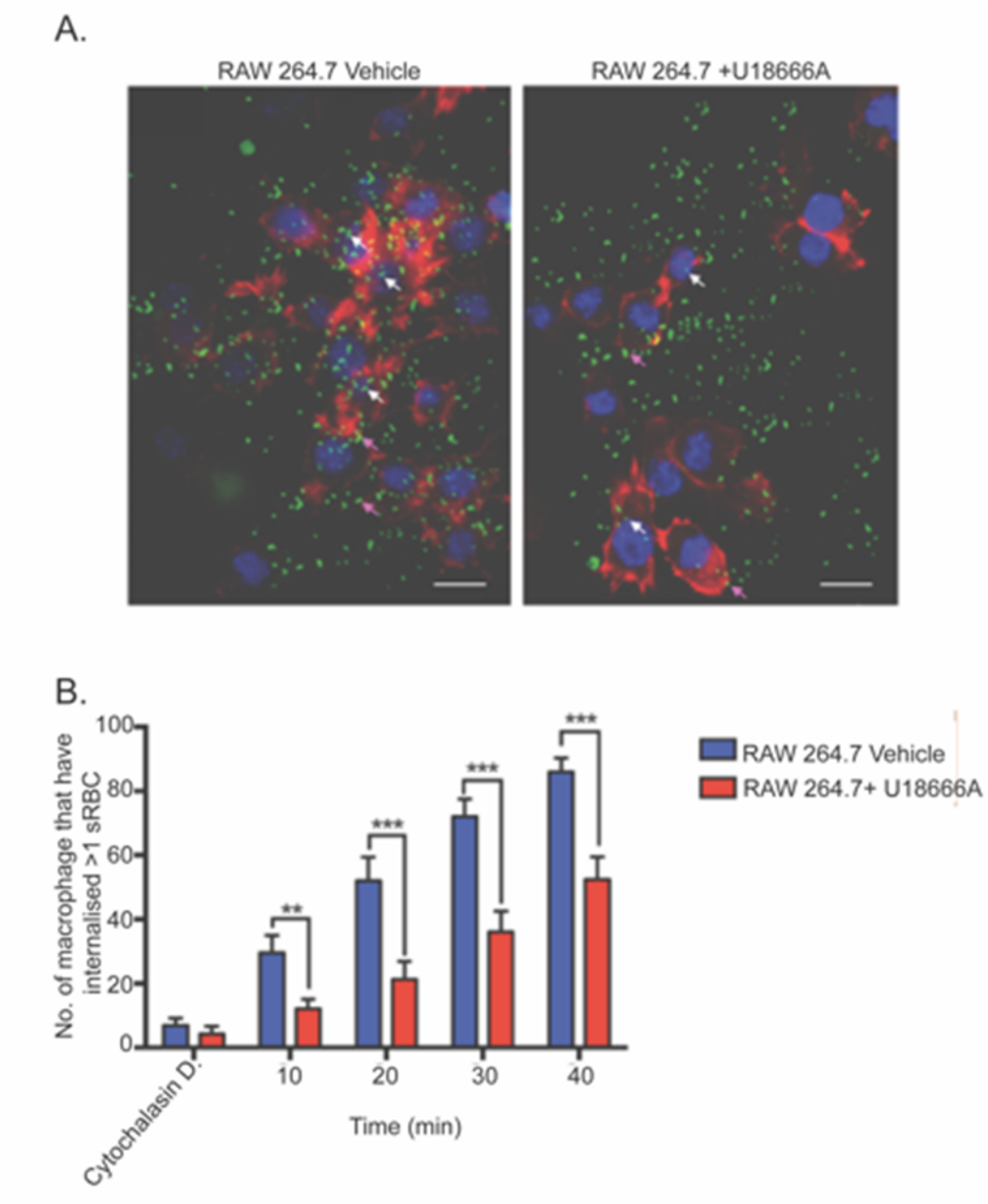


Figure 2.10. RAW 264.7 MΦ treated with U18666A show significantly reduced phagocytosis of Ox-sRBC: (A) Representative images of vehicle-treated MΦ (left panel) and U18666A-treated cells (right panel) incubated with CellTracker™, green labeled Ox-sRBC. Examples of internalised Ox-sRBC are indicated by white arrows, Examples of bound, but not internalised Ox-sRBC are indicated by magenta arrows. Blue = DAPI. Red = phalloidin. Scale bar =5 µm, 63x **(B)** Quantification of phagocytic activity. Vehicle-treated RAW 264.7 MΦ (blue columns) display significantly greater uptake of Ox-sRBC than U18666A-treated RAW 264.7 MΦ Mean ± SD. N=5, **p<0.01, ***p>0.001. (student's t-test with Welch's correction). Data is representative of three independent experiments.

FACS analysis confirmed a comparable deficit in uptake of Ox-sRBC by U18666A- treated RAW 264.7 MΦ (**Fig.2.11**). Fluorescence of vehicle-treated MΦ incubated with Ox-sRBC was significantly greater than that of U18666A-treated RAW 264.7 (MEFL=1937±58.1 as compared to MEFL=737±54.1). Vehicle RAW 264.7 MΦ showed a fluorescent frequency of 68.9% as compared to 39.4% in U18666A-treated RAW 264.7 MΦ. Representative FACS profiles and their quantification are shown in **Fig. 2.11.**

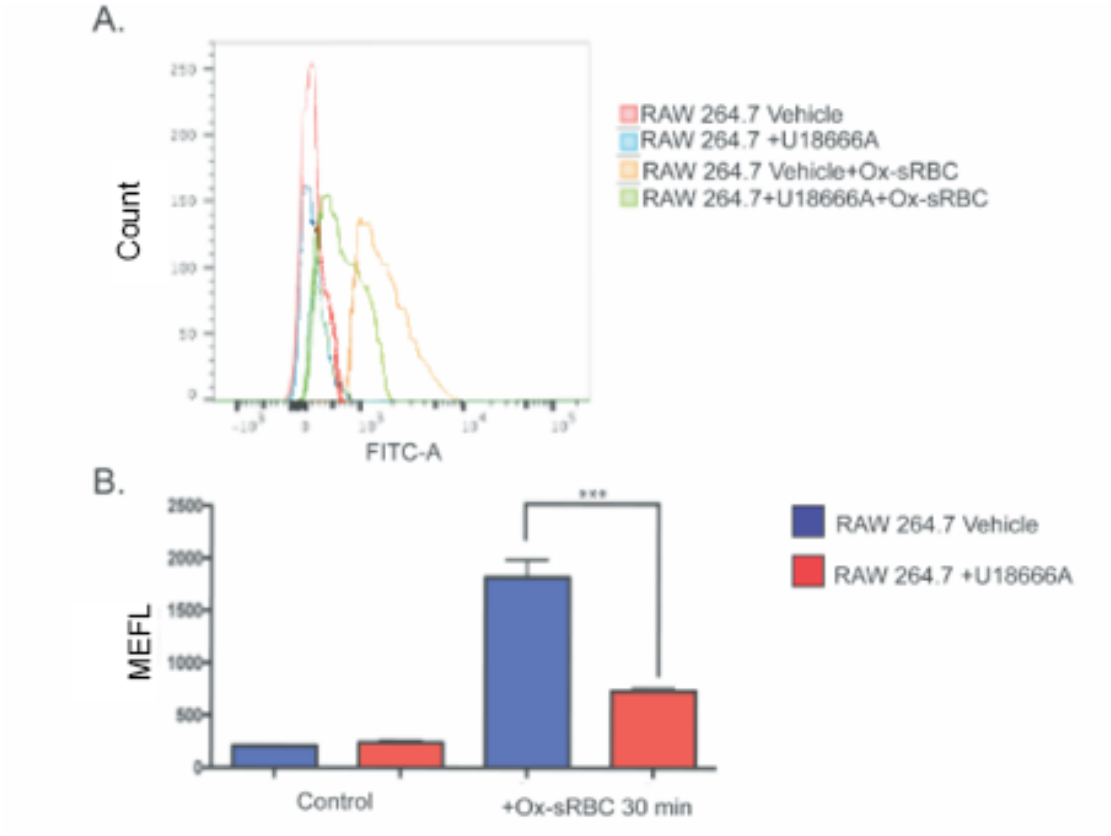


Figure 2.11. U18666A-treated RAW 264.7 MΦ display reduced phagocytosis of Ox-sRBC:
(A) FACS profiles showing greater fluorescence (x-axis) of vehicle-treated RAW 264.7 MΦ co-incubated with labelled Ox-sRBC (MOI 20:1) than U18666A-treated MΦ. **(B)** MEFLs of vehicle-treated (blue columns) and U18666A-treated RAW264.7 MΦ (red columns) incubated alone or with CellTracker™ green labelled Ox-sRBC for 30 min. Mean ± SD. N=4 *** $p<0.001$ (via *t*-test with Welch's correction). Data is representative of three independent experiments.

2.3.3.5 NPC RAW 264.7 cells display impaired phagocytosis of *Escherichia coli*; Analysis by microscopy and FACS.

We extended our investigations to include examining for phagocytosis of *Escherichia coli (E. coli).* Vehicle and U18666A-treated RAW 264.7 MΦ were overlaid with fluorescent pHrodo® green *E. coli* Bio Particles at RAW 264.7 MΦ**:** *E. coli* MOI of 1:25 (as recommended by manufacturer), co-incubated and analysed by confocal microscopy. After 10 min of co-incubation, 9.81% of U18666A-treated RAW 264.7 MΦ displayed evidence of internalisation (>1 *E. coli* per MΦ) as compared to 28.1% of vehicle-treated MΦ; at 20 min 16.7% of drug-treated RAW 264.7 had internalized bacteria as against 57.1% of vehicle-treated phagocytes; by 30 min, 51.2% of U18666A-treated RAW 264.7 MΦ displayed evidence of phagocytosis whereas it was 77.8% for control MΦ; at 40 min of co-incubation, 69.7% of U18666A-treated RAW 264.7 MΦ were scored positive for phagocytosis as compared to 88.4% of vehicle-treated RAW 264.7 MΦ (**Fig. 2.12**). The reduction in relative phagocytic activity in drug-treated MΦ was statistically significant at all time points (**Fig. 2.12B**). Uptake of *E. coli* was confirmed to be by a phagocytic mechanism because pre-treatment with cytochalasin D abolished almost all ingestion (images not shown)

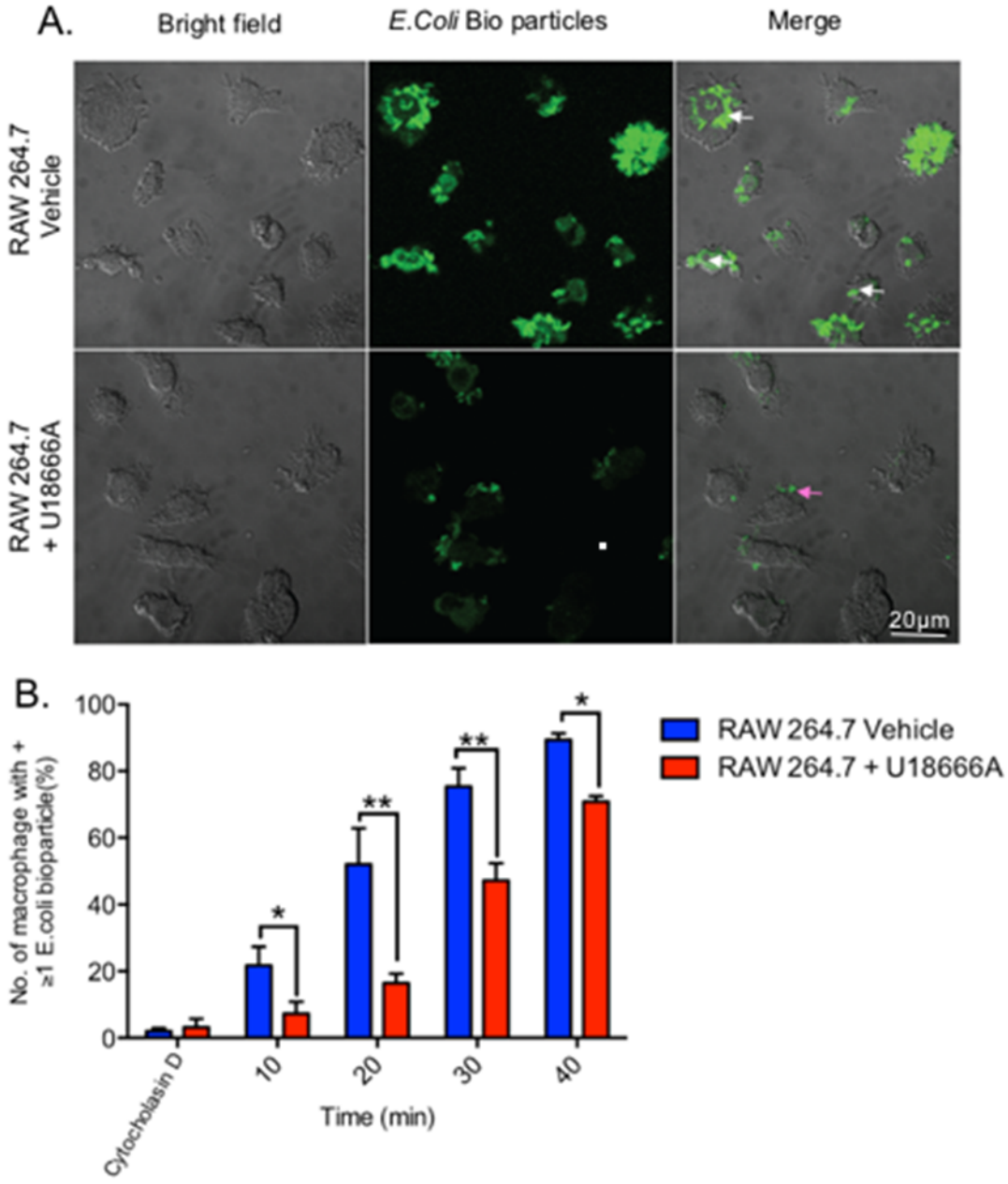


Figure 2.12. RAW 264.7 MΦ treated with U18666A show a significant reduction in phagocytosis of E. coli Bio particles: (A) Representative fields of vehicle-treated and U18666A-treated RAW 264.7 MΦ co-incubated with *E. coli* Bio particles (green) for 30 min. Red, phalloidin staining. Examples of internalized bacteria identified by white arrows. Examples of bound, but not internalized *E. coli* indicated by magenta arrow. Scale bar=20 µm,40x **(B)** Vehicle-treated RAW 264.7 MΦ (blue columns) display statistically significantly greater phagocytosis of *E. coli* than U18666A-treated RAW 264.7 MΦ (red columns). Mean ± SD. N=200 *p<0.05, **p<0.01 (student's t-test with Welch's correction). Data is representative of three independent experiments.

Phagocytosis of pHrodo® *E. coli* Bio particles was also assessed by FACS. Representative FACS profiles of control and U18666A-treated RAW 264.7 MΦ co-incubated with fluorescein labelled *E. coli* are shown in **Fig.2.13**. Relative to U18666A-treated cells, vehicle-treated RAW 264.7 MΦ showed two-fold greater fluorescence at 10 min (U18666A-treated MEFL= 3061±42.1; vehicle-treated MEFL=6901±71.41) and two-fold greater after incubation for 30 min (U18666A-treated MEFL=9841; untreated MEFL= 18941±110.4). Vehicle RAW 264.7 MΦ showed a fluorescent frequency of 7.1% after 10 min and 59.4% after 30 min compared to 21.3% and 71.1% in U18666A-treated RAW 264.7 MΦ. Representative FACS profiles and their quantification are shown in **Fig. 2.13.**

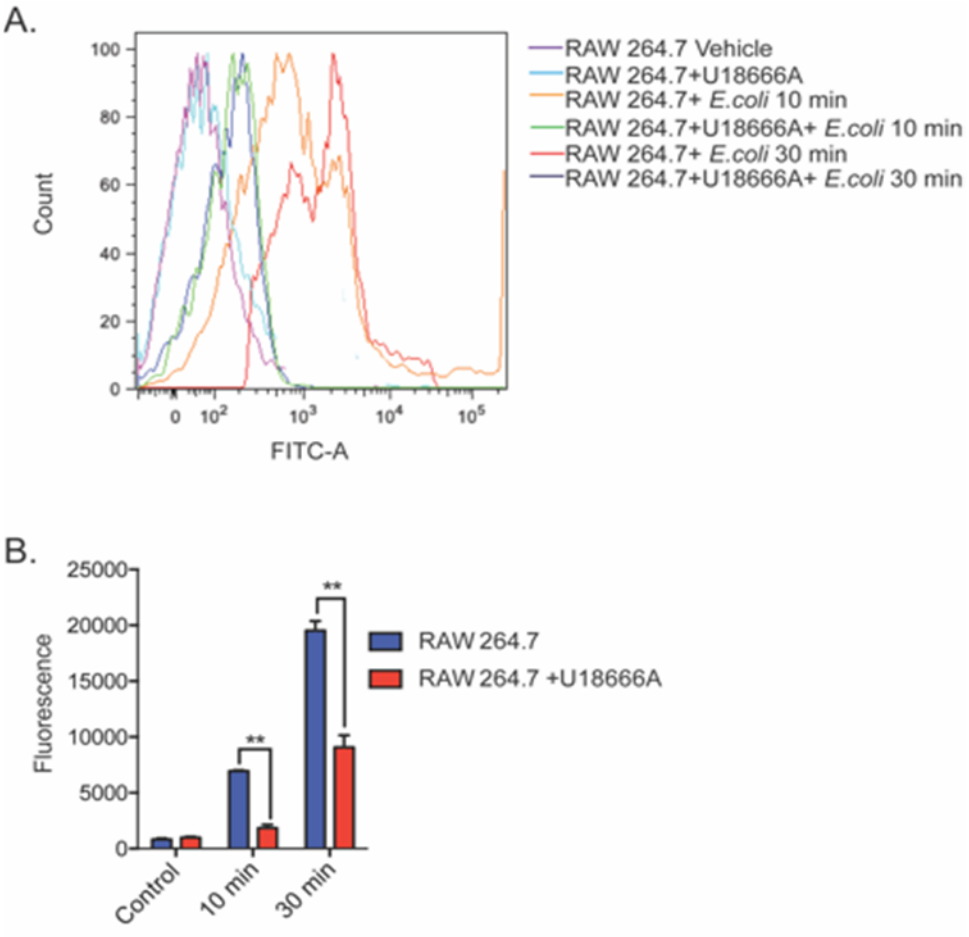


Figure 2.13. U18666A-treated RAW 264.7 MΦ display significantly reduced phagocytosis of E. coli Bio particles: (A) FACS profiles of vehicle-treated and U18666A-treated RAW 264.7 cells alone and co-incubated with fluorescent *E. coli* Bio particles. **(B)** Quantification of fluorescence of vehicle-treated (blue columns) and U18666A-treated (red columns) RAW 264.7 MΦ at 0 min, 10 min and 30 min of co-incubation with *E. coli*. Mean ± SD. N=4 ***p*<0.01 (*t*-test with Welch's correction). Data is representative of three independent experiments.

2.3.3.6 NPC RAW 264.7 MΦ show an insignificant decrease in phagocytosis of zymosan Bio particles; Analysis by microscopy and FACS

We analysed for phagocytosis of pHrodo® zymosan Bio particles, a heat-killed particulate preparation of *Saccharomyces cerevisiae,* which consists primarily of β1, 3-glucan, that has been used extensively to study the recognition of fungi by cells of the innate immune system (Underhill, 2003) (**Fig 2.14**). After 10 min of co-incubation, 14.9% of U18666A-treated RAW 264.7 cells showed evidence of phagocytosis (>1 zymosan particle per MΦ) as compared to 16.7% of vehicle-treated RAW 264.7 MΦ; at 20 min, internalisation of zymosan was apparent in 36.4% of U18666A-treated RAW 264.7 cells and 37.9% of vehicle-treated RAW 264.7 cells; at 30 min, 43.9% of U18666A-treated as compared to 44.7% of vehicle-treated RAW 264.7 MΦ had internalized zymosan; at 60 min of incubation, the frequencies of uptake were 61.9% of drug-treated and 70.44% of vehicle-treated RAW 264.7 cells and at 120 min internalisation was apparent in 83.6% of U18666A-treated RAW 264.7 and 87.1% of control Mϕ. There was minimal evidence of ingestion when Mϕ were pretreated with cytochalasin D (2.19% of U18666A-treated and 3.11% of vehicle-treated cells). There was no significant difference in phagocytosis of zymosan between U18666A-treated and vehicle-treated RAW 264.7 MΦ at all time points (**Fig 2.14B).**

Phagocytosis of zymosan by RAW 264.7 MΦ (vehicle and U18666A-treated) was also analysed by FACS. Representative FACS profiles are shown in **Fig.2.15**. There was a significant change in fluorescence between U18666A-treated RAW 264.7 following addition of zymosan (MEFL=3011.4 following addition of zymosan, MEFL=204.1±11.6 in control). A comparable shift in fluorescence was also seen in vehicle RAW 264.7 following incubation with zymosan for 30 min (MEFL=2744 following addition of zymosan in vehicle RAW 264.7, MEFL=99.7±8.7 in control RAW 264.7). Vehicle RAW 264.7 MΦ showed a fluorescent frequency of 57.1% compared to 64.1% in U18666A-treated RAW 264.7 MΦ. Representative FACS profiles and their quantification are shown in **Fig. 2.15.** Although the change in fluorescence was higher in the vehicle group, results were not statistically significant (N=4, p= 0.0541), complimenting the microscopy results.

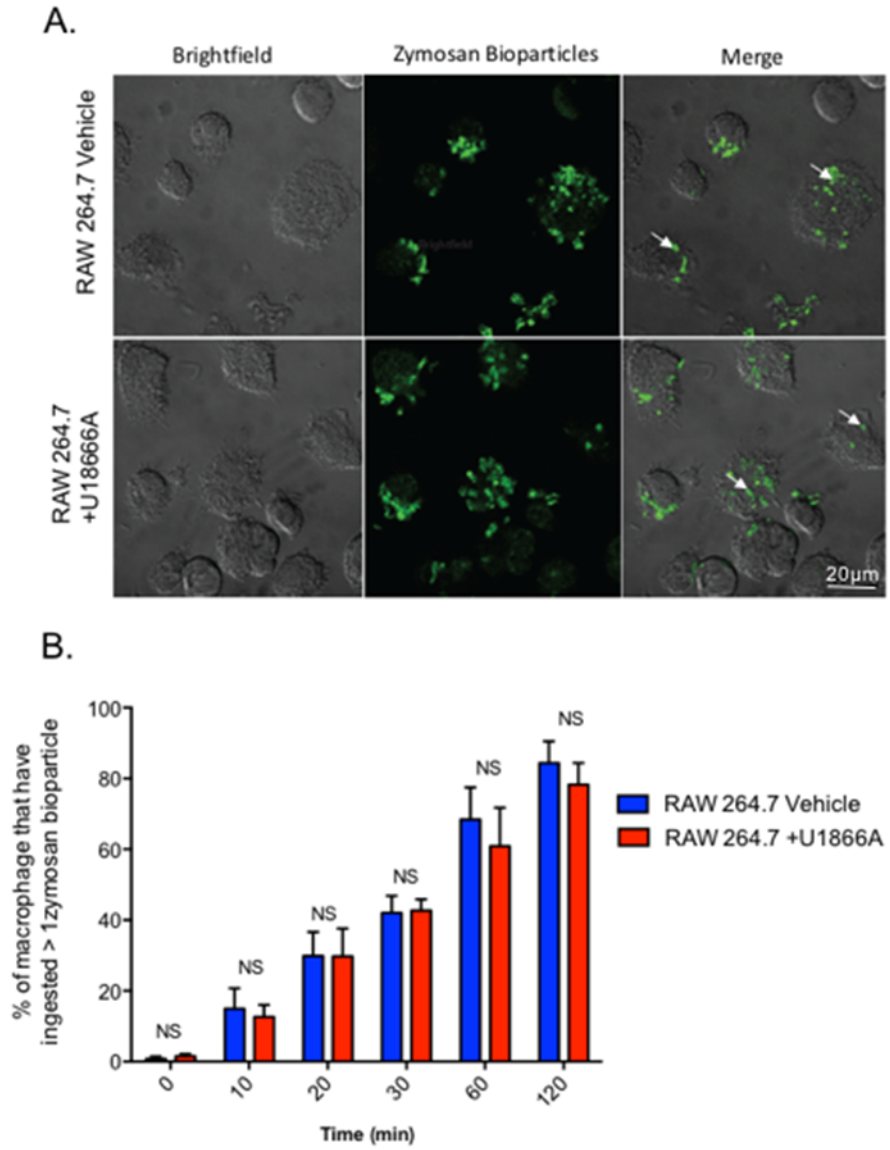


Figure 2.14 RAW 264.7 MΦ treated with U18666A do not show altered phagocytosis of zymosan Bio particles (A) Representative fields of vehicle or U18666A-treated RAW 264.7 co-incubated with zymosan Bio particles(green) for 60 min. Examples of ingested particles, white arrows. Red, phalloidin **(B)** Quantification of phagocytosis of zymosan Bio particles by vehicle (blue columns) and U18666A-treated (red columns) RAW 264.7 MΦ Mean ± SD. N=6 (Student's t-test with Welch's correction). Data is representative of three independent experiments.

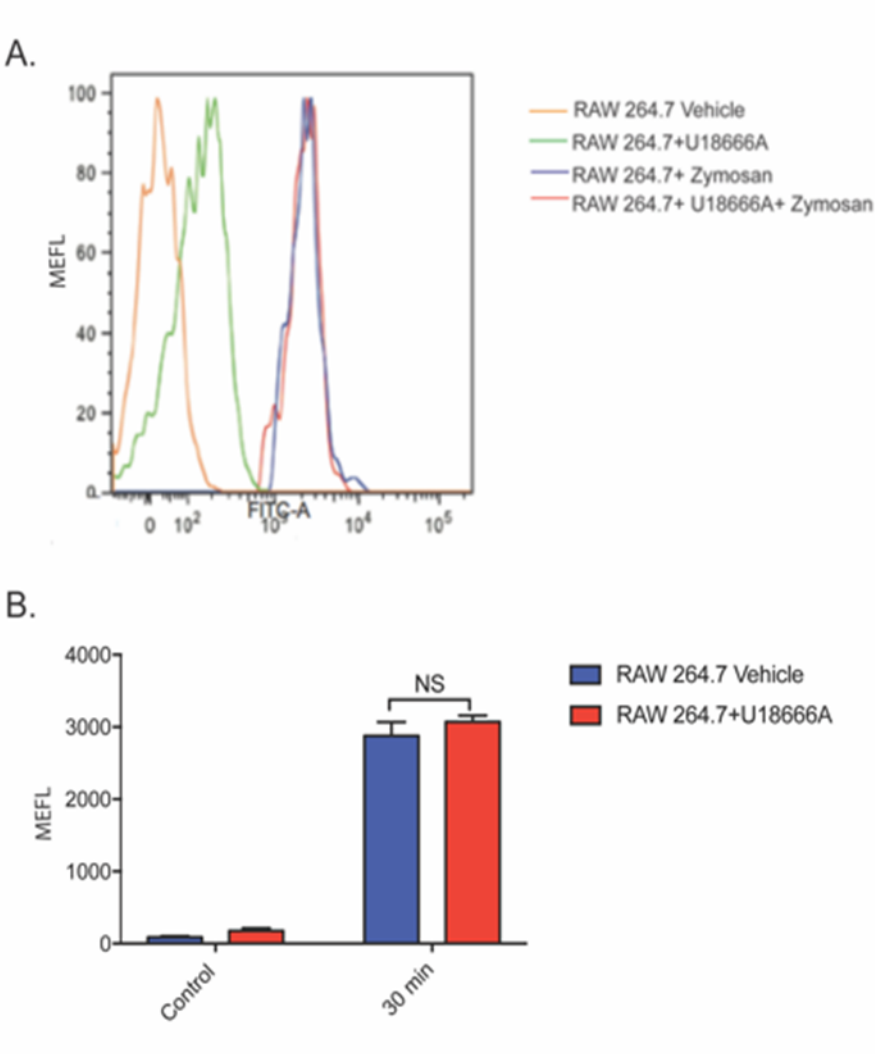


Figure 2.15. RAW 264.7 MΦ display defective phagocytosis of zymosan Bio particles as quantified by FACS: (A) FACS profiles of control RAW 264.7 MΦ and U18666A-treated RAW 264.7 MΦ co-incubated with zymosan Bio particles. **(B)** Mean fluorescence of RAW 264.7 MΦ 30 min after exposure to zymosan Bio particles). Fold change in mean fluorescence relative to control RAW 264.7 cells. Mean ± SD. N=4. ***p<0.001 versus untreated RAW 264.7 (via t-test with Welch's correction). Data is representative of two independent experiments.

2.3.4 Phagocytic defect in NPC J774A.1 and RAW 264.7 MΦ is independent of particle size.

Phagocytosis is responsible for ingestion of particles >0.5 μm in size. Although MΦ can phagocytosis particles <20 μm in diameter, size is an important parameter that affects the rate and capacity for internalization (Akira et al., 2006; Champion and Mitragotri, 2006; Champion et al., 2008). We investigated whether the phagocytic deficit of U18666A-treated J774A.1 MΦ and RAW 264.7 MΦ is dependent upon size of the phagocytic target by incubating macrophages with IgG opsonized spherical particles of defined size and measuring the extent of uptake.

Microscopy analysis of uptake by J774A.1 MΦ, revealed that greater than 80% of control MΦ ingested all sizes of beads tested over the time course of the experiment, whereas for U18666A-treated MΦ ingestion was maximal (60%) for 2 μm beads and only 40% for 10 μm beads (**Fig. 2.16**). U18666A-treated J774A.1MΦ phagocytosed statistically significantly fewer 3 μm, 6 μm and 10 μm polystyrene beads than did vehicle-treated cells. In the case of 2 μm particles, phagocytosis was not significantly different between groups.

This study was repeated using RAW 264.7 MΦ and similar results were obtained (**Fig. 2.16**). There was statistically significant greater uptake of all sizes of beads by vehicle-treated compared than by drug-treated MΦ at all time points except for ingestion of 2 μm beads at 10 and 15 min.

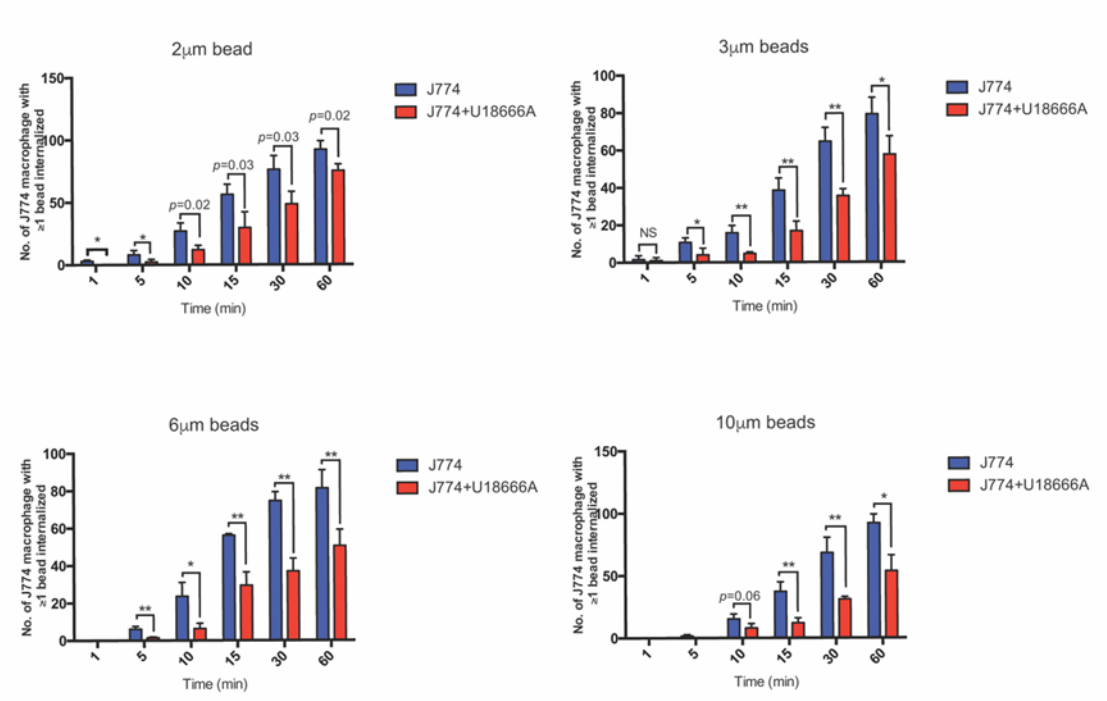
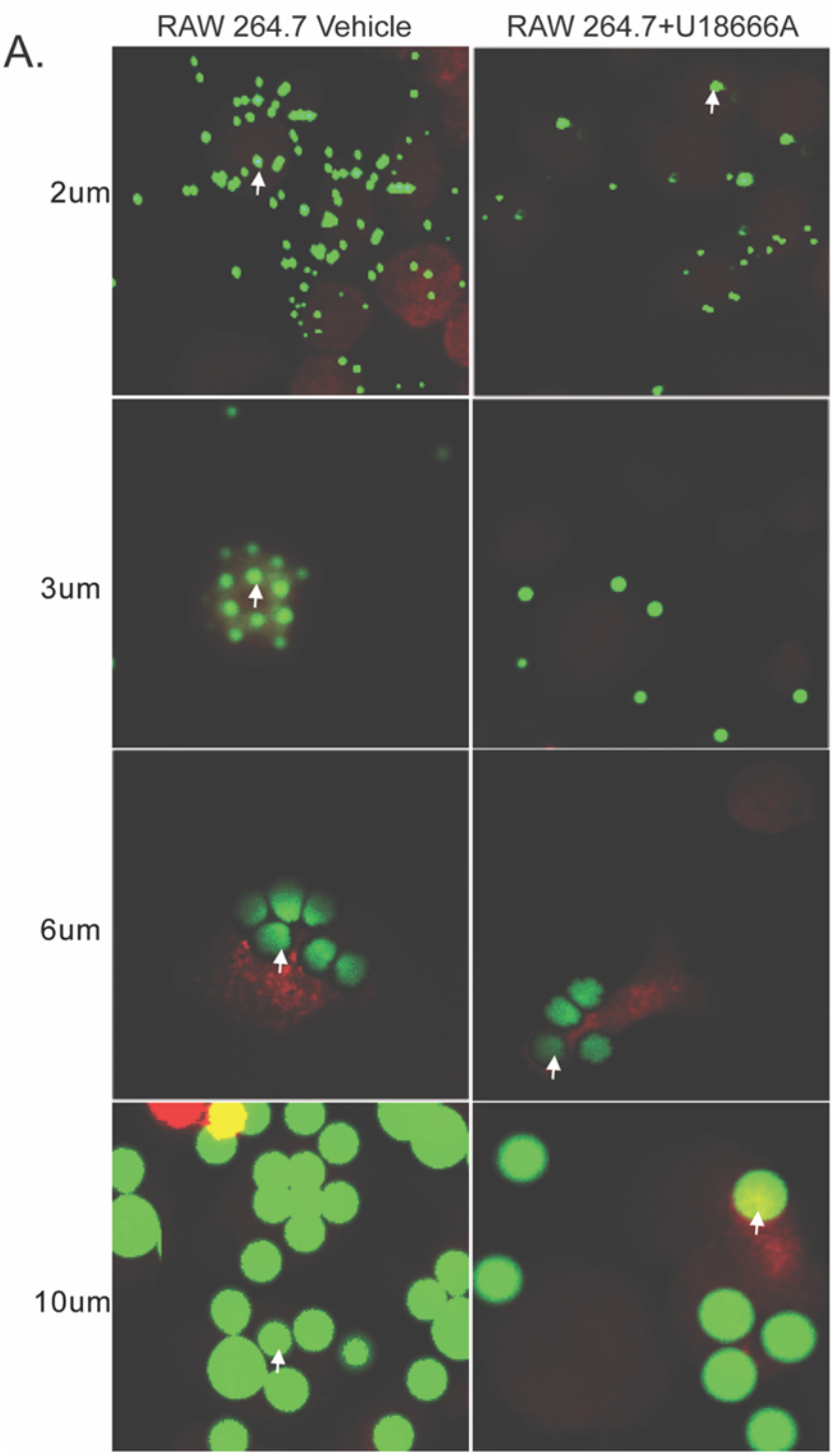


Figure 2.16. U18666A-treated J774A.1 MΦ display significantly reduced phagocytosis of IgG-opsonised polystyrene beads: Microscopy study reveals lower efficacy of J774A.1 treated with U18666A MΦ to phagocytize opsonized polystyrene beads. Representative confocal microscopy not shown. Histogram representation of phagocytosis. In all cases, untreated J774 cells ingested more beads, however, 2μm bead results were NS. Data is presented as mean ± SD. N=6, student's *t*-test evaluated; NS. $p>0.05$, *$p<0.05$, **$p<0.01$, ***$p<0.001$. Data is representative of three independent experiments.


A.
RAW 264.7 Vehicle
RAW 264.7+U18666A
2um
3um
6um
10um

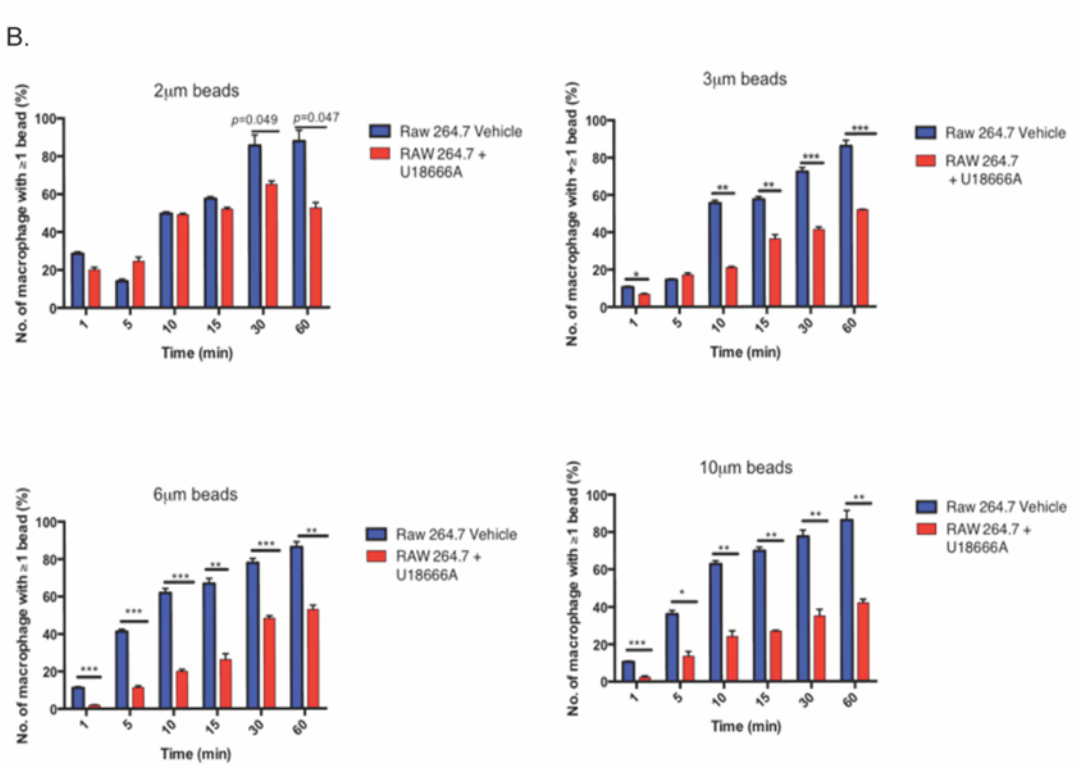


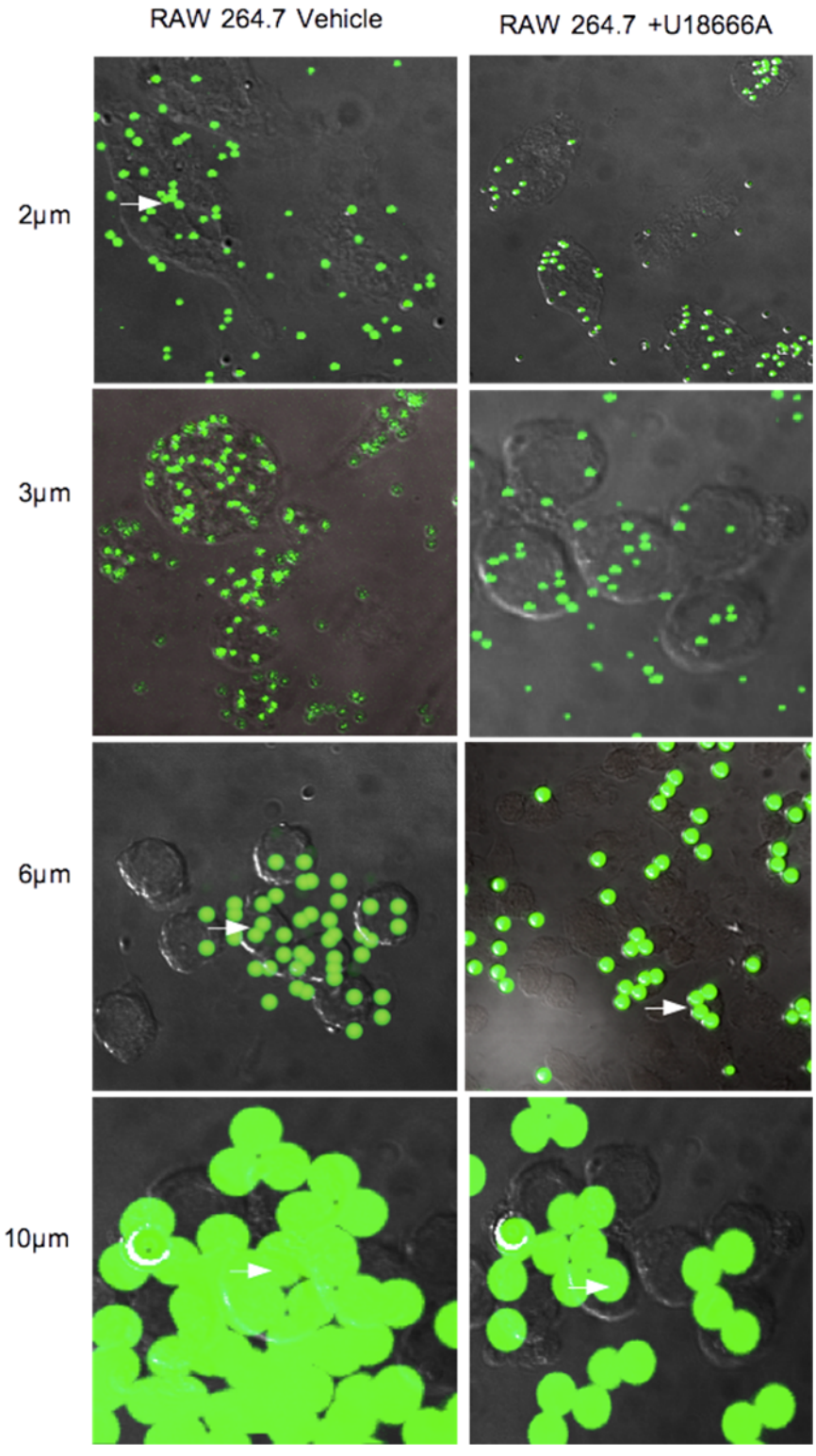
Figure 2.17. U18666A-treated RAW 264.7 MΦ display significantly reduced phagocytosis of IgG-opsonised polystyrene beads independent of their size: (A) Representative fields of Microscopy study reveals lower efficacy of RAW 264.7 treated with U18666A MΦ to phagocytize opsonized polysterene beads. Representative confocal microscopy images of untreated RAW 264.7 (left panels) and U18666A-treated RAW 264.7 MΦ (right panels) stained with phalloidin (red) that have been co-incubated with polystyrene beads 2 μm, 3 μm, 6 μm and 10 μm polystyrene beads; green for 30 min. Examples of ingested (white arrows) beads are indicated. Magnification=63x **(B)** Histogram representation, in all cases RAW 264.7 untreated MΦ ingested more beads. Data is presented as mean ± SD. N=6. NS. $p>0.05$, *$p<0.05$, **$p<0.01$, ***$p<0.001$. (student's *t*-test). Data shown is representative of three independent experiments.

We extended the investigation of the influence of bead size on uptake by measuring the phagocytosis of un-opsonized or “naked” beads (**Fig 2.18**). Results were significantly different for all beads tested, confirming that there was significantly lower phagocytosis of 3-10 μm beads by RAW 264.7 MΦ that had been treated with U18666A. Results when using 2 μm were insignificant. In the case of 2 μm particles, at 1 min 1.41% of U18666A-treated RAW 264.7 MΦ had ingested, in comparison to 1.91% of vehicle-treated MΦ; at 5 min of incubation, 9.15% of U18666A-treated RAW 264.7 MΦ showed evidence of internalization as compared to 11.51% of vehicle-treated RAW 264.7 MΦ; at 10 min the frequency was 20.5% of U18666A-treated cells and 28.6% of vehicle-treated; at 15 min it was 38.6% compared to 41.8% in untreated MΦ; at a 30 min time incubation, U18666A-treated RAW 264.7 MΦ had a mean internalisation 42.70% compared to a mean of 54.71% in untreated MΦ; at a 60 min incubation, RAW 264.7 MΦ treated with U18666A had a mean internalization of 56.53% compared to 60.41 % in untreated RAW 264.7 MΦ (**Fig. 2.18B**).

Phagocytosis assays were made for 3 μm, 6 μm and 10 μm beads (**Fig. 2.18 B**). In the case of 3 μm beads, at 1 min U18666A-treated RAW 264.7 MΦ had a mean value of 0.08% internalization as compared to 1.91% in untreated MΦ; at 5 min incubation, U18666A-treated RAW 2647. MΦ had a mean internalization of 8.15% internalization compared to 10.51% in untreated RAW 264.7 MΦ; at a 10 min incubation U18666A MΦ had a mean internalization of 11.41% compared to 33.0% in untreated MΦ; at a 15 min incubation U18666A MΦ had a mean internalization of 31.67% compared to 49.41% in untreated

MΦ; at a 30 min time incubation, U18666A-treated RAW 264.7 MΦ had a mean internalisation 44.41% compared to a mean of 78.40% in untreated MΦ; at a 60 min incubation, RAW 264.7 MΦ treated with U18666A had a mean internalization of 42.1% compared to 77.41 % in untreated RAW 264.7 MΦ

In the case of 6 μm beads, at 1 min U18666A-treated RAW 264.7 MΦ had a mean value of 0.18% internalization compared to 1.4% in untreated MΦ; at a 5 min incubation, U18666A-treated RAW 264.7 MΦ had a mean internalization of 8.13% internalization compared to 17.4% in untreated RAW 264.7 MΦ; at a 10 min incubation U18666A MΦ had a mean internalization of 11.1% compared to 24.5% in untreated MΦ; at a 15 min time incubation U18666A MΦ had a mean internalization of 20. 14% compared to 35.5% in untreated MΦ; at a 30 min time incubation, U18666A-treated RAW 264.7 MΦ had a mean internalisation 33.1% compared to a mean of 49.4% in untreated MΦ; at a 60 min incubation, RAW 264.7 MΦ treated with U18666A had a mean internalisation of 50.8% compared to 74.1 % in untreated RAW 264.7 MΦ.


RAW 264.7 Vehicle
RAW 264.7 +U18666A
2µm
3µm
6µm
10µm

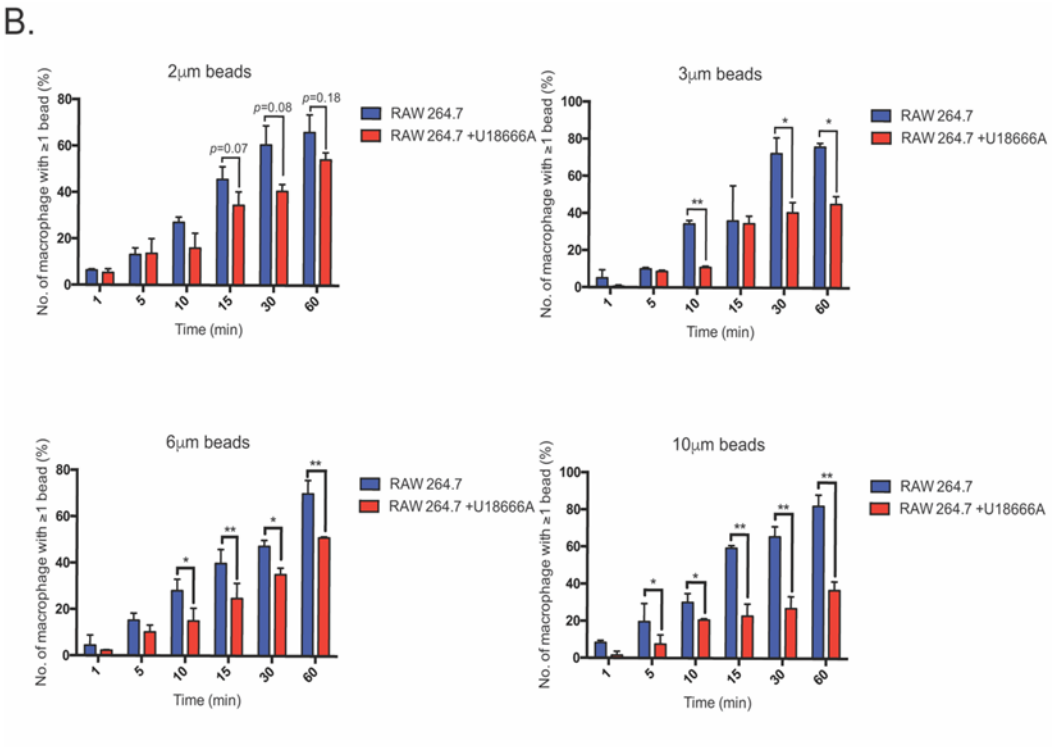


Figure 2.18. U18666A-treated RAW 264.7 MΦ display significantly reduced phagocytosis of different sized non-opsonised polystyrene beads: **(A)** Microscopy study reveals lower efficacy of RAW 264.7 treated with U18666A MΦ to phagocytize unopsonized polystyrene beads. Examples of ingested beads are indicated by white arrows. Magnification=63x **(B)** Histogram representation, in all cases RAW 264.7 untreated MΦ ingested more beads. Mean ± SD. N=6, NS $p>0.05$, *$p<0.05$, **$p<0.01$, ***$p<0.001$. (student's *t*-test evaluated). Data is representative of three independent experiments.

2.3.5 Receptors expression is not altered by treatment with U18666A.

A simple explanation for the phagocytic defect observed for U18666A-treated MΦ might be that the drug significantly reduces the expression of surface receptors required for phagocytosis. We therefore used FACS to determine the relative expression levels of specific receptors on vehicle and U18666A-treated RAW 264.7 MΦ by staining with antibodies.

We were unable to detect statistically significant differences in expression of FcγRIIA, FcγRIIB, FcγRIII between control and U18666A-treated cells (**Fig 2.19**)

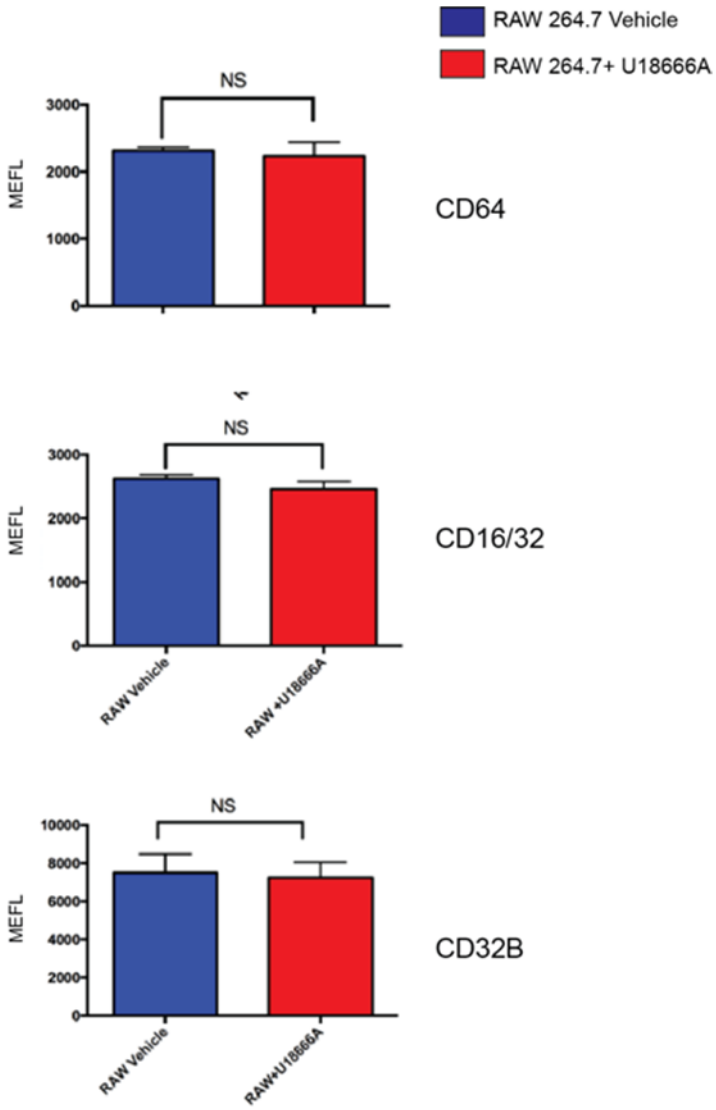


Figure 2.19. RAW 264.7 MΦ treated with U18666A show unaltered expression of specific receptors: MEFLs obtained by FACS for vehicle (blue columns) and U18666A-treated (red columns) RAW 264.7 cells, staining for receptors **(A)** CD64 **(B)** CD16/32 **(C)** CD32B. Fold change in mean fluorescence relative to vehicle RAW 264.7 (control). Mean ± SD N=4. NS. $p>0.05$. (*t*-test with Welch's correction). Data is representative of three independent experiments.

2.4 Discussion.

In this chapter we made *in vitro* investigations of the phagocytic activities of U18666A-treated J774A.1 and RAW 264.7 MΦ cell lines. In summary, our results showed that in comparison to control phagocytes, U18666A-treated MΦ showed significant impairment of their abilities to ingest a number of different particles that are internalised via distinct phagocytic mechanisms.

The murine MΦ cell lines J774.1 and RAW 264.7 MΦ have been used extensively for studies of phagocytosis and their capacity to internalise efficiently a range of particles using distinct phagocytic mechanisms has been well documented (Weinshank et al., 1988; Suzuki, 1991; Aderem and Underhill, 1999; Henry et al., 2004; Luo et al., 2005; Stuart and Ezekowitz, 2005; Fuentes et al., 2014; Lemaire et al., 2014).

We studied the uptake of particles bearing ligands that would target for internalisation by specific phagocytic mechanisms (**Table 1.1**) in the knowledge that the two cell lines express the relevant phagocytic receptors (e.g. for FcγR and CR mediated phagocytosis) as well as other non-opsonic receptors (e.g. scavenger receptors) (Indik et al., 1995; Pearson, 1996; Platt et al., 1999; Ravetch and Bolland, 2001; Rus et al., 2005; Rankin et al., 2006; Tohyama and Yamamura, 2006). For example, RAW 264.7 MΦ display significant FcγR mediated phagocytosis (Weinshank et al., 1988) (Weinshank et al., 1988) and J774A.1 have been exploited for studies of CR mediated uptake (May et al., 2000). We reasoned that by making studies of two independent cell lines we might exclude possible cell specific effects. Indeed, because we observed effects that were consistent between the two murine MΦ cell lines in our initial

investigations, we restricted our subsequent studies of FcγR mediated internalization to the use of RAW 264.7 MΦ.

As expected, we showed that treatment of RAW 264.7 and J774A.1 MΦ with U18666A induced cellular phenotypes indicative of NPC, such as expansion of the acidic compartment and the accumulation of cholesterol in the lysosome. U18666A-induced cholesterol accumulation and an increase in Lysotracker™ staining have been reported previously for RAW 264.7 cells (Lloyd-Evans et al., 2008; Te Vruchte et al., 2015) and J774A.1 MΦ {te Vruchte, 2004 #215}. Although we did not confirm them here, those studies also demonstrated the induction of other NPC phenotypes by U18666A, including storage and mistrafficking of GSLs and loss of lysosomal Ca^{2+} homeostasis. Although at the time of writing we cannot be completely confident of all the cellular targets of U18666A, direct binding of U18666A to NPC1 has been demonstrated recently (Lu, 2015).

We employed two independent methodologies to assess phagocytic activity. Confocal microscopy has the advantage of permitting visual evaluation of individual phagocytes for an extended period of time. A large number of microscopy-based studies of phagocytosis can be found in the published literature (Platt et al., 1996; Magenau et al., 2011; Mosser and Zhang, 2011; Samie et al., 2013). The use of fluorescence, by fluorescent labeling of particles and identification of the limit of the plasma membrane of MΦ by staining with labeled phalloidin enabled us to distinguish with confidence between particles that had been fully internalized and ones that remain bound to the phagocyte surface. However, the accumulation of sufficient data to be able to make statistically valid conclusions was time consuming. Preliminary experiments

were used to establish a suitable time course of co-incubation over which we could compare the phagocytic activities of control and drug-treated of J774A.1 and RAW 264.7 MΦ.

Major weaknesses of the method that requires direct visual inspection by fluorescent microscopy are that it is time consuming in respect of data collection (manual counting) and has the potential for observational bias by the investigator. We therefore also used FACS to quantify phagocytosis. The major advantage of this methodology, in which the fluorescent signal derived from internalised particles is an indicator of the frequency of phagocytes that have ingested particles and their relative phagocytic activities, is the rapid collection of data. However, in comparison to microscopy it has two disadvantages. First, the fluorescence intensity is relative and the absolute number of particles taken up cannot be determined. Second, it cannot discriminate between MΦ that have phagocytosed particles from those where targets remain bound and are extracellular. Despite these deficiencies, FACS has been frequently used to evaluate phagocytic activity (Stewart et al., 1986; Wan et al., 1993; Lehmann et al., 2000; Simons, 2010; Keogh et al., 2011). For these reasons we used both methods in our investigations of phagocytosis.

Because to our knowledge there have been no published studies of the effect of the NPC cellular phenotype upon phagocytosis, it was important that we undertook a broad investigation of phagocytic activities by examination of different uptake mechanisms. As we have discussed in Chapter 1, there is not a universal pathway that is responsible for all ingestion. Rather, the internalization of specific particles is determined by the phagocytic ligands they express and the receptors they engage. We could hypothesize distinct

possibilities in NPC cells; either multiple phagocytic mechanisms may be affected, none might be changed or that perhaps only selected ones are altered.

We used model systems, including IgG and complement opsonized sRBC and synthetic fluorescent beads for our investigations of phagocytosis by drug-induced NPC MΦ. The requirements for and parameters that affect FcγR and CR mediated phagocytosis has been well defined (Suzuki, 1991; Sutterwala et al., 1996; Swanson and Hoppe, 2004; Rus et al., 2005; Tohyama and Yamamura, 2006). We also used systems that are biologically relevant, such as the clearance of aged or oxidized sRBC, but for which the relevant receptors have not been fully defined (Olsson and Oldenborg, 2008). In summary, our studies showed that with one exception, phagocytosis by both opsonin-dependent and opsonin-independent mechanisms were significantly impaired in NPC RAW 264.7 and J774A.1 MΦ in comparison to control phagocytes. Therefore, the most important finding from these investigations was the demonstration that phagocytic activity was impaired, but not absolutely abolished in the pharmacological model of NPC. These data do not reveal how phagocytic mechanisms are affected in NPC cells, but we can draw important inferences from this series of initial investigations. The reduction in activity seen in multiple phagocytic mechanisms would suggest that that impairment is most likely to occur at a point(s) in the process of phagocytosis that is shared by or common to phagocytic mechanisms (which have been outlined in Chapter 1), rather than at the level of specific receptor types. However, the data are also compatible with disruption that might affect more broadly the properties of all receptors (such as changes to the composition of the plasma membrane). This

would be unlikely to be the absolute amount of receptor expression, because FACS analysis did not reveal a significant difference in expression of the receptors we looked at (**Fig 2.19**), but could possibly be due to something such as altered distribution of receptors within the membrane. Studies exploring possible mechanisms that may explain the reduction in phagocytosis by NPC cells will be presented in Chapter 4.

In contrast to the studies of uptake of other particles, we did not measure a significant difference in the ingestion of zymosan particles by control and U18666A-treated MΦ (**Fig 2.14**). As mentioned, zymosan has been used extensively to model the interaction between cells of the innate immune system and fungal pathogens and several receptors have been shown to be involved in its discrimination and ingestion (Underhill, 2003). Perhaps the receptor that can bind zymosan and which has been explored in the greatest detail is Dectin-1 (CLEC7A), a C-type lectin that is found primarily on MΦ, neutrophils and dendritic cells and is expressed by RAW 264.7 and J774A.1 MΦ (Brown, 2002). Currently we are unable to offer an obvious and simple explanation for why, unlike all the other systems we explored, phagocytosis of zymosan was not affected in U18666A-treated MΦ cell lines. Further experimental investigations will be required.

The recognition and uptake of particles by phagocytic cells are influenced not only by biological ligands but also by physical characteristics (Aderem and Underhill, 1999; Champion and Mitragotri, 2006; Champion et al., 2008). Our data showed that the reduction in phagocytosis by U18666A-treated immortalised murine MΦ as compared to controls was independent of particle diameter (<10 μm) and whether the bead was IgG opsonized or not opsonised

(**Fig 2.17 and Fig 2.18**). The lack of an obvious difference in the uptake of beads of 2 μm diameter by control and drug-treated phagocytes was most probably because particles of this size can also be internalized by non-phagocytic mechanisms, such a macropinocytosis (Besterman and Low, 1983). Our investigation into the role of particle size was in part, provoked by a previous report of impaired phagocytosis by MΦ with altered lysosomal Ca^{2+} homeostasis. Samie and colleagues (Samie et al., 2013) identified that MΦ lacking the TRP channel, TRPML1 display impaired phagocytosis of particle uptake, but the deficiency was restricted to phagocytosis of IgG opsonized particles greater than 6 μm in diameter. The factors that differentiate the phagocytosis of small and large particles are not fully understood, but a comparison between uptake in the absence of TRPML1 and that occurring in the absence of NPC may help dissect the different mechanisms and role of lysosomal Ca^{2+}.

Summary.

In summary, we have presented evidence of reduced phagocytosis by MΦ with a pharmacologically induced NPC phenotype. These studies provide the foundation for studies of genetically deficient cells, mechanisms that may underlie the phagocytic defect and the biological significance of the reduction in phagocytosis, which will be described in subsequent chapters.

Chapter 3. Defective Phagocytosis in NPC Primary Macrophages.

3.1 Introduction.

Experiments described in Chapter 2 were performed using the murine MΦ cell lines, RAW 264.7, and J774A.1. In summary, the results demonstrated that following treatment with U18666A (a drug which induces NPC cellular phenotypes) RAW 264.7 and J774A.1 MΦ displayed significantly reduced phagocytosis of a number of different particles. In order to validate the findings, we observed using the drug-induced cellular model of the disease; and to exclude the possibility that our results may result from off-target (i.e. Npc1-independent) effects of U18666A, we chose to investigate the phagocytic capacity of cells with genetic deficiency in Npc1 expression.

Whilst a number of different animal models of NPC disease have been described, including *Drosophila* (Huang et al., 2005; Fluegel et al., 2006), zebrafish (van der Meer et al., 2005; Schwend et al., 2011; Louwette et al., 2013; Sultana et al., 2016) and cat (Lowenthal et al., 1990; Brown et al., 1994; Somers et al., 2003), studies of which have enhanced our understanding of the disorder, mouse models of the disease have been studied to the greatest extent. Mice offer a number of advantages as experimental models, such as short generation time, relative ease of husbandry, defined genome and genetics, and availability of a wide range of specific reagents that can be used for experimental analyses (Leao et al., 2006; Vandamme, 2014).

3.1.1 NPC Mouse Model.

Although at least three other genetically modified mouse strains have been created in which the *Npc1* locus has been disrupted, the most intensively investigated has been the spontaneous mutant strain, BALB/cNctr- *Npc1*^{m1N}/J (previously known as npc*1*^{nih} or Npc1^{N} – and referred to in this thesis as Npc*1*$^{-/-}$). Pentchev and colleagues (Pentchev et al., 1984) were the first to characterize the strain at the genetic level. They identified that the strain encodes a frame-shift mutation in the coding region of Npc1 gene due insertion of a transposon into exon 9 that results in generation of an early termination codon and hence encodes a significantly truncated protein which lacks 11 of the 13 trans-membrane protein domains. Mice homozygous for the mutation (*Npc1*$^{-/-}$ mice) display extensive GSL accumulation, neuronal degeneration and an acute course of disease that recapitulates the pathological features characteristic of the human disorder (Higashi et al., 1993; Suzuki et al., 1995). An overview of disease progression in *Npc1*$^{-/-}$ mice is summarized in Table 3.1. This authentic animal model has been exploited to facilitate multiple investigations of the underlying pathological processes and evaluation of potential therapeutics (Smith et al., 2009).

Age (weeks)	Disease stage	Clinical symptoms and signs	Biochemical and histological changes
6-7	Early symptomatic	Weight loss, ataxia and gait abnormalities, progressive deterioration in motor and neurological function, tremor, lack of responsiveness to external stimuli and infertility	Hepatosplenomegaly and enlargement of lymph nodes, foam cells in liver and spleen, loss of cerebellar Purkinje cells, elevated levels of sphingomyelin and free cholesterol in the liver and spleen, significant reduction in the activity of sphingomyelinase in liver (to 30%), spleen (to 50%) and brain (to 70-80%).
8-10	Late symptomatic	Hepatosplenomegaly, progressive worsening of all neurological problems, inability to walk, eat or drink.	
12-14	End stage	Death	

Table 3.1 Characteristics of Disease Progression in the *Npc1$^{-/-}$ Mouse.*

We therefore took the experimental approach of isolating populations of MΦ from *Npc1*$^{+/+}$ (WT) and *Npc1*$^{-/-}$ (diseased) mice and compared their capacity to ingest different particles using *in vitro* phagocytosis assays described previously in Chapter 2. We hypothesized that we would observe phagocytic defects in genetically deficient phagocytes comparable to those we found using U18666A-induced NPC cells.

Major objectives of this chapter.

- Determine if the phagocytic deficiency previously seen with U18666A-treated MΦ is replicated by *ex-vivo Npc1*$^{-/-}$ murine MΦ.
- Investigate whether any reduction in phagocytic activity in *Npc1*$^{-/-}$ MΦ is restricted to the uptake of specific particles or is more general.
- Examine whether primary MΦ isolated from other murine or human models of specific LSDs also display evidence of impaired ingestion.

3.2 Materials and Methods.

3.2.1 Reagents.

Reagents identical to those listed in Section 2.2.1 were used for *in vitro* phagocytosis assays. Fluorescently-conjugated antibodies specific for CD16/32-PE, CD32b-PE, F4/80-PE were purchased from E-bioscience (Altrincham). Opsonizing antibodies (IgG and IgM) are described previously in Section 2.2.1. 3 μm polystyrene beads were purchased from Polysciences.

3.2.2 Mice.

The spontaneous mutant mouse model of NPC on the BALB/c genetic background, BALB/cNctr-*Npc1*^{m1N}/J, was obtained from The Jackson Laboratory (Maine, US(A) and maintained by mating of heterozygous animals. (Pentchev et al., 1984) All mice were bred and housed under specific pathogen-free conditions in the animal facilities at the University of Oxford (Oxford), with food and water available *ad libitum* and a 12-h light–dark cycle (light on from 6.00 a.m. until 6.00 p.m.) with a temperature range of 22-24°C and relative

humidity of 50-60%. All animal studies were conducted using protocols approved and licensed by the UK Home Office under Scientific Procedures, Laboratory Animals Act, 1986.

3.2.3 Genotyping of Mice.

3.2.3.1 *Npc1*$^{-/-}$ mice.

Genotypes of individual mice were determined by polymerase chain reaction (PCR) analysis of ear DNA, as described previously (Loftus et al., 1997; te Vruchte et al., 2004). Ear biopsies were collected from 10-day-old mice for DNA extraction. The tissue pieces were digested in alkaline lysis buffer (75 μl of 25 mM NaOH /0.2 mM EDTA) for 15 min at 95°C and neutralized with an equal volume of 40 mM Tris HCl (pH 5.5). PCR reactions to identify specific alleles of the *Npc1* locus composed Dream Taq Green PCR Master mix (Fisher), primers 8F-GGTGCTGGACAGCCAAGTA and INTR3- GATGGTCTGTTCTCCCATG (Invitrogen) and 2 μl of ear lysate in a total volume of 50μl. Cycling conditions were: initial denaturing at 94°C for 3 min; 35 cycles of 94°C for 30 seconds; annealing at 58°C for 30 seconds and extension at 72°C for 30 seconds, with a single final extension at 72°C for 7 min. Reaction products were separated on 1.5% agarose gel and visualized with ethidium bromide. Product sizes of 1048 bp and 1209 bp corresponded to WT and mutant alleles

3.2.3.2 Sandhoff disease (*hexb*$^{-/-}$) mice.

Genotypes of individual mice were determined by PCR analysis of ear DNA, as described previously (Loftus et al., 1997; te Vruchte et al., 2004; Kyrkanides et al., 2012). Ear biopsies were collected from 10-day-old mice for DNA extraction. The tissue pieces were digested in alkaline lysis buffer (75 μl of 25 mM NaOH

/0.2 mM EDTA) for 15 minutes at 95°C and neutralized with an equal volume of 40 mM Tris HCl (pH 5.5). PCR reactions to identify WT and mutant alleles of the *hexB* locus composed Dream Taq Green PCR Master mix (Fisher), primers 5′-AGTCCTGCCAGAATTTGATACC-3′ and 5′-ATTCCAAGTTCGACCATCC-3′ (Invitrogen) and 2 μl of ear lysate in a total volume of 50 μl. Cycling conditions were: initial denaturing at 94°C for 3 min; 35 cycles of 94°C for 30 seconds; annealing at 58°C for 30 seconds and extension at 72°C for 30 seconds, with a single final extension at 72°C for 7 min. Reaction products were separated on 1.5% agarose gel and visualized with ethidium bromide.

3.2.4 Isolation of peritoneal MΦ

3.2.4.1 Isolation of resident peritoneal MΦ (RPMΦ).

Seven-week-old mice were sacrificed, and RPMΦ were recovered by lavage of the peritoneum with PBS. Collected cells were centrifuged, counted and re-suspended in R10 at a density of $2.5x10^5$ cells/mL and plated onto sterile glass coverslips placed in the bottom of 24 well tissue culture plates, and incubated at 37ºC, 5% CO_2.

3.2.4.2 Isolation of elicited inflammatory peritoneal MΦ (EPMΦ).

Seven and eight-week old mice were injected (intraperitoneal) (Adam et al.) with 1mL of sterile thioglycollate broth (Beckton Dickinson) (3% w/v autoclaved stock prepared in water and stored for >4 weeks in the dark at room temperature before use). Four days' post-injection, mice were sacrificed and EPMΦ were recovered by peritoneal lavage with PBS. Cells were centrifuged

at 1200 RPM for 10 min, counted and re-suspended in R10 at a density of 2.5 x 10^5 cells/mL and plated onto sterile glass coverslips placed in the bottom of 24 well tissue culture plates and incubated at 37^{o}C, 5% CO_2. MΦ were collected and prepared for use in phagocytosis assays.

3.2.5 Isolation of thymocytes and induction of apoptosis.

Thymi from 2-4 week old Balb/c mice were mechanically dissociated to a single cell suspension, cultured in RPMI medium 1640 with 10% FCS containing 1 μM dexamethasone (Sigma) for 6h, washed with PBS and labeled with Celltracker™ green.

3.2.6 *In vitro* phagocytosis assay.

In vitro phagocytosis assays were performed as previously described in Section 2.2.11. Particles, including fluorescently labeled IgG opsonized sRBC (Section 2.2.6), complement opsonised sRBC (Section 2.2.6), Ox-sRBC (Section 2.2.7), *E. coli* Bio particles (Section 2.2.8), and zymosan Bio particles (Section 2.2.8) are described previously.

3.2.6.1 LysoTracker™ staining.

Lysotracker™ staining of RPMΦ and EPMΦ was performed as described previously in section 2.2.4.

3.2.6.1 Fluorescent microscopy.

As described previously in section 2.2.12

3.2.6.2 FACS staining and analysis.

As described previously in section 2.2.13.

3.2.7 Isolation of blood monocytes from Gaucher Disease patients and MΦ differentiation.

As part of an ongoing MRC funded Gaucherite Stratified Medicine grant, human blood was collected from normal and Gaucher Disease patients for analysis. In this instance, blood monocytes were isolated and kept in a biobank -80^{o}C freezer prior to usage. Blood monocytes were treated with macrophage colony stimulation factor (M-CSF) at a concentration of 10 ng/mL for 7 days to differentiate monocytes into blood monocyte-derived MΦ (performed by Dr. Kerri-Lee Wallom).

3.2.8 Preparation of coverslips.

Performed as described previously in Section 2.2.10.

3.2.9 Enzyme-linked immunoassay (ELIS(A) supernatant cytokines.

EPMΦ were collected and cultured as described. Phagocytosis assays involving ingestion of 3 μm polystyrene beads were performed (section 2.2.9) and supernatants were collected. Cytokine content of supernatants were measured using specific ELISA kits (ebioscience) according to manufacturer's instructions.

3.2.10 Measurement of reactive oxygen species (ROS) production.

A DCFDA Cellular Reactive Oxygen Species Detection Assay Kit (Abcam) was used to measure ROS production. EPMΦ were incubated with IgG opsonised sRBC or *E. coli* Bio particles for 60 min. MΦ were stained with DCFDA for 30

min, 37^{o}C, 5% CO2 and fluorescence measured by FACS. Change in ROS was determined as a percentage of control after subtraction of unstained background control.

3.2.11 Statistics.

Data are presented as the mean ± SD. Statistical comparisons were made using Student's *t*-test (Graphpad Prism) with Welch's correction. A *p* value < 0.05 was considered statistically significant.

3.3 Results.

3.3.1 Lysotracker^{TM} Staining and phenotyping of RPMΦ and EPMΦ.

RPMΦ were used initially for studies. To confirm an NPC phenotype in the RPMΦ isolated from *Npc1*$^{-/-}$ mice, we performed Lysotracker^{TM} staining to confirm expansion of the acidic compartment. In RPMΦ, Lysotracker^{TM} staining was increased 3-fold in *Npc1*$^{-/-}$ (MEFL=18468) relative to *Npc1*$^{+/+}$ RPMΦ (MEFL=1989) **(Fig.3.1).**

EPMΦ are a population of inflammatory phagocytes that have been recently recruited from the bone marrow and have entered the peritoneal cavity where they differentiate into cells with MΦ phenotypes (Gordon et al., 2014). In order to ensure that they also display the cellular characteristics of NPC we performed Lysostracker^{TM} staining to confirm expansion of the acidic compartment.

LysoTracker^{TM} staining was increased 12-fold in *Npc1*$^{-/-}$ (MEFL= 26184±689.1) relative to *Npc1*$^{+/+}$ EPMΦ (MEFL=1947±74.3) (**Fig.3.2**), indicative of an NPC phenotype.

To confirm that the peritoneal wash collected 4 days post injection of thioglycollate broth contained a significant frequency of EPMΦ we stained with F4/80 antibody, which is specific for the MΦ-restricted antigen, EMR1 (Hamann et al., 2007) and analysed for expression by FACS. Analysis confirmed that greater than 60% of cells from both *Npc1*$^{+/+}$ and *Npc1*$^{-/-}$ mice were F4/80 positive (*Npc1*$^{+/+}$, 71.4%; *Npc1*$^{-/-}$, 67.3%) (**Fig 3.3**). When subsequently plated onto glass coverslips and non-adherent cells were removed by washing, the frequency of F4/80^{+} cells increased to >90% (not shown).

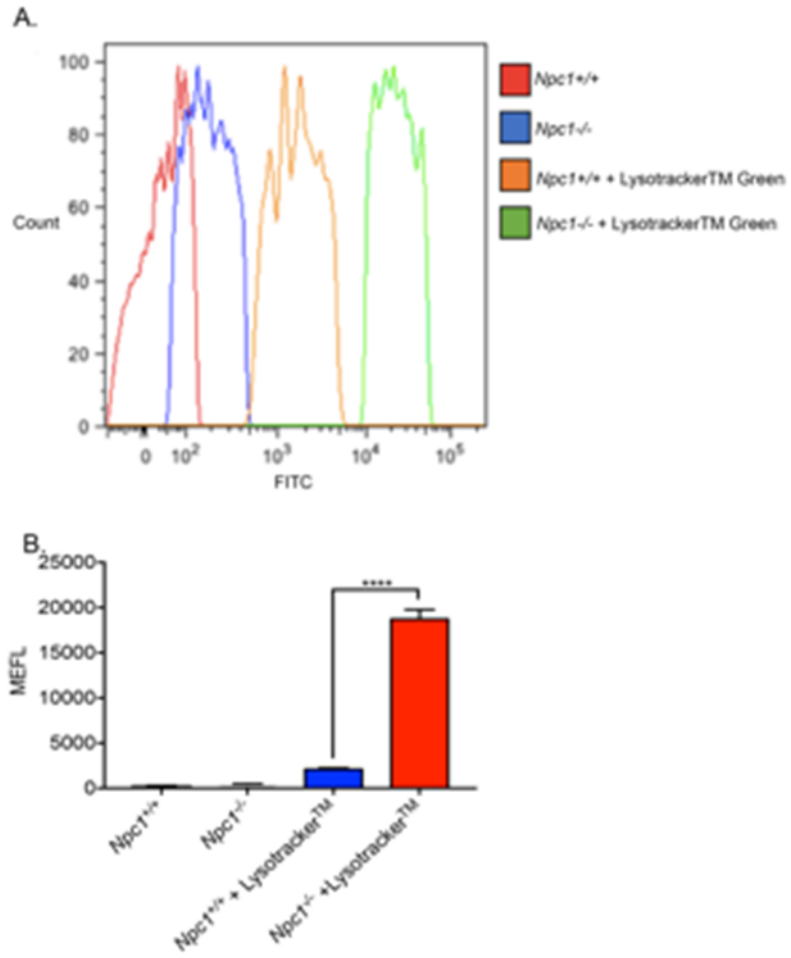


Figure 3.1. RPMΦ show NPC phenotype as determined by increased Lysotracker™ fluorescence measured by FACS: (A) FACS profiles of *Npc1*$^{+/+}$ and *Npc1*$^{-/-}$ RPMΦ unstained or stained with LysoTracker™. **(B)** Histogram of MEFL of LysoTracker™ green stained *Npc1*$^{+/+}$ (blue column) and *Npc1*$^{-/-}$ (red column) RPMΦ. Mean ± SD. N=4 ***p*<0.01 Data representative of greater than 10 independent experiments.

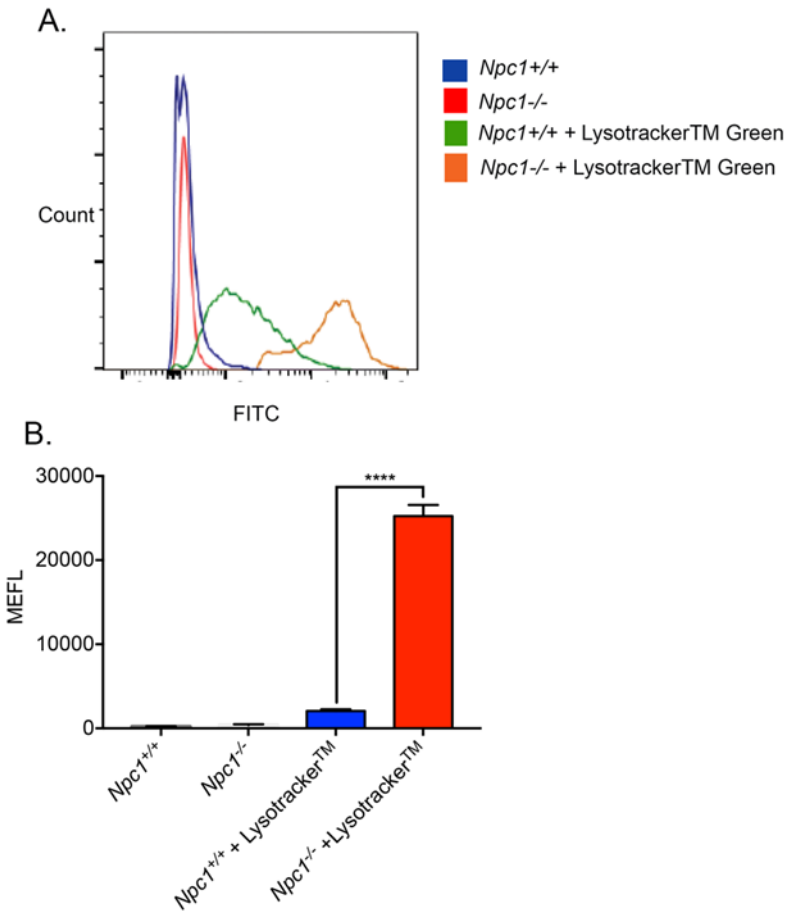


Figure 3.2. EPMΦ show NPC phenotype as determined by increased Lysotracker™ fluorescence measured by FACS: (A) FACS profiles of *Npc1*$^{+/+}$ and *Npc1*$^{-/-}$ EPMΦ unstained or stained with LysoTracker™. **(B)** Histogram of MEFL of LysoTracker™ green stained *Npc1*$^{+/+}$ (blue column) and *Npc1*$^{-/-}$ (red column) EPMΦ. Mean ± SD. N = 4 $^{**}p<0.01$ Data representative of greater than 10 independent experiments.

3.3.2. *Npc1*$^{-/-}$ RPMΦ display reduced phagocytosis of IgG-sRBC in comparison to *Npc1*$^{+/+}$ RPMΦ.

RPMΦ from *Npc1*$^{-/-}$ and *Npc1*$^{+/+}$ mice on coverslips were overlaid with fluorescently-labelled IgG-sRBC and incubated at 37^{o}C for 30, 60, 90, or 120 min. After lysis of non-internalised sRBC and extensive washing with PBS, RPMΦ were fixed, coverslips mounted and subsequently examined by fluorescent microscopy. The frequency of RPMΦ that had internalized >1 IgG-sRBC per MΦ was determined for a minimum of 200 cells across fields selected randomly.

Inspection of representative fields revealed that at 30 min 38.70% of *Npc1* $^{-/-}$ RPMΦ contained ingested IgG-sRBC; at 60 min, 47.16%; at 90 min, 61.57% and at 120 min, 69.81% (**Fig.3.3B**, red columns), whereas for *Npc1*$^{+/+}$ cells, at 30 min 62.61% contained ingested IgG-sRBC; at 60 min, 73.44%; at 90 min, at 80.91% and at 120 min, 86.73% (**Fig.3.3B**, blue columns). The reduction in uptake by *Npc1*$^{-/-}$ in comparison to that of *Npc1*$^{+/+}$ cells was statistically significant at all time points (30 min p=0.031; 60 min p=0.0023; 90 min p=0.0073; 120 min p=0.015; **Fig 3.3B**).

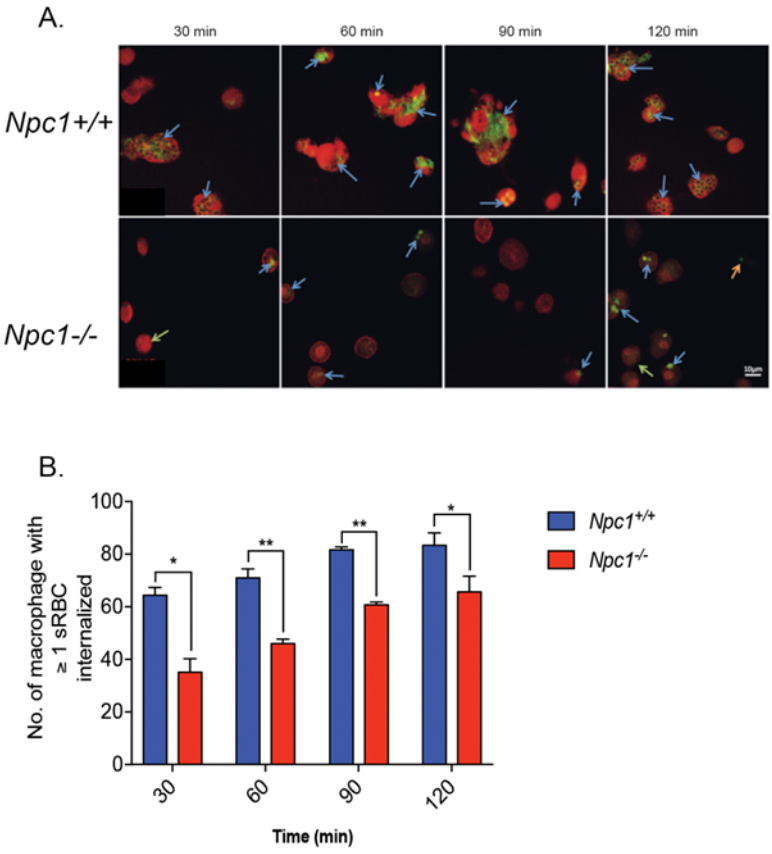


Figure 3.3. RPMΦ from *Npc1*$^{-/-}$ mice display impaired phagocytosis of IgG –sRBC: (A) Representative confocal microscopy images of WT RPMΦ (upper panels) and *Npc1*$^{-/-}$ RPMΦ (lower panels) stained with phalloidin (red) that have been co-incubated with IgG-sRBC (green) for the indicated times. Examples of ingested (blue arrows), bound, but non-internalised IgG-sRBC (green arrows) and IgG-sRBC that are neither bound or internalized (orange arrows) are indicated**.** **(B**) *Npc1*$^{-/-}$ show significantly decreased phagocytosis. Data presented as mean ± SD for 3 replicates per condition. N=4, **p*<0.05, ***p*<0.01 versus control (via student's *t*-test with Welch's correction).

3.3.3. *Npc1*$^{-/-}$ EPMΦ display reduced phagocytosis of IgG-sRBC; Analysis by microscopy and FACS

We performed *in vitro* phagocytosis assays as described previously to investigate the phagocytic activities of *Npc1*$^{+/+}$ and *Npc1*$^{-/-}$ EPMΦ.

We confirmed significantly reduced phagocytosis of IgG-sRBC by *Npc1*$^{-/-}$ EPMΦ in comparison to *Npc1*$^{+/+}$ cells. For *Npc1*$^{-/-}$ cells, 22.41% had ingested IgG-sRBC after 10 min of co-incubation; 28.71% at 20 min; 36.55% at 30 min; and 51.67% at 40 minutes (**Fig.3.4**; red columns); in comparison, 52.76%of *Npc1*$^{+/+}$ cells had internalised IgG-sRBC within 10 min; 77.66% within 20 min; 79.43% by 30 min, and 82.79% by 40 min (**Fig. 3.4**; blue columns). The difference in phagocytic uptake between *Npc1*$^{+/+}$ and *Npc1*$^{-/-}$ EPMΦ was statistically significant at all time points (10 min p=0.0041; 20 min p=0.0008; 30 min p=0.0074; 40 min p=0.011; **Fig 3.4**).

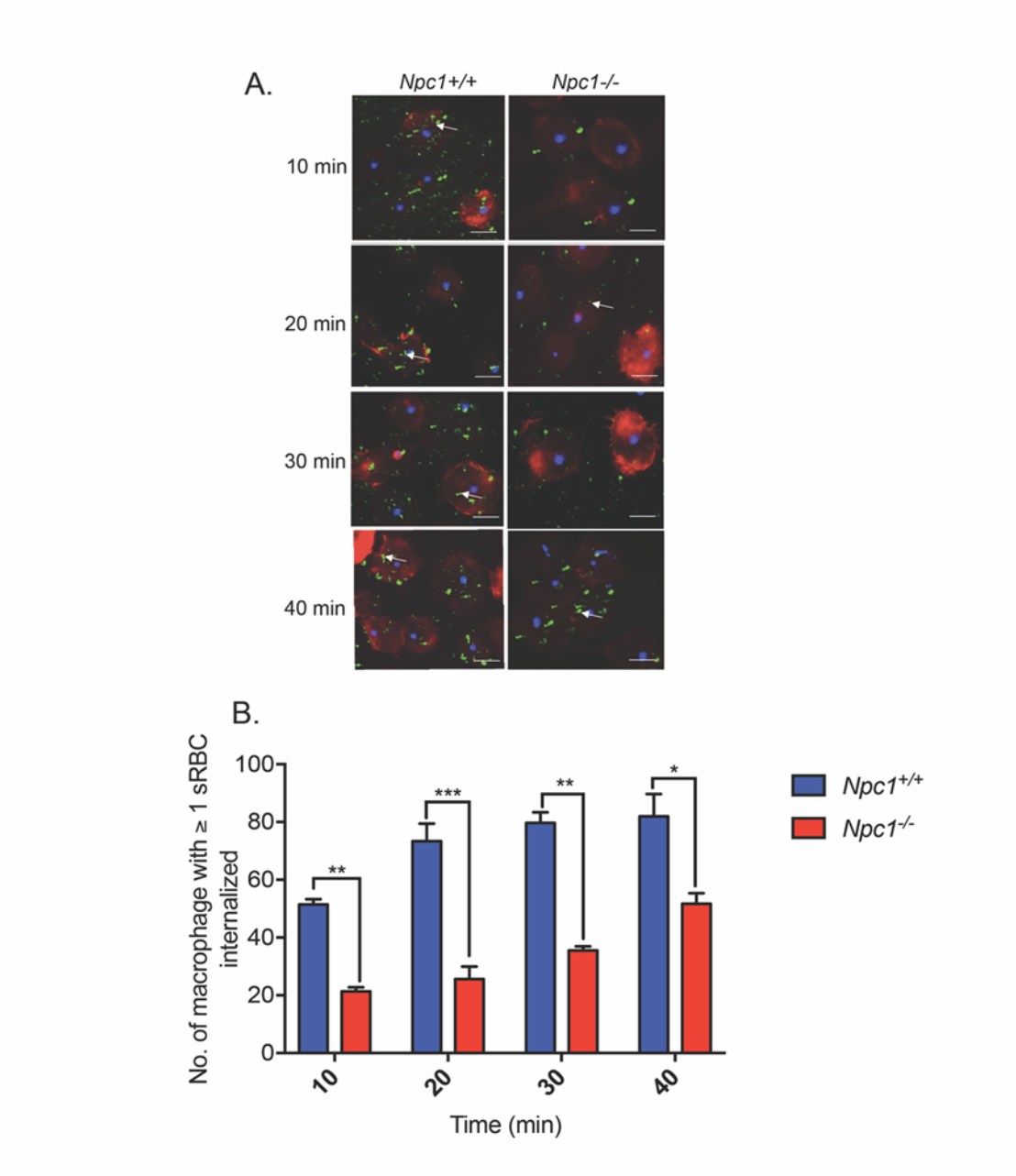


Figure 3.4. EPMΦ display defective phagocytosis of sRBC by FcyR mediated pathway: (A) Representative confocal microscopy images of *Npc1*$^{+/+}$ (left panel) and *Npc1*$^{-/-}$ (right panel) stained with Phallodin (red) that have been co-incubated with IgG-sRBC (green) for the indicated times. Examples of internalised sRBC within *Npc1*$^{+/+}$ and *Npc1*$^{-/-}$ EPMΦ are indicated by white arrows. Scale bar = 5µm. (**B)** *Npc1*$^{-/-}$ show significantly decreased phagocytosis at 4 of 5 tested time points. Data presented as mean ±SD for 3 replicates per condition. N=4, *p<0.05, **p<0.01, ***p<0.001, versus control (via student's t-test with Welch's correction).

As for our investigations employing U1888A-treated MΦ we used a second methodology (FACS) to compare the phagocytic activities of *Npc1*$^{+/+}$ and *Npc1*$^{-/-}$ EPMΦ. Representative FACS profiles of *Npc1*$^{+/+}$ and *Npc1*$^{-/-}$ EPMΦ that had been co-incubated with Celltracker^{TM} green labeled IgG-sRBC are shown in **Fig. 3.5**. *Npc1*$^{+/+}$ EPMΦ displayed approximately 2-fold greater fluorescent intensity (mean MEFL=17431±211) in comparison to *Npc1*$^{-/-}$ EPMΦ (mean MEFL=8943±106), indicative of greater ingestion of labeled IgG-sRBC. These data are presented in **Fig.3.5.**

FACS analysis also confirmed a significantly lower frequency of fluorescent *Npc1*$^{-/-}$ EPMΦ (32.3%) in comparison to that of fluorescent *Npc1*$^{+/+}$ EPMΦ (71.4%).

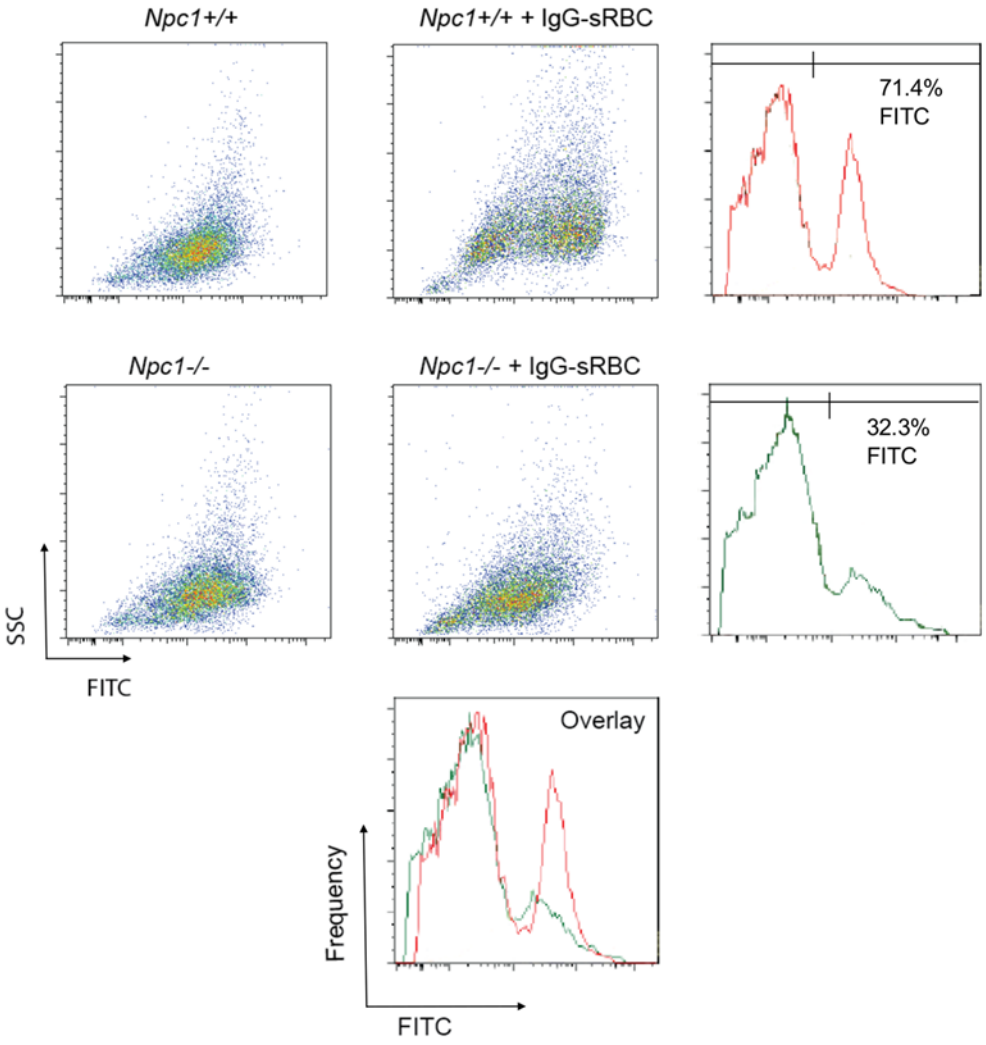


Figure 3.5. *Npc1*$^{-/-}$ EPMΦ display decreased frequency of fluorescence as quantified by FACS MOI 20:1: FACS profiles of EPMΦ from *Npc1*$^{+/+}$ and *Npc1*$^{-/-}$ mice co-incubated with Cell Tracker™ green IgG-sRBC. 71.4% of *Npc1*$^{+/+}$ EPMΦ are gated as positive in comparison to 32.3% of *Npc1*$^{-/-}$ EPMΦ. Representative of three independent experiments.

3.3.3.1 Phagocytic efficiency is impaired in *Npc1*$^{-/-}$ EPMΦ.

In order to quantify phagocytic activity in our fluorescent microscopy-based phagocytosis assay, we determined the frequency of MΦ that had engulfed > 1 particle (3 μm polystyrene bead, opsonised with IgG) (**Fig 3.6**). However, this methodology may not fully reflect phagocytic activity because it fails to take into account the actual number of particles each MΦ has ingested as well as the frequency of MΦ that have taken up particles (i.e.phagocytic efficiency). We therefore incubated *Npc1*$^{+/+}$ and *Npc1*$^{-/-}$ EPMΦ with fluorescently-labeled IgG-opsonised sRBC as previously and determined the frequency of MΦ that had ingested 1, 2, 3, 4 or more sRBCs. Representative fields and quantification are shown in **Fig 3.6**. The data confirm that although *Npc1*$^{-/-}$ MΦ retain the capacity to internalise particles they are less efficient, and take up significantly fewer particles per MΦ in comparison to *Npc1*$^{+/+}$ EPMΦ.

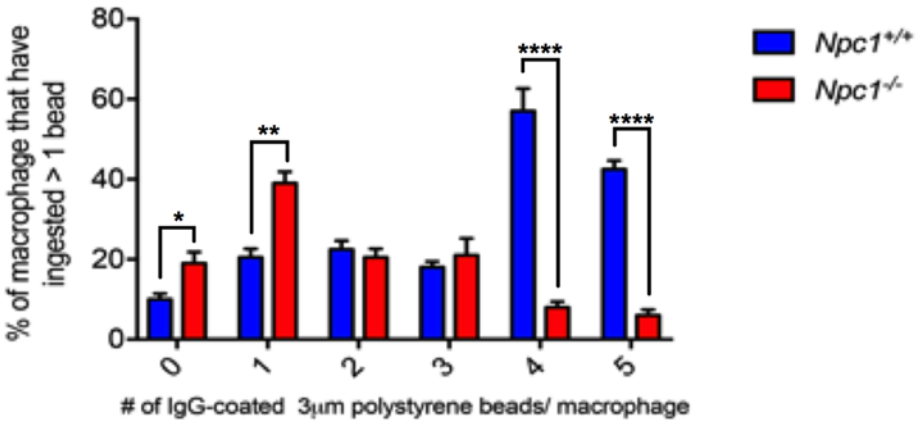


Figure 3.6. Phagocytic efficiency is impaired in NPC: *Npc1*$^{-/-}$ and *Npc1*$^{+/+}$ EPMΦ were overlaid with IgG opsoised 3μm polystyrene beads. Phagocytosis was assessed by confocal microsopy. Counts were made as the number of EPMΦ that had ingested 0,1,2,3,4 and 5+ beads. At least 200 MΦ were analyzed per group. Histogram representation of results. Percentage of internalization was calculated for *Npc1*$^{-/-}$ and *Npc1*$^{+/+}$. The mean (bars) represent quantification of interlization. *Npc1*$^{+/+}$ MΦ were more efficient (blue bars) meaning they ingested more beads per MΦ than *Npc1*$^{-/-}$, N=6.*p<0.05, **p<0.01, ****p<0.0001

3.3.3.2 *Npc1*$^{-/-}$ EPMΦ display reduced phagocytosis of sRBC opsonised with complement; Analysis by microscopy and FACS

We prepared complement-opsonised labelled sRBC in order to target their ingestion via CR and investigated for the possibility of reduced uptake by this pathway in *Npc1*$^{-/-}$ cells. EPMΦ were overlaid with opsonised sRBC at a MOI of 1:20; EPMΦ: sRBC and incubated at 37^{o}C. Within 10 min of co-incubation a

mean of 32.87% of *Npc1*$^{-/-}$ EPMΦ displayed evidence of internalisation (>1 CR-sRBC per MΦ) as compared to a mean of 62.31% for *Npc1*$^{+/+}$ (**Fig. 3.7**); at 20 min 38.51% *Npc1*$^{-/-}$ had internalized sRBC as compared to 77.19% of *Npc1*$^{+/+}$ EPMΦ; by 30 min, uptake was seen for 41.2% of *Npc1*$^{-/-}$ cells and 86.4% for *Npc1*$^{+/+}$ EPMΦ and lastly, at 40 min co-incubation, ingestion was obvious in 56.41% of *Npc1*$^{-/-}$ EPMΦ was approximately half (mean 56.41%) that of *Npc1*$^{+/+}$ EPMΦ (mean 90.8%). The reduction in relative phagocytic activity of *Npc1*$^{-/-}$ EPMΦ was statistically significant at all four time points examined (10 min p=0.00041; 20 min p=0.0104; 30 min p=0.00037; 40 min p=0.00043; **Fig 3.7**). The highest frequency of phagocytosis by *Npc1*$^{-/-}$ EPMΦ was significantly lower than that of *Npc1*$^{+/+}$ EPMΦ and within the time course used did not reach the maximal level of that of *Npc1*$^{+/+}$ cells.

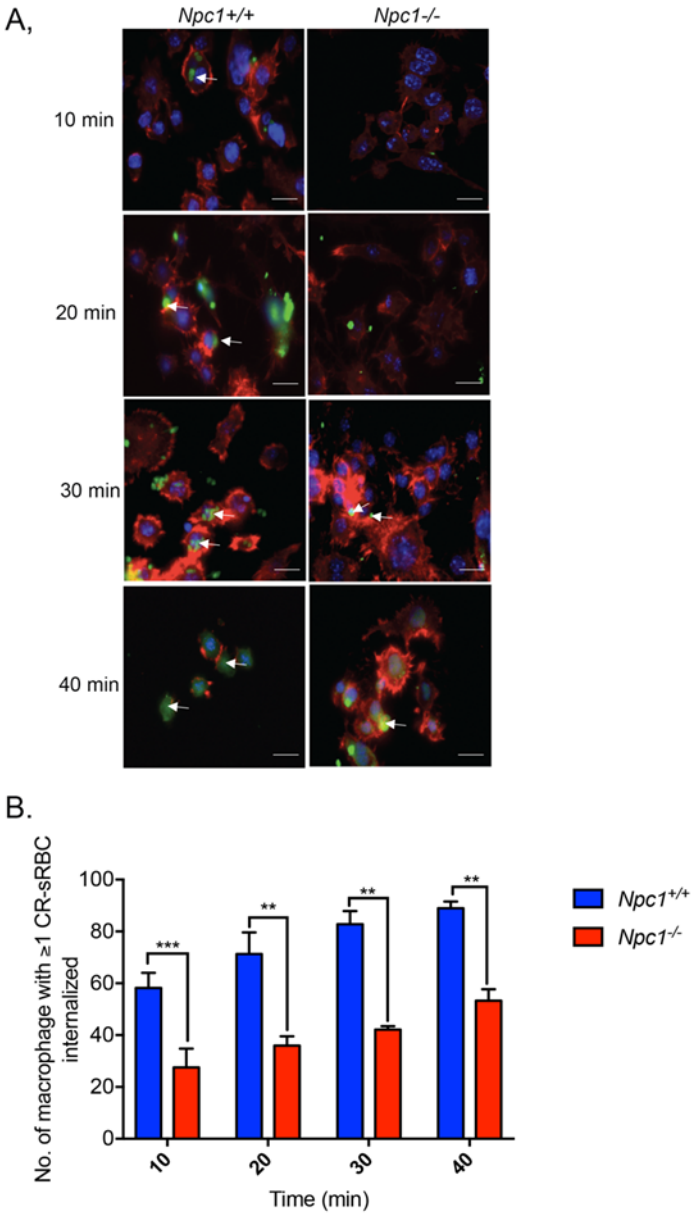


Figure 3.7. *Npc1*$^{-/-}$ EPMΦ display defective phagocytosis of complement-sRBC.

(A) Representative confocal microscopy images of *Npc1*$^{+/+}$ (left panel) and *Npc1*$^{-/-}$ (right panel) stained with phalloidin (red) that have been co-incubated with complement-sRBC (green) for the indicated times. Examples of internalised sRBC within *Npc1*$^{+/+}$ and *Npc1*$^{-/-}$ EPMΦ are indicated by white arrows. Blue=DAPI. Scale bar = 5µm. (**B)** *Npc1*$^{-/-}$ EPMΦ (red columns) show significantly decreased phagocytosis at all tested time points as compared to *Npc1*$^{+/+}$ EPMΦ (blue columns). Data presented as mean ± SD. N=4, **p*<0.05, ***p*<0.01, ****p*<0.001, *****p*< 0.0001 versus control (via student's *t*-test with Welch's correction).

We also used the FACS based phagocytosis assay to determine the phagocytic activity of *Npc1*$^{+/+}$ and *Npc1*$^{-/-}$ EPMΦ for sRBC opsonised with complement. Representative FACS profiles of *Npc1*$^{+/+}$ and *Npc1*$^{-/-}$ EPMΦ co-incubated with Celltracker^{TM} green labeled CR-sRBC are shown in **Fig.3.8**. *Npc1*$^{+/+}$ EPMΦ showed approximately 4-fold greater fluorescence (MEFL=6461±62.9) as compared to *Npc1*$^{-/-}$ EPMΦ (MEFL=1304±17.5), indicative of a statistically greater ingestion (**Fig.3.8).**

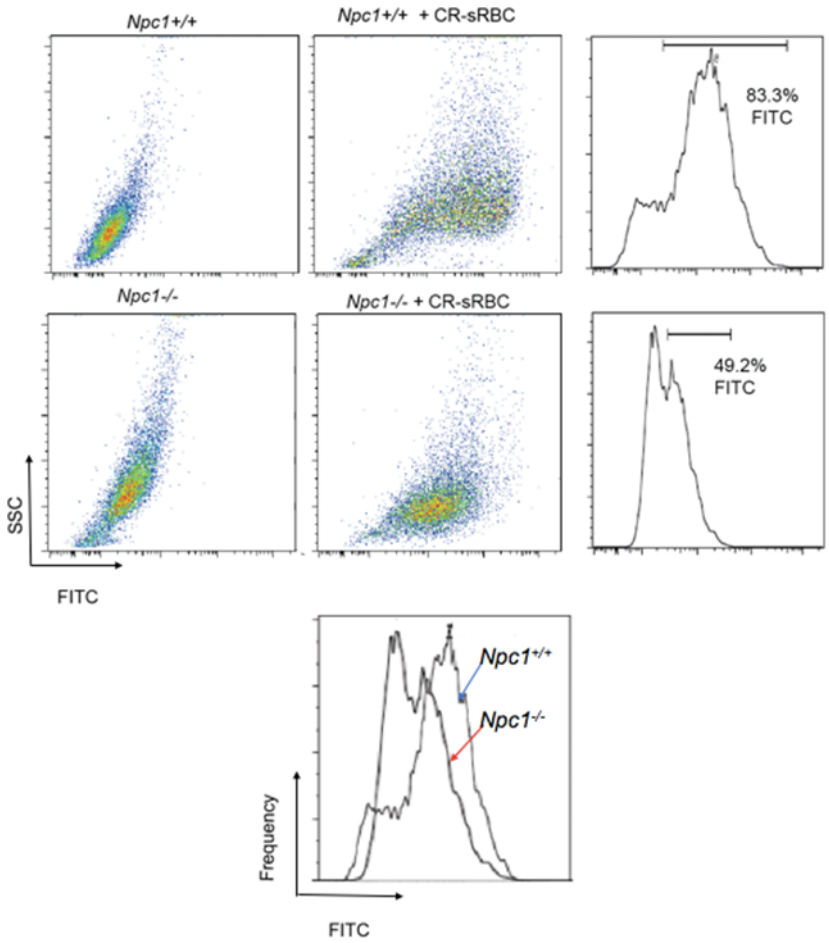


Figure 3.8. *Npc1*$^{-/-}$ EPMΦ display decreased frequency of fluorescence as quantified by FACS MOI 20:1: FACS profiles of EPMΦ from *Npc1*$^{+/+}$ and *Npc1*$^{-/-}$ mice co-incubated with Cell Tracker™ green complement opsonised sRBC. 83.3% of *Npc1*$^{+/+}$ EPMΦ are gated as positive in comparison to 49.2% of *Npc1*$^{-/-}$ EPMΦ. representative of three independent experiments.

3.3.3.3 *Npc1*$^{-/-}$ EPMΦ display reduced phagocytosis of Ox-sRBC; Analysis by microscopy and FACS

sRBCs were oxidised with copper *in vitro* (Olsson and Oldenborg, 2008) , labelled with Celltracker^{TM} green, and overlaid onto *Npc1*$^{+/+}$ and *Npc1*$^{-/-}$ EPMΦ at EPMΦ**:** Ox-sRBC MOI of 1:20 and co-incubated. At 10 min of co-incubation 10.32% of *Npc1*$^{-/-}$ EPMΦ displayed evidence of ingestion (>1 Ox-sRBC ingested per MΦ) as compared to 29.41% of 31.44% of *Npc1*$^{+/+}$ EPMΦ; at 20 min, 24.14% of *Npc1*$^{-/-}$ as compared to 53.64% of *Npc1*$^{+/+}$EPMΦ had internalised sRBC; at 30 min, the frequencies were 41.62% and 77.43% respectively and lastly at 40 min, uptake was detectable for 63.21% of *Npc1*$^{-/-}$ and 89.11% for *Npc1*$^{+/+}$ EPMΦ. EPMΦ pretreated with cytochalasin D showed minimal uptake of Ox-sRBC (2.15% of *Npc1*$^{-/-}$ and 3.41% of *Npc1*$^{+/+}$cells, images not shown) confirming that phagocytosis was the mechanism by which Ox-sRBC were ingested (**Fig 3.9**). The phagocytic ingestion by EPMΦ isolated from symptomatic *Npc1*$^{-/-}$ mice of Ox-sRBC was significantly lower than that of *Npc1*$^{+/+}$cells at all time points (10 min p=0.0041; 20 min p=0.0032; 30 min p=0.043; 40 min p= 0.024; **Fig 3.9**).

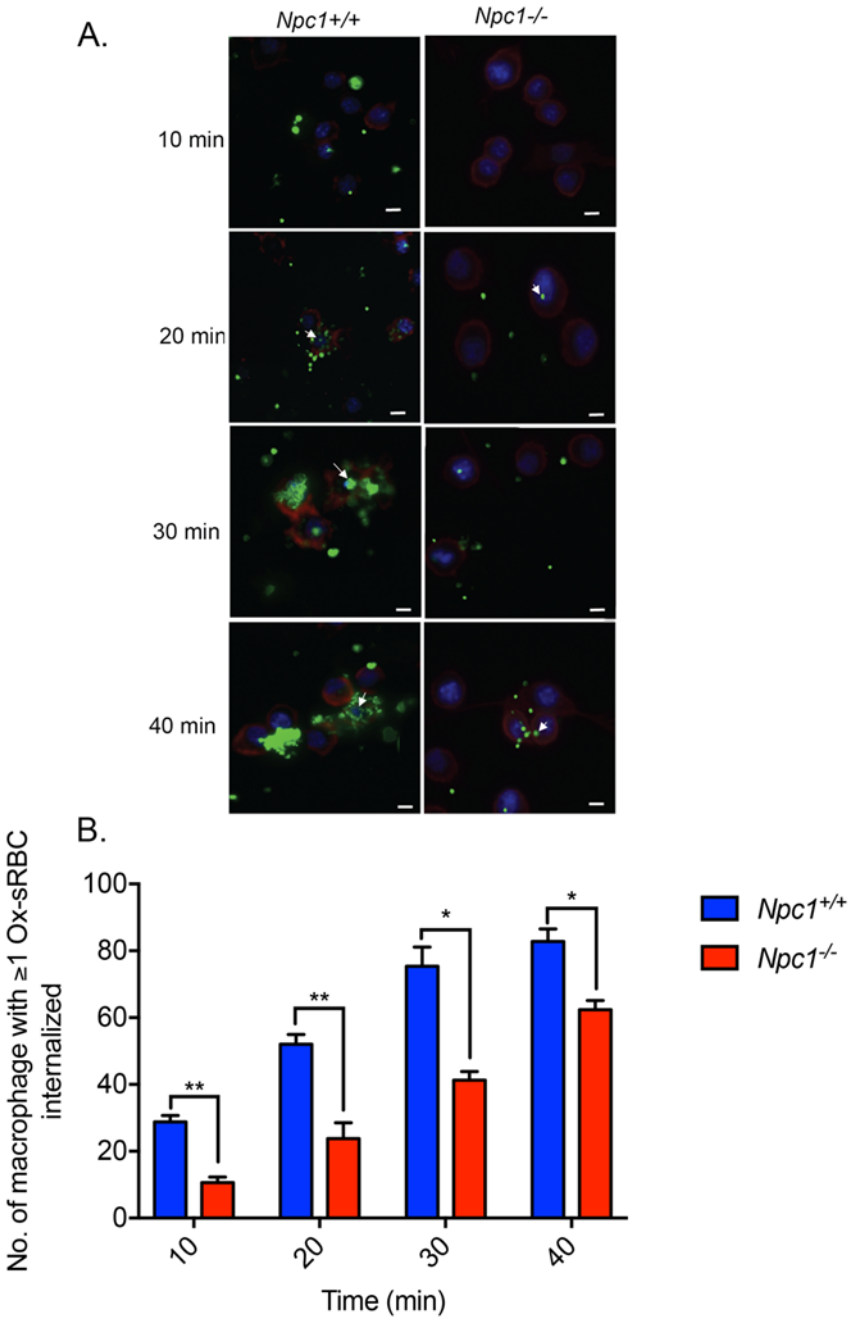


Figure 3.9. *Npc1*$^{-/-}$ EPMΦ display defective phagocytosis of Ox-sRBC:(A) Representative confocal microscopy images of *Npc1*$^{+/+}$ (left panels) and *Npc1*$^{-/-}$ (right panels) stained with phalloidin (red) that have been co-incubated with Ox-sRBC (green) for the indicated times. Examples of internalised sRBC are indicated by white arrows. Blue = DAPI. Scale bar = 5 µm. (**B)** *Npc1*$^{-/-}$ EPMΦ show significantly decreased phagocytosis as compared to *Npc1*$^{+/+}$ EPMΦ (blue columns). Data presented as mean ± SD. N=4 *p<0.05, **p<0.011 versus control (via student's t-test with Welch's correction).

We also analyzed phagocytosis of CMFDA labelled Ox-sRBC by *Npc1*$^{+/+}$ and *Npc1*$^{-/-}$ EPMΦ using FACS. Examples of FACS profiles for *Npc1*$^{+/+}$ and *Npc1*$^{-/-}$ EPMΦ co-incubated with fluorescent Ox-sRBC are shown in **Fig.3.10**. *Npc1*$^{+/+}$ EPMΦ displayed approximately 3-fold higher fluorescence (mean MEFL=10691±318.1) in comparison to *Npc1*$^{-/-}$ EPMΦ (mean MEFL=3016), indicative of significantly greater ingestion of Ox-sRBC (**Fig. 3.10)**.

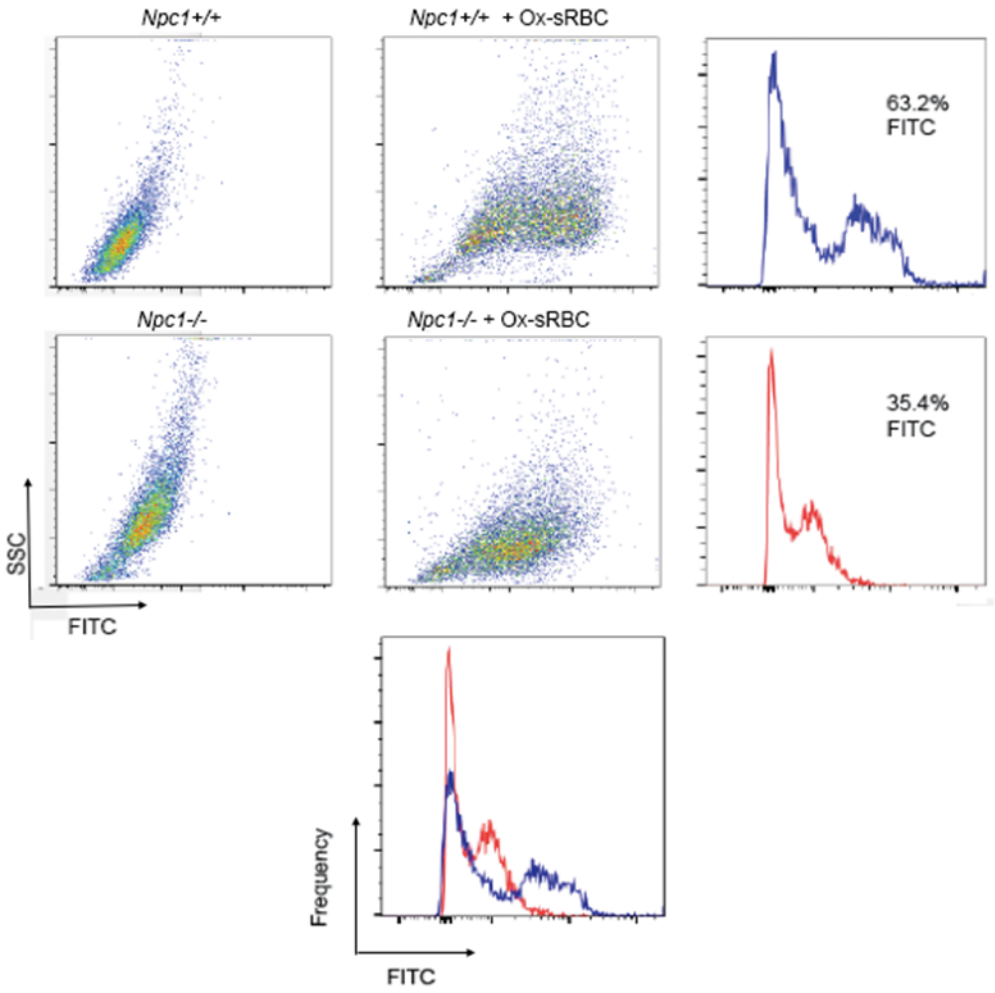


Figure 3.10. *Npc1*$^{-/-}$ EPMΦ display defective phagocytosis of Ox-sRBC as quantified by FACS: FACS profiles of EPMΦ from *Npc1*$^{+/+}$ and *Npc1*$^{-/-}$ mice incubated with CellTracker™ labelled Ox-sRBC. 63.2% of *Npc1*$^{+/+}$ cells are gated as fluorescent, indicating internalised Ox-sRBC whereas only 35.4 % of *Npc1*$^{-/-}$ MΦ fall within the same gate. Data is representative of three independent experiments.

3.3.3.4 *Npc1*$^{-/-}$ EPMΦ display reduced phagocytosis of *E. coli*; Analysis by microscopy and FACS

Phagocytosis is a critical innate immune activity that protects the host against infectious pathogens (Janeway and Medzhitov, 2002). We investigated whether engulfment of bacteria by *Npc1*$^{-/-}$ EPMΦ was lower in comparison to uptake by *Npc1*$^{+/+}$phagocytes. EPMΦ were overlaid with fluorescent *E. coli* Bio particles at EPMΦ**:** *E. coli* MOI of 1:30 and co-incubated. At 10 min co-incubation 15.410% of *Npc1*$^{-/-}$ EPMΦ showed evidence of internalized bacteria (i.e. contained >1 *E. coli* per MΦ) and 35.61% of *Npc1*$^{+/+}$ EPMΦ showed evidence of uptake; at 20 min the frequency had increased to 18.41% for *Npc1*$^{-/-}$ EPMΦ and 60.41% *Npc1*$^{+/+}$ cells; after 30 min of incubation 31.41% of *Npc1*$^{-/-}$ EPMΦ had internalised at least a minimum of one bacterium, with the frequency being 79.41% for *Npc1*$^{+/+}$ EPMΦ and at 40 min 43.15% of *Npc1*$^{-/-}$ EPMΦ were scored as positive in comparison 89.52% of *Npc1*$^{+/+}$. EPMΦ pretreated with cytochalasin D showed minimal uptake of *E. coli* (0.47% of *Npc1*$^{-/-}$, 1.85% of *Npc1*$^{+/+}$ EPMΦ, images not shown), confirming ingestion was dependent upon phagocytosis. The reduction in phagocytic activity of EPMΦ isolated from symptomatic *Npc1*$^{-/-}$ mice as compared to that of *Npc1*$^{+/+}$ cells was significant at all time points (10 min p=0.031; 20 min p=0.00054; 30 min p=0.0001; 40 min p=0.00067; **Fig.3.11**)

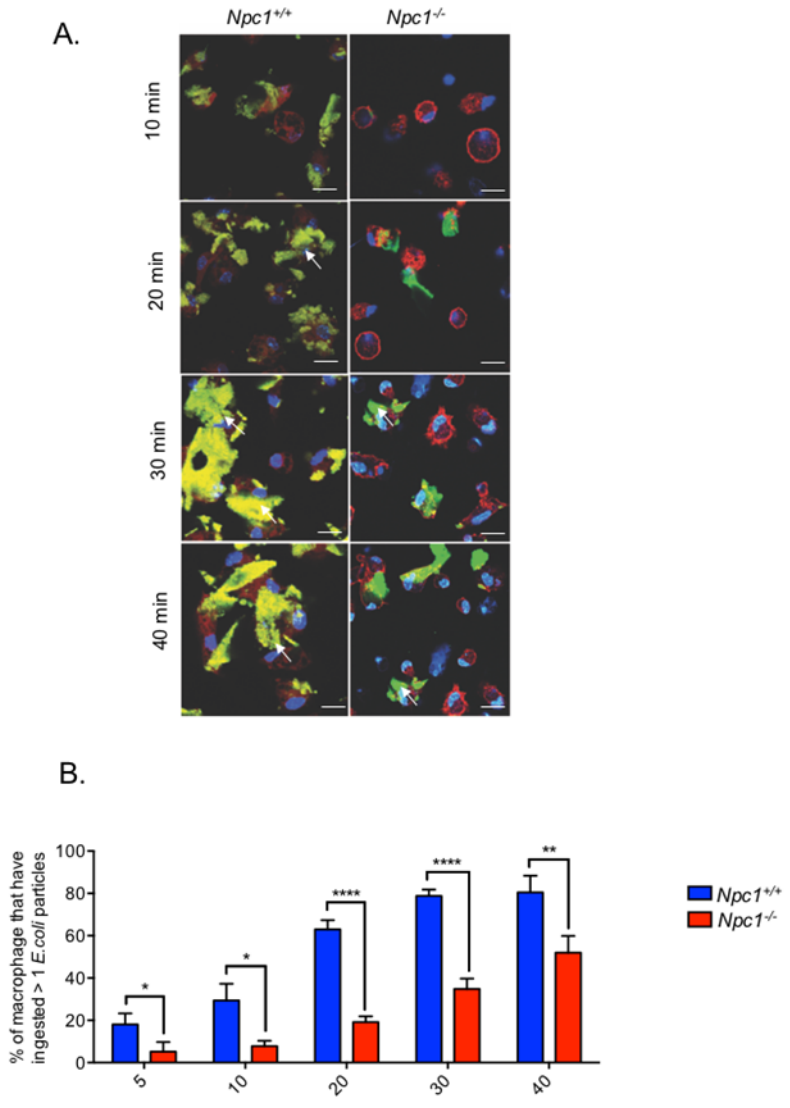


Figure 3.11. EPMΦ display defective phagocytosis of *E. coli* bio particles: (A) *Npc1*$^{+/+}$ EPMΦ (left panels) and *Npc1*$^{-/-}$ EPMΦ (right panels) were co-incubated with *E. coli* Bio particles (green) and examined at specific times. Examples of internalised *E. coli* in *Npc1*$^{+/+}$ and *Npc1*$^{-/-}$ are indicated by white arrows. Red = phalloidin, blue = DAPI. Scale bar =10 µm.
(**B)** *Npc1*$^{-/-}$ EPMΦ (red columns) show significantly decreased phagocytosis at all 4 time points in comparison to *Npc1*$^{+/+}$ EPMΦ (blue columns). Data presented as mean ±SD. N=5 cells *p<0.05, **p<0.01, ***p<0.001, ****p<0.0001 versus control (via student's *t*-test with Welch's correction).

We also analysed phagocytosis of *E. coli* by *Npc1*$^{+/+}$ and *Npc1*$^{-/-}$ EPMΦ by FACS, with the intensity of fluorescence derived from internalised bacteria as a measure of the extent of uptake by EPMΦ. Representative FACS profiles for *Npc1*$^{+/+}$ and *Npc1*$^{-/-}$ EPMΦ co-incubated with *E.coli* Bio particles are shown in **Fig.3.12**. *Npc1*$^{+/+}$ EPMΦ showed approximately 2-fold higher fluorescence (mean MEFL=13491±208) as compared to that of *Npc1*$^{-/-}$ EPMΦ (mean MEFL=8993±197), indicative of reduced internalization of bacteria by genetically deficient EPMΦ **Fig.3.12.**

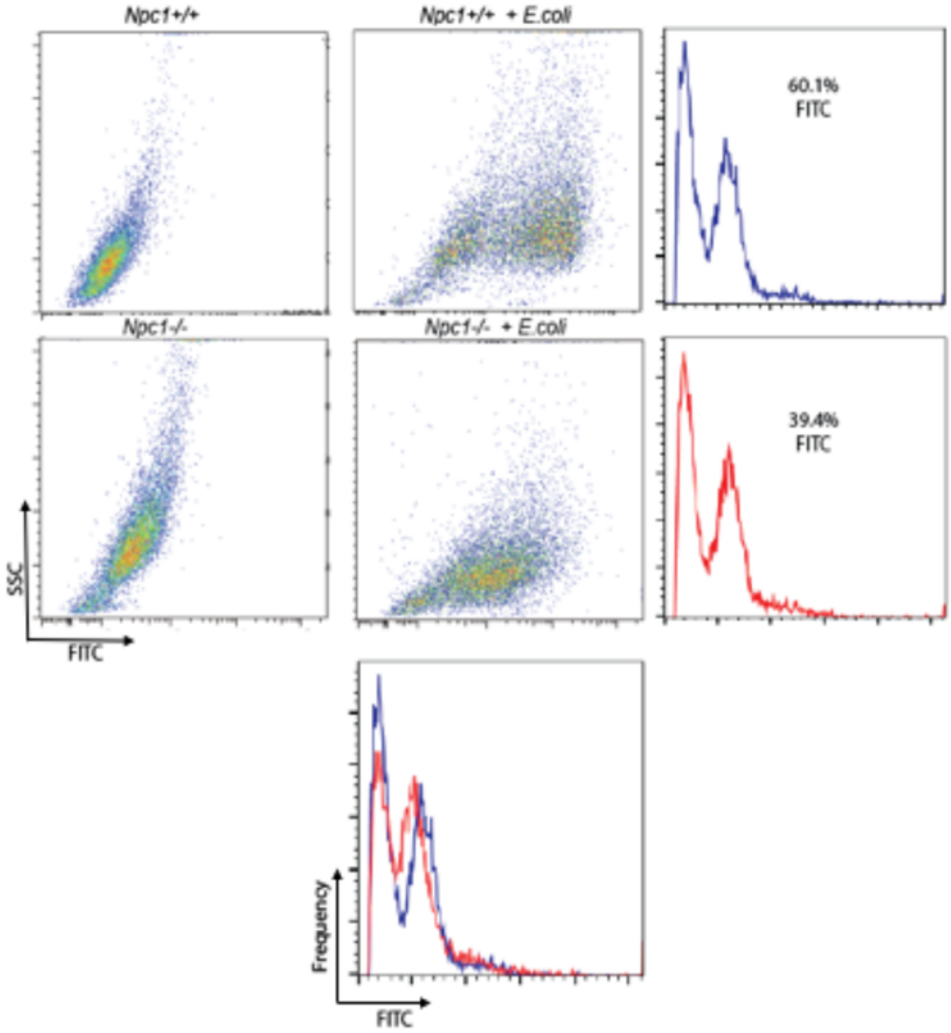


Figure 3.12. *Npc1*$^{-/-}$ EPMΦ display defective phagocytosis of *E. coli* Bio particles as quantified by FACS. FACS profiles of *Npc1*$^{+/+}$ and *Npc1*$^{-/-}$ EPMΦ that have been co-incubated with *E. coli* Bio particles (green) rom *Npc1*$^{+/+}$ and *Npc1*$^{-/-}$ mice. 60% of *Npc1*$^{+/+}$ were gated as fluorescent, indicating ingestion, as compared to 39.4% of *Npc1*$^{-/-}$ EPMΦ. Data is representative of three independent experiments.

3.3.3.5 *Npc1*$^{-/-}$ EPMΦ display reduced phagocytosis of zymosan Bio particles; Analysis by microscopy and FACS

We incubated EPMΦ with zymosan bio-particles conjugated with Alexa Fluor 488 at MOI 1:30 and at defined times, examined for evidence of internalisation by fluorescent microscopy. After 5 min of co-incubation, 0.971% of *Npc1*$^{-/-}$ EPMΦ displayed evidence of internalization of *zymosan* (>1 *zymosan* particle per MΦ) as compared to 11.68% of *Npc1*$^{+/+}$ EPMΦ; at 10 min, 10.41% of *Npc1*$^{-/-}$ EPMΦ were positive for yeast uptake as compared to 36.68% of *Npc1*$^{+/+}$ EPMΦ; at 20 min, internalisation of Bio particles was apparent in 61.85% of *Npc1*$^{+/+}$ EPMΦ but only 28.67% of *Npc1*$^{-/-}$ EPMΦ; at 30 min, the frequency of EPMΦ with evidence of ingestion was 49.74% for *Npc1*$^{-/-}$ and 69.79% for *Npc1*$^{+/+}$ cells; at 40 minutes, phagocytic activity of *Npc1*$^{-/-}$ EPMΦ remained lower, with 79.15% having ingested a minimum of a single zymosan particle in comparison to 88.44% of *Npc1*$^{+/+}$ EPMΦ (**Fig.3.13**). There was minimal uptake by EPMΦ pretreated with cytochalsin D (1.19% of *Npc1*$^{-/-}$ and 2.09% of *Npc1*$^{+/+}$ EPMΦ) indicating that *zymosan* was taken up via phagocytosis (**Fig. 3.13**). The reduction in phagocytic activity of EPMΦ isolated from symptomatic *Npc1*$^{-/-}$ mice in comparison to that of *Npc1*$^{+/+}$ cells was statistically significant at 4 of 5 time points (20 min p=0.0541; 30 min p=0.043; 40 min p=0.0103; 60 min p=0.037) (**Fig. 3.13B**).

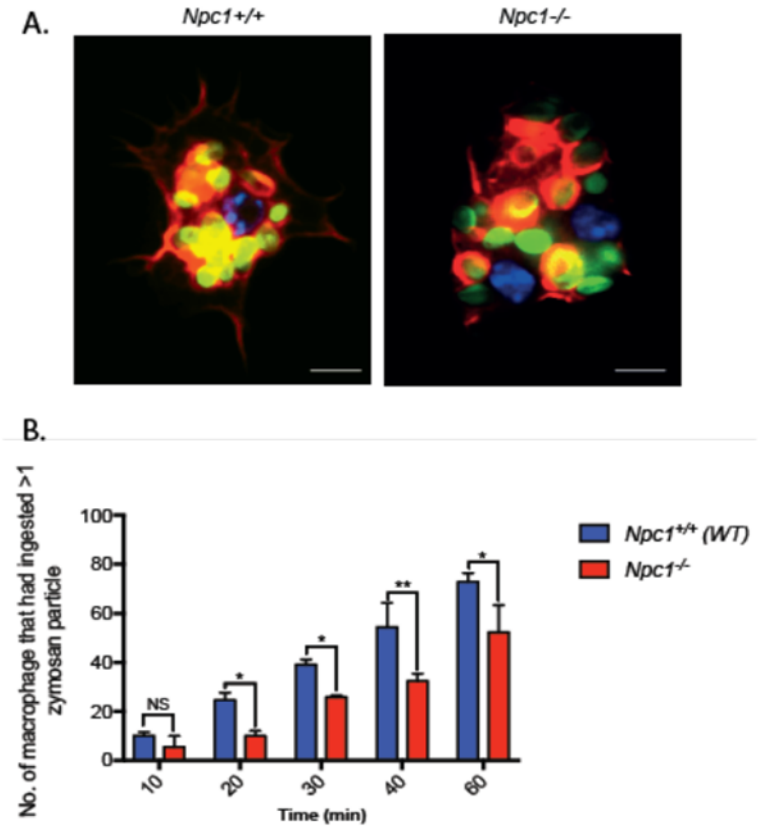


Figure 3.13. *Npc1*$^{-/-}$ EPMΦ display defective phagocytosis of zymosan bio particles.
(A) Representative confocal microscopy images of *Npc1*$^{+/+}$ EPMΦ (left panels) and *Npc1*$^{-/-}$ EPMΦ (right panels) stained with phalloidin (red) that have been co-incubated with zymosan Bio particles (green) for 30 min. Internalised zymosan are yellow, whereas extracellular particles remain green **(B)** *Npc1*$^{-/-}$ EPMΦ display significantly decreased phagocytosis at all time points with the exception of 10 min. Data presented as mean ± SD. N=5, **p*<0.05, ***p*<0.01 versus control (via student's *t*-test with Welch's correction).

Phagocytosis of zymosan was also analysed by FACS. Representative FACS profiles of *Npc1*$^{+/+}$ and *Npc1*$^{-/-}$ EPMΦ co-incubated with fluorescent zymosan Bio particles are shown in **Fig.3.14**. *Npc1*$^{+/+}$ EPMΦ displayed an approximate higher fluorescence (mean MEFL =9741±129) as compared to that of *Npc1*$^{-/-}$ EPMΦ (mean MEFL=6943±179), which was statistically significant (**Fig 3.14**).

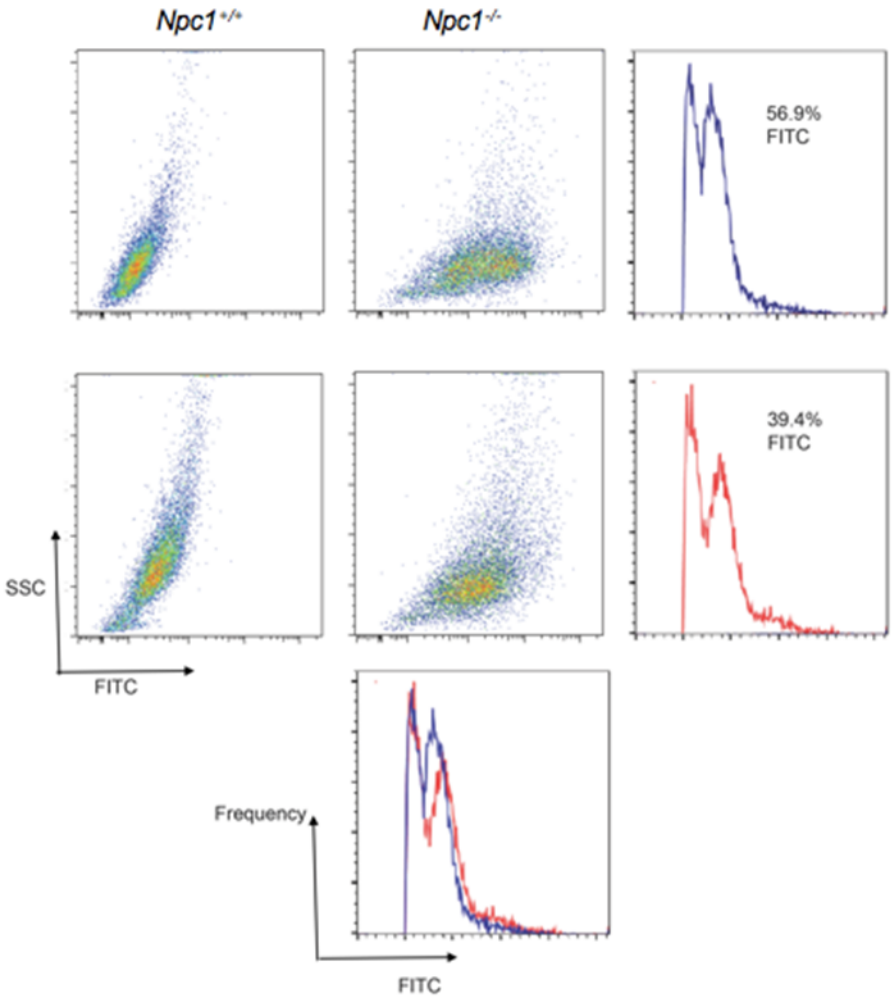


Figure 3.14 *Npc1*$^{-/-}$ EPMΦ display defective phagocytosis of zymosan Bio particles as quantified by FACS. FACS profiles of *Npc1*$^{+/+}$ and *Npc1*$^{-/-}$ EPMΦ co-incubated with zymosan Bio particles (green). 56.9% of *Npc1*$^{+/+}$ EPMΦ were gated as fluorescent, indicating ingestion of zymosan as compared to 39.4% of *Npc1*$^{-/-}$ EPMΦ. Data is representative of three independent experiments.

3.3.3.6 *Npc1*$^{-/-}$ EPMΦ show impaired phagocytosis of apoptotic thymocytes.

Phagocytosis of apoptotic cells by MΦ and other populations of phagocytes is essential for tissue homeostasis and is dependent upon the exposure of specific ligands on the dying cell that mediates their recognition via multiple receptors (Poon et al., 2014). We incubated fluorescently labelled apoptotic thymocytes with EPMΦ at MOI of 1:20 and determined the frequency of MΦ containing >1 apoptotic thymocyte per MΦ at specific time points. After 10 min co-incubation, a mean of 23.41% of *Npc1*$^{-/-}$ EPMΦ exhibited evidence of internalized thymocytes as compared to 51.67% of *Npc1*$^{+/+}$ EPMΦ; at 20 min, the incidence for *Npc1*$^{-/-}$ EPMΦ was 44.13% and 67.91% for *Npc1*$^{+/+}$ EPMΦ; 36.33% of *Npc1*$^{-/-}$ and 74.14% of *Npc1*$^{+/+}$ EPMΦ had evidence of phagocytic activity at 30 min; had reached 73.51% and 89.32% for *Npc1*$^{-/-}$ and *Npc1*$^{+/+}$ EPMΦ respectively at 40 min of co-incubation and finally 77.91% of *Npc1*$^{-/-}$ and 90.44% of *Npc1*$^{+/+}$ EPMΦ had ingested apoptotic thymocytes by 60 min. EPMΦ pretreated with cytochalasin D, showed minimal ingestion of apoptotic thymocytes (1.39% of *Npc1*$^{-/-}$ and 2.31% of *Npc1*$^{+/+}$) confirming thymocyte uptake was via phagocytosis. Statistically, the reduction in phagocytic activity of *Npc1*$^{-/-}$ EPMΦ isolated from symptomatic mice in comparison to *Npc1*$^{+/+}$ EPMΦ was significant at 10 min (p= <0.0001), 20 min (p=0.00032) and 30 min (p=0.00017, but not significant at 40 min (p=0.051) and 60 min (p=0.063) (**Fig.3.15**).

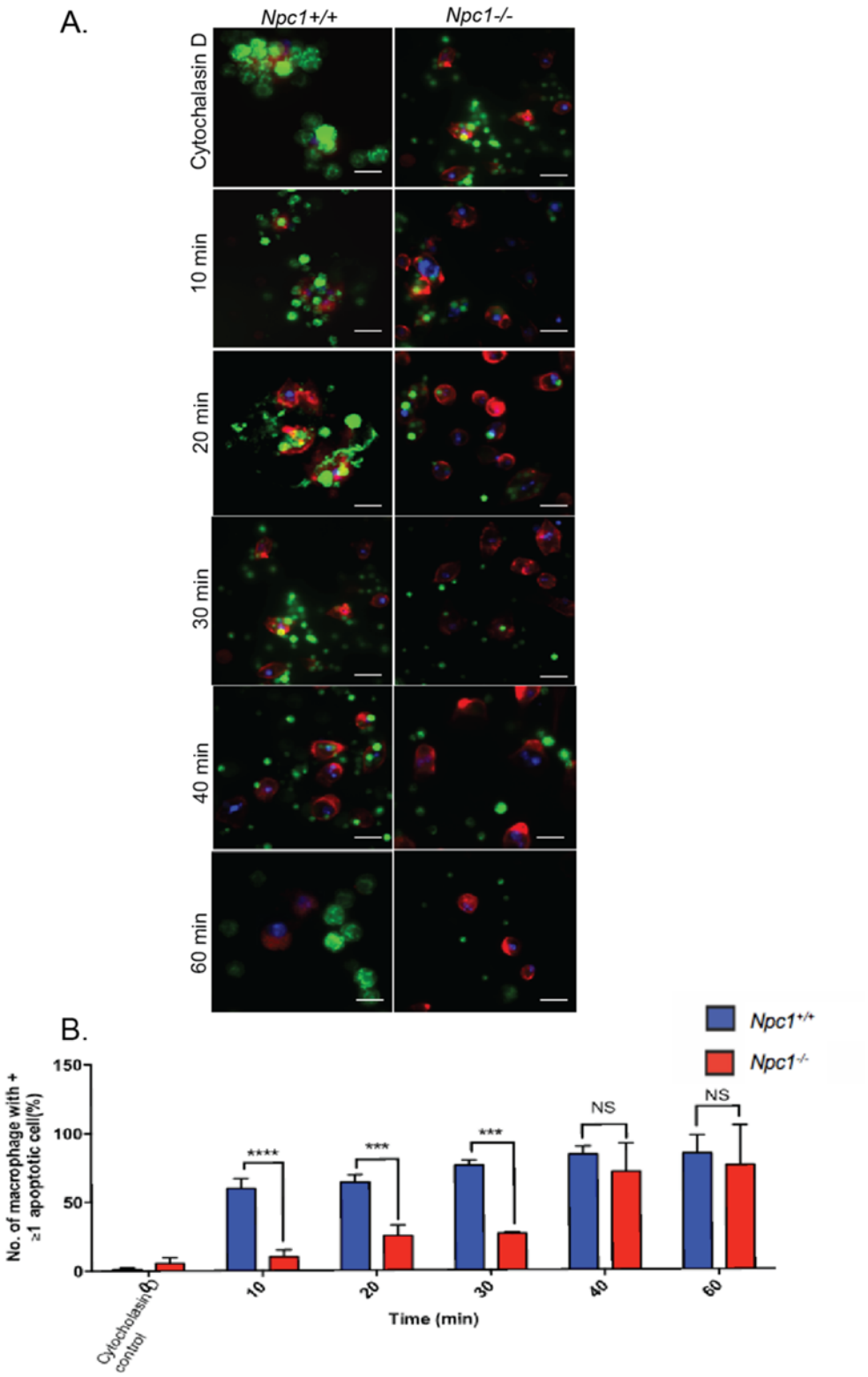

A.
Npc1+/+
Npc1-/-
Cytochalasin D
10 min
20 min
30 min
40 min
60 min
B.
Npc1+/+
Npc1-/-
No. of macrophage with + ≥1 apoptotic cell(%)
150
100
50
0
****
***
***
NS
NS
Cytochalasin D control
10
20
30
40
60
Time (min)

Figure 3.15 *Npc1*$^{-/-}$ EPMΦ display decreased phagocytosis of apoptotic thymocytes. (A) *Npc1*$^{+/+}$ EPMΦ (left panels) and *Npc1*$^{-/-}$ EPMΦ (right panels) stained with phalloidin (red) that have been co-incubated with apoptotic thymocytes (green). Blue = DAPI. Scale bar = 10 μm**,**63X **(B)** *Npc1*$^{-/-}$ EPMΦ (red columns) display significantly reduced phagocytosis of apoptotic thymocytes at 10, 20 and 30 min of co-incubation as compared to *Npc1*$^{+/+}$ EPMΦ. Data presented as mean ±SD. N=6. ****p*<0.001, *****p*<0.0001, NS *p*>0.05 versus control (via Student's *t*-test with Welch's correction).

3.3.4 Expression of specific receptors is apparently normal in *Npc1*$^{-/-}$ EPMΦ.

Phagocytic activity is reliant on the adequate expression of specific receptors on the surface of phagocytes that mediate binding and internalization of the target particle(Cannon and Swanson, 1992). Therefore, absence of or a decrease in receptor(s) expression would be very likely to have a negative impact on the phagocytic capacity of the cell. In order to exclude the possibility that this might underlie the generalized reduction in phagocytic activities of *Npc1*$^{-/-}$ MΦ in comparison to *Npc1*$^{+/+}$ cells, we used immunostaining and FACS analysis to compare the relative levels of expression.

Representative examples of FACS profiles of fluorescent antibody stained *Npc1*$^{+/+}$ and *Npc1*$^{-/-}$ EPMΦ are shown in **Fig 3.16**. Our data confirmed that there was no statistically significant difference in the fluorescent signal (MEFL) of *Npc1*$^{+/+}$ and *Npc1*$^{-/-}$ EPMΦ stained with anti-CD16/32 antibody (specific for low affinity FcγRIII and FcγRII, **Fig 3.16 (A)**; and anti-CD32B (specific for FcγRIIB, **Fig 3.16B**). These results would suggest that the reduced phagocytic activity

of homozygous deficient EPMΦ are not the result of altered levels of expression of specific receptors.

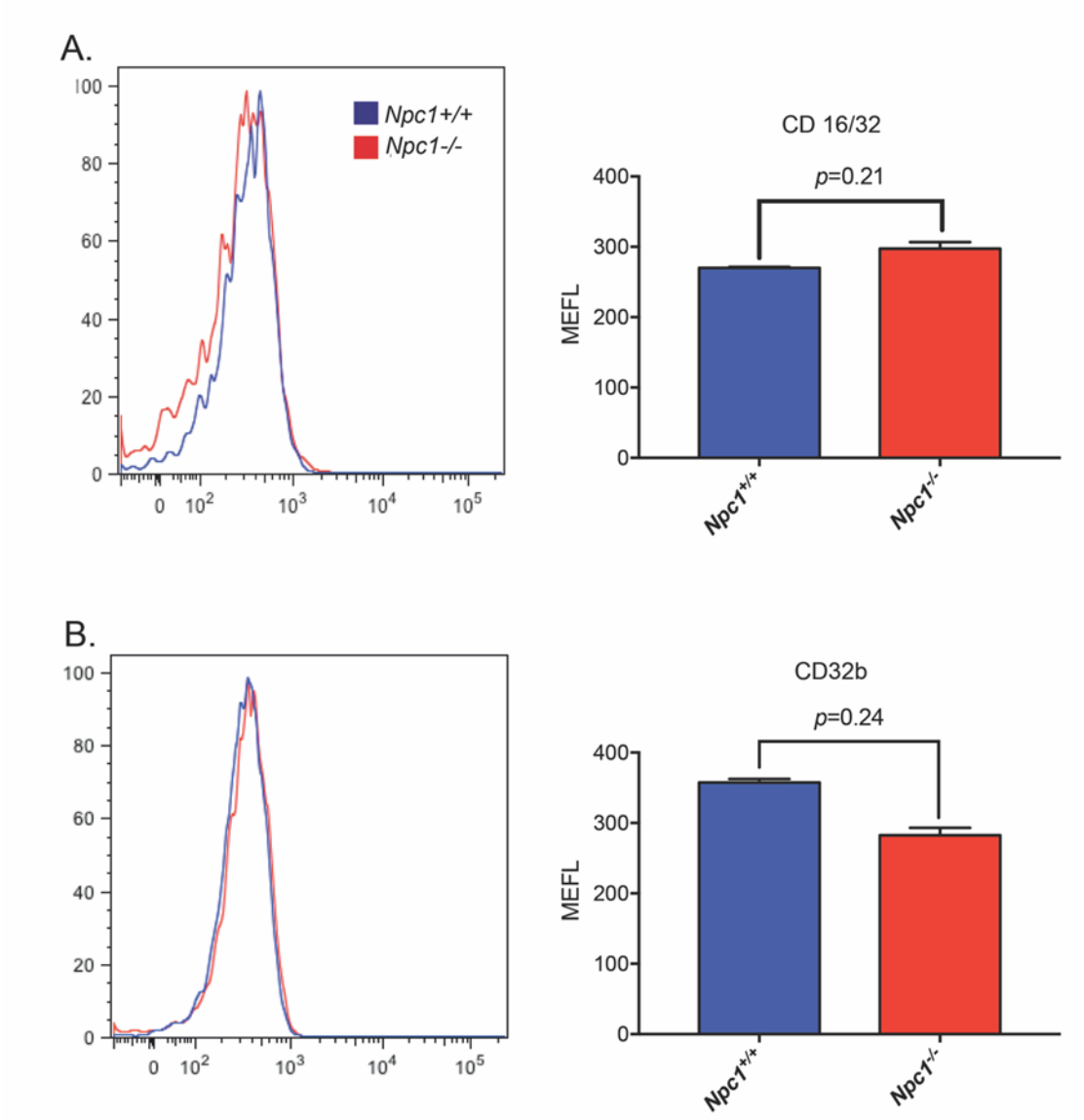


Figure 3.16. *Npc1*$^{-/-}$ EPMΦ show unaltered expression of specific phagocytic receptors. FACS profiles (left panels) and MEFLs (right panels) of *Npc1*$^{+/+}$ (blue columns) and *Npc1*$^{-/-}$ EPMΦ (red columns). **(A)** CD16/32 and **(B)** CD32B. Mean ± SD N=4, NS, $p>0.05$ (via *t*-test with Welch's correction).

.

3.3.5 *Npc1*$^{-/-}$ EPMΦ produce lower levels of pro-inflammatory cytokines after incubation with IgG-sRBC.

The process of phagocytosis as previsouly mentioned is a key immune regulatory action that internalised and disposes of unwanted particles. During this process, the MΦ responds by producing specific cytokines to initiate the immune processing. Of most interest in phagocytosis is the production of reactive oxygen species (ROS), TNF-α, and IL-6. Significantly lower amounts of IL-6 (p=<0.001) and TNF-α (p=<0.001) were produced by *Npc1*$^{-/-}$ EPMΦ following incubation with IgG-sRBC (Fig. 3.17).

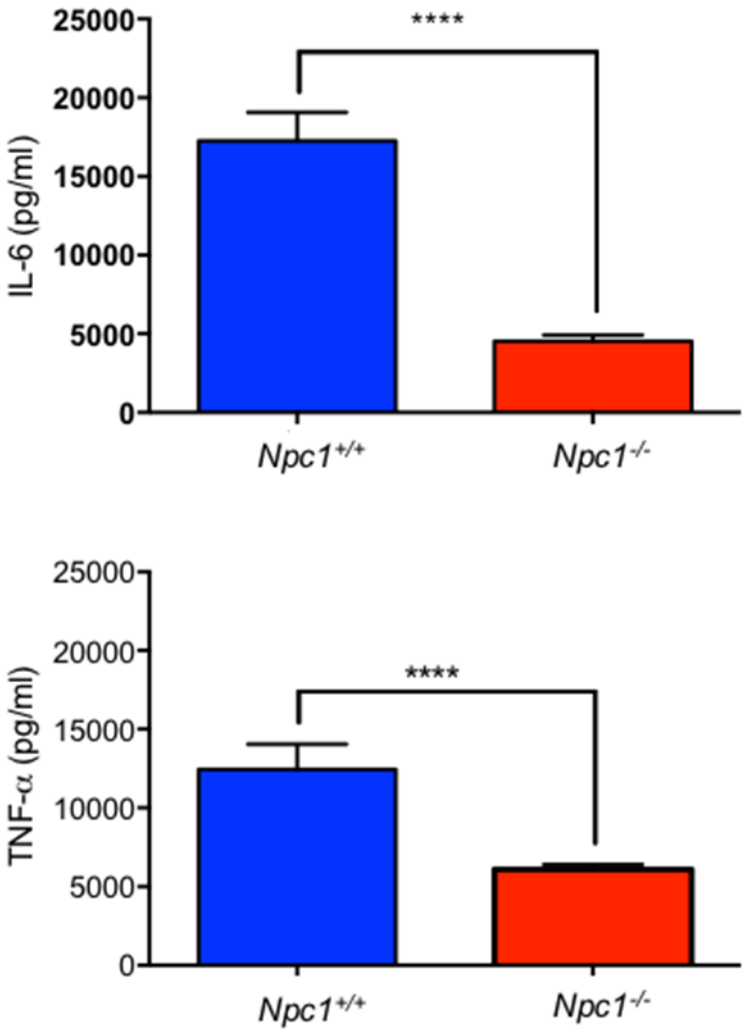


Figure 3.17 Decreased cytokine production by *Npc1*$^{-/-}$ EPMΦ incubated with polystyrene beads. *Npc1*$^{-/-}$ EPMΦ (red columns) secreted significantly lower amounts of IL-6 and TNFα in comparison to *Npc1*$^{+/+}$ EPMΦ (blue columns) following incubation with IgG-sRBC. Mean ± SD. N=2. ****p<0.0001 versus *Npc1*$^{+/+}$ EPMΦ (via One-way ANOVA).

3.3.6 Decreased production of ROS by *Npc1*$^{-/-}$ EPMΦ after co-incubation with IgG-sRBC or *E. coli* Bio particles.

Npc1$^{-/-}$ EPMΦ showed significantly reduced production of ROS following incubation with IgG-sRBC **(Fig.3.18)**. (*Npc1*$^{-/-}$, p=0.0102) compared with correct controls. ROS production was decreased following exposure to *E.coli* and MΦ activation with LPS, but the decrease was NS (*E.coli*, p=0.0491; LPS p=0.694).

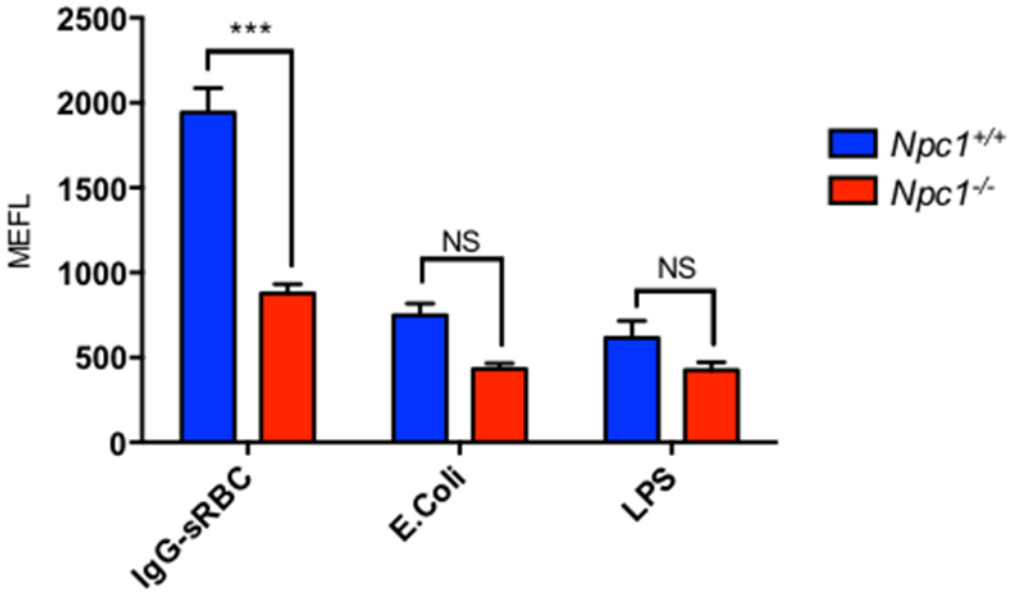


Figure 3.18 *Npc1*$^{-/-}$ EPMΦ show reduced ROS production in response to phagocytosis of IgG-sRBC. Following phagocytosis, ROS production increased substantially in *Npc1*$^{+/+}$ MΦ. *Npc1*$^{-/-}$ showed a significantly lower change in fluorescence in comparison to *Npc1*$^{+/+}$ indicating decreased production of ROS. Data collected as mean change in fluorescence of EPMΦ 30 min after labelling with DCFDA. Fold change in mean fluorescence relative to control *Npc1*$^{+/+}$. Mean SD of 3 biological replicates per group. N=3 **p<0.01 (via t-test with Welch's correction).

.

3.3.7 Phagocytic activities of MΦ with phenotypes of other LSDs

3.3.7.1 EPMΦ from Sandhoff disease (*hexb*$^{-/-}$) mice do not display impaired phagocytosis of IgG-sRBC

We wished to define the phagocytic activity of MΦ with cellular phenotypes characteristic of other LSDs in order to determine whether impairment may be unique to NPC or potentially a feature common to this group of disorders.

We isolated EPMΦ from symptomatic *hexb*$^{-/-}$ mice, a mouse model of Sandhoff disease, which has an acute course of disease and phenotypes that include neurodegeneration and CNS inflammation (Jeyakumar et al., 2003). We employed the microscope-based *in vitro* assay to compare the phagocytic activities of *hexb*$^{+/+}$ and *hexb*$^{-/-}$ EPMΦ. Representative results are shown in **Fig. 3.19**. Assays were established using EPMΦ overlaid with Celltracker^{TM} green labelled IgG-opsonised sRBC at MOI of 1:20; at 10 min co-incubation, 32.7% of *hexb*$^{-/-}$ EPMΦ showed evidence of internalised IgG-sRBC as compared to 36.9% of *hexb*$^{+/+}$ EPMΦ; at 20 min, it was 44.5% and 49.3% for *hexb*$^{-/-}$ and *hexb*$^{+/+}$ cells respectively; it had reached 66.9% and 64.1% at 30 min and by 40 min was 73.2% and 79.14% for *hexb*$^{-/-}$ and *hexb*$^{+/+}$ EPMΦ. Pre-treatment of MΦ with cytochalasin D inhibited phagocytosis (*hexb*$^{+/+}$ 1.78%, *hexb* $^{-/-}$ 1.93%) indicating that phagocytosis was the mechanism used to internalise IgG-sRBC. There was no statistically significant difference in phagocytosis between *hexb*$^{-/-}$ and *hexb*$^{+/+}$ EPMΦ at all time points. (10 min p=0.279; 20 min p=0.192; 30 min p=0.574; 40 min p=0406; **Fig.3.19B**).

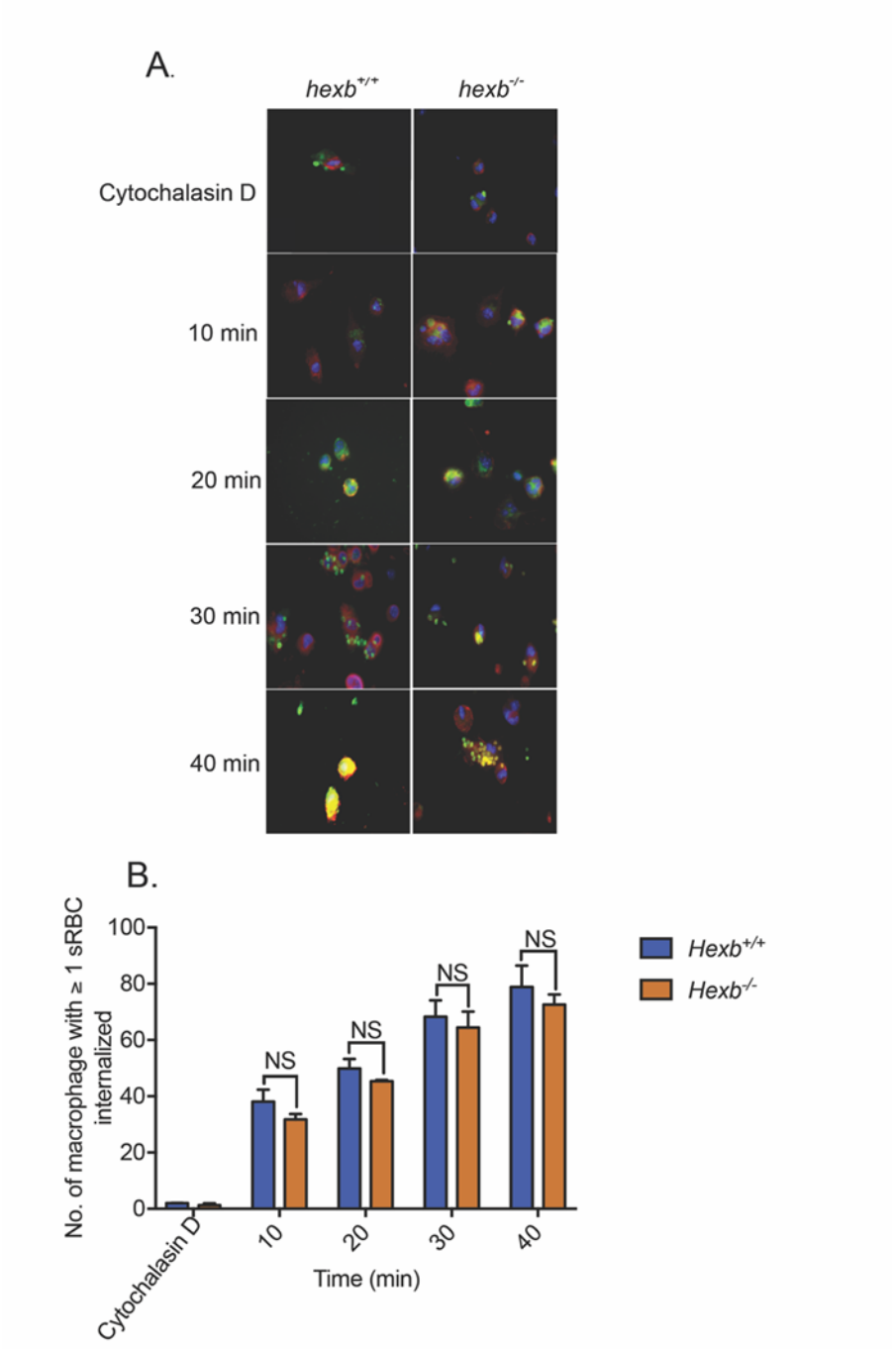

A.
hexb+/+
hexb-/-
Cytochalasin D
10 min
20 min
30 min
40 min
B.
No. of macrophage with ≥ 1 sRBC internalized
100
80
60
40
20
0
NS
NS
NS
NS
Cytochalasin D
10
20
30
40
Time (min)
Hexb+/+
Hexb-/-

Figure 3.19. EPMΦ from Sandhoff mice display normal phagocytic activity: **(A)** EPMΦ from Sandhoff mice were overlaid with CellTracker™ green labelled IgG-sRBC for listed times. **(B)** Histogram representation of phagocytic activity. *hexb*$^{+/+}$ (shown by blue bars) and *hexb*$^{-/-}$ (shown by brown bars) show non-significant differences in phagocytosis at all time points. N=5, data presented as mean ± SD of 3 biological replicates per group, ns $p>0.05$; WT (*hexb*$^{+/+}$) vs Sandhoff (*hexb*$^{-/-}$) (via student's *t*-test with Welch's correction)

3.3.7.2 Monocyte-derived MΦ from Gaucher Disease patients do not display impaired phagocytosis of IgG-sRBC or polystyrene beads.

In collaboration with Dr. Kerri-Lee Wallom (University of Oxford, Department of Pharmacology) we investigated whether monocyte-derived MΦ derived from patients with Gaucher Disease show altered phagocytic activities. Cells were co-incubated with IgG-sRBC or 3 μm polystyrene beads for defined periods of time and the extent of uptake determined by FACS. Representative profiles of MΦ co-incubated with IgG-sRBC are shown in **Fig. 3.20**. At 10 min, of co-incubation, 40.4% of Gaucher MΦ had ingested IgG-sRBC and 51% had ingested beads; at 20 min, 56.3% of cells showed evidence of internalisation of IgG-sRBC and 63.7% for beads; at 30 min, 71.8% of cells had taken up IgG-sRBC and 73.1% had internalised beads; at 40 min, 79.9% had ingested IgG-sRBC and 84.7 had internalised beads. Frequency of ingestion by WT cells at 10 min was 49.3% for IgG-sRBC and 47.4% for beads; at 20 min, 53.4% had internalised IgG-sRBC and 60.1% had ingested beads; at 30 min, 70.3% had ingested IgG-sRBC and 77.9% had internalised beads and at 40 min 86.4% had internalised IgG-sRBC and 79.3% had taken up beads (**Fig.3.21,**

corresponding images, histogram not shown). There was no significant difference in the extent of ingestion between healthy and Gaucher Disease MΦ for either particle and at all time points (10 min p=0.218; 20 min p=0.631; 30 min p=0.071; 40 min

p=0.24**.**

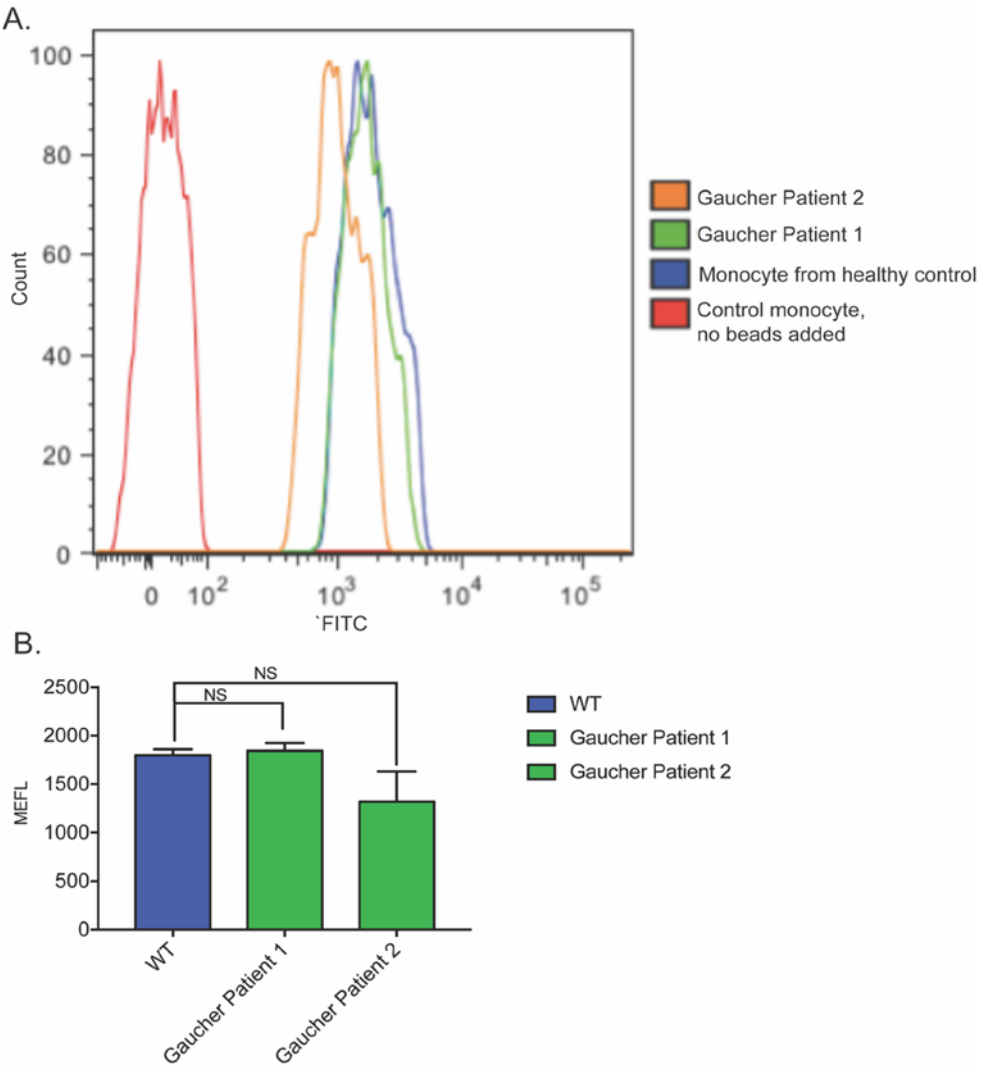


Figure 3.20 Primary Gaucher MΦ show normal phagocytic behaviour as quantified by FACS: MEFL of primary MΦ exposed to Celltracker labelled IgG-sRBC. Fold change in mean fluorescence relative to control WT. Mean SD of 3 biological replicates tested per group.
*p<0.05, ns p>0.05 versus Gaucher MΦ (via t-test with Welch's correction.

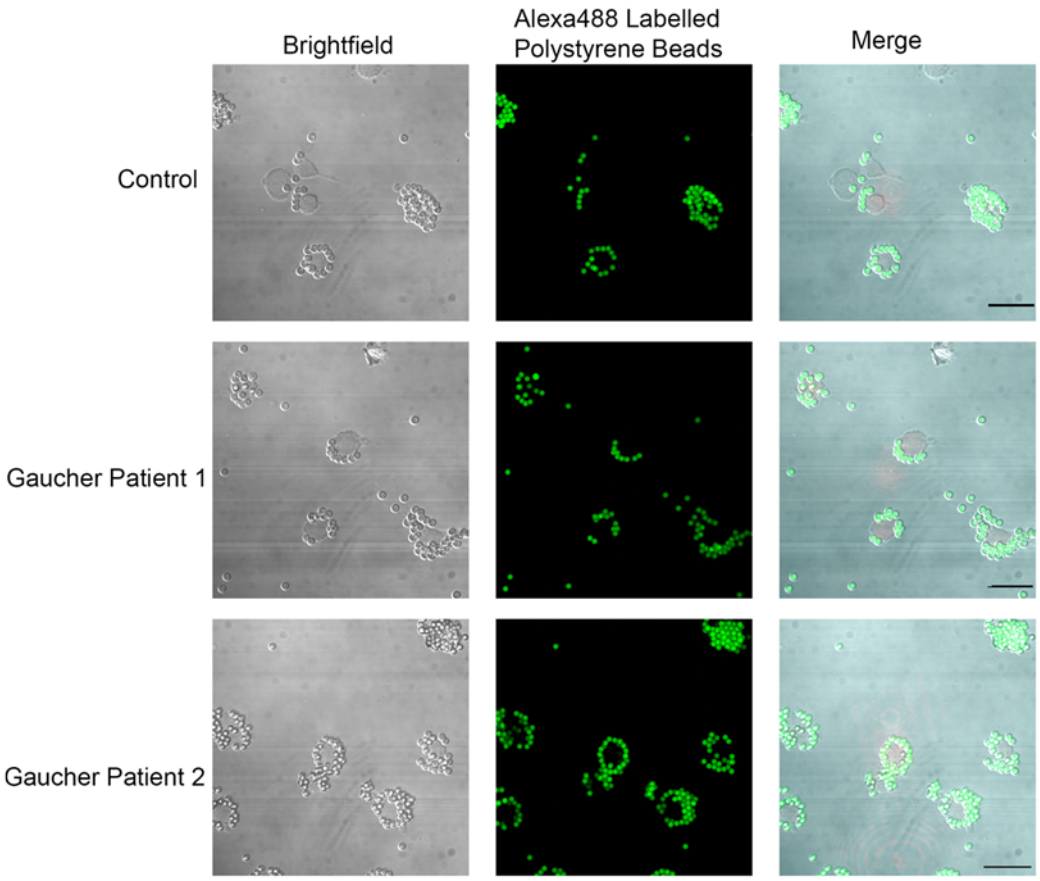


Figure 3.21. Gaucher Disease patient monocyte derived MΦ show normal phagocytosis of 3 μm polystyrene beads: (A) Primary MΦ from two Gaucher patients as well as a control sample have been co-incubated with 3 μm polystyrene beads (green). Phagocytosis of 3 μm polystyrene beads is comparable to control as indicated by comparing uptake of beads. Scale bar =10μm, 63X.

3.4 Discussion

In this chapter we investigated the *ex-vivo* phagocytic activities of murine MΦ populations isolated from an authentic mouse model of NPC. In summary, our results showed that *Npc1*$^{-/-}$ MΦ have a significant impairment in their ability to ingest a number of different particles *in vitro* in comparison to MΦ isolated from *Npc1*$^{+/+}$ animals. These data suggest the possibility of phagocytic deficiencies *in vivo* that may impact significantly upon pathological phenotypes and disease progression.

In Chapter 1 we provided a detailed description of phagocytosis and discussed its importance for host defense and maintenance of tissue homeostasis. There are known deleterious consequences that result from reduced or absence of phagocytic function, which include significantly increased susceptibility to pathogens (Andrews and Sullivan, 2003; Rawat et al., 2014) and the triggering of damaging autoimmune responses when the removal of dying cells is compromised (Munoz et al., 2010; Taylor et al., 2010). Therefore, in the context of investigating altered innate immune activities in NPC, phagocytosis warranted study.

In order to facilitate our initial studies into the potential consequences of NPC on phagocytosis we exploited drug-based induction of the cellular phenotype in transformed murine MΦ cell lines. However, as previously mentioned, although U18666A has been demonstrated to bind directly to NPC1 (Lu, 2015), the drug is also known to be an inhibitor of sterol biosynthesis (Cenedella, 2009) and may have other, as yet unidentified targets. This may complicate interpretation of results generated using the drug-induced cellular model because of the possibility of off targets of U18666A. We performed therefore comparable

investigations using cells genetically deficient in the Npc1 protein isolated from a well-characterized murine model of NPC. Because the biological function(s) of Npc1 remain controversial (Walkley and Suzuki, 2004; Lloyd-Evans et al., 2008; Lu, 2015), we do not have an assay with which to quantify any residual activity that may remain in cells from the *Npc1*$^{-/-}$ mouse that may have the potential to influence the extent of phagocytosis. However, because the insertion of a retrotransposon in this mouse strain results in a significantly truncated open reading frame, which encodes only the first three exons of the protein, it is considered to be the equivalent of a null allele(Loftus et al., 1997). This is consistent with the less severe phenotypes shown by two independent mouse strains that harbor point mutations in *Npc1* (Maue et al., 2012; Praggastis et al., 2015).

Specific populations of murine tissue MΦ can be isolated relatively easily from mice in sufficient quantity. To be suitable for experimentation it would be necessary that *ex-vivo* cells display the cellular hallmarks of NPC. For example, although large numbers of bone marrow derived MΦ can be generated from a single *Npc1*$^{-/-}$ mouse via *in vitro* differentiation of precursors in the presence of M-CSF (Manzanero, 2012), this population does not show significant expansion of the acidic compartment, cholesterol accumulation etc. most likely because of relatively low throughput in the endolysosomal system (Dr N. Platt, personal communication). We chose to analyse the phagocytic activities of two different populations of murine tissue MΦ which we confirmed had NPC cellular phenotypes. RPMΦ are the resident myeloid cell population of the peritoneum, which can be recovered at a frequency of typically 1-2 x 10^6 cells per mouse and are a relatively long-lived cell population. In contrast inflammatory EPMΦ,

such as the population elicited by intraperitoneal injection of sterile thioglycollate broth, are generated in greater numbers and at 96 h after the stimulus ~ 5-10 x 10^6 cells can be obtained from a single mouse, thereby facilitating experiments that require input of larger numbers of phagocytes (e.g. the FACS based phagocytosis assay). We chose to isolate MΦ from early symptomatic *Npc1*$^{-/-}$ mice because preliminary studies demonstrated NPC cellular phenotypes in *ex-vivo* cells obtained from animals of 7 weeks of age (not shown). Confirmation of storage disease phenotypes was seen as expansion of acidic compartment volumes of both RPMΦ and EPMΦ isolated from *Npc1*$^{-/-}$ mice by LysoTracker™ staining (**Fig. 3.3**)

In order to bind and internalize the very broad range of infectious and non-infectious particles that may be encountered, which differ widely in their molecular composition, phagocytosis has evolved to be a complex process that includes a number of discrete systems, which can efficiently recognize and remove particulates (Stuart and Ezekowitz, 2008). In particular, coating or opsonisation of targets with host-derived molecules such as IgG or complement proteins (opsonins) or the direct detection of ligands borne by microbes (i.e. pattern recognition or molecular pattern molecules) identifies particles for efficient ingestion via specific phagocytic receptors (Cannon and Swanson, 1992; Stuart and Ezekowitz, 2005; Akira et al., 2006). Therefore, in the absence of available data that could inform our investigations (i.e. direct us to study ingestion via particular receptor-mediated pathways), we undertook a broad study of phagocytosis involving different particles in order to evaluate whether only some, or perhaps all of them might be affected as a consequence of loss of Npc1 function. In essence, this was the same approach that we adopted in

our studies of the drug-induced cellular model of NPC described in Chapter 2. Our expectation was that results obtained by this approach could discriminate the alternatives of either reduction or absence of an activity required for only a single phagocytic mechanism or one that might affect phagocytosis more globally. We adopted two complementary methods, employed previously in the studies described in Chapter 2, to analyse phagocytic activity: a fluorescent microscopy phagocytosis assay that permitted visual inspection of individual phagocytes and a FACS based assay that enabled a higher throughput of samples.

In vitro phagocytosis assays that involve examination by microscopy have been well documented (Aderem and Underhill, 1999; Akira et al., 2006). Co-incubation of phagocytes and targets for a pre-determined period(s) of time, established at a MOI to ensure particles are in sufficient excess so as to not be limiting, and the assay terminated by washing away of non-ingested material has become a standardized approach (Platt and Fineran, 2015). We adopted a comparable methodology for our studies (here and in Chapter 2). On the other hand, methods used for the quantification of phagocytic capacity have tended to be more varied because determination of internalization frequencies by visual inspection (i.e. counting of ingested particles) can be time consuming for the investigator. The capacity of phagocytes to ingest particles is related not only to the frequency that display evidence of having ingested at least one particle, but also a measure of how phagocytic they are (i.e. the number of particles that each phagocyte has consumed). For example, authors have created a “phagocytic index” by multiplying the percentage of phagocytes that contain a minimum of a single particle

multiplied by the mean number of particles per positive cell (Hu et al., 2000). In contrast, assays that include FACS-based evaluation (Bjerknes, 1984; Lehmann et al., 2000) has allowed for much more rapid quantification than is possible by microscopy and facilitated studies that involve significantly greater number of samples. As we have already explained, we adopted both approaches within our investigations in order to combine the advantages of each methodology.

We found a significant reduction in the phagocytic activity of *Npc1*$^{-/-}$ MΦ for all particles that were tested, which included ones opsonized with IgG and complement, bacterial and fungal microbes, synthetic beads and apoptotic cells, although the extent of the reduction was not identical for all – for example, ingestion of IgG-sRBC and Ox-sRBC by *Npc1*$^{+/+}$ EPMΦ was, respectively, two and three fold greater than that by *Npc1*$^{-/-}$ EPMΦ, but internalization of zymosan by *Npc1* deficient MΦ was only half that of *Npc1*$^{+/+}$. The most significant conclusion that we can make from the demonstration of impaired uptake of all of the particles that we examined is that the level at which loss of Npc1 dependent activities impacts upon phagocytosis is common to different mechanisms and is not restricted to any particular one. This would, for instance, exclude the likelihood of inactivation of molecules that are essential for only a single uptake mechanism. For example, two distinct mechanisms have been identified which differentiate between CR3 and FcγR mediated phagocytosis (Caron and Hall, 1998). Although both require members of the Rho guanosine triphosphate (GTPase) family to facilitate re-organisation of the actin cytoskeleton, uptake dependent upon the IgG receptor involves Cdc42 and Rac whilst internalization by CR3 requires Rho. Our data would therefore, not be

explained by inactivation of a particular GTPase, but would be compatible if all members of the family were affected in NPC.

We measured only a relatively modest, but significant reduction in phagocytosis of zymosan particles by *Npc1*$^{-/-}$ EPMΦ **(Fig 3.16)**. It may be relevant that we failed to detect impaired ingestion of the same particle by U18666A-treated RAW 264.7 MΦ (**Fig. 2.14, Fig. 2.15**). These data may suggest that the phagocytic mechanism responsible for the uptake of yeast particles is relatively resistant to the consequences of loss of Npc1.

Although there were statistically significant differences in phagocytic activities between *Npc1*$^{-/-}$ and *Npc1*$^{+/+}$ MΦ, we did not detect a measurable reduction in *Npc1*$^{+/-}$ cells (Figures not shown). This was perhaps not unexpected because extensive studies of our mouse colony have failed to identify changes in behavior or other significant phenotypes for *Npc1*$^{+/-}$ mice at 7 weeks of age (Dave Smith, personal communication). However, it has been reported that fibroblasts derived from heterozygous patients showed an intermediate phenotype for cholesterol esterification as compared to wild type and homozygous deficient cells (Pentchev et al., 1984; Vanier, 2010). In addition, evidence of motor dysfunction has recently been claimed in 9-week-old *Npc1*$^{+/-}$ mice (Hung et al., 2016). We would suggest that study of aged *Npc1*$^{+/-}$ mice (heterozygous animals have a normal lifespan) would likely be the most appropriate strategy to investigate whether heterozygosity may impact upon phagocytosis because it would allow for accumulation of any deleterious events that result from reduced gene dosage. Unfortunately, cohorts of suitably aged *Npc1*$^{+/-}$ and *Npc1*$^{+/+}$ mice were not available to us during the course of our studies.

The microscopy-based phagocytosis assay was established with the aim of being able to quantify differences between the phagocytic activities of *Npc1*$^{-/-}$ cells in comparison to *Npc1*$^{+/+}$ cells. If loss of Npc1 were to impact upon phagocytosis we might predict multiple distinct phenotypic possibilities. First, we thought it very unlikely that phagocytosis would be increased by loss of Npc1 because to our knowledge there is an absence of published evidence showing mutation-dependent phagocytic gain-of-function. More probable scenarios would be that phagocytic activities of *Npc1*$^{-/-}$ cells may be unchanged, perhaps as a result of up regulation of compensatory mechanisms (although considered perhaps unlikely in view of the data we had obtained for U18666A-treated MΦ cell lines in Chapter 2) or reduced relative to that of *Npc1*$^{+/+}$ MΦ. If the latter, the extent of reduction could be greater than that seen with the drug-induced model as a result of either enhanced inherent phagocytic activities of RAW264.7 and J774A.1 MΦ cell lines relative to that of *ex-vivo* MΦ, or because treatment with U18666A under the regime used did not completely block all Npc1 activity. On the other hand, compensatory mechanisms that may have been stimulated *in vivo* prior to cell isolation might be insufficient to recover full phagocytic activities, but be enough to lessen the deficit as compared to *Npc1*$^{+/+}$ MΦ. In essence, because of these considerations we did not attempt a direct side-by-side comparison of the models but investigated for phenotypic trends that were consistent between the two studies.

Although we detected statistically diminished phagocytosis by *Npc1*$^{-/-}$ RPMΦ and EPMΦ, loss of the lysosomal protein Npc1 did not prevent all phagocytic activity – ingestion by MΦ in the presence of cytochalasin D, a fungal toxin that binds to actin filaments and prevents its polymerization (Goddette and Frieden,

1986; Cooper, 1987) was significantly lower than that of *Npc1*$^{-/-}$ MΦ. We therefore designed assays to enable analyses of the kinetics and efficiency of phagocytosis by MΦ with the two different genotypes.

Over the time course of co-incubation used, we measured a continuous increase in the percentage of *Npc1*$^{+/+}$ MΦ that had ingested particles, indicating that under these conditions phagocytic capacity had not been exceeded; yet, the rate of internalisation over the duration of the assay was not linear. Phagocytosis by *Npc1*$^{-/-}$ MΦ was significantly lower than for *Npc1*$^{+/+}$ cells at each comparable time point, with no evidence of an initial deficit or delay in uptake that subsequently recovered to the level of *Npc1*$^{+/+}$ MΦ by the end of the assay, indicating that impairment of phagocytosis was not transient. However, we can be absolutely confident of that being the case only under the conditions (time period of co-incubation) we used. Unfortunately, we anticipate experiments involving extended co-incubation times could be problematic to evaluate because evidence of internalized particles would be dependent upon not only the rate of ingestion, but also that of their clearance (i.e. lysosome-mediated destruction). A characteristic of NPC is a block in endolysosome fusion events and maturation (Kaufmann et al., 2009; Platt et al., 2012), which could mean that whilst phagocytosis is reduced, particles that have been internalized persist for a longer period of time, thereby providing an impression of greater phagocytic activity. Accurate and quantitative discrimination between rate of uptake and that of particle destruction within the cell would require different experimental design, such as that described by Panicker *et al* (Panicker et al., 2012).

Other than confirming that multiple phagocytic systems are affected in *Npc1*$^{-/-}$ MΦ *in vitro*, the results presented here do not address the underlying molecular mechanism(s) that may be responsible for the deficiencies. As previously described in Chapter 1, the process of phagocytosis is dependent upon expression of specific receptors on the plasma membrane of the phagocyte that are responsible for particle binding and induction of signaling events that promote re-organisation of the cytoskeleton, which facilitates particle engulfment to form a phagosome. Many publications have demonstrated that removal of receptor availability, such as by antibody blockade (Kurlander, 1983) or genetic deletion (Norsworthy et al., 2004) significantly reduces or ablates specific particle uptake. We therefore examined whether reduced phagocytic activity of *Npc1*$^{-/-}$ RPMΦ might be explained by lower receptor expression. Expression levels, as measured by FACS of FcγRIII and FcγRII, FcγRI and FcγRIIB, which are important for IgG mediated uptake, were unaltered as compared to *Npc1*$^{+/+}$ RPMΦ. However, these data do not exclude the possibility that phagocytosis is compromised at level of phagocytic receptors in NPC. Cholesterol is a major component of the plasma membrane and known to play an essential role in determining its fluidity and architecture, but its distribution and trafficking are affected in NPC (accumulation in late endosome/ lysosome and relative depletion from the plasma membrane (Garver and Heidenreich, 2002; Blom et al., 2003; te Vruchte et al., 2004; Tang et al., 2009; Lloyd-Evans and Platt, 2010; Peake and Vance, 2010). The normally tightly controlled cholesterol (and other lipids) content of the plasma membrane is critical for maintaining ordered segregation of lipid raft microdomains and associated proteins (Simons and Ikonen, 1997). Because successful

completion of phagocytosis is dependent upon receptor motility within the membrane and subsequent confinement at the site of the bound particle (Freeman and Grinstein, 2014) the altered lipid content of NPC cells could affect the biophysical behaviour of phagocytic receptors and inhibit their lateral movement and localization to sites of particle binding. To our knowledge there have been no published studies of individual phagocytic receptor dynamics and movement in NPC cells.

Our data that demonstrated generation of lower levels of specific pro-inflammatory cytokines and ROS by mutant phagocytes were consistent with the reduced phagocytic activities of *Npc1*$^{-/-}$ PMΦ. Induction of the effector molecules is triggered by ingestion of particles via specific phagocytic mechanisms, such as FcγRs, and their production is critical for the elimination of pathogens(Nimmerjahn and Ravetch, 2008).

Because of the significant reduction of phagocytic activities, we found for *Npc1*$^{-/-}$ MΦ we wondered whether it could be a feature shared by myeloid cells of other LSDs. Although we could examine only two other LSDs we did not find evidence of impaired phagocytosis in either. The murine model of GM2 gangliosidosis (*hexb*$^{-/-}$ mice) has an acute disease course that features CNS inflammation(Jeyakumar et al., 2003) and a life span that is only moderately longer than that of *Npc1*$^{-/-}$ mice (15-17 weeks as against 10-13 weeks respectively). We were unable to find evidence of reduced phagocytosis by EPMΦ isolated from symptomatic mice. We also looked at monocyte-derived MΦ generated from Gaucher Disease patients and again were unable to detect a phagocytic phenotype. The latter observation is in agreement with a study of MΦ differentiated from induced pluripotent stem cells generated from Gaucher

Disease patients, which also reported unchanged phagocytic activities (Panicker et al., 2012). Although it is probably unsafe to make definitive statements about the frequency of altered phagocytosis amongst different LSDs, based on a very small sample, we can suggest that it is not likely to be a universal feature of these disorders. What is not obvious however, is whether it may be specific to NPC because of the combination of cellular phenotypes that are unique to the disease. We can presume that accumulation of GM2 ganglioside alone is not sufficient because it occurs in both Sandhoff disease and NPC (Tatematsu et al., 1981; Yamato et al., 2004). However, It might be of interest and potentially informative to examine phagocytosis in related LSDs, such as Niemann Pick Diseases Type A and B, which are similar to NPC because all accumulate sphingomyelin (Lloyd-Evans et al., 2008; Schuchman and Wasserstein, 2015).

Summary:

In summary, our results found a generalized reduction in phagocytic activity in *Npc1*$^{-/-}$ PMΦ that was not restricted to specific pathways of phagocytosis, suggesting inhibition occurred at a point or stage common to all phagocytic mechanisms. Also, we could not find evidence of a comparable reduction in phagocytosis in the other LSDs that we studied, suggesting that impairment may be restricted to NPC. In the next chapter we investigate whether the phagocytic deficit in NPC may be due to changes in the properties of the cytoskeleton and the involvement of particular species of GSLs.

Chapter 4. The Actin Cytoskeleton, GSLs and Phagocytosis.

4.1. Introduction.

Results presented in the two previous chapters confirmed impaired phagocytic activity in both drug-induced and genetically deficient NPC MΦ. Importantly, reduction in phagocytosis was apparent for all of the phagocytic mechanisms we investigated and expression of specific phagocytic receptors such as FcγRs was apparently not affected. These findings imply that perturbation of particle uptake was very likely to occur at a stage in phagocytosis that is common to all mechanisms and very probably downstream of individual receptor type. We therefore sought to identify the common point of convergence and its possible relationship with the other cellular phenotypes characteristic of NPC.

Several lines of evidence prompted us to focus on cytoskeletal defects and alterations in GSL metabolism in NPC. First, as outlined in Chapter 1, remodeling of the actin cytoskeleton is essential for completion of phagocytosis (May and Machesky, 2001). Second, Allie Colaco, a D.Phil student working in the Platt Lab (University of Oxford, Department of Pharmacology), performed an unbiased genetic screen to identify binding partners for the yeast orthologue of NPC1 (Ncr1) and identified several cytoskeletal or cytoskeleton-associated proteins (data not shown). Third, during the course of the microscopy-based *in vitro* phagocytosis assays we discerned a clear difference in the appearance of the actin cytoskeleton between resting *Npc1*$^{+/+}$ and *Npc1*$^{-/-}$ EPMΦ when

visualized with fluorescently conjugated phalloidin. Finally, multiple investigations have demonstrated that lipid metabolism is key for normal phagocytosis (Steinberg and Grinstein, 2008). Although as far as we are aware there is no published evidence of changes in NPC to phospholipid species (such as specific phosphatidylinositol phosphates) that are known to be important signaling intermediates in phagocytosis, the distribution of cholesterol is profoundly altered in NPC (Peake and Vance, 2010). In normal cells cholesterol is differentially distributed to the plasma membrane where it is critical for establishment of membrane micro-domains (lipid rafts) that are required for signal transduction and membrane trafficking, whereas in NPC cells cholesterol is relatively depleted from the plasma membrane as a result of its accumulation in the lysosome (Ioannou, 2005; Peake and Vance, 2010). The levels and intracellular distribution of GSLs are also profoundly altered in NPC cells (Lloyd-Evans and Platt, 2010) but there have been relatively few reports of the role of these lipids in phagocytosis. In this chapter we therefore describe investigations into the cytoskeleton and GSLs in *Npc1*$^{-/-}$ MΦ.

4.2. Materials and Methods.

4.2.1. Cells.

RAW 264.7 cells and mouse EPMΦ (*Npc1*$^{+/+}$ and *Npc1*$^{-/-}$) were obtained and cultured as described in Section 2.2.2 and Section 3.2.4.2 respectively. RAW 264.7 cells were treated with U18666A as described in Section 2.2.3.

4.2.2.1. Visualisation of actin by microscopy.

Imaging of the cytoskeleton was performed with assistance from Dr. Esther Garcia at the Weatherall Institute of Molecular Medicine, John Radcliffe Hospital, Oxford. EPMΦ were plated onto 13 mm glass coverslips, fixed with 4% (w/v) PFA for 10 min on ice. Actin was stained using CytoPainter F-actin Staining Kit (Abcam) according to the manufacturer's instructions. Images were collected using a Zeiss 510 inverted confocal microscope.

4.2.2.2. Nuclear Staining.

Nuclei were stained by 5 min incubation with 0.33 µg/mL Hoechst nuclear stain (Life Technologies) at room temperature. Alternatively, a staining solution made up of 40 µl HCS Nuclearmask^{TM} (ThermoFisher) in 10 mL of R10 medium was prepared and added to MΦ on coverslips at a concentration of 100 µl/ well for 30 min followed by fixation with 4% PFA.

4.2.3. Particle binding assay.

To examine particle binding by MΦ, we prepared IgG opsonized sRBC and IgG opsonized 3 µm polystyrene beads. MΦ plated onto glass coverslips were overlaid with IgG-sRBC or beads and incubated on ice to prevent particle uptake for <30 min. The coverslips were gently washed with ice-cold R10 to remove unbound IgG-sRBC, fixed and examined by confocal microscopy for evidence of rosettes, consisting of multiple IgG-sRBC bound to a central MΦ. Alternatively, phagocytosis was inhibited by pre-treatment of MΦ with cytochalasin D before addition of IgG-sRBC or beads. The number of rosettes formed by a minimum of 200 MΦ was determined.

4.2.4. Assay of phagocytic cup formation.

Latex beads (3 μm diameter) (Sigma-Aldrich) were opsonized with 0.5 mg/mL human IgG (Sigma-Aldrich) for 12h at room temperature, washed with PBS extensively, and suspended in RPMI1640 containing 1% FCS and 10 mM 3-methyladenine (3-MA) (Cambridge Biosciences). These experiments were performed initially using RAW 264.7 MΦ and repeated using *Npc1*$^{-/-}$ and *Npc1*$^{+/+}$ EPMΦ. Identical procedures were followed for each cell type. MΦ were plated onto glass coverslips, placed in 6-well culture plates and were incubated in pre-warmed serum-free medium containing 10 mM 3-MA for 30 min at 37 °C. The culture medium was removed and cells overlaid with 0.5 mL of ice-cold opsonized latex bead suspension at a MOI of 10-50 beads per MΦ and incubated at 4 °C for 10 min to permit binding of beads.

Formation of phagocytic cups was initiated by the addition of 1.5 mL of pre-warmed RPMI1640 containing 1% FCS and 10 mM 3-MA, and cells were incubated at 37 °C for a further 15 min. Phagocytic cup formation was stopped by fixation in 4% (w/v) paraformaldehyde for 10 min, and cells were permeabilized and blocked with PBS 0.1% (w/v) saponin and 1% (w/v) bovine serum albumin for 5 min. Phagocytic cups were visualized by F-actin staining with Alexa 568-phalloidin (Invitrogen) and examined under a fluorescence microscope (Zeiss 510 inverted confocal). To quantify phagocytosis and phagocytic cup formation, we scored percentage of cells with evidence of ingestion and the frequency of cells with phagocytic cups. A minimum of 200 cells were analyzed for each condition.

4.2.5. Preparation of opsonised polystyrene particles.

Described previously in Section 2.2.9. In specific experiments non-internalised 3 μm IgG opsonised polystyrene beads were identified by staining with Alexa 594, anti-IgG antibody (Polysciences) at a 1:1000 dilution for 30 min on ice prior to fixation

4.2.6. Phagocytosis assay.

Phagocytosis assay is described in Section 2.2.11.

4.2.7 Live cell imaging of phagocytosis.

This was performed at the Weatherall Institute of Molecular Medicine at John Radcliffe Hospital, Oxford UK with the assistance of Dr. Esther Garcia. A Zeiss 780 inverted confocal microscope was used to perform analysis, with environmental chamber pre-heated to 37^{o}C. MΦ plated onto coverslips were placed in glass chambers 6h prior to analysis. To initiate each experiment, 1x10^{6} polystyrene beads were added and intensity of the FITC signal was adjusted. Images were collected at intervals of 30s for a period of 30 min.

4.2.8. Measuring phasosomal/ lysosomal fusion.

Coverslips plated with MΦ were loaded overnight in 24 well plates with 50 μg/mL of Hydrazide Alexa 594 in RPMI +L929 (25 μg/mL). The following day, hydrazide was removed from coverslips and washed 3x with PBS. Coverslips were incubated in fresh media for up to 12h (5h, 8h, 12h) to chase hydrazide to the lysosome. Cells were fixed with 4% PFA in PBS for 10 min at RT. Aldehyde groups were quenched using 100 mM glycine in PBS for 20 min. Cells were permeabilised using PBS with 5% goat serum and 0.1% saponin (0.22 μm filtered) at RT for 30 min. Coverslips were then stained with anti-

LAMP-1 (1/100) in PBS with 5% goat serum and 0.1% saponin for 1h RT followed by wash (3x) with PBS+0.01% saponin. Coverslips were mounted with prolong gold overnight and analysed by microscopy.

4.2.9. Intracellular distribution of lipid species.

4.2.9.1. Localisation of GM1 with cholera toxin B (CtxB).

Coverslips plated with MΦ were washed twice with cold R10 prior to incubation with 2 µg/mL fluorescently labelled CtxB in R10 for 30 min at room temperature Media was removed and replaced with fresh R10 and incubated for 2h at 37ºC. Post-incubation coverslips were washed with 3 x 1mL 1% bovine serum albumin (BSA) (Sigma-Aldrich) in PBS

4.2.10. GSL analysis.

4.2.10.1. Extraction and purification of GSLs.

Cell pellets were homogenised in 0.55 mL Milli-Q water. Lipids were extracted according to (Svennerholm and Fredman, 1980). 2 mL chloroform: methanol, 1:2 (v/v) was added to 0.5 mL of aqueous homogenate to the ratio of chloroform: methanol: water, 4: 8: 3 (v/v/v) and were extracted by gently spiramixing at room temperature for 3h. Samples were centrifuged at 1,000g for 10 min. Tissue pellets were discarded and supernatants were transferred to fresh tubes and 0.5 mL PBS and 0.5 mL volume of chloroform were added. After vortexing, samples were centrifuged at 1,000g for 10min to achieve phase separation. The lower phase was removed to a new tube, dried down under a stream of nitrogen and re-suspended in 50 µl of chloroform: methanol, 1: 3 (v/v). The re-dissolved lower phase was added to and mixed with the upper phase again. The extracted lipids were then purified using SepPak C18 columns (Waters) according to (Neville et al., 2004). C18 columns were pre-equilibrated

with 4 x 1 mL methanol and 2 x 1 mL water. Combined phase lipid extract was applied to the column and washed with 4 mL water. Total GSLs were eluted in 1 mL chloroform: methanol, 98: 2 (v/v), 2 mL chloroform: methanol, 1:3 (v/v) and 1 mL methanol. Purified GSLs from cells were concentrated by drying under nitrogen, re-suspended in a smaller volume of chloroform: methanol, 2: 1 and re-dried again.

4.2.10.2. Ceramide glycanase digestion.

Dried GSLs were re-dissolved in 90 µl sodium acetate buffer (50 mM sodium acetate, 1 mg/mL sodium taurodeoxycholate, pH 5.0) containing 2 µl endoglyoceramidase (prepared *in house* from the medicinal leech *Hirudo medicinalis*/*verbenA)* and gently mixed. Enzyme-GSL mix was incubated at 37°C for 16h.

4.2.10.3. 2-Anthranilic acid (2AA) labeling.

Released oligosaccharides were fluorescently labelled with 2AA as described (Anumula and Dhume, 1998), with the following modifications. 310 µl of labelling mixture (30 mg/mL 2AA, 45 mg/mL sodium cyanoborohydride, 4% sodium acetate trihydrate (w/v) and 2% boric acid (w/ v) in methanol) were added to the digested samples and heated to 80°C for 60min. Labelled oligosaccharides were cooled to room temperature before addition of 3 mL of acetonitrile: water, 97: 3. Unconjugated 2AA was removed over an amide column (Neville et al., 2009). Discovery DPA-6S columns (Supelco) were pre-equilibrated with 1 mL acetonitrile, 2 mL water, and 2 mL acetonitrile sequentially, before labelled sugars in acetonitrile/water mix were loaded. Free 2AA was removed by washing with 4 mL acetonitrile: water, 95: 5. Purified

labelled oligosaccharides were eluted with 0.6mL Milli-Q water and stored at −20 °C.

4.2.11. Normal Phase High-Performance Liquid Chromatography (NP-HPLC).

Purified 2AA-labelled oligosaccharides were separated and quantified by Normal Phase High-Performance Liquid Chromatography (NP-HPLC) as described (Neville et al., 2004). The solid phase was a 4.6 x 250mm TSK gel-Amide 80 column (Anachem, Luton, UK) and HPLC system consisted of a Waters Alliance 2695 separations module with an in-line Waters 2475 multi λ-fluorescence detector set at Exλ 360nm and Emλ 425nm. All chromatography was performed at 30°C. Solvent A was 100% acetonitrile, solvent B was 100% Milli-Q water and solvent C was 100 mM ammonium acetate hydroxide pH 3.85 with acetic acid. Data were collected and processed using Empower software. Individual GSLs were identified by their glucose unit values determined following comparison with a 2AA-labelled glucose oligomer ladder, derived from a partial hydrolysate of dextran. Finally, the measured amount of GSLs of each sample was standardised to protein concentration of the corresponding sample.

4.2.12. Measurement of protein concentration.

Protein concentrations were determined using the BCA protein assay (Sigma-Aldrich) according to manufacturer's instruction. Briefly, a working solution was prepared, and added to a multiwall plate at a volume of 100μl/well, a gradient volume is standard protein was added to each well (2mg/mL) and sample protein was added to each well (5μl/well). The plate was incubated at 37ºC for 30 min and absorbance was measured at 562nm on a plate reader.

4.2.13. Addition of exogenous lipids to EPMΦ in culture.

3M Lipid stocks were prepared in sodium acetate buffer (0.05M, pH 5) and diluted with R10 media and added to cells to a final concentration of 3 μM, and incubated at 37^{o}C, 5% CO_2 for defined periods.

4.2.14. Statistics.

Statistical analyses were performed using GraphPad Prism (GraphPad Software). Specific descriptions of statistical analysis for each experiment are listed in figure legends.

4.3. Results.

4.3.1. Reduced binding of IgG-sRBC and IgG opsonised polystyrene beads by U18666A-treated RAW 264.7 and *Npc1*$^{-/-}$ EPMΦ.

The initial event in the process of phagocytosis is receptor-dependent binding or tethering of the particle by the phagocyte, prior to internalization (Diakonova et al., 2002). MΦ bind erythrocytes to form a cluster of erythrocytes surrounding the central phagocyte, known as an erythrocyte rosette (Ribacke et al., 2013). Fluorescently labelled particles were used to determine the extent of binding by EPMΦ.

The analysis was intially performed using U18666A-treated RAW 264.7 MΦ where we performed a rosetting assay to look for particle recogntion and adherance. Cells (200) were analysed for the presence of rosettes (>5 bound IgG-sRBC per MΦ). 64.6% of control RAW 264.7 MΦ formed rosettes as compared to 34.1% of U18666A-treated RAW 264.7 MΦ (**Fig. 4.1**).

The study was repeated with *Npc1*$^{+/+}$ and *Npc1*$^{-/-}$ EPMΦ using both IgG-sRBC and IgG opsonised 3 μm polystyrene beads. Whilst 67.3% of *Npc1*$^{+/+}$ EPMΦ formed rosettes of IgG-sRBC, they were observed for only 29.7% of *Npc1*$^{-/-}$ EPMΦ (p=0.00053). Although rosettes of 3 μm polystyrene beads were less well defined than those of IgG-sRBC, 79.3% of *Npc1*$^{+/+}$ EPMΦ showed evidence of adherance of beads, compared to 19.3% for *Npc1*$^{-/-}$ EPMΦ (p=0.00037). (**Fig. 4.2 and Fig. 4.3**).

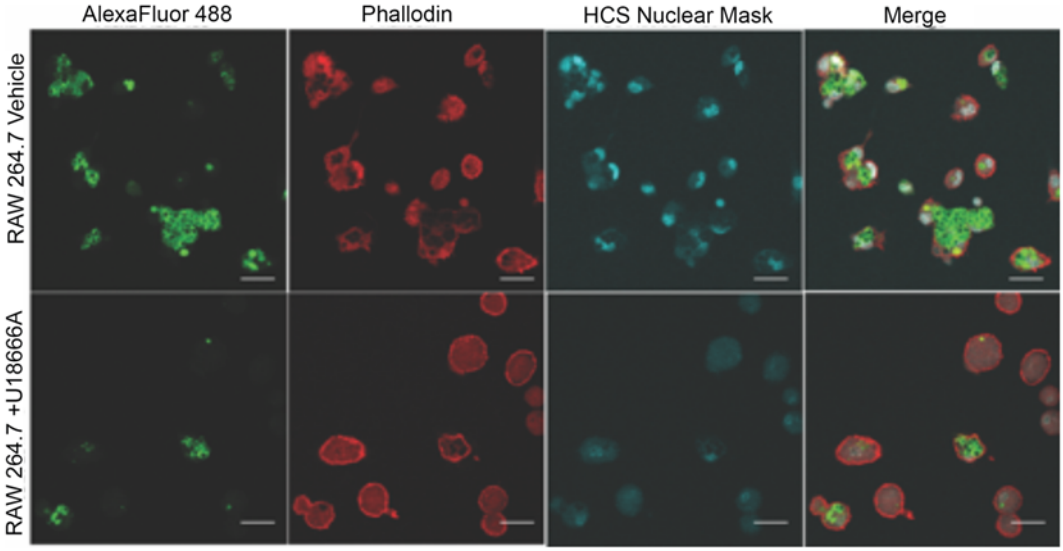


Figure 4.1 U18666A-treated RAW 264.7 MΦ show reduced formation of IgG-sRBC rosettes: Vehicle-treated RAW 264.7 MΦ (upper panel) and U18666A-treated RAW 264.7 MΦ (lower panel) were incubated with IgG-sRBC and examined for the extent of IgG-sRBC rosette formation. U18666A-treated MΦ displayed significantly reduced binding and few rosettes. Scale bar= 5 μm, 63X. Green = Celltracker™ green; red = phalloidin; blue = HCS Nuclear Mask.

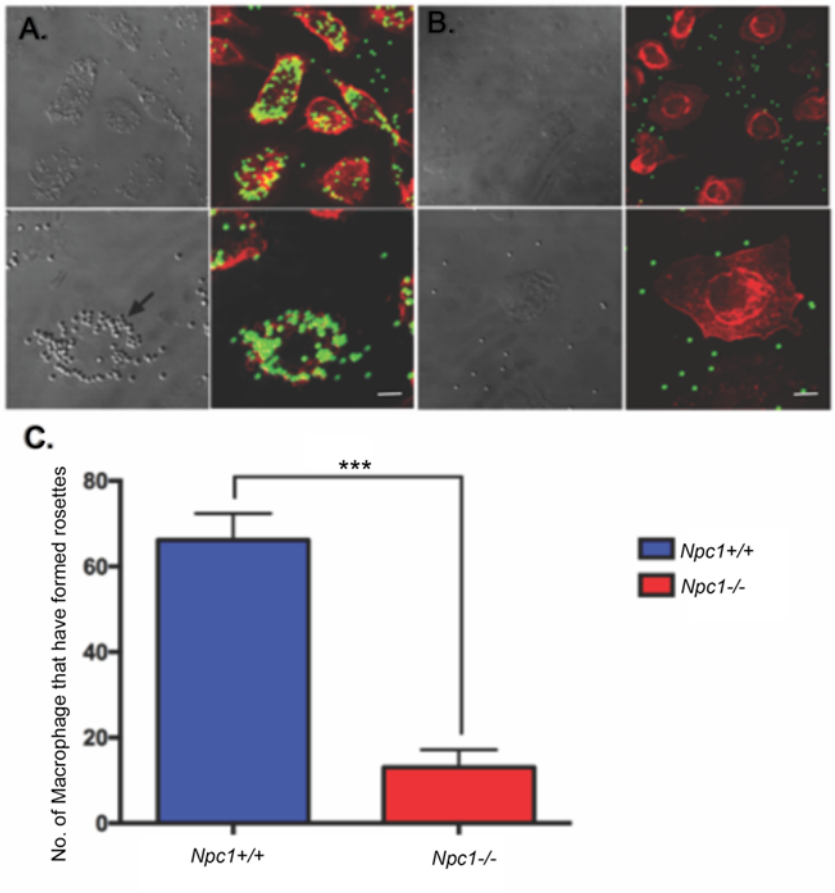


Figure 4.2 Fewer IgG-sRBC rosettes are formed with *Npc1*$^{-/-}$ EPMΦ than with *Npc1*$^{+/+}$ EPMΦ: (A) *Npc1*$^{+/+}$ and **(B)** *Npc1*$^{-/-}$ were incubated with IgG-sRBC (green) and examined for rosette formation (black arrow). *Npc1*$^{-/-}$ EPMΦ showed significantly less binding and few rosettes. Red = phalloidin. Scale bar = 5μm, 63x. **(C)** *Npc1*$^{-/-}$ EPMΦ (red column) display significantly decreased formation of rosettes as compared to *Npc1*$^{+/+}$ EPMΦ (blue column). Data presented as mean ± SD N=2 ***p<0.001 (student's t-test with Welch's correction). Data is representative of 3 independent experiments with a minimum of 200 MΦ considered for each group.

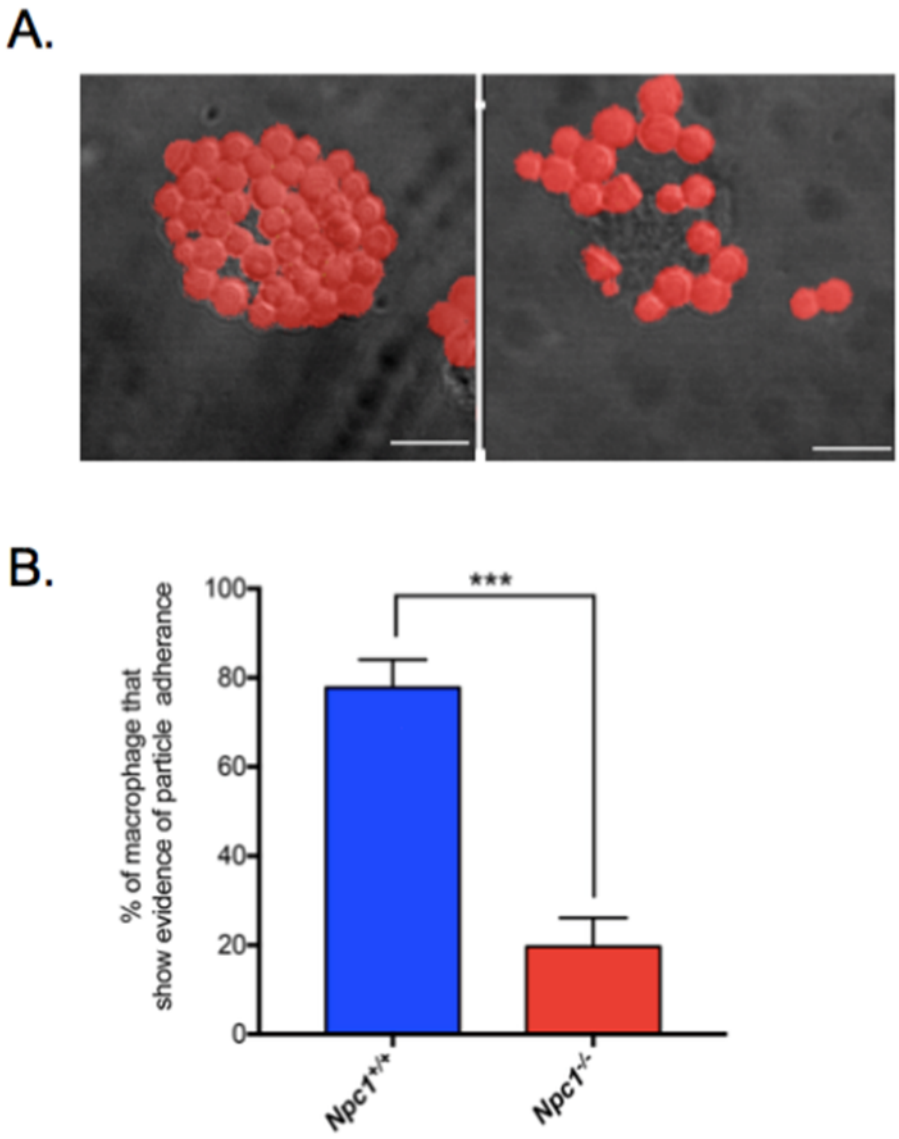


Figure 4.3 *Npc1*$^{-/-}$ EPMΦ display decreased binding of IgG opsonised polystyrene beads: (A) EPMΦ (top panel) were incubated on ice with IgG opsonised 3 μm beads (red). *Npc1*$^{-/-}$ EPMΦ (right panel) display significantly less binding of beads than *Npc1*$^{+/+}$ EPMΦ (right panel). The distribution of actin on *Npc1*$^{+/+}$ (left panel) and *Npc1*$^{-/-}$ (right panel) EPMΦ. Red = 3μm polystyrene beads. Scale bar = 10 μm. (B) Quantification of adherent particles. *Npc1*$^{-/-}$ EPMΦ bind significantly fewer beads than *Npc1*$^{+/+}$ EPMΦ (blue column). Data presented as mean ±SD N= 2, ***p<0.001, (student's t-test with Welch's correction). Data is representative of 3 independent experiments.

4.3.2 Formation of phagocytic cups by *Npc1*$^{-/-}$ EPMΦ and U18666A-treated RAW 264.7 MΦ is impaired.

As described in Chapter 1, during FcγR-mediated phagocytosis the cytoskeleton is remodeled by F-actin nucleation and polymerization to facilitate extension of pseudopods to surround the particle (May and Machesky, 2001). During this process there occurs transient invagination of the plasma membrane and localized accumulation of filamentous actin beneath the particle ("phagocytic cup"), which dissolves once the material is internalized into the phagosome. The appearance of phagocytic cups can be visualized by staining with fluorescently conjugated phalloidin, a fungal toxin that binds specifically to F-actin (Berepiki et al., 2011). We therefore analysed for the frequency of phagocytic cup formation in *Npc1*$^{+/+}$ and *Npc1*$^{-/-}$ EPMΦ and vehicle-treated and U18666A-treated RAW 264.7 MΦ incubated with IgG-opsonised latex beads (**Fig. 4.4** and **Fig. 4.5**). Although phagocytic cups were seen to form in both *Npc1*$^{+/+}$ and *Npc1*$^{-/-}$ EPMΦ and vehicle and U18666A-treated RAW 264.7 MΦ there were significantly fewer in U18666A-treated RAW 264.7 MΦ (p=0.031) and *Npc1*$^{-/-}$ EPMΦ (p=0.0022) (**Fig 4.4 and 4.5**).

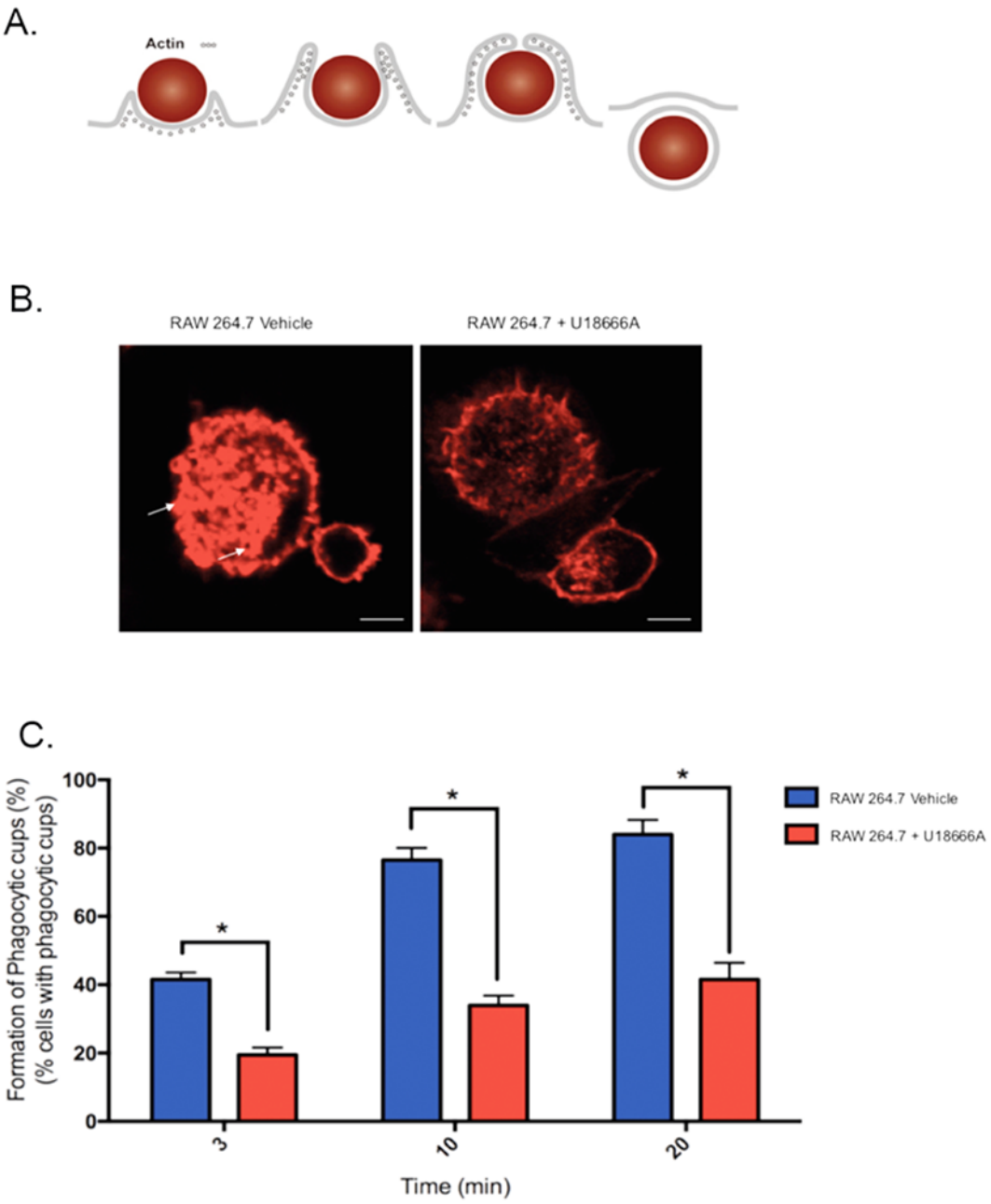


Figure 4.4 Abnormal phagocytic cup formation in U18666A-treated RAW 264.7 MΦ: (A) Cartoon of phagocytic cup formation, figure adapted from (Egami et al., 2011) **(B)** Vehicle-treated RAW 264.7 MΦ (left image) with a large number of visible phagocytic cups (white arrows); U18666A-treated RAW 264.7 MΦ (right image) has few obvious phagocytic cups. Scale bar= 10μm, 63x. **(C)** Histogram of frequency of phagocytic cups in RAW 264.7 MΦ (vehicle and U18666A-treated) determined by microscopy. Data presented as mean ± SD for 3 replicates per condition. *p<0.05, versus control (via student's t-test with Welch's correction)

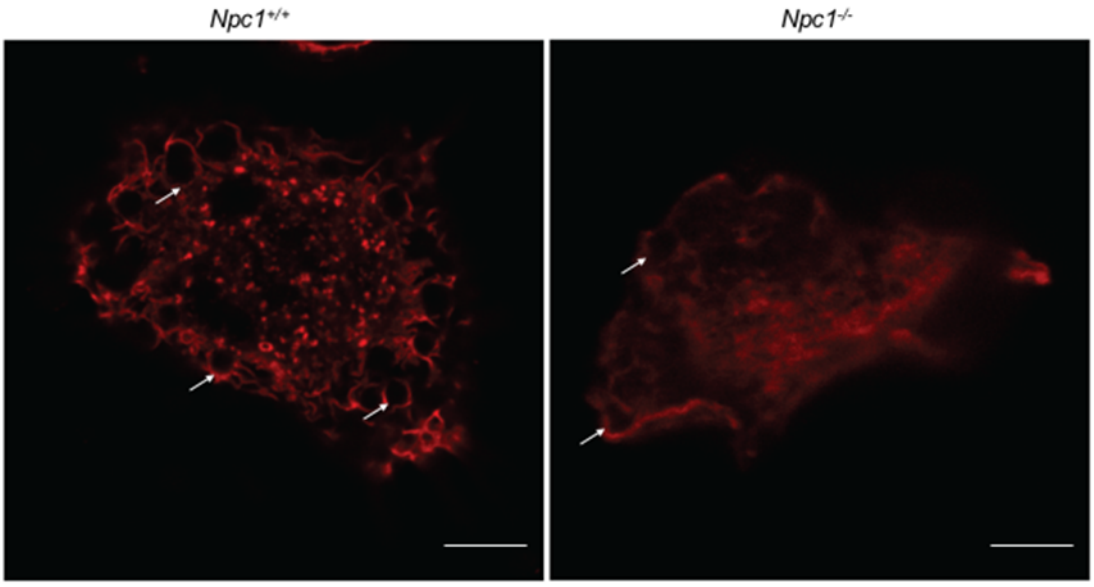


Figure 4.5 Impaired phagocytic cup formation in *Npc1*$^{-/-}$ EPMΦ: *Npc1*$^{+/+}$ EPMΦ (left image) with a large number of visible phagocytic cups (white arrows);*Npc1*$^{-/-}$ EPMΦ (right image) has few obvious phagocytic cups. Scale bar =10 μm, 100x.

4.3.4 Live cell microscopy confirms altered F-actin dynamics during phagocytic cup formation in NPC MΦ.

We used live cell confocal imaging to examine actin dynamics in formation of phagocytic cups during polystyrene bead binding and ingestion. For *Npc1*$^{+/+}$ EPMΦ we were able to observe recruitment and concentration of F-actin at the base of the cup concurrent with binding of the bead, sustained actin staining during the period of plasma membrane extension to surround the particle and then dissipation of F-actin from the cup with completion of cup closure and generation of the phagosome **(Fig. 4.6)**. In contrast, when analyzing *Npc1*$^{-/-}$ EPMΦ although actin polymerization occurred at the membrane at the point of bead binding, and pseudopod extensions were visible, the observation of actin

remodeling marking internalisation and formation of the phagocytic cup was much weaker , less defined, and occurred at a slower rate **(Fig. 4.6)**.

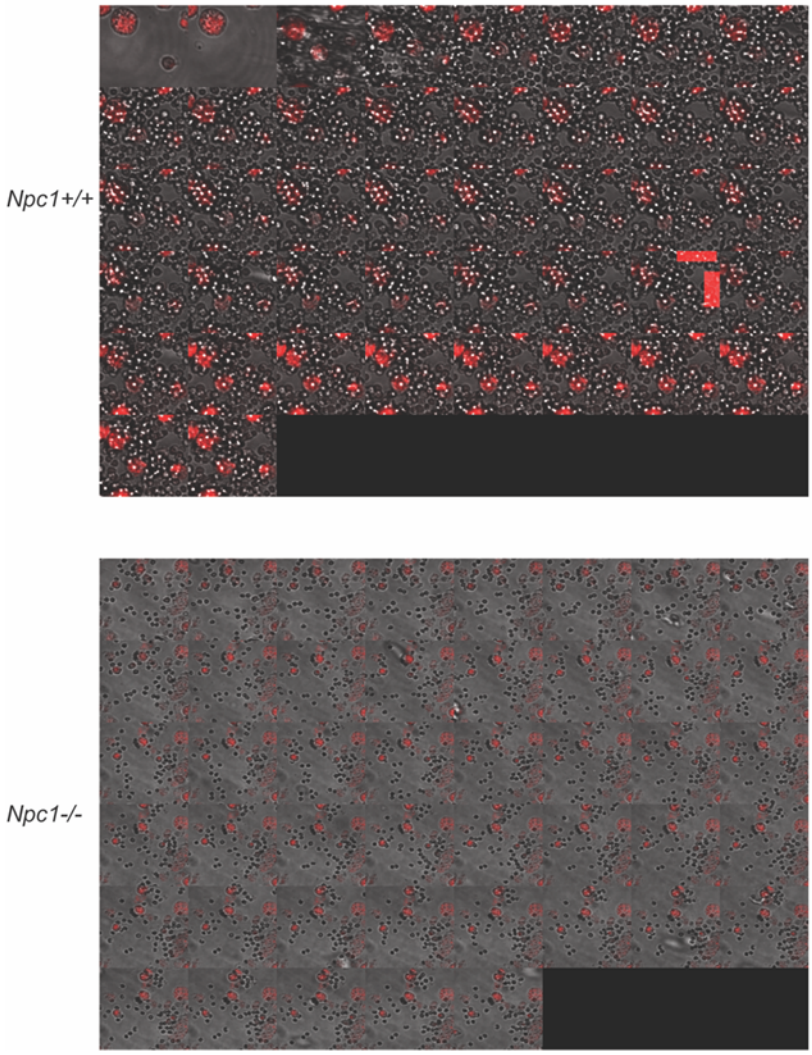


Figure 4.6 Compilation of Live Cell Microscopy: Top row: *Npc1*$^{+/+}$ EPMΦ sections showing rearrangement of actin to internalize an opsonised bead rapidly. Bottom row: A comparable segment of video images showing actin in *Npc1*$^{-/-}$ following exposure to IgG opsonised bead. In the *Npc1*$^{-/-}$ video we see less rapid organization of actin, fewer pseudopod extensions, and less formation of phagocytic cups in video analysis. Red=Phallodin. Beads=colourless.

4.3.5 Accumulation of GSLs and defective lipid trafficking in *Npc1*$^{-/-}$ EPMΦ.

The phenotype of NPC cells includes accumulation and mistrafficking of cholesterol and a variety of other lipid species within the endolysosomal system (Peake and Vance, 2010). However, the profile of GSL species that accumulate is dependent upon cell type. We performed GSL analyses of *Npc1*$^{+/+}$ and *Npc1*$^{-/-}$ EPMΦ. Representative HPLC profiles are shown in **Fig. 4.7**. In *Npc1*$^{-/-}$ EPMΦ we were able to detect a significant increase in the amounts of the most abundant GSLs, GM1a, GD1a and GA1 (**Fig**. **4.7**). Levels of GM1a and GA1 in *Npc1*$^{-/-}$ EPMΦ were approximately 2-fold higher than for *Npc1*$^{+/+}$ EPMΦ (**Fig. 4.7**).

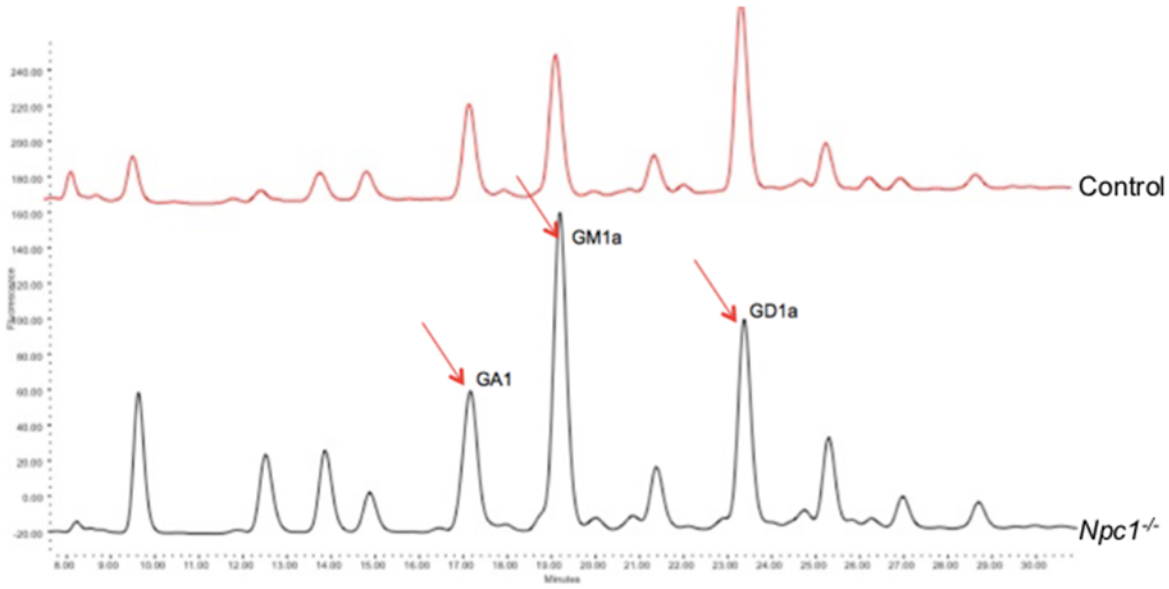


Figure 4.7 Representative GSL HPLC Traces from *Npc1*$^{+/+}$ and *Npc1*$^{-/-}$ EPMΦ: EPMΦ from *Npc1*$^{-/-}$ mice. Major GSL species are indicated. *Npc1*$^{-/-}$ EPMΦ Higher GA1, GM1a, and GD1a peaks (red arrows) seen in *Npc1*$^{-/-}$ EPMΦ compared to *Npc1*$^{+/+}$ (not shown).

4.3.6 Abnormal phagosome/ lysosome fusion allows for GM1 accumulation in the endolysosome thus depleting GM1 from the plasma membrane of *Npc1*$^{-/-}$ EPMΦ.

Phagosome/lysosome fusion is a key step in phagocytosis and particle elimination (Swanson, 2002; Flannagan et al., 2012). We observed decreased phagosome/ lysosome fusion in *Npc1*$^{-/-}$ by chasing hydrazide to the lysosome (**Fig. 4.8**). We found evidence of delayed overlap between the lysosome and hydrazide, where in *Npc1*$^{+/+}$ samples the overlap occurred in a standard 8h chase, in *Npc1*$^{-/-}$ overlap was not noticeable until a 24h chase, indicating delayed or defective fusion of the phagosome/ lysosome in NPC.

Mistrafficking and impaired re-cycling of GSLs in NPC cells results in their accumulation within the endolysosome and their relative depletion from other cellular compartments (Lloyd-Evans and Platt, 2010). We determined the relative distribution of GM1 in *Npc1*$^{-/-}$ and *Npc1*$^{+/+}$ EPMΦ by confocal microscopy. Analyses of fixed and permeabilised NPC cells stained with fluorescently conjugated CtxB. (**Fig. 4.8)** showed intracellular accumulation of GM1.

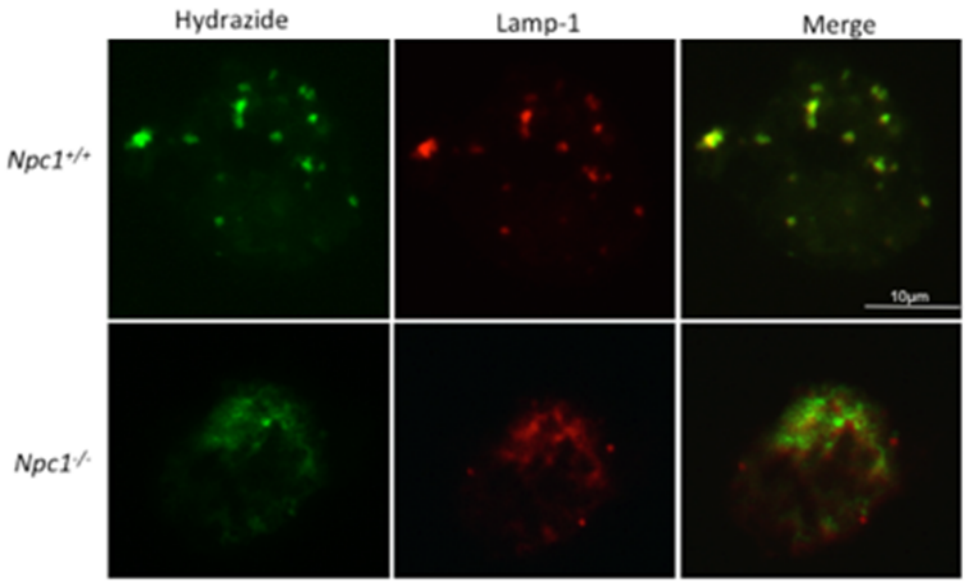


Figure 4.8 Hydrazide trafficking appears delayed in *Npc1*$^{-/-}$ EPMΦ: Phagosomal/lysosomal fusion is a key end step in the process of phagocytosis. To analyze fusion of the phagosome to the lysosome, we analyzed EPM from *Npc1*$^{+/+}$ and *Npc1*$^{-/-}$ mouse to confirm hydrazide localization. EPMΦ were incubated with Hydrazide A594 overnight, washed and fixed with PFA (4%), and stained with LAMP-1 (primary antibody) for a 6h chase, and anti-rat 488 (secondary antibody). Overlap of hydrazide (green) and LAMP-1 (red) is indicative of normal phagosomal/lysosomal fusion. Overlap occurred equally in both *Npc1*$^{+/+}$ and *Npc1*$^{-/-}$ MΦ, however in *Npc1*$^{-/-}$ overlap occurred at a much longer chase time.

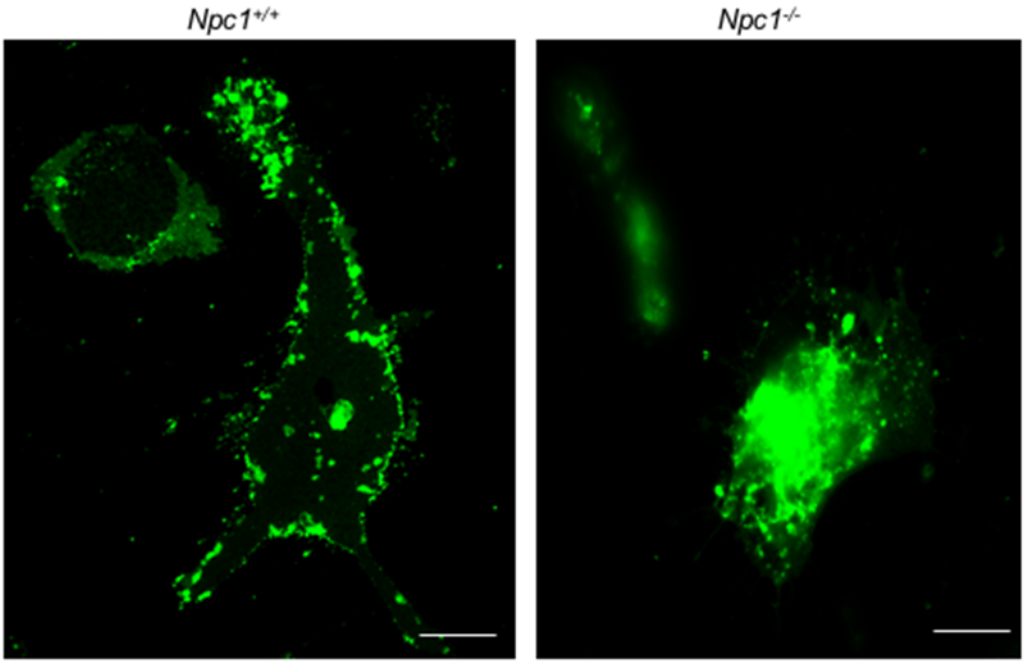


Figure 4.9 Plasma membrane associated GM1 is reduced in NPC: Cell surface staining of EPMΦ with CtxB. *Npc1*$^{+/+}$, and *Npc1*$^{-/-}$ cells were incubated with CtxB-Alexa488 for 30 min on ice and imaged with a Zeiss inverted microscope. Internalized GM1 is more concentrated in *Npc1*$^{-/-}$ EPMΦ, whereas *Npc1*$^{+/+}$ have increased concentration GM1 on plasma membrane (bright green). Scale bar = 2 μm, 63x.

4.3.7 Exogenous GM1 ganglioside increases the level of plasma membrane-associated GM1 in *Npc1*$^{-/-}$ EPMΦ.

We tested whether addition of exogenous GM1 ganglioside to the culture medium could increase the level of GM1 associated with the plasma membrane of *Npc1*$^{-/-}$ EPMΦ. This method was adapted from Tafesse *et al*. (Tafesse et al., 2015) and was used for rationale behind addition of GM1. Following addition of GM1 for 1h, we saw an increase in GM1 associated with the plasma membrane (**Fig. 4.10**). GM1 was added exogenously to cell media. After 30 min, *Npc1*$^{-/-}$ showed less accumulation of GM1 within the cell and showed more evidence

of GM1 on the surrounding membrane indicating addition of GM1 was partially correcting GM1 at the plasma membrane (Fig. 4.9).

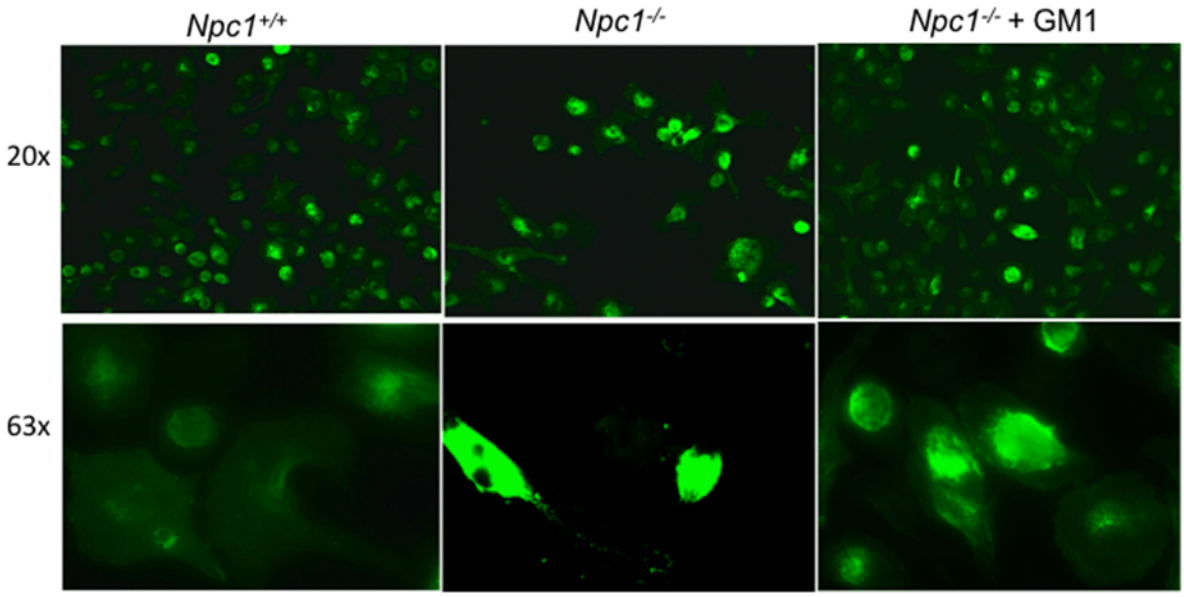


Figure 4.10 Exogenous GM1 partially restores plasma membrane- associated GM1 in *Npc1*$^{-/-}$ EPMΦ: *Npc1*$^{+/+}$ (left panels), *Npc1*$^{-/-}$ (center panels) and *Npc1*$^{-/-}$ EPMΦ treated with GM1 for 1h (right panels) were incubated with CtxB-Alexa 488 for 30 min on ice and imaged with a Zeiss inverted microscope. *Npc1*$^{-/-}$ cells show high level of internal GM1 and little associated with the plasma membrane as compared to *Npc1*$^{+/+}$ EPMΦ; exogenous ganglioside partially restores the level of plasma membrane GM1 in *Npc1*$^{-/-}$ cells. 63x.

4.3.8 Addition of exogenous GM1 partially corrects phagocytic activities in *Npc1*$^{-/-}$ EPMΦ

We hypothesized that diminished levels of GM1 in the plasma membrane might be responsible for the reduced phagocytic activity of *Npc1*$^{-/-}$ EPMΦ based on a literature review of lipid biosynthesis and phagocytosis (Tafesse et al., 2015). We therefore added exogenous GM1 ganglioside, incubated for 30 min and

then co-incubated with IgG-opsonised 3 μm fluorescent polystyrene beads to test whether increasing the GM1 content of the membrane could affect phagocytosis. As can be seen in **Fig. 4.11**, there was a statistically significant increase in phagocytic activity of GM1-treated cells at 5 min (p=0.0013), 10 min (p=0.0034) and 20 min (p=0.010) relative to untreated *Npc1*$^{-/-}$ EPMϕ (**Fig.4.10**).

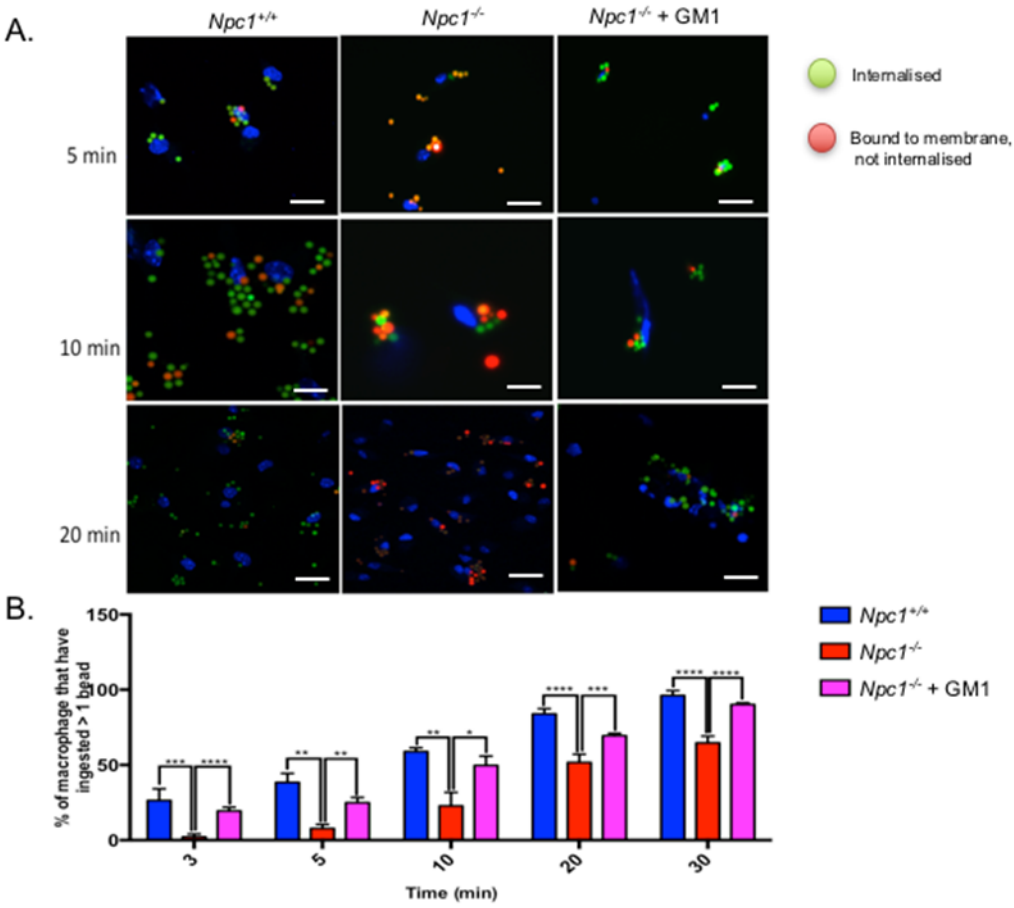
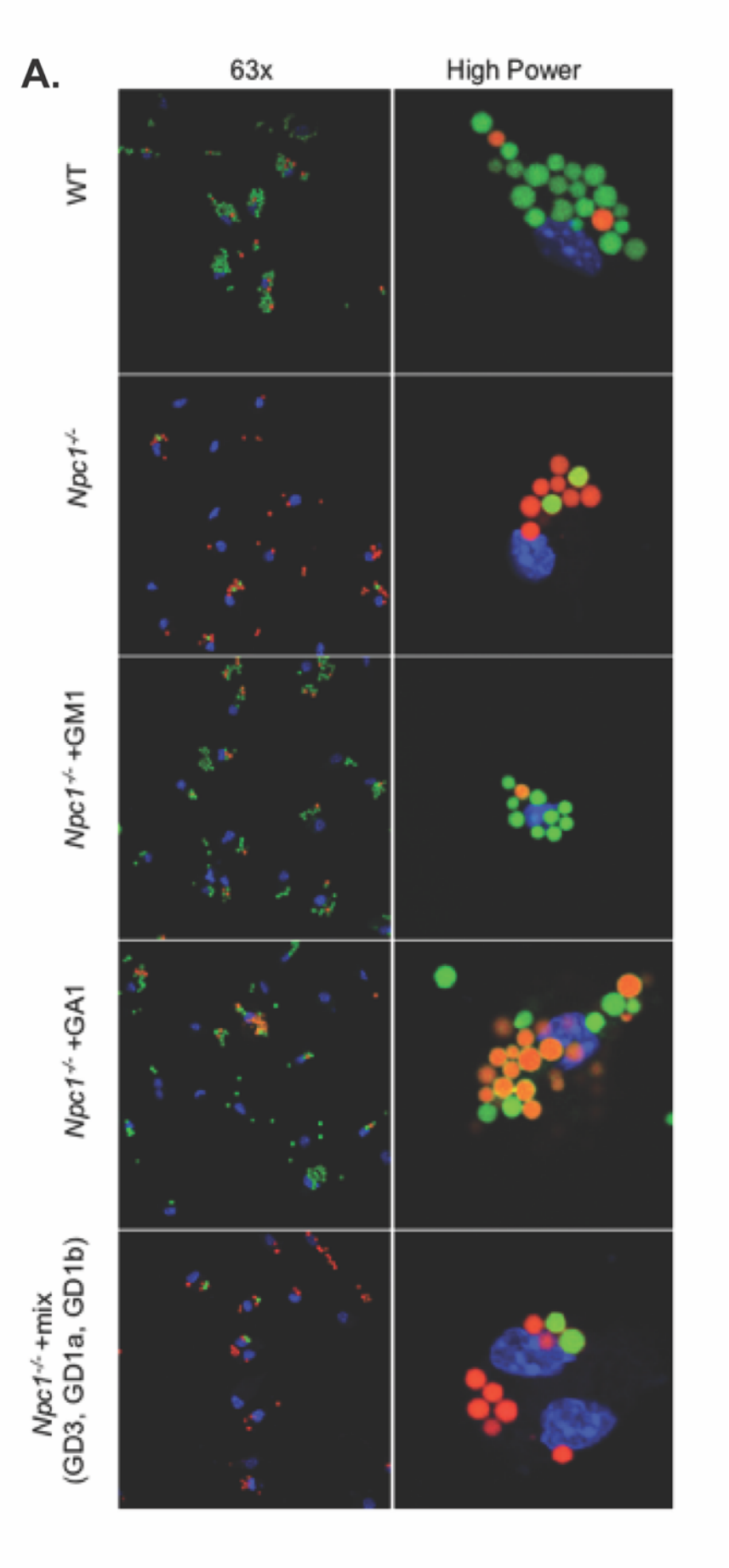


Figure 4.11 Extracellular addition of GM1 partially restores phagocytic activity in *Npc1*$^{-/-}$ EPMΦ. (A) Images of *Npc1*$^{+/+}$ (left panels), *Npc1*$^{-/-}$ (centre panels) and *Npc1*$^{-/-}$ + GM1 (right panels) EPMΦ co-incubated with IgG-opsonized 3 μm polystyrene beads for indicated times. Green = beads that have been internalized, Red = beads remaining bound to plasma membrane (counter stained with Alexa-594), Blue = Hoescht nuclear stain. Images collected with Live cell Olympus confocal microscope. Scale bar = 5 μm,63x. **(B)** Exogenous GM1 addition to *Npc1*$^{-/-}$ EPMΦ (pink columns) significantly enhances phagocytosis as compared to control *Npc1*$^{-/-}$ EPMΦ (red columns). Phagocytosis by *Npc1*$^{+/+}$ cells is shown as blue columns. Data is presented as mean ± SD where a minimum of 200 EPMΦ in triplicate were counted for each treatment. N=5 $^{**}p<0.001$, $^{*}p<0.05$. $^{***}p<0.001$ versus *Npc1*$^{-/-}$ EPMΦ (via *t*-test with Welch's correction).

4.3.9 Impact of exogenous additions of GSLs on phagocytosis

4.3.9.1 Exogenous GM1, but not GA1 or a cocktail of GM3, GD1a and GD1b, partially restores phagocytic activity in *Npc1*$^{-/-}$ EPMΦ.

We next examined whether addition of related GSLs or combinations of GSLs (**Table 4.1**) could also augment phagocytosis by *Npc1*$^{-/-}$ EPMΦ. The binding and phagocytosis of IgG opsonised 3 μm polystyrene beads by lipid-treated cells was analysed by fluorescent microscopy **(Fig. 4.12)**. GA1 had no appreciable effect on phagocytosis, nor did addition of a mixture of GSLs that included GM3, GD1a and GD1b (**Fig. 4.12**).


A.
63x
High Power
WT
Npc1-/-
Npc1-/- +GM1
Npc1-/- +GA1
Npc1-/- +mix
(GD3, GD1a, GD1b)

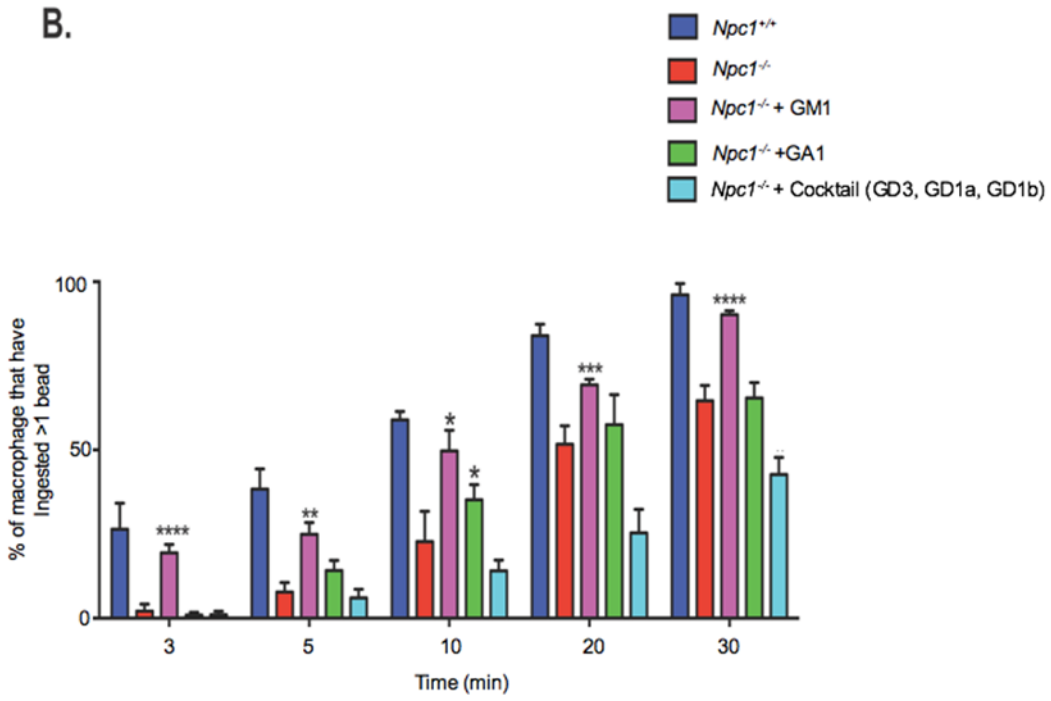


Figure 4.12 Related GSLs have no significant impact on phagocytosis: (A) Lipids discussed in section 4.3.7 were added to EPM media and phagocytosis was examined. Green beads are internalized; red beads are associated or bound to the cell membrane but not internalized. Cells were imaged with a Zeiss inverted microscope **(B)** Histogram representation showing significant differences in *Npc1*$^{-/-}$ phagocytic ability (red bar) following lipid addition. Data is presented as mean ±SD of 3 biological replicates per group. **p<0.05**, p<0.001,* ****p*<0.001, *****p*<0.0001, N=5 (via student's *t*-test with Welch's correction).

4.3.9.2 GM1 and GA1, but not a cocktail of GM3, GD1a and GD1b increase binding of IgG opsonized particles by *Npc1*$^{-/-}$ EPMΦ.

We analysed whether or not any of the GSL additions assisted in target recognition in terms of association with the membrane. We found through microscopy analysis that GM1 (p=0.0204) and GA1 (p=0.0332) increased the number of opsonised particles associated with (stuck to) the membrane,

however, a mixture of GM3, GD1a and GD1b showed no significant improvement (p=0.403, NS) (**Fig. 4.13**).

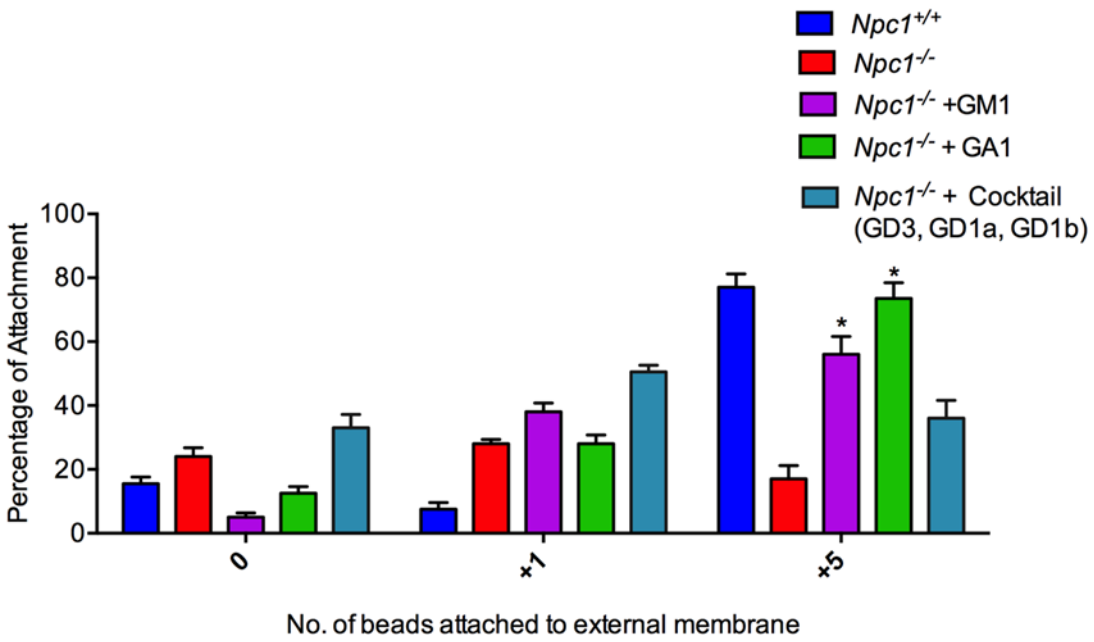


Figure 4.13 GM1 and GA1 increase *Npc1*$^{-/-}$ MΦ target recognition efficacy: Phagocytic recognition efficiency can be determined by analyzing number of target particles that are associated with the membrane (internalized or not) as likely when a particle is bound to the membrane it will become internalized in due time. Following addition of GM1 and GA1, *Npc1*$^{-/-}$ displayed a higher concentration of membrane bound particles in comparison to untreated *Npc1*$^{-/-}$. Data was collected through counting via inverted confocal microscopy. Data presented as mean ±SD of 3 biological replicates per group. *$p < 0.05$ (via student's t-test with Welch's correction).

4.3.9.3. Exogenous Lac-Cer, Glc-Cer and GM3 partially restore phagocytic activity in *Npc1*$^{-/-}$ EPMΦ.

We tested other lipids to determine if any had a comparable effect to GM1. Phagocytosis of IgG opsonized polystyrene beads was assessed by FACS analysis. Only Lac-Cer (p=0.0014), Glc-Cer (p=0.00031), GM1 (p=0.0016) and GM3 (p=0.0103) were found to significantly enhance phagocytosis. For Lac-Cer and Glc-Cer there was a 3-fold increase in fluorescence (MEFL=31885; MEFL=34941) as compared to untreated *Npc1*$^{-/-}$ EPMΦ. For GM1 and GM3 there was a two-fold increase in fluorescence (MEFL=20419, MEFL=23221) relative to untreated *Npc1*$^{-/-}$ (MEFL= 11094) (**Fig. 4.13**).

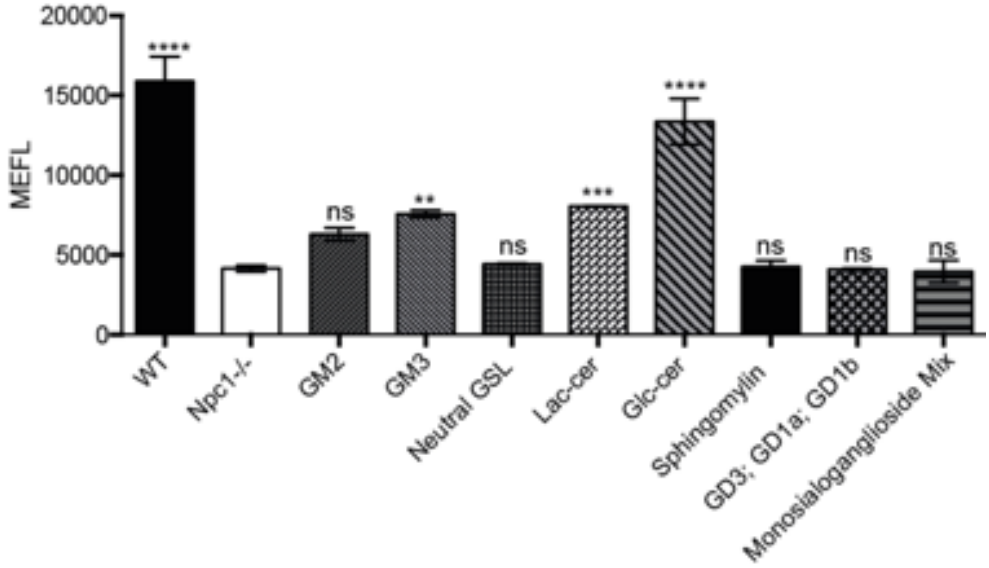


Figure 4.13 GM1, GM3, Lac-Cer and Glc-Cer improve phagocytosis: Mean fluorescence of EPMΦ 30 min after exposure to 3μm polystyrene beads. Fold change in mean fluorescence relative to control (untreated *Npc1*$^{-/-}$). N=12, Mean SD of 3 biological replicates per group.**p<0.01, ***p<0.001, ****p<0.0001 versus *Npc1*$^{-/-}$ EPMΦ (via student's t-test with Welch's correction).

4.3.9.4 Exogenous Glc-Cer is rapidly metabolized to GM1 in *Npc1*$^{-/-}$ EPMΦ.

We hypothesized that the beneficial effect of exogenous Glc-Cer on phagocytic activity may not be a direct consequence of the lipid itself, but possibly a result of metabolism through to more complex GSLs. We therefore pulsed EPMΦ with exogenous Glc-Cer for different lengths of time (10 min, 1h, 4h) and performed GSL analysis of cell extracts by HPCL, with assistance from Mylene Huebecker and Dr. David Priestman (Department of Pharmacology, University of Oxford). Within 10 min of addition of lipid there was a measurable increase of GM1 in *Npc1*$^{-/-}$ and *Npc1*$^{+/+}$ EPMΦ; at 1hr after addition of Glc-Cer the amount of GM1 in *Npc1*$^{-/-}$ with added Glc-Cer were shown and to be comparable to *Npc1*$^{+/+}$ GM1 levels with no added Glc-Cer indicating addition of Glc-cer to *Npc1*$^{-/-}$ was able to partially restore GM1 levels on the external membrane (**Fig.4.14**).

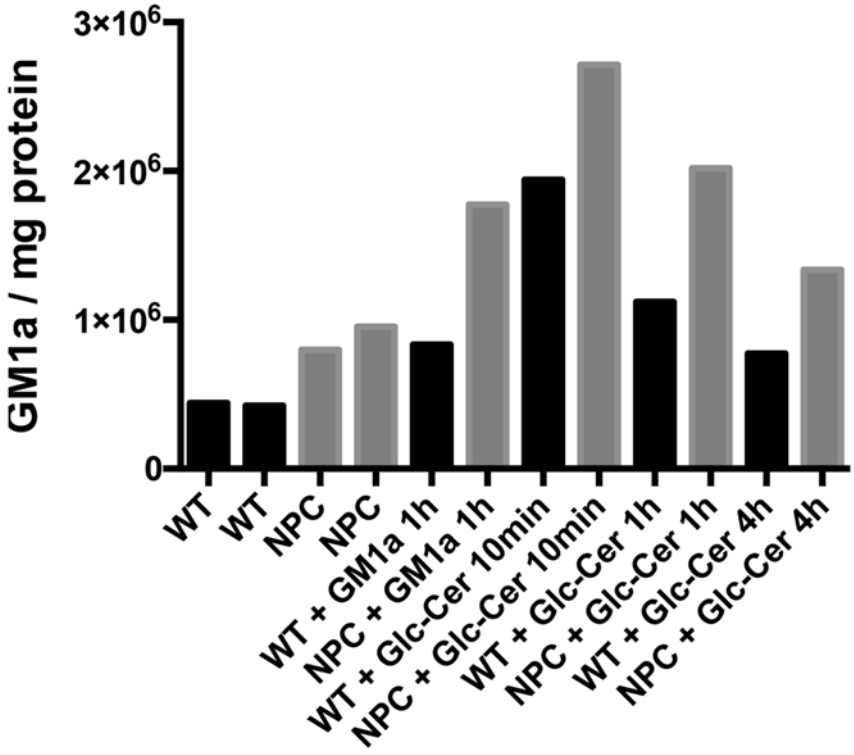


Figure 4.14 Glc-Cer is metabolized to GM1 in *Npc1*$^{-/-}$ EPMΦ: Following addition of Glc-cer at 10 min, 1h and 4h intervals, MΦ were tested by HPLC and protein analysis for lipid profiles. Rapidly after addition of Glc-Cer in *Npc1*$^{+/+}$ and *Npc1*$^{-/-}$ EPMΦ, there was an increase in GM1 concentration. This increase continued over time, and subsequent Glc-Cer concentrations decreased in parallel. This indicates that Glc-Cer is being metabolized to GM1 before accumulating within the cell.

4.4 Discussion

In this chapter we investigated cellular defects that might underlie the broad phagocytic deficiency identified in NPC MΦ. We confirmed impaired formation of phagocytic cups beneath particles that was associated with reduced F-actin polymerization in mutant cells. We showed that *Npc1*$^{-/-}$ EPMΦ have diminished levels of GM1 associated with the plasma membrane and demonstrated that

this contributes to the reduction in phagocytic activity because addition of exogenous ganglioside was capable of partially recovering phagocytosis. Other ganglioside species, such as Glc-Cer were also able to partially restore activity, but this most likely was due to their rapid processing through to GM1 ganglioside.

In order to identify cell biological defects that could be responsible for impaired phagocytosis by NPC MΦ, we chose to analyse FcγR dependent ingestion of IgG opsonized particles because it is a phagocytic mechanism that has been well characterized (Diakonova et al., 2002; Gallo et al., 2010). Although phagocytosis is a complex process, distinct stages of FcγR mediated internalization have been identified: initial particle engagement and binding and signaling, dynamic changes to the cytoskeleton that permit extension of pseudopods to surround the particle and finally concentration of actin beneath and then termination of polymerization and sealing of the phagosome (Freeman and Grinstein, 2014). We focused therefore on these steps, with the objective of determining whether some or all might be perturbed in NPC cells. Our expectation was when identified, we might then be able to speculate how such alterations to the phagocytic mechanism could result from the loss of Npc1.

Our data confirmed that binding of IgG opsonized particles, the initial step in the process of phagocytosis was impaired in *Npc1*$^{-/-}$ EPMΦ and U18666A-treated RAW 264.7 MΦ. The reduction in erythrocyte rosetting (binding) would impact directly upon the number of IgG opsonized particles that could be subsequently internalized. Tethering of IgG opsonized targets is recognized to involve the lateral movement of FcγRs in the membrane and their concentration at the site of particle contact with the cell. The evidence is that in resting cells

mobility of receptors is restricted by the cytoskeleton and their diffusion within the plasma membrane is facilitated by signals that originate from initial interactions with the particle (Flannagan et al., 2010). The requirement for FcγRs to concentrate in the membrane to enable binding is consistent with the relatively low affinity of FcγR for the Fc portion of IgG, meaning multiple receptor-ligand complexes are needed to be formed to secure the particle to the cell surface. This would suggest that alterations to either the composition or ordering of molecules in the plasma membrane could very likely affect FcR behavior. A crucial feature of NPC cells is disorder of the intracellular transport of cholesterol and GSLs. Sillence and colleagues (te Vruchte et al., 2004) confirmed large increases in the GSL content of microdomains and mistargeting of specific proteins within the membrane. Although we confirmed in Chapter 3 that the expression levels of specific FcγRs were not significantly altered in *Npc1*$^{-/-}$ EPMΦ, it is very possible that receptor distribution within the bilayer might be changed and their mobility curtailed, thereby preventing the clustering of receptors that is required for tethering of IgG opsonized particles. The consequences of the curtailing of FcγR motility or their distribution within the membrane leaflet could be more profound; prevention of clustering may also not allow recruitment of signaling proteins to the cytoplasmic domains of the receptors and thereby inhibit signal transduction that is responsible for initiating the remodeling of the cytoskeleton (Underhill and Goodridge, 2012). For example, phosphorylation of FcγRIIA that induces actin rearrangement is blocked when lipid rafts are disrupted (Kwiatkowska et al., 2003)

Re-modeling of the actin cytoskeleton to shape the membrane around the tethered particle is critical for the mechanism of phagocytosis (Flannagan et al.,

2012; Freeman and Grinstein, 2014). Indeed, inhibiting actin polymerization with the fungal toxin cytochalasin D and subsequent observation of the prevention of particle uptake is the standard methodology to confirm that mechanism responsible is phagocytosis (Ting-Beall et al., 1995). The clearest evidence of recruitment and polymerization of filamentous actin during the events of phagocytosis can be obtained with the use of a fluorescently labeled phalloidin probe, which binds specifically to F-actin(Burkel et al., 2007). In our studies we were able to visualize actin dynamics in both fixed and living cells with the aid of live cell confocal microscopy. A defining step in the contribution of actin rearrangement to particle ingestion is the formation of phagocytic cups beneath a particle when it is intimate contact with the induced curvature of the plasma membrane (Flannagan et al., 2012). In brief, for normal cells the dynamics of actin are: 1) actin is recruited and concentrated at the base of the cup and 2) it is sustained there during the time when pseudopods extend around the particle 3) decreases in concentration (depolymerizes) concurrent with closure and isolation of the phagosome. This was the pattern of actin dynamics we observed in *Npc1*$^{+/+}$ EPMΦ and control RAW 264.7 MΦ. On the other hand, in *Npc1*$^{-/-}$ EPMΦ and U18666A-treated MΦ we observed delayed recruitment of actin after addition of IgG opsonized targets and reduced concentration of actin at the base of the cup, extension of pseudopods was impaired, significantly fewer phagocytic cups were formed and were often abnormal in appearance in comparison to those of *Npc1*$^{+/+}$ MΦ. Furthermore, successful completion of cup formation was much less frequent. These observations are all consistent with impairment or disruption of the actin cytoskeleton in NPC.

A hallmark feature of NPC cells is storage and mistrafficking of GSLs that results in their altered distributions with cellular compartments (Lloyd-Evans and Platt, 2010). We confirmed that the relative level of GM1 was reduced at the plasma membrane of *Npc1*$^{-/-}$ EPMΦ as compared to control cells, suggesting the possibility that the lower ganglioside content at the plasma membrane (due to sequestration in late endosome/ lysosome) could affect the process of phagocytosis. We tested this hypothesis by first demonstrating that addition of exogenous GM1 was able to increase the amount of ganglioside associated with the plasma membrane and then showing that there was partial restoration of phagocytic activity in *Npc1*$^{-/-}$ EPMΦ following exogenous addition of GM1. We focused our efforts on GM1 because the availability of CtxB as a specific probe simplified and facilitated our analyses. These data would suggest that the ganglioside composition of the plasma membrane is critically important for phagocytosis/actin dynamics. GSLs are known to be important for a number of activities that have the possibility of perturbing phagocytosis. It has been suggested that GSs are employed for the trafficking of endogenous proteins that are critical for cell physiology through their capacity to form specialized microdomains in the membrane bilayer and interactions with GSL-binding proteins (Khine et al., 1998; Wolf et al., 1998). Disturbance of GSL trafficking has the potential to affect either the normal composition of the plasma membrane by preventing trafficking of specific molecules associated with GSLs to the compartment (ones that can contain GSL-binding domains) or by affecting their specific distribution within the membrane, or a combination of the two. To our knowledge, although there has been a study showing distorted distribution and sorting of microdomain-associated proteins such as annexin 2

and 6 (te Vruchte et al., 2004) there have been no investigations of proteins known to be involved in phagocytosis. It would be of particular interest to examine the distribution of FcγRs within the bilayer of resting phagocytes and track their movement (or lack of movement) triggered with the addition of IgG opsonized particles. At what step(s) GM1 exerts its effect(s) on phagocytosis is also an open question. The evidence that GSL contribution to phagocytosis may well be lipid-specific is supported by our demonstration of normal phagocytic activity of *hexb*$^{-/-}$ EPMΦ in which the metabolism of GM2 ganglioside is affected (Chapter 3 Section 3.3.5.1).

Interestingly, we found that restoration of phagocytic activity in *Npc1*$^{-/-}$ EPMΦ was only achieved with the addition of specific GSLs (GM1, Glc-Cer and Lac-Cer), indicating that the precise biochemical and biophysical properties of the lipid are important. Unexpectedly, although addition of Glc-Cer promoted phagocytic activity, the evidence was that this was very likely due to its very rapid metabolism to complex GSLs, including GM1. These data indicate that although GSL trafficking is significantly perturbed in NPC cells, the biosynthetic route that requires trafficking of precursors through the trans-Golgi network, where complex GSLs are generated is apparently not significantly affected, at least when the lipid is delivered exogenously. This observation deserves further attention.

There have been several studies showing the influence of sphingolipids on phagocytosis. Whilst inhibition of *de novo* ceramide synthesis was demonstrated to enhance phagocytosis of opsonized red blood cells (Hinkovska-Galcheva et al., 2003), a recent study of the uptake of *Candida albicans* showed that inhibition of sphingolipid biosynthesis had the opposite

effect (Tafesse et al., 2015). The authors reported that DC2.4 cells, a dendritic cell line, treated with myriocin or fumonisin, which block sphingolipid biosynthesis, or engineered for homozygous loss of serine palmitoyl-CoA transferase (*Sptlc*) gene activity, which catalyses the rate-limiting reaction in the sphingolipid biosynthetic pathway, displayed significantly impaired phagocytosis of fungal particles. Pertinently, they also observed failure to form of phagocytic cups in sphingolipid-depleted cells and that addition of exogenous GM1 was capable of restoring phagocytic activity in *Sptlc*$^{-/-}$ cells. In that study they did not test other GSLs for their capacity to correct the phagocytic defect. Therefore, sphingolipids and GSLs have the potential to affect the complex mechanism that is phagocytosis by direct effects related to their contributions to specific membrane or cellular compartments or indirectly via their involvement in biosynthetic and trafficking pathways. One speculation is that GM1 may be involved in promoting the organisation of cell surface proteins that intersect with the actin cytoskeleton and this merits detailed investigations in the future.

Summary.

The data shown in this chapter revealed that the phagocytic deficiency in *Npc1*$^{-/-}$ MΦ is paralleled by altered actin cytoskeleton dynamics during phagocytosis. Second, GSL composition of the plasma membrane contributes to the impairment of phagocytosis because exogenous GM1 ganglioside partially recovered activity. In the next chapter we test whether normalizing specific biochemical changes that characterise the disease by use of NPC therapies are able to recover phagocytic activity.

Chapter 5. Impact of NPC Therapies on Phagocytosis.

5.1 Introduction.

Data in the previous chapters supports a model in which an abnormal innate immune response directly contributes to NPC pathology by disrupting clearance of invading pathogens and aged cells by phagocytosis. Currently, NPC therapeutics consist of only one EMA approved drug, miglustat, as well as 3 others currently in clinical trials. We therefore investigated whether therapies used in the treatment of NPC would correct the phagocytic defect In NPC MΦ.

Below the therapies in clinical use, in clinical trials or preclinical compounds that have shown efficacy in *Npc1*$^{-/-}$ mice are reviewed briefly.

5.1.1 Miglustat.

N-butyl-deoxynojirimycin (*N*B-DNJ), also called Zavesca (trade name) or miglustat (generic name), was originally developed as a therapeutic for type 1 Gaucher Disease (Cox et al., 2000). It functions by inhibiting glucosylceramide synthase, the enzyme which catalyzes the first step in the GSL biosynthetic pathway. Its action results in a reduction of both glucosylceramide and other more complex GSLs **(Fig.5.1)** and provides benefit by the mechanism known as substrate reduction therapy (Jeyakumar et al., 2005). NPC animals treated with miglustat have increased lifespan, as well as delayed onset of neurological disease progression as analyzed with behavioural testing (Zervas et al., 2001).

The feline model of NPC disease following miglustat treatment showed decreased accumulation of GM2 ganglioside and a slightly delayed development of neurological symptoms (Stein et al., 2012). In the *Npc1*$^{-/-}$ mice, miglustat reduced ganglioside storage (Lloyd-Evans and Platt, 2010) and extended survival by about 40% (Smith et al., 2009). In patients, miglustat has been shown to modestly extend lifespan and produce some neurological improvement as it slows disease progression (Patterson et al., 2007). Currently, miglustat is the only licensed therapy for NPC (worldwide, with the exception of USA).

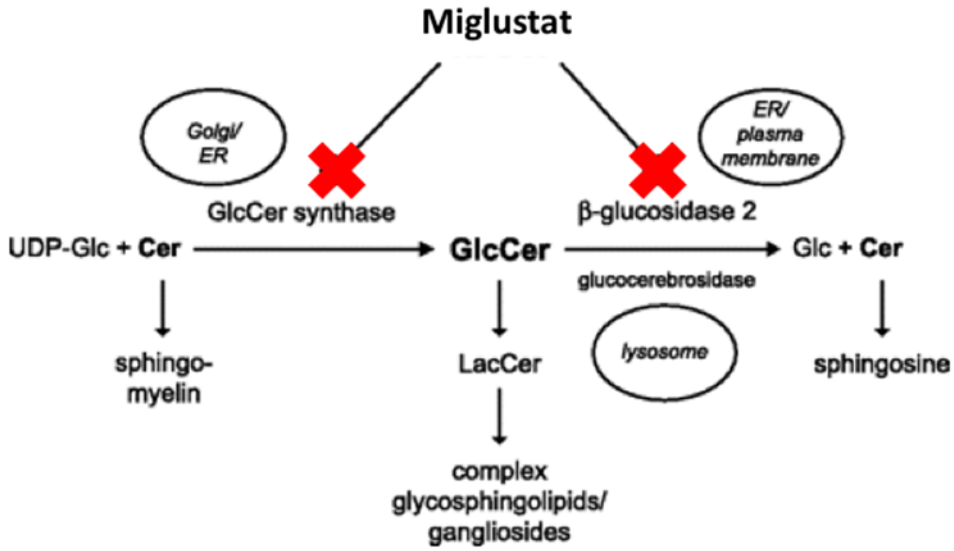


Figure 5.1. Miglustat and the metabolism of Glc-Cer and related sphingolipids: The biosynthesis of Glc-Cer takes place in an early Golgi compartment. The reaction is catalyzed by Glc-Cer synthase. Glc-Cer can then be converted to Lac-Cer and more complex GSLs. Glc-Cer can be catabolized by two enzymes. At non-lysosomal locations, Glc-Cer can be cleaved by β-glucosidase 2 (GBA2), and in the lysosome, Glc-Cer can be cleaved by GBA1. Both Glc-Cer synthase and GBA2 (and to a much lesser extent GB(A) can be inhibited by miglustat. Figure adapted from Walden *et al*. (Walden et al., 2007)

5.1.2 2-hydroxypropyl-β-cyclodextrin (HPβCD).

HPβCD is part of the family of cyclodextrin's named cyclic oligosaccharides. They consist of a hydrophilic exterior carbohydrate ring with a hydrophobic interior making them ideal for use as vehicles for drug delivery (Ottinger et al., 2014). More recently, HPβCD has been shown to be is beneficial in NPC. This finding stemmed from the use of HPβCD to deliver allopregnanolone to the CNS of *Npc1*$^{-/-}$ mice (Liao et al., 2009). Unexpectedly, It was found that HPβCD alone led to a clinical improvement in the *Npc1*$^{-/-}$ mice with delayed symptom onset

and increased survival (Liao et al., 2009). *Npc1*$^{-/-}$ mice showed decreased levels of GSL, sphingosine and cholesterol following treatment with HPβCD (Liao et al., 2009; Vance and Peake, 2011; Liu, 2012; Ottinger et al., 2014). The rationale is that cyclodextrin binds to cholesterol and is then able to extract cholesterol from lipid membranes or stimulate exocytosis by signaling plasma membrane damage (Chen et al., 2010). Thus it is assumed that this ability to remove cellular cholesterol and other stored lipids was responsible for the beneficial effect of HPβCD in NPC (Vance and Peake, 2011). However, the precise mechanism by which HPβCD is therapeutically active remains contentious, particularly because of the lack of evidence that it can cross the blood-brain barrier (Pontikis et al., 2013).

5.1.3 Curcumin.

A unique phenotype of NPC is the loss of lysosomal Ca^{2+} homeostasis (Lloyd-Evans et al., 2008). The reduction in Ca^{2+} release from the lysosome is responsible for the downstream defects in endocytic trafficking and lysosomal fusion. Curcumin, which is derived from turmeric (Gupta et al., 2012) is able to compensate for the reduced lysosomal Ca^{2+} release in NPC (Lloyd-Evans et al., 2008) **(Fig. 5.2)**. It functions by inhibiting the sarcoplasmic reticulum Ca^{2+} ATPase (SERCA), which acts to move Ca^{2+} from the cytosol to the lumen of the ER (Patergnani et al., 2011). If SERCA is inhibited, the movement of Ca^{2+} is impaired, resulting in a rise in cytosolic Ca^{2+}. Oral treatment of *Npc1*$^{-/-}$ mice with curcumin has been shown to be beneficial (Lloyd-Evans et al., 2008); (Williams et al., 2014).

Curcumin has also been suggested to benefit other disorders including cancer, depression and Alzheimer's disease (Perry and Howes, 2011; Maiti et al., 2016;

Wen et al., 2016; Yue et al., 2016). In NPC, the advantageous effect of curcumin is related to its Ca^{2+}-modulating properties because chelating cytosolic Ca^{2+} with BAPTA-AM (1,2-bis(o-aminophenoxy) Ethane-N, N, N', N'-tetraacetic acid) abolishes the correction of NPC cells (Lloyd-Evans et al., 2008). Furthermore, when co-administered to *Npc1*$^{-/-}$ mice with the anti-inflammatory drug ibuprofen, it had a synergistic effect, which indicates that curcumin is not acting via an anti-inflammatory mechanism (Williams et al., 2014).

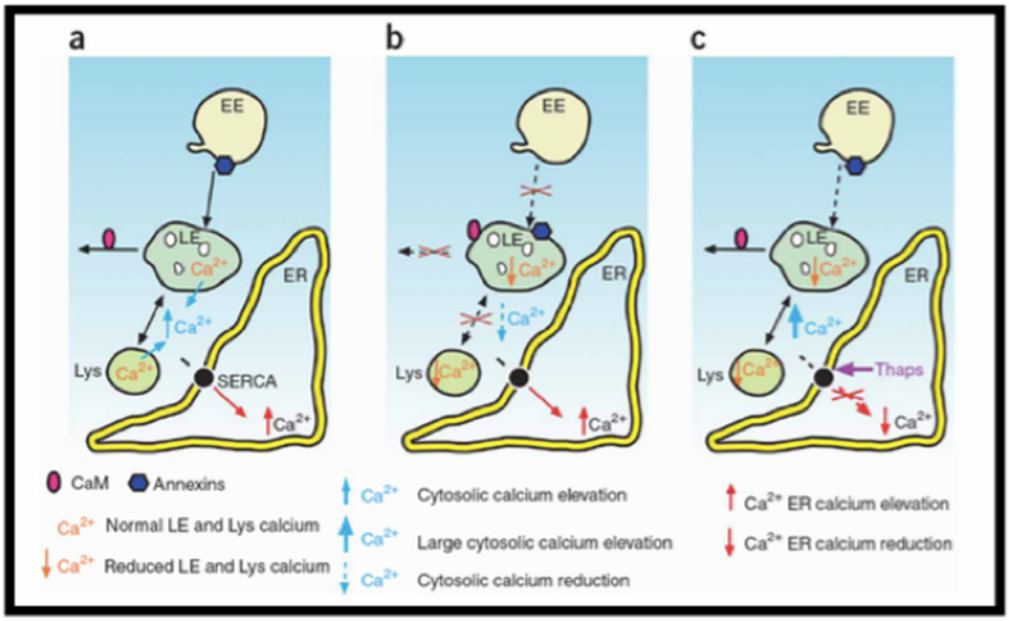


Figure 5.2. Schematic representation of the effect of curcumin on compensating for reduced acidic compartment calcium release in NPC1 cells. Figure taken from Lloyd-Evans *et al.* (Lloyd-Evans et al., 2008)

5.2 Methods.

5.2.1 Reagents.

Media and cell culture reagents are described in Section 2.2 and 3.2.

5.2.2 Cells.

Npc1$^{-/-}$ and *Npc1*$^{+/+}$ EPMΦ were obtained and cultured as described previously in Section 3.2.4.2.

5.2.3 Drug treatment and cholesterol storage measurment

RAW 264.7 MΦ grown on coverslips were treated with 2 μg/ml U18666A for 24h to induce cholesterol accumulation and other NPC phenotypes. Coverslips were washed and treated with NPC therapies diluted in R-10. Concentrations of drugs used and the length of treatment are listed in **Table 5.1**.

Therapy	**Parameters**
Miglustat (Actelion)	50 μM, 72h
HPβCD	250 μM, 24h
Curcumin (Enzo)	30 μM, 24h

Table 5.1 NPC therapeutics with corresponding dosage parameters.

Following treatment, coverslips were fixed with 4% PFA (10 min on ice) and cholesterol distribution determined via staining with filipin (as detailed in section 2.2.5). Microscopy analysis was performed as described in Chapter 2.2.5.

5.2.4 Correction of phagocytic defects in *Npc1*$^{-/-}$ EPMΦ by NPC therapies.

EPMΦ were isolated from *Npc1*$^{-/-}$ and *Npc1*$^{+/+}$ mice as described in section 3.2.5.2**.** Cells were plated onto coverslips and treated with drugs (**Table 5.1**). Phagocytosis assays were performed according to methods outlined in Chapter 2 (Section 2.2). Following co-incubation with IgG-sRBC labelled with Celltracker^{TM} green, MΦ were fixed with 4% PFA for 10 minutes on ice, and stained for actin using F-actin rhodamine Phalloidin (Thermo Scientific) and the nucleus stained with DAPI. Microscopy was performed as described in Section 2.2.12.

5.2.5 FACS assays to assess effectiveness of NPC therapies on phagocytosis.

EPMΦ were seeded overnight in 6-well plates (1x10^6 per well). Following confirmation of confluency (>80%,) cells were washed and fresh media (containing therapeutics) was added. Concentrations and durations of treatment were as indicated (**Table 5.1**). Cells were overlaid with Celltracker^{TM} green labeled IgG-sRBC for 30 minutes. Cells were fixed with PFA (4% PFA, 10 min on ice), harvested, and levels and frequency of fluorescence (indicative of intracellular sRBC) were quantified using FACS (10,000 events collected per sample).

5.2.6 Enzyme-linked immunoassay (ELISA) analysis of supernatant cytokines.

Described in Section 3.2.8.

5.3 Results.

5.3.1 NPC Therapies correct U18666A-induced cholesterol storage.

Filipin staining was increased in both U18666A-treated RAW 264.7 MΦ and *Npc1*$^{-/-}$ EPMΦ relative to controls **(Fig.5.3)**. Treatment of both U18666A-treated RAW 264.7 and *Npc1*$^{-/-}$ EPMΦ with HPβCD, miglustat and curcumin partially corrected the phenotype **(Fig 5.3)**.

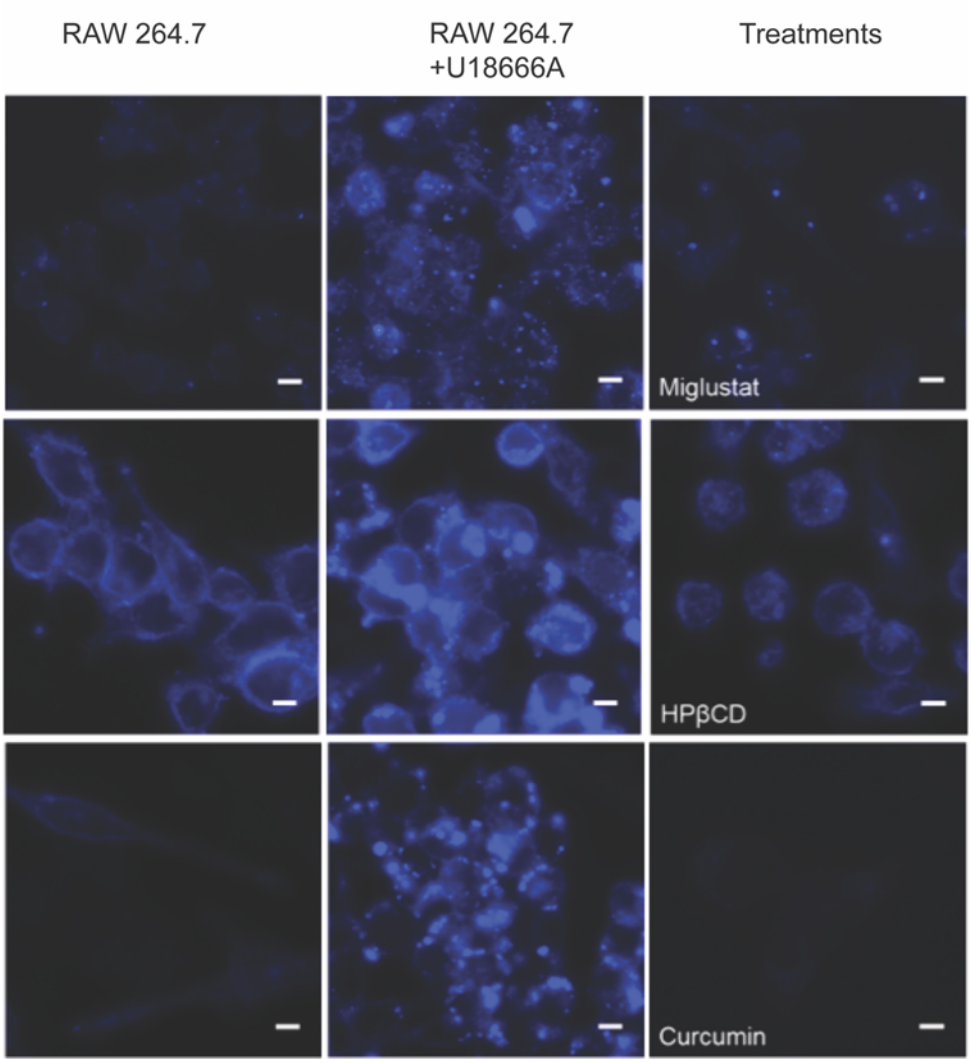


Figure 5.3 U18666A induces cholesterol accumulation in LE/ Lys of RAW 264.7 MΦ which can be corrected with miglustat, HPβCD or curcumin. Filipin staining (blue) confirms U18666A treatment (centre panels) causes lysosomal accumulation of cholesterol that can be corrected by miglustat, HPβCD or curcumin (right panels). Scale bar = 10μm.

5.3.2 Miglustat and curcumin correct phagocytic defects in *Npc1*$^{-/-}$ EPMΦ; HPβCD has no significant on phagocytosis by *Npc1*$^{-/-}$ EPMΦ.

Following treatment with miglustat (50 μM, 72h) *Npc1*$^{-/-}$ EPMΦ showed increased phagocytosis of IgG-sRBC. Microscopy analysis of *Npc1*$^{-/-}$ following treatment with miglustat showed a higher incidence of IgG-sRBC within the MΦ in comparison to untreated. *Npc1*$^{-/-}$. Histogram representation determined a significant difference in uptake between *Npc1*$^{-/-}$ and *Npc1*$^{-/-}$ treated with miglustat at all time points (10 min. *Npc1*$^{-/-}$ mean= 9.647%; *Npc1*$^{-/-}$+miglustat mean= 33.64%, p=<0.0012; 20 min. *Npc1*$^{-/-}$ mean=18.395, *Npc1*$^{-/-}$ +miglustat mean=58.751, p=0.00033; 40 min. *Npc1*$^{-/-}$ mean=42.331, *Npc1*$^{-/-}$ +miglustat mean=73.029, p=0.0027) **(Fig. 5.4)**.

Analysis by FACS confirmed that *Npc1*$^{-/-}$ EPMΦ showed a 3-fold increase in fluorescence (*Npc1*$^{-/-}$ mean MEFL=3841; *Npc1*$^{-/-}$+miglustat mean MEFL=16541; p=0.00103). For *Npc1*$^{+/+}$, 73.1% of EPMΦ were positive (indicating phagocytosis of IgG-sRBC), whereas for untreated *Npc1*$^{-/-}$ 36.4% were scored as positive; following treatment with miglustat, 59.7% of *Npc1*$^{-/-}$ cells were gated for phagocytosis of IgG-sRBC. **(Fig. 5.5)**. Therefore, miglustat increased the frequency and activity of *Npc1*$^{-/-}$ EPMΦ to ingest IgG-sRBC.

Microscopy analysis of *Npc1*$^{-/-}$ EPMΦ following treatment with curcumin showed an increased incidence of IgG-sRBC ingestion in comparison to untreated *Npc1*$^{-/-}$ MΦ. A significant difference in uptake between *Npc1*$^{-/-}$

EPMΦ and *Npc1*$^{-/-}$ EPMΦ treated with curcumin was observed at all time points (10 min. *Npc1*$^{-/-}$ mean= 9.647%; *Npc1*$^{-/-}$+curcumin mean= 28.99%, *p*=0.0023; 20 min. *Npc1*$^{-/-}$ mean=18.395, *Npc1*$^{-/-}$ +curcumin mean=58.285, *p*=0.0003;40 min. *Npc1*$^{-/-}$ mean=42.331, *Npc1*$^{-/-}$ + curcumin mean=78.073, *p*=0.0012) **(Fig. 5.4)**.

Following treatment with 30 μm curcumin for 24h, *Npc1*$^{-/-}$ EPMΦ were analyzed by FACS for their ability to ingest IgG-sRBC. Curcumin treated EPMΦ showed a 2-fold increase in fluorescence (MEFL=7319) in comparison to untreated *Npc1*$^{-/-}$ EPMΦ (MEFL=3461) (*p*=0.010), and 56.7% of curcumin treated *Npc1*$^{-/-}$ scored fluorescently positive (indicating uptake) in comparison to 26.8% of *Npc1*$^{-/-}$. This is indicative of greater uptake of CMFDA-labeled IgG-sRBC by curcumin treated *Npc1*$^{-/-}$ EPMΦ **(Fig. 5.5)**.

Microscopy analysis of *Npc1*$^{-/-}$ MΦ following treatment with HPβCD showed no obvious increase of IgG-sRBC in comparison to untreated.

There was no significant difference in uptake between *Npc1*$^{-/-}$ and *Npc1*$^{-/-}$ treated with HPβCD at all time points (10 min. *Npc1*$^{-/-}$ mean= 9.647%; *Npc1*$^{-/-}$ +HPβCD mean= 12.418%, *p*=<0.061; 20 min. *Npc1*$^{-/-}$ mean=18.395, *Npc1*$^{-/-}$ + HPβCD mean=25.612, *p*=0.092; 40 min. *Npc1*$^{-/-}$ mean=42.331, *Npc1*$^{-/-}$ + HPβCD mean=42.322, *p*=0.142) **(Fig. 5.4)**.

Following treatment with HPβCD for 24h**,** *Npc1*$^{-/-}$ EPMΦ phagocytosis was assessed by FACS. The *Npc1*$^{-/-}$ EPMΦ treated with HPβCD showed a small increase in fluorescence (*Npc1*$^{-/-}$ MEFL=3841; *Npc1*$^{-/-}$+ HPβCD MEFL=4281; *p*=0.051), where 48.1% of *Npc1*$^{-/-}$ + HPβCD showed evidence of uptake compared to 37.4% of *Npc1*$^{-/-}$ indicating a slightly higher, and borderline

significant number of EPMΦ had internalized Celltracker™ green-labeled IgG-sRBC **(Fig. 5.5)**.

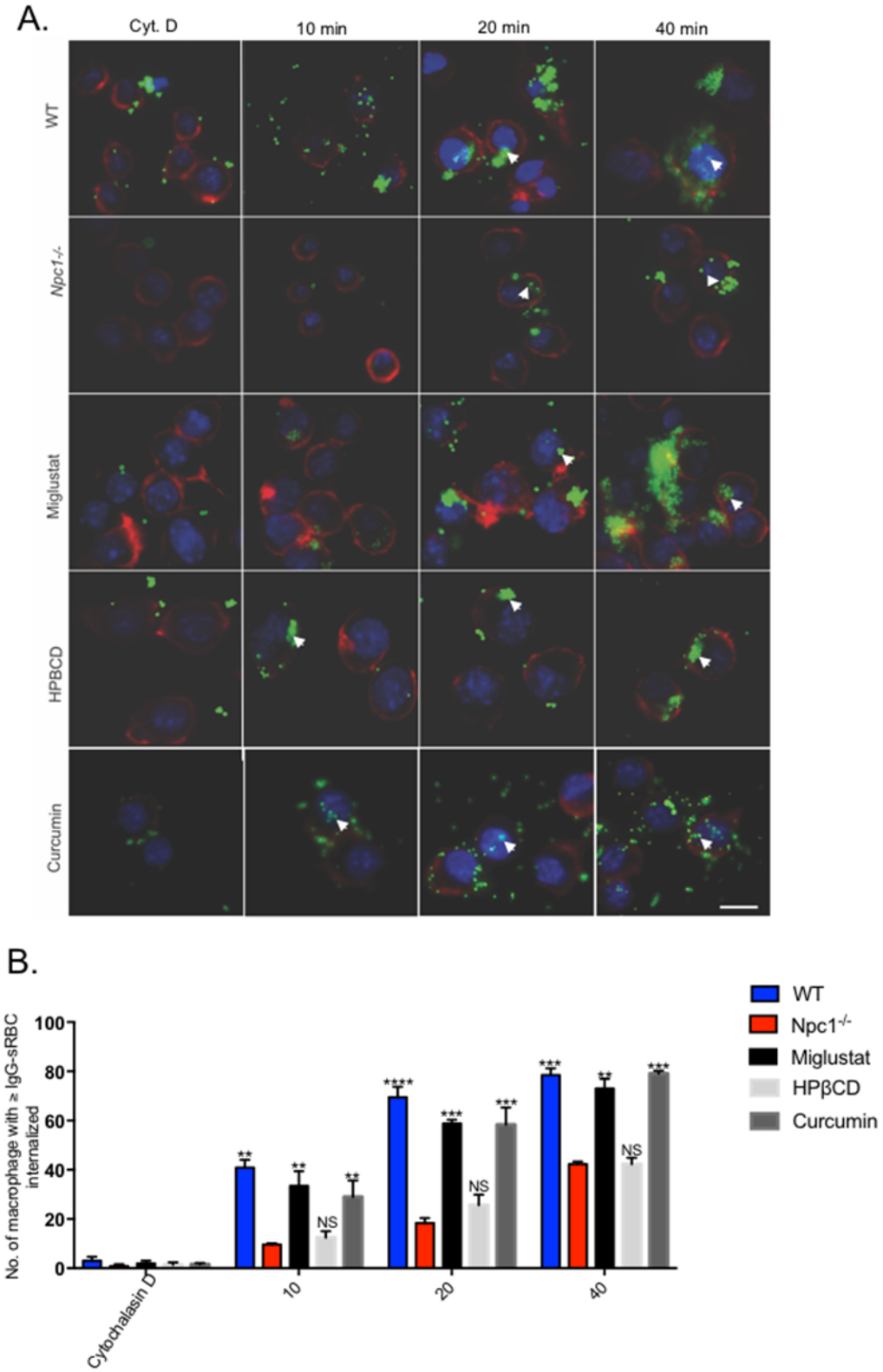

A.
Cyt. D
10 min
20 min
40 min
WT
Npc1-/-
Miglustat
HPBCD
Curcumin
B.
No. of macrophage with ≥ IgG-sRBC internalized
100
80
60
40
20
0
Cytochalasin D
10
20
40
NS
WT
Npc1-/-
Miglustat
HPβCD
Curcumin

Figure 5.4 Miglustat and curcumin treatment improve the phagocytic activity of *Npc1*$^{-/-}$ EPMΦwhereas HPβCD has no significant effect: **(A)**Representative fields of control, miglustate, curcumin or HPβCD-treated *Npc1*$^{+/+}$ and *Npc1*$^{-/-}$ EPMΦ at 10, 20 and 40 min of co-incubation with CMFDA labelled IgG-sRBC (green). Red = Phalloidin. Blue = DAPI. Scale bar = 5 µm **(B)** Quantification of relative phagocytic activitiy of *Npc1*$^{+/+}$ (blue columns), *Npc1*$^{-/-}$ untreated (red columns), miglustat treated (black columns) and curcumin treated (dark grey) show significantly increased phagocytic activity as compared to control *Npc1*$^{-/-}$ (red columns) EPMΦ. HPβCD treatment (pale grey columns) has no significant effect on phagocytosis. Data presented as mean ± SD for 3 replicates per condition N=5 **p*<0.05 ***p*<0.01 ****p*<0.001 versus untreated *Npc1*$^{-/-}$ EPMΦ (via student's *t*-test with Welch's correction).

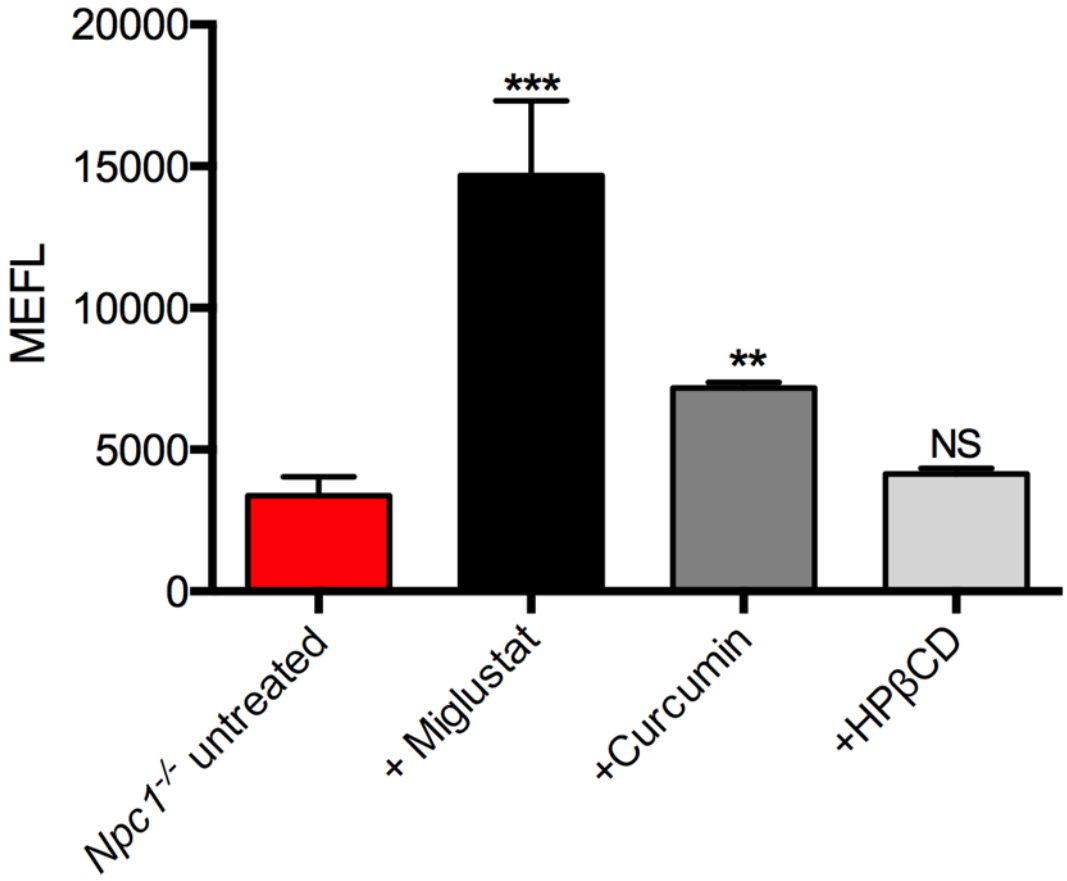


Figure 5.5 Miglustat improves the phagocytic activity of *Npc1*$^{-/-}$ EPMΦ whereas HPβCD has no significant effect (analysis by FACS). *Npc1*$^{+/+}$ and *Npc1*$^{-/-}$ cells were exposed to Celltracker^{TM}-labeled IgG-sRBC. *Npc1*$^{-/-}$ showed a 3-fold increase in CMFDA fluorescence following treatment with miglustat indicating increased internalisation of IgG-sRBC within the cell. *Npc1*$^{-/-}$ EPMΦ treated with HPβCD showed a less than 1-fold, non-significant increase in CMFDA fluorescence indicating minimal increase in phagocytosis. Data is presented as mean +/-SD of 3 biological replicates per group. N=4, $^{**}p<0.01$, $^{***}p<0.001$, NS $p>0.05$, versus *Npc1*$^{-/-}$ EPMΦ (via *t*-test with Welch's correction).

5.3.3 Impact of NPC therapies on MΦ inflammatory responses to phagocytosis.

As shown previously in Chapter 3 *Npc1*$^{-/-}$ EPMΦ secreted lower amounts of TNFα and IL-6 following phagocytosis of IgG-opsonised 3 μm polystyrene beads in comparison to *Npc1*$^{+/+}$ EPMΦ (Section 3.3.5). We investigated whether treatment with miglustat and HPβCD affected cytokine production. *Npc1*$^{-/-}$ EPMΦ treated with miglustat and incubated with IgG beads showed significantly increased production of TNFα and IL-6 in comparison to untreated cells and the levels were not significantly lower than those secreted by *Npc1*$^{+/+}$ EPMΦ (IL-6 p=<0.0001; TNFα p=0.00104) **(Fig. 5.6)**. In contrast, HPβCD had no significant impact on secretion by *Npc1*$^{-/-}$ EPMΦ (IL-6 p=0.041; TNFα p=0.022) **(Fig. 5.6)**.

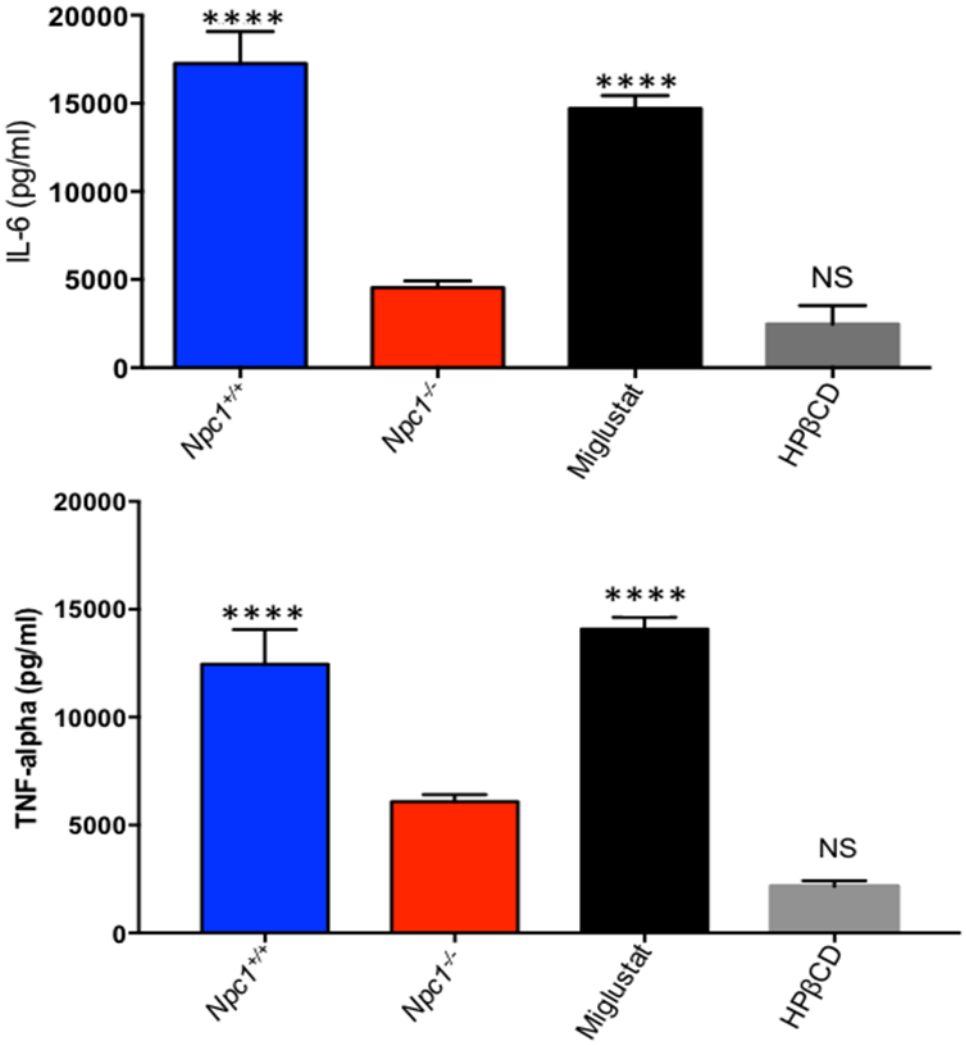


Figure 5.6. Miglustat but not HPβCD treatment increases the secretion of pro-inflammatory cytokines by *Npc1*$^{-/-}$ EPMΦ after co-incubation with IgG beads. Following treatment with miglustat (black columns) and incubation with IgG beads *Npc1*$^{-/-}$ produced significantly more IL-6 (upper panel) and TNFα (lower panel) than control *Npc1*$^{-/-}$ EPMΦ , the levels of which were not significantly different from those produced by *Npc1*$^{+/+}$ EPMΦ (blue columns). Treatment of *Npc1*$^{-/-}$ EPMΦ with HPβCD (grey columns) did not show a significant increase in secretion of IL-6 or TNFα. Mean N=5, NS $p>0.05$, ***$p<0.001$. Analysis was determined by one-way ANOVA.

Discussion.

In this chapter, we demonstrated that treating *Npc1*$^{-/-}$ EPMΦ with miglustat or curcumin resulted in a significant increase in phagocytic activity, whereas HPβCD had no significant effect. The same two drugs also enhanced the secretion of two pro-inflammatory cytokines induced by FcγR mediated phagocytosis and cyclodextrin was again without significant effect.

The three drugs act therapeutically at different points in the pathological cascade in NPC. Miglustat provides therapeutic benefit in LSDs by inhibiting the activity of glucosylceramide synthase, the enzyme involved in the first step of GSL biosynthesis (Lachmann et al., 2004; Patterson et al., 2007). In NPC cells and cells treated with U18666A GSLs accumulate in membrane microdomains within the endolysosomal system and are depleted from the plasma membrane (te Vruchte et al., 2004). Inhibiting the production of GSLs results not only in reduced delivery of substrates to the lysosome, thereby limiting accumulation in the organelle but also to a significant extent, normalises the distribution of GSLs between different cellular compartments (te Vruchte et al., 2004). Although we observed that inhibition of GSL biosynthesis with miglustat resulted in lower lysosomal accumulation of cholesterol, as revealed by filipin staining, te Vruchte *et al* (te Vruchte et al., 2004) reported only a modest decrease in total cellular cholesterol after treatment with the amino sugar. Therefore, it would seem that the enhancement of phagocytic activity of *Npc1*$^{-/-}$ EPMΦ that we measured following treatment is most likely due to restoration of GSL content at the plasma membrane. This hypothesis is supported by our demonstration that addition of exogenous GM1 was able to

increase plasma membrane-associated ganglioside and enhance phagocytosis by NPC MΦ (Chapter 4 Section 4.3.8)

Lloyd-Evans and colleagues (Lloyd-Evans et al., 2008) demonstrated that NPC is a disease caused by the loss of lysosomal Ca^{2+} homeostasis. The authors showed that sphingosine accumulation in the lysosome resulted in impaired filling of the store and that Ca^{2+} modulating drugs were able to correct cellular phenotypes, including sphingolipid trafficking. Oral curcumin, a weak SERCA antagonist that raised the level of cytosolic Ca^{2+}, significantly extended survival of *Npc1*$^{-/-}$ mice, improved their neurological symptoms and reduced GSL accumulation. The length of time for which we cultured *Npc1*$^{-/-}$ EPMΦ with curcumin, prior to testing of phagocytic activity, was of sufficient duration to significantly reduce cholesterol accumulation (**Fig 5.3**). Although we did not confirm it here, the period of treatment with curcumin should also have been sufficient to significantly reduce GSL storage (based on studies performed by Dr Paul Fineran, under revision). Again, we would suggest that changes to GSL distribution is the most likely explanation for the improvement in phagocytic activity achieved with curcumin.

The best evidence that we obtained that would argue against the enhancement of phagocytic activity resulting from changes to cholesterol metabolism was the inability of HPβCD to affect phagocytosis. Multiple studies have reported therapeutic benefit with cyclodextrins in different models of NPC (Ramirez et al., 2010; Pontikis et al., 2013; Vite et al., 2015). At the cellular level, the evidence indicates that HBβCD acts by reducing cellular cholesterol through stimulating lysosomal exocytosis (Chen et al., 2010). We would suggest that such a mechanism would be unlikely to restore plasma membrane GSLs, but

to our knowledge this has not been examined. The failure of HPβCD to affect phagocytosis was re-enforced with the demonstration of unaltered secretion of FcγR triggered pro-inflammatory cytokines.

Summary.

In this chapter, we demonstrated that treatment of *Npc1*$^{-/-}$ MΦ with miglustat and curcumin was able to promote phagocytosis of IgG-sRBC. We hypothesize that the ability to improve phagocytosis is dependent on correction of the GSL distribution in the plasma membrane. However, further studies on the mechanism by which these therapeutic(s) impact innate immune activity both *ex vivo* and *in vivo* will require further investigation as will explanation of the failure of HBβCD to rescue phagocytosis and the inflammatory response.

Chapter 6: Defective Phagocytosis *In Vivo.*

6.1 Introduction.

Our studies have identified phagocytic defects in both pharmacological and genetic models of NPC *in vitro* that could be partially corrected by treatment with miglustat and curcumin. We now wished to make preliminary investigations for evidence of altered phagocytosis *in vivo* that would support the proposal that impairment is likely to contribute to pathologies associated with the disease

Major objectives of this chapter:

- Investigate phagocytosis in vivo using *Npc1*$^{-/-}$ mice.
- Compare in vivo data with current research linking defective phagocytosis to other NPC pathologies.

6.2 Materials and Methods

6.2.1 Mice.

All animal experiments were performed according to Home office regulations (as detailed in Chapter 3). BALB/c *Npc1*$^{-/-}$ and *Npc1*$^{+/+}$ were obtained as described in Section 3.2.2. The mice used in experiments were 7 weeks of age.

In investigations of liver histology, selected *Npc1*$^{-/-}$ mice were treated with miglustat added to the diet at a dose of 600 mg/ kg/ day from weaning (3-weeks of age)

6.2.2 Preparation of IgG beads.

3 μm fluorescent polystyrene spheres were opsonized with rabbit anti-sRBC antibody by adsorption. Full protocol is described in section 2.2.9.1.

6.2.3 In vivo phagocytosis of IgG-opsonised beads.

Mice were injected with 1 ml of sterile 4% thioglycollate broth into the peritoneum (Chapter 3 Section 3.2.4.2)**.** 96 h later, mice were injected via the same route with $2x10^7$ fluorescently labeled beads. After 60 min, mice were killed, the peritoneum was lavaged with PBS and the washout collected. Cells were pelleted by centrifugation (1500 rpm for 5 min), re suspended, counted and stained with F4/80 antibody as described earlier (Chapter 3 Section 3.3.1) and analysed immediately by FACS.

6.2.4 Histology.

PFA fixed samples were processed using an automated Shandon ExcelsiorTM ES tissue processor (Thermo Fisher Scientific Inc., Fisher Scientific UK Ltd, Loughborough, Leicestershire) using following protocol: Formalin (30 min), 70% alcohol (1:30h), 90% alcohol (1:30h), 100% alcohol (1:30h), 100% alcohol (1h), 100% alcohol (1:30h), 100% alcohol (1:30h), histoclear (1:30h), histoclear (1:30h), histoclear (2h), wax (1h), wax (1h), wax (2h). Samples were paraffin-embedded, 4 μm sections were prepared (Leica RM2126 microtome) and stained with haematoxylin and eosin (H&E). Samples were kindly processed by Richard Stillion, Sir William Dunn School of Pathology, University of Oxford.

6.2.5 Statistics.

To compare differences between 2 groups, an unpaired Student's *t* test was used, and changes between multiple groups were analyzed using a 1-way ANOVA followed by Bonferroni multiple comparison test. All analyses were

performed Graph Pad Prism. Values are expressed as mean ± SD, and *p* values <0.05 were considered significant.

6.3 Results.

6.3.1 *Npc1*$^{-/-}$ EPMΦ display reduced phagocytosis of 3μm polystyrene beads in vivo.

We used FACS analysis to distinguish between the frequency and fluorescent intensity of populations of EPMΦ that were either F4/80^{+} IgG bead^{+} (EPMΦ that had ingested fluorescent polystyrene beads) and F4/80^{+} IgG bead^{-} (EPMΦ that had not ingested fluorescent polystyrene beads). After 60 min time period, a mean of 68.0 % *Npc1*$^{+/+}$ EPMΦ showed evidence of ingestion (F4/80^{+} IgG bead^{+}) whereas only a mean of 41.9% of *Npc1*$^{-/-}$ were double positive **(Fig.6.1)** There was a significant difference in the frequencies of *Npc1*$^{+/+}$ and *Npc1*$^{-/-}$ EPMΦ that had ingested beads (p=0.00103).

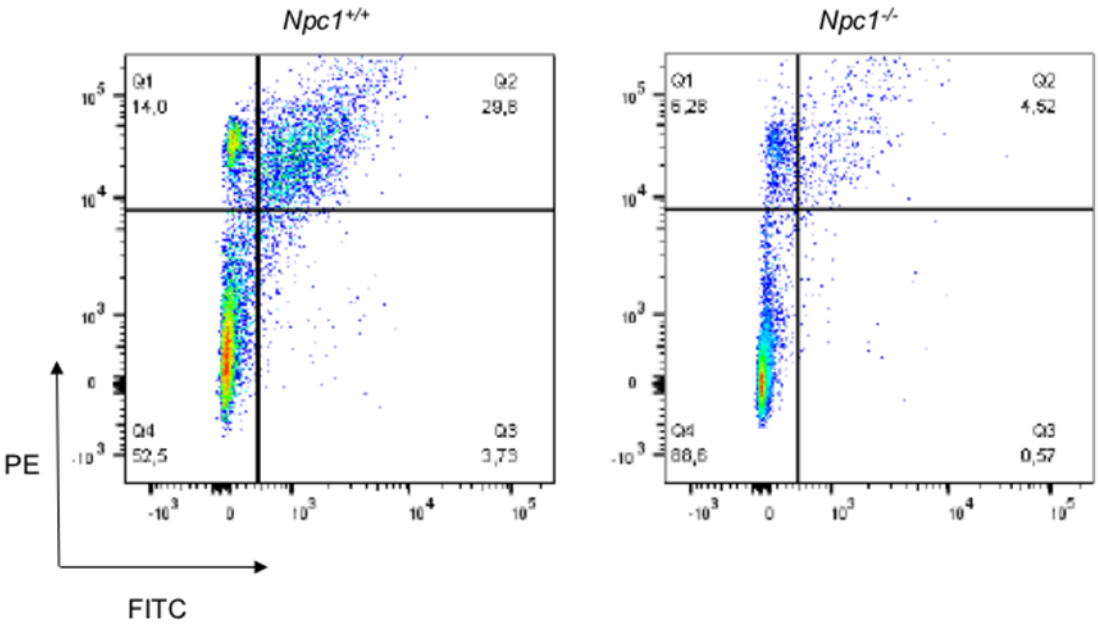


Figure 6.1 *Npc1*$^{-/-}$ EPMΦ EPMΦ display reduced phagocytosis of 3 μm polystyrene beads *in vivo.* Representative FACS plots of *ex-vivo Npc1*$^{+/+}$ (left panel) and *Npc1*$^{-/-}$ (right panel) EPMΦ. The top right quadrant contains F4/80 PE^{+} EPMΦ that have ingested FITC^{+} 3 μm beads; the top left quadrant contains F4/80 PE^{+} EPMΦ that have not ingested FITC^{+} 3 μm beads. Difference in double fluorescence detection between *Npc1*$^{-/-}$ and *Npc1*$^{+/+}$ was significantly different (p=0.00301) N=2, where each experimental condition was tested using 3 biological replicates

6.3.2 Abnormal accumulation of RBC in liver of NPC mouse, that is improved with miglustat treatment.

Spleens and livers of *Npc1*$^{-/-}$ mice were found to be significantly heavier than organs taken from *Npc1*$^{+/+}$ of the same age **(Fig.6.2)**. In order to identify possible changes to tissue organization and composition that might underlie the increase in mass we examined liver sections prepared from the two

genotypes that had been stained with H&E and toluidine. Examination of *Npc1*$^{-/-}$ liver tissue revealed the presence of foamy MΦ with subcellular storage bodies **(Fig. 6.3) and** adjacent to them the abnormal accumulation of erythrocytes. We did not observe these accumulations in our examinations of *Npc1*$^{+/+}$ livers. **(Fig.6.3)**.

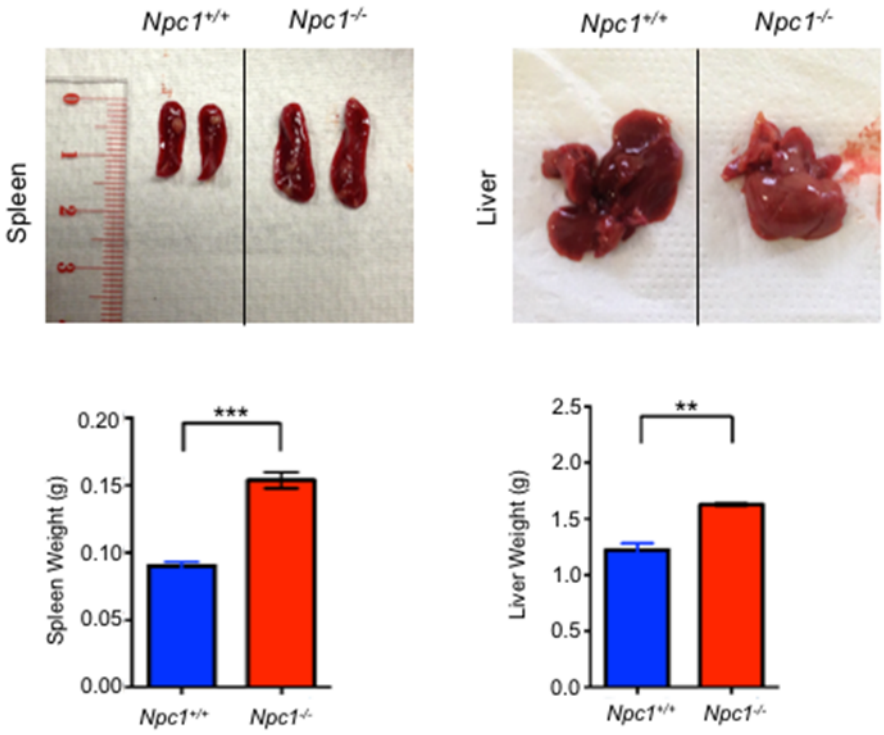


Figure 6.2 Increased splenic and liver weight in *Npc1*$^{-/-}$ mouse: Representative spleens (left upper panel) and livers (upper right panel) taken from 9-week old *Npc1*$^{+/+}$ and *Npc1*$^{-/-}$ mice. Spleens (left lower panel) and livers (right lower panel) of *Npc1*$^{-/-}$ mice (red columns) are significantly heavier than organs of *Npc1*$^{+/+}$ mice (blue columns). Data shown as Mean ± SD. N=6. ***p*<0.01 ****p*<0.001. (student *t*-test). Data from Oscar Chen.

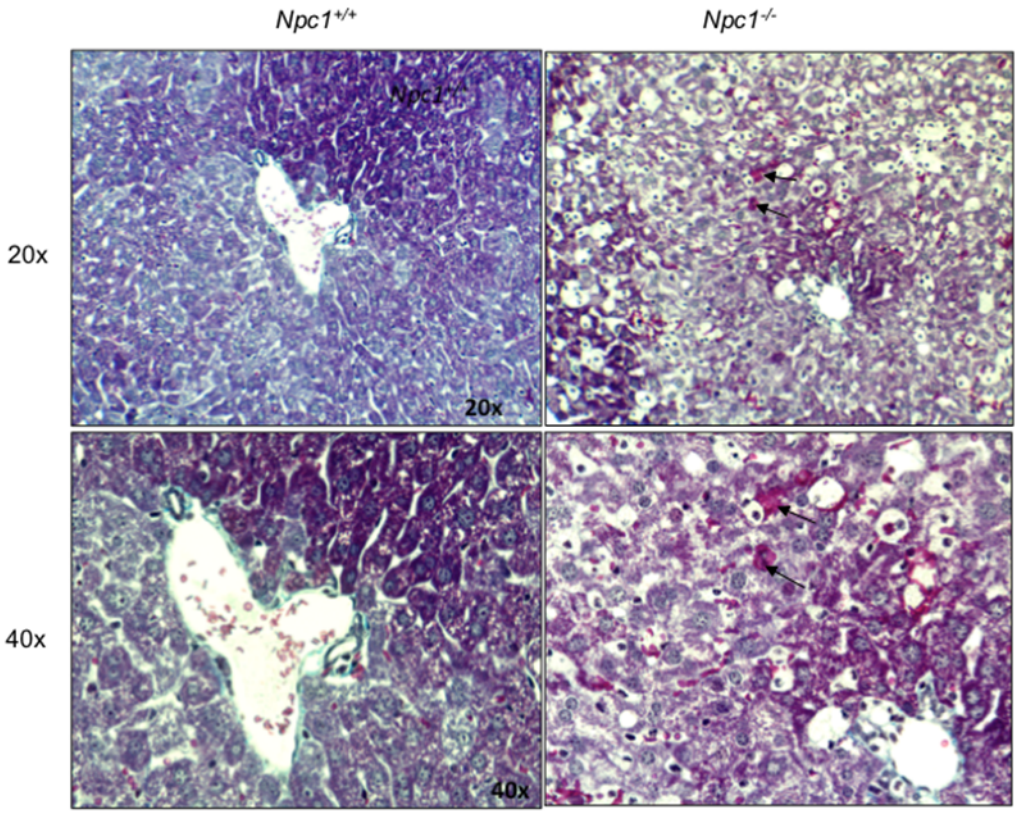


Figure 6.3 Abnormal accumulation of RBCs in sinusoids adjacent to foamy MΦ in *Npc1*$^{-/-}$ liver: H and E staining of *Npc1*$^{+/+}$ (left panels) and *Npc1*$^{-/-}$ livers (right panels) reveals abnormal clusters of RBC (pink, indicated by black arrows) in the sinusoids adjacent to foamy MΦ. This accumulation of RBC was not apparent in *Npc1*$^{+/+}$ liver.

6.3.3 Treatment with miglustat reduces the accumulation of RBCs in liver of *Npc1*$^{-/-}$ mice.

In order to obtain initial evidence that accumulation of RBCs in the liver of *Npc1*$^{-/-}$ mice is a pathological feature of the disease we undertook histological comparison of livers taken from 11-week old *Npc1*$^{+/+}$ and *Npc1*$^{-/-}$ mice and *Npc1*$^{-/-}$ animals that had been treated orally with miglustat. Inspection of representative tissue sections confirmed evidence of the accumulation of RBCs in *Npc1*$^{-/-}$ liver, their absence from *Npc1*$^{+/+}$ mice and a reduction in their frequency in *Npc1*$^{-/-}$ animals that had been treated with miglustat **(Fig.6.4).**

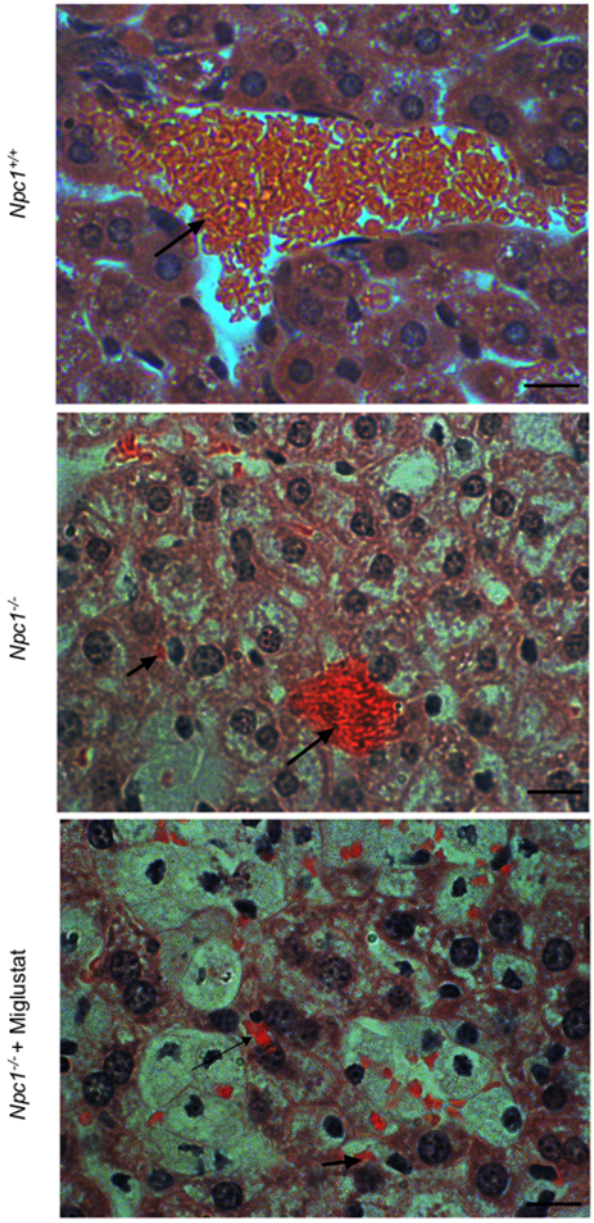


Figure 6.4 Treatment with miglustat decreases accumulation of RBC in *Npc1*$^{-/-}$ liver: Representative liver sections, stained with H&E, of *Npc1*$^{+/+}$ (top), untreated *Npc1*$^{-/-}$ (middle) and miglustat-treated *Npc1*$^{-/-}$ (bottom) mice. In *Npc1*$^{+/+}$, RBCs (pink) are restricted to within vessels. In untreated *Npc1*$^{-/-}$ liver there are RBC accumulations adjacent to Kupffer cells (black arrow). Accumulations of RBC are far less obvious in *Npc1*$^{-/-}$ mice that had been treated with miglustat. Scale bar = 12 μm N=3, where 4 biological replicates were examined.

6.4 Discussion.

We performed preliminary investigations for the purpose of obtaining evidence indicative of impaired phagocytic activity in *Npc1*$^{-/-}$ mice *in vivo*. We were able to demonstrate decreased phagocytosis by *Npc1*$^{-/-}$ EPMΦ of exogenous particles introduced into the peritoneum of *Npc1*$^{-/-}$ animals. Second, there was an accumulation of RBCs in the liver of mutant animals that could be consistent with impaired clearance of senescent cells.

In our introductory chapter we discussed the significant consequences that may result from diminished phagocytic activities. In brief, the persistence of pathogens can significantly enhance susceptibility to infection and the failure to remove endogenous cells can provoke and sustain damaging pro-inflammatory and autoimmune responses (Underhill and Ozinsky, 2002; Savill et al., 2003).

We used an *in vivo* peritoneal model to investigate the phagocytic activity of inflammatory *Npc1*$^{-/-}$ MΦ. We measured significantly lower ingestion of IgG opsonized beads under the conditions used. This model has been exploited in published studies, such as that made by Taylor *et al* (Taylor et al., 2000) to examine the role of the complement protein C1q in apoptotic cell clearance and offers technical advantages that facilitate experimental manipulation. For example, introduction of a bolus of exogenous particles, such as was undertaken in our study, is restricted to the peritoneum in the short term and is not subject to systemic dispersal that could limit availability to local phagocytes. Second, the induction of a localized pro-inflammatory response (peritonitis),

such as by injection of sterile thioglycollate broth into the peritoneum stimulates the recruitment of populations of inflammatory leukocytes, the first of which to enter are predominantly neutrophils that subsequently undergo apoptosis and are removed by inflammatory MΦ that have infiltrated the compartment (Ben-Baruch et al., 1995; Cotena et al., 2004).Therefore future studies of *Npc1*$^{-/-}$ mice can include study of the clearance of endogenous host cells.

We also examined for evidence of accumulation of cells in *Npc1*$^{-/-}$ mice that could result from insufficient or inefficient phagocytic activity. We found significantly increased mass of spleens and liver in mutant mice and accumulation of RBCs in liver that were not detected in *Npc1*$^{+/+}$ animals. The removal of senescent RBCs (erythrophagocytosis) that occurs primarily in the spleen and liver (Bratosin et al., 1998) is critical to the regulation of iron levels in tissues through re-cycling of heme (Kristiansen et al., 2001). The likelihood of perturbed phagocytosis of RBC in NPC is supported by evidence of reduction in serum iron and ferritin levels in *Npc1*$^{-/-}$ mice and patients (Chen, in preparation). We have therefore provided the foundation for future studies of RBC clearance and if altered, its potential consequences in NPC.

Finally, a recent study has highlighted the high penetrance of Crohn's disease in NPC patients (Schwerd et al., 2016). Crohn's is a disorder that is characterized by mishandling of microbes, which could also result from impaired phagocytosis.

Summary.

In this Chapter we have generated preliminary data that is consistent with reduced phagocytic activity in NPC *in vivo*. Further investigations are therefore merited.

Chapter 7 Conclusions.

In conclusion, the work presented in this thesis provides evidence supporting a model in which innate immune dysfunction alters cellular phagocytic activity that like contributes to NPC disease pathology. This defect in phagocytosis is mediated through various cellular processes including actin remodeling and lipid trafficking to the plasma membrane where abnormal lysosomal trafficking and endolysosomal fusion inhibit recognition, adherence, and internalisation of particles. The subsequent induction of NPC cellular phenotypes, particularly the accumulation of GM1 and defects in intracellular trafficking provide a plasma membrane environment that is inhibitory to phagocytosis.

This work provides a mechanistic framework which is complementary to previous observations of immune dysfunction in NPC, including abnormal inflammatory response (Platt et al., 2016), decreased numbers of iNKT cells (Speak et al., 2014), and abnormal microbe handling associated with inflammatory bowel disease (Schwerd et al., 2016). We have also provided evidence that a functional NPC pathway is required for uptake and metabolism of erythrocytes and apoptotic thymocytes *in vitro*. This finding may hold important implications for NPC patients, who due to NPC pathway dysfunction may have clinical subsidies of anemia and pro-inflammatory related disorders that are associated with clearance of apoptotic cells.

Mechanistically, our findings show that abnormal placement and trafficking of GSLs, particular Glc-Cer and GM1 play a key role in phagocytosis. Although other related LSDs (Gaucher and Sandhoff) did not show a similar phagocytic defect to that seen in NPC, it is likely that developing a more advanced

understanding of how abnormal sphingolipid biosynthesis and trafficking impact cellular events, particularly during immunological responses can contribute positively to a more developed understanding of LSDs and other related disorders. Future work should focus on developing more advanced knowledge of how GSLs regulate the cellular membrane response to unwanted pathogens in infected NPC mice as well as other disorders such as GM1 deficient mice.

The most exciting consequence of the above findings is the promise it holds for development of new therapeutics for NPC that target the immune system. Currently, only one NPC therapeutic is available for use, with various others in clinical trial. However, our result provide insight into some of the abnormal inflammatory pathologies of NPC and will likely assist in developing new combined therapies that focus on GSL metabolism as well as decreasing the abnormal pro-inflammatory response that occurs in NPC patients. Our results may also contribute to assisting in the progress of trialed NPC therapeutics such as omaya reservoir implantation for HPβCD therapy (Ottinger et al., 2014). This clinical trial was placed on hold following *Propionibacterium acnes* infection in NPC patients (a microbe that is normally a skin commensal) that is likely in part due to abnormal clearance of bacteria and microbe handling. By targeting phagocytosis and immune response in NPC it is likely this combination will be clinically successful. Demonstration of the efficacy of anti-inflammatory and immunological regulating treatment in combination with current NPC therapies in infected mice is therefore a priority for future work.

Most importantly, this project demonstrates the need and importance of rare disease research. Although NPC is a rare condition, affecting less than 0.001%

of the population, the links already made between NPC and Ebola (Carette et al., 2011; Zhao et al., 2016), HIV(Tang et al., 2009), and Crohn's disease (Schwerd et al., 2016) as well as the like between immunological dysfunction in NPC that is also seen in many other common diseases may prove relevant to the development of therapies for various other human infectious diseases.

References

Adam D, Philipp P, and Belohradsky BH (1971) Studies on the influence of host defence mechanisms on the antimicrobial effect of chemotherapeutic agents. Effect of antibiotics on phagocytosis of mouse-peritoneal-macrophages in vitro. *Arztl Forsch* **25:**181-184.

Aderem A and Underhill DM (1999) Mechanisms of phagocytosis in macrophages. *Annu Rev Immunol* **17:**593-623.

Akira S, Uematsu S, and Takeuchi O (2006) Pathogen recognition and innate immunity. *Cell* **124:**783-801.

Alberts B, Johnson, A., Lewis, J. (2002) *Molecular Biology of the Cell: 4th Edition*. Garland Science, New York

Allen LA and Aderem A (1996) Molecular definition of distinct cytoskeletal structures involved in complement- and Fc receptor-mediated phagocytosis in macrophages. *J Exp Med* **184:**627-637.

Andrews T and Sullivan KE (2003) Infections in patients with inherited defects in phagocytic function. *Clin Microbiol Rev* **16:**597-621.

Anumula KR and Dhume ST (1998) High resolution and high sensitivity methods for oligosaccharide mapping and characterization by normal phase high performance liquid chromatography following derivatization with highly fluorescent anthranilic acid. *Glycobiology* **8:**685-694.

Appelmans F, Wattiaux R, and De Duve C (1955) Tissue fractionation studies. 5. The association of acid phosphatase with a special class of cytoplasmic granules in rat liver. *Biochem J* **59:**438-445.

Appelqvist H, Waster P, Kagedal K, and Ollinger K (2013) The lysosome: from waste bag to potential therapeutic target. *J Mol Cell Biol* **5:**214-226.

Argmann CA, Houten SM, Zhu J, and Schadt EE (2016) A Next Generation Multiscale View of Inborn Errors of Metabolism. *Cell Metab* **23:**13-26.

Bajic G, Yatime L, Sim RB, Vorup-Jensen T, and Andersen GR (2013) Structural insight on the recognition of surface-bound opsonins by the integrin I domain of complement receptor 3. *Proc Natl Acad Sci U S A* **110:**16426-16431.

Ballabio A (2016) The awesome lysosome. *EMBO Mol Med* **8:**73-76.

Ben-Baruch A, Xu L, Young PR, Bengali K, Oppenheim JJ, and Wang JM (1995) Monocyte chemotactic protein-3 (MCP3) interacts with multiple leukocyte receptors. C-C CKR1, a receptor for macrophage inflammatory protein-1 alpha/Rantes, is also a functional receptor for MCP3. *J Biol Chem* **270:**22123-22128.

Berepiki A, Lichius A, and Read ND (2011) Actin organization and dynamics in filamentous fungi. *Nat Rev Microbiol* **9:**876-887.

Besterman JM and Low RB (1983) Endocytosis: a review of mechanisms and plasma membrane dynamics. *Biochem J* **210:**1-13.

Betto R, Teresi A, Fachechi-Cassano G, Salviati G, and Sabbadini RA (1992) Sphingosine inhibits calcium release from sarcoplasmic reticulum membranes. *Adv Exp Med Biol* **311:**403-404.

Bjerknes R (1984) Flow cytometric assay for combined measurement of phagocytosis and intracellular killing of Candida albicans. *J Immunol Methods* **72:**229-241.

Blom TS, Linder MD, Snow K, Pihko H, Hess MW, Jokitalo E, Veckman V, Syvanen AC, and Ikonen E (2003) Defective endocytic trafficking of NPC1 and NPC2 underlying infantile Niemann-Pick type C disease. *Hum Mol Genet* **12:**257-272.

Bosch ME and Kielian T (2015) Neuroinflammatory paradigms in lysosomal storage diseases. *Front Neurosci* **9:**417.

Bratosin D, Mazurier J, Tissier JP, Estaquier J, Huart JJ, Ameisen JC, Aminoff D, and Montreuil J (1998) Cellular and molecular mechanisms of senescent erythrocyte phagocytosis by macrophages. A review. *Biochimie* **80:**173-195.

Brown DE, Thrall MA, Walkley SU, Wenger DA, Mitchell TW, Smith MO, Royals KL, March PA, and Allison RW (1994) Feline Niemann-Pick disease type C. *Am J Pathol* **144:**1412-1415.

Brown J, O'Callaghan CA, Marshall AS, Gilbert RJ, Siebold C, Gordon S, Brown GD, and Jones EY (2007) Structure of the fungal beta-glucan-binding immune receptor dectin-1: implications for function. *Protein Sci* **16:**1042-1052.

Burkel BM, von Dassow G, and Bement WM (2007) Versatile fluorescent probes for actin filaments based on the actin-binding domain of utrophin. *Cell Motil Cytoskeleton* **64:**822-832.

Cannon GJ and Swanson JA (1992) The macrophage capacity for phagocytosis. *J Cell Sci* **101 (Pt 4):**907-913.

Carette JE, Raaben M, Wong AC, Herbert AS, Obernosterer G, Mulherkar N, Kuehne AI, Kranzusch PJ, Griffin AM, Ruthel G, Dal Cin P, Dye JM, Whelan SP, Chandran K, and Brummelkamp TR (2011) Ebola virus entry requires the cholesterol transporter Niemann-Pick C1. *Nature* **477:**340-343.

Caron E and Hall A (1998) Identification of two distinct mechanisms of phagocytosis controlled by different Rho GTPases. *Science* **282:**1717-1721.

Cenedella RJ (2009) Cholesterol synthesis inhibitor U18666A and the role of sterol metabolism and trafficking in numerous pathophysiological processes. *Lipids* **44:**477-487.

Champion JA and Mitragotri S (2006) Role of target geometry in phagocytosis. *Proc Natl Acad Sci U S A* **103:**4930-4934.

Champion JA, Walker A, and Mitragotri S (2008) Role of particle size in phagocytosis of polymeric microspheres. *Pharm Res* **25:**1815-1821.

Chen FW, Li C, and Ioannou YA (2010) Cyclodextrin induces calcium-dependent lysosomal exocytosis. *PLoS One* **5:**e15054.

Cluzeau CV, Watkins-Chow DE, Fu R, Borate B, Yanjanin N, Dail MK, Davidson CD, Walkley SU, Ory DS, Wassif CA, Pavan WJ, and Porter FD (2012) Microarray expression analysis and identification of serum biomarkers for Niemann-Pick disease, type C1. *Hum Mol Genet* **21:**3632-3646.

Cooper JA (1987) Effects of cytochalasin and phalloidin on actin. *J Cell Biol* **105:**1473-1478.

Costa SC, Ribeiro C, Girard PA, Zumbihl R, and Brehelin M (2005) Modes of phagocytosis of Gram-positive and Gram-negative bacteria by Spodoptera littoralis granular haemocytes. *J Insect Physiol* **51:**39-46.

Cotena A, Gordon S, and Platt N (2004) The class A macrophage scavenger receptor attenuates CXC chemokine production and the early infiltration of neutrophils in sterile peritonitis. *J Immunol* **173:**6427-6432.

Cox T, Lachmann R, Hollak C, Aerts J, van Weely S, Hrebicek M, Platt F, Butters T, Dwek R, Moyses C, Gow I, Elstein D, and Zimran A (2000)

Novel oral treatment of Gaucher's disease with N-butyldeoxynojirimycin (OGT 918) to decrease substrate biosynthesis. *Lancet* **355:**1481-1485.
Crowley MT, Costello PS, Fitzer-Attas CJ, Turner M, Meng F, Lowell C, Tybulewicz VL, and DeFranco AL (1997) A critical role for Syk in signal transduction and phagocytosis mediated by Fcgamma receptors on macrophages. *J Exp Med* **186:**1027-1039.
Debaisieux S, Lachambre S, Gross A, Mettling C, Besteiro S, Yezid H, Henaff D, Chopard C, Mesnard JM, and Beaumelle B (2015) HIV-1 Tat inhibits phagocytosis by preventing the recruitment of Cdc42 to the phagocytic cup. *Nat Commun* **6:**6211.
Desnick JP, Kim J, He X, Wasserstein MP, Simonaro CM, and Schuchman EH (2010) Identification and characterization of eight novel SMPD1 mutations causing types A and B Niemann-Pick disease. *Mol Med* **16:**316-321.
Diakonova M, Bokoch G, and Swanson JA (2002) Dynamics of cytoskeletal proteins during Fcgamma receptor-mediated phagocytosis in macrophages. *Mol Biol Cell* **13:**402-411.
Doshi N and Mitragotri S (2010) Macrophages recognize size and shape of their targets. *PLoS One* **5:**e10051.
Egami Y, Fukuda M, and Araki N (2011) Rab35 regulates phagosome formation through recruitment of ACAP2 in macrophages during FcgammaR-mediated phagocytosis. *J Cell Sci* **124:**3557-3567.
Elliott MR and Ravichandran KS (2010) Clearance of apoptotic cells: implications in health and disease. *J Cell Biol* **189:**1059-1070.
Erwig LP and Henson PM (2008) Clearance of apoptotic cells by phagocytes. *Cell Death Differ* **15:**243-250.
Eskelinen EL (2006) Roles of LAMP-1 and LAMP-2 in lysosome biogenesis and autophagy. *Mol Aspects Med* **27:**495-502.
Essner E and Novikoff AB (1961) Localization of acid phosphatase activity in hepatic lysosomes by means of electron microscopy. *J Biophys Biochem Cytol* **9:**773-784.
Fan M, Sidhu R, Fujiwara H, Tortelli B, Zhang J, Davidson C, Walkley SU, Bagel JH, Vite C, Yanjanin NM, Porter FD, Schaffer JE, and Ory DS (2013) Identification of Niemann-Pick C1 disease biomarkers through sphingolipid profiling. *J Lipid Res* **54:**2800-2814.
Flannagan RS, Cosio G, and Grinstein S (2009) Antimicrobial mechanisms of phagocytes and bacterial evasion strategies. *Nat Rev Microbiol* **7:**355-366.
Flannagan RS, Harrison RE, Yip CM, Jaqaman K, and Grinstein S (2010) Dynamic macrophage "probing" is required for the efficient capture of phagocytic targets. *J Cell Biol* **191:**1205-1218.
Flannagan RS, Jaumouille V, and Grinstein S (2012) The cell biology of phagocytosis. *Annu Rev Pathol* **7:**61-98.
Fluegel ML, Parker TJ, and Pallanck LJ (2006) Mutations of a Drosophila NPC1 gene confer sterol and ecdysone metabolic defects. *Genetics* **172:**185-196.
Freeman SA and Grinstein S (2014) Phagocytosis: receptors, signal integration, and the cytoskeleton. *Immunol Rev* **262:**193-215.

Friedland N, Liou HL, Lobel P, and Stock AM (2003) Structure of a cholesterol-binding protein deficient in Niemann-Pick type C2 disease. *Proc Natl Acad Sci U S A* **100:**2512-2517.

Fuentes AL, Millis L, Vapenik J, and Sigola L (2014) Lipopolysaccharide-mediated enhancement of zymosan phagocytosis by RAW 264.7 macrophages is independent of opsonins, laminarin, mannan, and complement receptor 3. *J Surg Res* **189:**304-312.

Futerman AH and van Meer G (2004) The cell biology of lysosomal storage disorders. *Nat Rev Mol Cell Biol* **5:**554-565.

Gadola SD, Koch M, Marles-Wright J, Lissin NM, Shepherd D, Matulis G, Harlos K, Villiger PM, Stuart DI, Jakobsen BK, Cerundolo V, and Jones EY (2006) Structure and binding kinetics of three different human CD1d-alpha-galactosylceramide-specific T cell receptors. *J Exp Med* **203:**699-710.

Gallo P, Goncalves R, and Mosser DM (2010) The influence of IgG density and macrophage Fc (gamma) receptor cross-linking on phagocytosis and IL-10 production. *Immunol Lett* **133:**70-77.

Garver WS and Heidenreich RA (2002) The Niemann-Pick C proteins and trafficking of cholesterol through the late endosomal/lysosomal system. *Curr Mol Med* **2:**485-505.

Giese AK, Mascher H, Grittner U, Eichler S, Kramp G, Lukas J, te Vruchte D, Al Eisa N, Cortina-Borja M, Porter FD, Platt FM, and Rolfs A (2015) A novel, highly sensitive and specific biomarker for Niemann-Pick type C1 disease. *Orphanet J Rare Dis* **10:**78.

Ginhoux F, Lim S, Hoeffel G, Low D, and Huber T (2013) Origin and differentiation of microglia. *Front Cell Neurosci* **7:**45.

Goddette DW and Frieden C (1986) Actin polymerization. The mechanism of action of cytochalasin D. *J Biol Chem* **261:**15974-15980.

Gordon S, Pluddemann A, and Martinez Estrada F (2014) Macrophage heterogeneity in tissues: phenotypic diversity and functions. *Immunol Rev* **262:**36-55.

Gupta SC, Patchva S, Koh W, and Aggarwal BB (2012) Discovery of curcumin, a component of golden spice, and its miraculous biological activities. *Clin Exp Pharmacol Physiol* **39:**283-299.

Hall AB, Gakidis MA, Glogauer M, Wilsbacher JL, Gao S, Swat W, and Brugge JS (2006) Requirements for Vav guanine nucleotide exchange factors and Rho GTPases in FcgammaR- and complement-mediated phagocytosis. *Immunity* **24:**305-316.

Hamann J, Koning N, Pouwels W, Ulfman LH, van Eijk M, Stacey M, Lin HH, Gordon S, and Kwakkenbos MJ (2007) EMR1, the human homolog of F4/80, is an eosinophil-specific receptor. *Eur J Immunol* **37:**2797-2802.

Helmy KY, Katschke KJ, Jr., Gorgani NN, Kljavin NM, Elliott JM, Diehl L, Scales SJ, Ghilardi N, and van Lookeren Campagne M (2006) CRIg: a macrophage complement receptor required for phagocytosis of circulating pathogens. *Cell* **124:**915-927.

Henry RM, Hoppe AD, Joshi N, and Swanson JA (2004) The uniformity of phagosome maturation in macrophages. *J Cell Biol* **164:**185-194.

Higashi Y, Murayama S, Pentchev PG, and Suzuki K (1993) Cerebellar degeneration in the Niemann-Pick type C mouse. *Acta Neuropathol* **85:**175-184.

Hinkovska-Galcheva V, Boxer L, Mansfield PJ, Schreiber AD, and Shayman JA (2003) Enhanced phagocytosis through inhibition of de novo ceramide synthesis. *J Biol Chem* **278:**974-982.

Hochreiter-Hufford A and Ravichandran KS (2013) Clearing the dead: apoptotic cell sensing, recognition, engulfment, and digestion. *Cold Spring Harb Perspect Biol* **5:**a008748.

Hoglinger D, Haberkant P, Aguilera-Romero A, Riezman H, Porter FD, Platt FM, Galione A, and Schultz C (2015) Intracellular sphingosine releases calcium from lysosomes. *Elife* **4**.

Hu B, Sonstein J, Christensen PJ, Punturieri A, and Curtis JL (2000) Deficient in vitro and in vivo phagocytosis of apoptotic T cells by resident murine alveolar macrophages. *J Immunol* **165:**2124-2133.

Huang X, Suyama K, Buchanan J, Zhu AJ, and Scott MP (2005) A Drosophila model of the Niemann-Pick type C lysosome storage disease: dnpc1a is required for molting and sterol homeostasis. *Development* **132:**5115-5124.

Hung YH, Walterfang M, Churilov L, Bray L, Jacobson LH, Barnham KJ, Jones NC, O'Brien TJ, Velakoulis D, and Bush AI (2016) Neurological Dysfunction in Early Maturity of a Model for Niemann-Pick C1 Carrier Status. *Neurotherapeutics* **13:**614-622.

Iftakhar EKI, Koide N, Hassan F, Noman AS, Dagvadorj J, Tumurkhuu G, Naiki Y, Komatsu T, Yoshida T, and Yokochi T (2009) Novel mechanism of U18666A-induced tumour necrosis factor-alpha production in RAW 264.7 macrophage cells. *Clin Exp Immunol* **155:**552-558.

Indik ZK, Park JG, Hunter S, and Schreiber AD (1995) The molecular dissection of Fc gamma receptor mediated phagocytosis. *Blood* **86:**4389-4399.

Ioannou YA (2005) Guilty until proven innocent: the case of NPC1 and cholesterol. *Trends Biochem Sci* **30:**498-505.

Janeway CA, Jr. and Medzhitov R (2002) Innate immune recognition. *Annu Rev Immunol* **20:**197-216.

Jeyakumar M, Dwek RA, Butters TD, and Platt FM (2005) Storage solutions: treating lysosomal disorders of the brain. *Nat Rev Neurosci* **6:**713-725.

Jeyakumar M, Thomas R, Elliot-Smith E, Smith DA, van der Spoel AC, d'Azzo A, Perry VH, Butters TD, Dwek RA, and Platt FM (2003) Central nervous system inflammation is a hallmark of pathogenesis in mouse models of GM1 and GM2 gangliosidosis. *Brain* **126:**974-987.

Jiang X and Ory DS (2016) Towards a New Diagnostic Standard for Niemann-Pick C Disease. *EBioMedicine* **4:**18-19.

Karageorgos L, Lancaster MJ, Nimmo JS, and Hopwood JJ (2011) Gaucher disease in sheep. *J Inherit Metab Dis* **34:**209-215.

Kaufmann AM, Goldman SD, and Krise JP (2009) A fluorescence resonance energy transfer-based approach for investigating late endosome-lysosome retrograde fusion events. *Anal Biochem* **386:**91-97.

Kedzierska K, Azzam R, Ellery P, Mak J, Jaworowski A, and Crowe SM (2003) Defective phagocytosis by human monocyte/macrophages following HIV-1 infection: underlying mechanisms and modulation by adjunctive cytokine therapy. *J Clin Virol* **26:**247-263.

Keogh MJ, Spoon T, Ridgway SH, Jensen E, Van Bonn W, and Romano TA (2011) Simultaneous measurement of phagocytosis and respiratory burst of leukocytes in whole blood from bottlenose dolphins (Tursiops

truncatus) utilizing flow cytometry. *Vet Immunol Immunopathol* **144:**468-475.
Khine AA, Firtel M, and Lingwood CA (1998) CD77-dependent retrograde transport of CD19 to the nuclear membrane: functional relationship between CD77 and CD19 during germinal center B-cell apoptosis. *J Cell Physiol* **176:**281-292.
Ko DC, Gordon MD, Jin JY, and Scott MP (2001) Dynamic movements of organelles containing Niemann-Pick C1 protein: NPC1 involvement in late endocytic events. *Mol Biol Cell* **12:**601-614.
Kristiansen M, Graversen JH, Jacobsen C, Sonne O, Hoffman HJ, Law SK, and Moestrup SK (2001) Identification of the haemoglobin scavenger receptor. *Nature* **409:**198-201.
Kumar H, Kawai T, and Akira S (2011) Pathogen recognition by the innate immune system. *Int Rev Immunol* **30:**16-34.
Kurlander RJ (1983) Blockade of Fc receptor-mediated binding to U-937 cells by murine monoclonal antibodies directed against a variety of surface antigens. *J Immunol* **131:**140-147.
Kwiatkowska K, Frey J, and Sobota A (2003) Phosphorylation of FcgammaRIIA is required for the receptor-induced actin rearrangement and capping: the role of membrane rafts. *J Cell Sci* **116:**537-550.
Kyrkanides S, Brouxhon SM, Tallents RH, Miller JN, Olschowka JA, and O'Banion MK (2012) Conditional expression of human beta-hexosaminidase in the neurons of Sandhoff disease rescues mice from neurodegeneration but not neuroinflammation. *J Neuroinflammation* **9:**186.
Lachmann RH, te Vruchte D, Lloyd-Evans E, Reinkensmeier G, Sillence DJ, Fernandez-Guillen L, Dwek RA, Butters TD, Cox TM, and Platt FM (2004) Treatment with miglustat reverses the lipid-trafficking defect in Niemann-Pick disease type C. *Neurobiol Dis* **16:**654-658.
Leao IC, Maciel M, and Hildreth JE (2006) Production and characterization of a monoclonal antibody against Niemann Pick type C protein. *Hybridoma (Larchmt)* **25:**216-224.
Lehmann AK, Sornes S, and Halstensen A (2000) Phagocytosis: measurement by flow cytometry. *J Immunol Methods* **243:**229-242.
Lekstrom-Himes JA and Gallin JI (2000) Immunodeficiency diseases caused by defects in phagocytes. *N Engl J Med* **343:**1703-1714.
Lemaire S, Mingeot-Leclercq MP, Tulkens PM, and Van Bambeke F (2014) Study of macrophage functions in murine J774 cells and human activated THP-1 cells exposed to oritavancin, a lipoglycopeptide with high cellular accumulation. *Antimicrob Agents Chemother* **58:**2059-2066.
Liao G, Cheung S, Galeano J, Ji AX, Qin Q, and Bi X (2009) Allopregnanolone treatment delays cholesterol accumulation and reduces autophagic/lysosomal dysfunction and inflammation in Npc1-/- mouse brain. *Brain Res* **1270:**140-151.
Liu B (2012) Therapeutic potential of cyclodextrins in the treatment of Niemann-Pick type C disease. *Clin Lipidol* **7:**289-301.
Liu R, Lu P, Chu JW, and Sharom FJ (2009) Characterization of fluorescent sterol binding to purified human NPC1. *J Biol Chem* **284:**1840-1852.

Lloyd-Evans E, Morgan AJ, He X, Smith DA, Elliot-Smith E, Sillence DJ, Churchill GC, Schuchman EH, Galione A, and Platt FM (2008) Niemann-Pick disease type C1 is a sphingosine storage disease that causes deregulation of lysosomal calcium. *Nat Med* **14:**1247-1255.

Lloyd-Evans E and Platt FM (2010) Lipids on trial: the search for the offending metabolite in Niemann-Pick type C disease. *Traffic* **11:**419-428.

Loftus SK, Morris JA, Carstea ED, Gu JZ, Cummings C, Brown A, Ellison J, Ohno K, Rosenfeld MA, Tagle DA, Pentchev PG, and Pavan WJ (1997) Murine model of Niemann-Pick C disease: mutation in a cholesterol homeostasis gene. *Science* **277:**232-235.

Louwette S, Regal L, Wittevrongel C, Thys C, Vandeweeghde G, Decuyper E, Leemans P, De Vos R, Van Geet C, Jaeken J, and Freson K (2013) NPC1 defect results in abnormal platelet formation and function: studies in Niemann-Pick disease type C1 patients and zebrafish. *Hum Mol Genet* **22:**61-73.

Lowell CA (2011) Src-family and Syk kinases in activating and inhibitory pathways in innate immune cells: signaling cross talk. *Cold Spring Harb Perspect Biol* **3**.

Lowenthal AC, Cummings JF, Wenger DA, Thrall MA, Wood PA, and de Lahunta A (1990) Feline sphingolipidosis resembling Niemann-Pick disease type C. *Acta Neuropathol* **81:**189-197.

Lu F, Liang, Q., Abi-Mosleh, L., Das, A., De Brabander, J.K., Goldstein, J.L., Brown, M.S. (2015) Identification of NPC1 as the target of U18666A, an inhibitor of lysosomal cholesterol export and Ebola infection. *Elifesciencs*

Luo Y, Tucker SC, and Casadevall A (2005) Fc- and complement-receptor activation stimulates cell cycle progression of macrophage cells from G1 to S. *J Immunol* **174:**7226-7233.

Luzio JP, Pryor PR, and Bright NA (2007) Lysosomes: fusion and function. *Nat Rev Mol Cell Biol* **8:**622-632.

Maceyka M and Spiegel S (2014) Sphingolipid metabolites in inflammatory disease. *Nature* **510:**58-67.

Maekawa N, Satoh S, Kawabe T, Maeda Y, Hosoda M, Iwata S, Nakamura K, Klein E, Okada H, and Yodoi J (1993) Enhancement of Fc epsilon RII/CD23 expression on U937 cells with opsonized zymosan: the requirement of a Fc gamma RI/CD64 mediated signal associated phagocytosis. *Mol Immunol* **30:**1265-1272.

Magenau A, Benzing C, Proschogo N, Don AS, Hejazi L, Karunakaran D, Jessup W, and Gaus K (2011) Phagocytosis of IgG-coated polystyrene beads by macrophages induces and requires high membrane order. *Traffic* **12:**1730-1743.

Maiti P, Hall TC, Paladugu L, Kolli N, Learman C, Rossignol J, and Dunbar GL (2016) A comparative study of dietary curcumin, nanocurcumin, and other classical amyloid-binding dyes for labeling and imaging of amyloid plaques in brain tissue of 5x-familial Alzheimer's disease mice. *Histochem Cell Biol*.

Manzanero S (2012) Generation of mouse bone marrow-derived macrophages. *Methods Mol Biol* **844:**177-181.

Maue RA, Burgess RW, Wang B, Wooley CM, Seburn KL, Vanier MT, Rogers MA, Chang CC, Chang TY, Harris BT, Graber DJ, Penatti CA, Porter DM, Szwergold BS, Henderson LP, Totenhagen JW, Trouard TP,

Borbon IA, and Erickson RP (2012) A novel mouse model of Niemann-Pick type C disease carrying a D1005G-Npc1 mutation comparable to commonly observed human mutations. *Hum Mol Genet* **21:**730-750.

May RC, Caron E, Hall A, and Machesky LM (2000) Involvement of the Arp2/3 complex in phagocytosis mediated by FcgammaR or CR3. *Nat Cell Biol* **2:**246-248.

May RC and Machesky LM (2001) Phagocytosis and the actin cytoskeleton. *J Cell Sci* **114:**1061-1077.

Mazzacuva F, Mills P, Mills K, Camuzeaux S, Gissen P, Nicoli ER, Wassif C, Te Vruchte D, Porter FD, Maekawa M, Mano N, Iida T, Platt F, and Clayton PT (2016) Identification of novel bile acids as biomarkers for the early diagnosis of Niemann-Pick C disease. *FEBS Lett* **590:**1651-1662.

Mengel E, Klunemann HH, Lourenco CM, Hendriksz CJ, Sedel F, Walterfang M, and Kolb SA (2013) Niemann-Pick disease type C symptomatology: an expert-based clinical description. *Orphanet J Rare Dis* **8:**166.

Mitchell MA, Huang MM, Chien P, Indik ZK, Pan XQ, and Schreiber AD (1994) Substitutions and deletions in the cytoplasmic domain of the phagocytic receptor Fc gamma RIIA: effect on receptor tyrosine phosphorylation and phagocytosis. *Blood* **84:**1753-1759.

Mizukami H, Mi Y, Wada R, Kono M, Yamashita T, Liu Y, Werth N, Sandhoff R, Sandhoff K, and Proia RL (2002) Systemic inflammation in glucocerebrosidase-deficient mice with minimal glucosylceramide storage. *J Clin Invest* **109:**1215-1221.

Mogensen TH (2009) Pathogen recognition and inflammatory signaling in innate immune defenses. *Clin Microbiol Rev* **22:**240-273, Table of Contents.

Mohammadi A, Perry RJ, Storey MK, Cook HW, Byers DM, and Ridgway ND (2001) Golgi localization and phosphorylation of oxysterol binding protein in Niemann-Pick C and U18666A-treated cells. *J Lipid Res* **42:**1062-1071.

Mosser DM and Zhang X (2011) Measuring opsonic phagocytosis via Fcgamma receptors and complement receptors on macrophages. *Curr Protoc Immunol* **Chapter 14:**Unit 14 27.

Mulcahy LA, Pink RC, and Carter DR (2014) Routes and mechanisms of extracellular vesicle uptake. *J Extracell Vesicles* **3**.

Munoz LE, Lauber K, Schiller M, Manfredi AA, and Herrmann M (2010) The role of defective clearance of apoptotic cells in systemic autoimmunity. *Nat Rev Rheumatol* **6:**280-289.

Neville DC, Coquard V, Priestman DA, te Vruchte DJ, Sillence DJ, Dwek RA, Platt FM, and Butters TD (2004) Analysis of fluorescently labeled glycosphingolipid-derived oligosaccharides following ceramide glycanase digestion and anthranilic acid labeling. *Anal Biochem* **331:**275-282.

Neville DC, Dwek RA, and Butters TD (2009) Development of a single column method for the separation of lipid- and protein-derived oligosaccharides. *J Proteome Res* **8:**681-687.

Nimmerjahn F and Ravetch JV (2008) Fcgamma receptors as regulators of immune responses. *Nat Rev Immunol* **8:**34-47.

Norsworthy PJ, Fossati-Jimack L, Cortes-Hernandez J, Taylor PR, Bygrave AE, Thompson RD, Nourshargh S, Walport MJ, and Botto M (2004) Murine

CD93 (C1qRp) contributes to the removal of apoptotic cells in vivo but is not required for C1q-mediated enhancement of phagocytosis. *J Immunol* **172:**3406-3414.

Olsson M and Oldenborg PA (2008) CD47 on experimentally senescent murine RBCs inhibits phagocytosis following Fcgamma receptor-mediated but not scavenger receptor-mediated recognition by macrophages. *Blood* **112:**4259-4267.

Ottinger EA, Kao ML, Carrillo-Carrasco N, Yanjanin N, Shankar RK, Janssen M, Brewster M, Scott I, Xu X, Cradock J, Terse P, Dehdashti SJ, Marugan J, Zheng W, Portilla L, Hubbs A, Pavan WJ, Heiss J, Vite CH, Walkley SU, Ory DS, Silber SA, Porter FD, Austin CP, and McKew JC (2014) Collaborative development of 2-hydroxypropyl-beta-cyclodextrin for the treatment of Niemann-Pick type C1 disease. *Curr Top Med Chem* **14:**330-339.

Panicker LM, Miller D, Park TS, Patel B, Azevedo JL, Awad O, Masood MA, Veenstra TD, Goldin E, Stubblefield BK, Tayebi N, Polumuri SK, Vogel SN, Sidransky E, Zambidis ET, and Feldman RA (2012) Induced pluripotent stem cell model recapitulates pathologic hallmarks of Gaucher disease. *Proc Natl Acad Sci U S A* **109:**18054-18059.

Patergnani S, Suski JM, Agnoletto C, Bononi A, Bonora M, De Marchi E, Giorgi C, Marchi S, Missiroli S, Poletti F, Rimessi A, Duszynski J, Wieckowski MR, and Pinton P (2011) Calcium signaling around Mitochondria Associated Membranes (MAMs). *Cell Commun Signal* **9:**19.

Patterson MC, Hendriksz CJ, Walterfang M, Sedel F, Vanier MT, Wijburg F, and Group N-CGW (2012) Recommendations for the diagnosis and management of Niemann-Pick disease type C: an update. *Mol Genet Metab* **106:**330-344.

Patterson MC, Vecchio D, Prady H, Abel L, and Wraith JE (2007) Miglustat for treatment of Niemann-Pick C disease: a randomised controlled study. *Lancet Neurol* **6:**765-772.

Peake KB and Vance JE (2010) Defective cholesterol trafficking in Niemann-Pick C-deficient cells. *FEBS Lett* **584:**2731-2739.

Pearson AM (1996) Scavenger receptors in innate immunity. *Curr Opin Immunol* **8:**20-28.

Pentchev PG, Boothe AD, Kruth HS, Weintroub H, Stivers J, and Brady RO (1984) A genetic storage disorder in BALB/C mice with a metabolic block in esterification of exogenous cholesterol. *J Biol Chem* **259:**5784-5791.

Perry E and Howes MJ (2011) Medicinal plants and dementia therapy: herbal hopes for brain aging? *CNS Neurosci Ther* **17:**683-698.

Platt FM, Boland B, and van der Spoel AC (2012) The cell biology of disease: lysosomal storage disorders: the cellular impact of lysosomal dysfunction. *J Cell Biol* **199:**723-734.

Platt N, da Silva RP, and Gordon S (1999) Class A scavenger receptors and the phagocytosis of apoptotic cells. *Immunol Lett* **65:**15-19.

Platt N and Fineran P (2015) Measuring the phagocytic activity of cells. *Methods Cell Biol* **126:**287-304.

Platt N, Speak AO, Colaco A, Gray J, Smith DA, Williams IM, Wallom KL, and Platt FM (2016) Immune dysfunction in Niemann-Pick disease type C. *J Neurochem* **136 Suppl 1:**74-80.

Platt N, Suzuki H, Kurihara Y, Kodama T, and Gordon S (1996) Role for the class A macrophage scavenger receptor in the phagocytosis of apoptotic thymocytes in vitro. *Proc Natl Acad Sci U S A* **93:**12456-12460.

Poh MK, Shui G, Xie X, Shi PY, Wenk MR, and Gu F (2012) U18666A, an intracellular cholesterol transport inhibitor, inhibits dengue virus entry and replication. *Antiviral Res* **93:**191-198.

Pollock JD, Williams DA, Gifford MA, Li LL, Du X, Fisherman J, Orkin SH, Doerschuk CM, and Dinauer MC (1995) Mouse model of X-linked chronic granulomatous disease, an inherited defect in phagocyte superoxide production. *Nat Genet* **9:**202-209.

Ponnappan S and Ponnappan U (2011) Aging and immune function: molecular mechanisms to interventions. *Antioxid Redox Signal* **14:**1551-1585.

Pontikis CC, Davidson CD, Walkley SU, Platt FM, and Begley DJ (2013) Cyclodextrin alleviates neuronal storage of cholesterol in Niemann-Pick C disease without evidence of detectable blood-brain barrier permeability. *J Inherit Metab Dis* **36:**491-498.

Poon IK, Lucas CD, Rossi AG, and Ravichandran KS (2014) Apoptotic cell clearance: basic biology and therapeutic potential. *Nat Rev Immunol* **14:**166-180.

Praggastis M, Tortelli B, Zhang J, Fujiwara H, Sidhu R, Chacko A, Chen Z, Chung C, Lieberman AP, Sikora J, Davidson C, Walkley SU, Pipalia NH, Maxfield FR, Schaffer JE, and Ory DS (2015) A murine Niemann-Pick C1 I1061T knock-in model recapitulates the pathological features of the most prevalent human disease allele. *J Neurosci* **35:**8091-8106.

Ramirez CM, Liu B, Taylor AM, Repa JJ, Burns DK, Weinberg AG, Turley SD, and Dietschy JM (2010) Weekly cyclodextrin administration normalizes cholesterol metabolism in nearly every organ of the Niemann-Pick type C1 mouse and markedly prolongs life. *Pediatr Res* **68:**309-315.

Rankin CT, Veri MC, Gorlatov S, Tuaillon N, Burke S, Huang L, Inzunza HD, Li H, Thomas S, Johnson S, Stavenhagen J, Koenig S, and Bonvini E (2006) CD32B, the human inhibitory Fc-gamma receptor IIB, as a target for monoclonal antibody therapy of B-cell lymphoma. *Blood* **108:**2384-2391.

Ravetch JV and Bolland S (2001) IgG Fc receptors. *Annu Rev Immunol* **19:**275-290.

Rawat A, Singh S, Suri D, Gupta A, Saikia B, Minz RW, Sehgal S, Vaiphei K, Kamae C, Honma K, Nakagawa N, Imai K, Nonoyama S, Oshima K, Mitsuiki N, Ohara O, Chan KW, and Lau YL (2014) Chronic granulomatous disease: two decades of experience from a tertiary care centre in North West India. *J Clin Immunol* **34:**58-67.

Reddy SM, Hsiao KH, Abernethy VE, Fan H, Longacre A, Lieberthal W, Rauch J, Koh JS, and Levine JS (2002) Phagocytosis of apoptotic cells by macrophages induces novel signaling events leading to cytokine-independent survival and inhibition of proliferation: activation of Akt and inhibition of extracellular signal-regulated kinases 1 and 2. *J Immunol* **169:**702-713.

Ribacke U, Moll K, Albrecht L, Ahmed Ismail H, Normark J, Flaberg E, Szekely L, Hultenby K, Persson KE, Egwang TG, and Wahlgren M (2013) Improved in vitro culture of Plasmodium falciparum permits

establishment of clinical isolates with preserved multiplication, invasion and rosetting phenotypes. *PLoS One* **8:**e69781.

Rus H, Cudrici C, and Niculescu F (2005) The role of the complement system in innate immunity. *Immunol Res* **33:**103-112.

Saftig P (2006) Physiology of the lysosome, in: *Fabry Disease: Perspectives from 5 Years of FOS* (Mehta A, Beck M, and Sunder-Plassmann G eds), Oxford.

Saftig P and Klumperman J (2009) Lysosome biogenesis and lysosomal membrane proteins: trafficking meets function. *Nat Rev Mol Cell Biol* **10:**623-635.

Samie M, Wang X, Zhang X, Goschka A, Li X, Cheng X, Gregg E, Azar M, Zhuo Y, Garrity AG, Gao Q, Slaugenhaupt S, Pickel J, Zolov SN, Weisman LS, Lenk GM, Titus S, Bryant-Genevier M, Southall N, Juan M, Ferrer M, and Xu H (2013) A TRP channel in the lysosome regulates large particle phagocytosis via focal exocytosis. *Dev Cell* **26:**511-524.

Sarantis H and Grinstein S (2012) Subversion of phagocytosis for pathogen survival. *Cell Host Microbe* **12:**419-431.

Sardiello M, Palmieri M, di Ronza A, Medina DL, Valenza M, Gennarino VA, Di Malta C, Donaudy F, Embrione V, Polishchuk RS, Banfi S, Parenti G, Cattaneo E, and Ballabio A (2009) A gene network regulating lysosomal biogenesis and function. *Science* **325:**473-477.

Savill J, Gregory C, and Haslett C (2003) Cell biology. Eat me or die. *Science* **302:**1516-1517.

Schengrund CL (2015) Gangliosides: glycosphingolipids essential for normal neural development and function. *Trends Biochem Sci* **40:**397-406.

Schuchman EH and Wasserstein MP (2015) Types A and B Niemann-Pick disease. *Best Pract Res Clin Endocrinol Metab* **29:**237-247.

Schwend T, Loucks EJ, Snyder D, and Ahlgren SC (2011) Requirement of Npc1 and availability of cholesterol for early embryonic cell movements in zebrafish. *J Lipid Res* **52:**1328-1344.

Schwerd T, Pandey S, Yang HT, Bagola K, Jameson E, Jung J, Lachmann RH, Shah N, Patel SY, Booth C, Runz H, Duker G, Bettels R, Rohrbach M, Kugathasan S, Chapel H, Keshav S, Elkadri A, Platt N, Muise AM, Koletzko S, Xavier RJ, Marquardt T, Powrie F, Wraith JE, Gyrd-Hansen M, Platt FM, and Uhlig HH (2016) Impaired antibacterial autophagy links granulomatous intestinal inflammation in Niemann-Pick disease type C1 and XIAP deficiency with NOD2 variants in Crohn's disease. *Gut*.

Settembre C, Fraldi A, Medina DL, and Ballabio A (2013) Signals from the lysosome: a control centre for cellular clearance and energy metabolism. *Nat Rev Mol Cell Biol* **14:**283-296.

Simons ER (2010) Measurement of phagocytosis and of the phagosomal environment in polymorphonuclear phagocytes by flow cytometry. *Curr Protoc Cytom* **Chapter 9:**Unit9 31.

Simons K and Ikonen E (1997) Functional rafts in cell membranes. *Nature* **387:**569-572.

Smith D, Wallom KL, Williams IM, Jeyakumar M, and Platt FM (2009) Beneficial effects of anti-inflammatory therapy in a mouse model of Niemann-Pick disease type C1. *Neurobiol Dis* **36:**242-251.

Somers KL, Royals MA, Carstea ED, Rafi MA, Wenger DA, and Thrall MA (2003) Mutation analysis of feline Niemann-Pick C1 disease. *Mol Genet Metab* **79:**99-103.

Speak AO, Platt N, Salio M, te Vruchte D, Smith DA, Shepherd D, Veerapen N, Besra GS, Yanjanin NM, Simmons L, Imrie J, Wraith JE, Lachmann RH, Hartung R, Runz H, Mengel E, Beck M, Hendriksz CJ, Porter FD, Cerundolo V, and Platt FM (2012) Invariant natural killer T cells are not affected by lysosomal storage in patients with Niemann-Pick disease type C. *Eur J Immunol* **42:**1886-1892.

Speak AO, Te Vruchte D, Davis LC, Morgan AJ, Smith DA, Yanjanin NM, Simmons L, Hartung R, Runz H, Mengel E, Beck M, Imrie J, Jacklin E, Wraith JE, Hendriksz C, Lachmann R, Cognet C, Sidhu R, Fujiwara H, Ory DS, Galione A, Porter FD, Vivier E, and Platt FM (2014) Altered distribution and function of natural killer cells in murine and human Niemann-Pick disease type C1. *Blood* **123:**51-60.

Stein VM, Crooks A, Ding W, Prociuk M, O'Donnell P, Bryan C, Sikora T, Dingemanse J, Vanier MT, Walkley SU, and Vite CH (2012) Miglustat improves purkinje cell survival and alters microglial phenotype in feline Niemann-Pick disease type C. *J Neuropathol Exp Neurol* **71:**434-448.

Steinberg BE and Grinstein S (2008) Pathogen destruction versus intracellular survival: the role of lipids as phagosomal fate determinants. *J Clin Invest* **118:**2002-2011.

Stewart CC, Lehnert BE, and Steinkamp JA (1986) In vitro and in vivo measurement of phagocytosis by flow cytometry. *Methods Enzymol* **132:**183-192.

Stuart LM and Ezekowitz RA (2005) Phagocytosis: elegant complexity. *Immunity* **22:**539-550.

Stuart LM and Ezekowitz RA (2008) Phagocytosis and comparative innate immunity: learning on the fly. *Nat Rev Immunol* **8:**131-141.

Sultana S, Truong NY, Vieira DB, Wigger JG, Forrester AM, Veinotte CJ, Berman JN, and van der Spoel AC (2016) Characterization of the Zebrafish Homolog of beta-Glucosidase 2: A Target of the Drug Miglustat. *Zebrafish* **13:**177-187.

Sutterwala FS, Rosenthal LA, and Mosser DM (1996) Cooperation between CR1 (CD35) and CR3 (CD 11b/CD18) in the binding of complement-opsonized particles. *J Leukoc Biol* **59:**883-890.

Suzuki K, Parker CC, Pentchev PG, Katz D, Ghetti B, D'Agostino AN, and Carstea ED (1995) Neurofibrillary tangles in Niemann-Pick disease type C. *Acta Neuropathol* **89:**227-238.

Suzuki T (1991) Signal transduction mechanisms through Fc gamma receptors on the mouse macrophage surface. *FASEB J* **5:**187-193.

Svennerholm L and Fredman P (1980) A procedure for the quantitative isolation of brain gangliosides. *Biochim Biophys Acta* **617:**97-109.

Swanson JA (2002) The extraordinary phagosome. *Nature* **418:**286-287.

Swanson JA and Hoppe AD (2004) The coordination of signaling during Fc receptor-mediated phagocytosis. *J Leukoc Biol* **76:**1093-1103.

Tafesse FG, Rashidfarrokhi A, Schmidt FI, Freinkman E, Dougan S, Dougan M, Esteban A, Maruyama T, Strijbis K, and Ploegh HL (2015) Disruption of Sphingolipid Biosynthesis Blocks Phagocytosis of Candida albicans. *PLoS Pathog* **11:**e1005188.

Tang Y, Leao IC, Coleman EM, Broughton RS, and Hildreth JE (2009) Deficiency of niemann-pick type C-1 protein impairs release of human immunodeficiency virus type 1 and results in Gag accumulation in late endosomal/lysosomal compartments. *J Virol* **83:**7982-7995.

Tatematsu M, Imaida K, Ito N, Togari H, Suzuki Y, and Ogiu T (1981) Sandhoff disease. *Acta Pathol Jpn* **31:**503-512.

Taylor AE, Finney-Hayward TK, Quint JK, Thomas CM, Tudhope SJ, Wedzicha JA, Barnes PJ, and Donnelly LE (2010) Defective macrophage phagocytosis of bacteria in COPD. *Eur Respir J* **35:**1039-1047.

Taylor PR, Carugati A, Fadok VA, Cook HT, Andrews M, Carroll MC, Savill JS, Henson PM, Botto M, and Walport MJ (2000) A hierarchical role for classical pathway complement proteins in the clearance of apoptotic cells in vivo. *J Exp Med* **192:**359-366.

te Vruchte D, Lloyd-Evans E, Veldman RJ, Neville DC, Dwek RA, Platt FM, van Blitterswijk WJ, and Sillence DJ (2004) Accumulation of glycosphingolipids in Niemann-Pick C disease disrupts endosomal transport. *J Biol Chem* **279:**26167-26175.

Te Vruchte D, Wallom KL, and Platt FM (2015) Measuring relative lysosomal volume for monitoring lysosomal storage diseases. *Methods Cell Biol* **126:**331-347.

Ting-Beall HP, Lee AS, and Hochmuth RM (1995) Effect of cytochalasin D on the mechanical properties and morphology of passive human neutrophils. *Ann Biomed Eng* **23:**666-671.

Tohyama Y and Yamamura H (2006) Complement-mediated phagocytosis--the role of Syk. *IUBMB Life* **58:**304-308.

Underhill DM (2003) Macrophage recognition of zymosan particles. *J Endotoxin Res* **9:**176-180.

Underhill DM and Goodridge HS (2012) Information processing during phagocytosis. *Nat Rev Immunol* **12:**492-502.

Underhill DM and Ozinsky A (2002) Phagocytosis of microbes: complexity in action. *Annu Rev Immunol* **20:**825-852.

van der Meer DL, van den Thillart GE, Witte F, de Bakker MA, Besser J, Richardson MK, Spaink HP, Leito JT, and Bagowski CP (2005) Gene expression profiling of the long-term adaptive response to hypoxia in the gills of adult zebrafish. *Am J Physiol Regul Integr Comp Physiol* **289:**R1512-1519.

Vance JE and Peake KB (2011) Function of the Niemann-Pick type C proteins and their bypass by cyclodextrin. *Curr Opin Lipidol* **22:**204-209.

Vandamme TF (2014) Use of rodents as models of human diseases. *J Pharm Bioallied Sci* **6:**2-9.

Vanier MT (1999) Lipid changes in Niemann-Pick disease type C brain: personal experience and review of the literature. *Neurochem Res* **24:**481-489.

Vanier MT (2010) Niemann-Pick disease type C. *Orphanet J Rare Dis* **5:**16.

Vellodi A (2005) Lysosomal storage disorders. *Br J Haematol* **128:**413-431.

Vicente-Manzanares M and Sanchez-Madrid F (2004) Role of the cytoskeleton during leukocyte responses. *Nat Rev Immunol* **4:**110-122.

Vite CH, Bagel JH, Swain GP, Prociuk M, Sikora TU, Stein VM, O'Donnell P, Ruane T, Ward S, Crooks A, Li S, Mauldin E, Stellar S, De Meulder M, Kao ML, Ory DS, Davidson C, Vanier MT, and Walkley SU (2015)

Intracisternal cyclodextrin prevents cerebellar dysfunction and Purkinje cell death in feline Niemann-Pick type C1 disease. *Sci Transl Med* **7:**276ra226.

Vitner EB, Platt FM, and Futerman AH (2010) Common and uncommon pathogenic cascades in lysosomal storage diseases. *J Biol Chem* **285:**20423-20427.

Vivier E, Raulet DH, Moretta A, Caligiuri MA, Zitvogel L, Lanier LL, Yokoyama WM, and Ugolini S (2011) Innate or adaptive immunity? The example of natural killer cells. *Science* **331:**44-49.

Walden CM, Sandhoff R, Chuang CC, Yildiz Y, Butters TD, Dwek RA, Platt FM, and van der Spoel AC (2007) Accumulation of glucosylceramide in murine testis, caused by inhibition of beta-glucosidase 2: implications for spermatogenesis. *J Biol Chem* **282:**32655-32664.

Walkley SU and Suzuki K (2004) Consequences of NPC1 and NPC2 loss of function in mammalian neurons. *Biochim Biophys Acta* **1685:**48-62.

Wan CP, Park CS, and Lau BH (1993) A rapid and simple microfluorometric phagocytosis assay. *J Immunol Methods* **162:**1-7.

Wassif CA, Cross JL, Iben J, Sanchez-Pulido L, Cougnoux A, Platt FM, Ory DS, Ponting CP, Bailey-Wilson JE, Biesecker LG, and Porter FD (2016) High incidence of unrecognized visceral/neurological late-onset Niemann-Pick disease, type C1, predicted by analysis of massively parallel sequencing data sets. *Genet Med* **18:**41-48.

Weinshank RL, Luster AD, and Ravetch JV (1988) Function and regulation of a murine macrophage-specific IgG Fc receptor, Fc gamma R-alpha. *J Exp Med* **167:**1909-1925.

Wen X, Cheng X, Hu D, Li W, Ha J, Kang Z, Zhang M, Huang Y, and Wu S (2016) Combination of Curcumin with an Anti-Transferrin Receptor Antibody Suppressed the Growth of Malignant Gliomas In vitro. *Turk Neurosurg* **26:**209-214.

West MA, Wallin RP, Matthews SP, Svensson HG, Zaru R, Ljunggren HG, Prescott AR, and Watts C (2004) Enhanced dendritic cell antigen capture via toll-like receptor-induced actin remodeling. *Science* **305:**1153-1157.

Williams IM, Wallom KL, Smith DA, Al Eisa N, Smith C, and Platt FM (2014) Improved neuroprotection using miglustat, curcumin and ibuprofen as a triple combination therapy in Niemann-Pick disease type C1 mice. *Neurobiol Dis* **67:**9-17.

Wolf AA, Jobling MG, Wimer-Mackin S, Ferguson-Maltzman M, Madara JL, Holmes RK, and Lencer WI (1998) Ganglioside structure dictates signal transduction by cholera toxin and association with caveolae-like membrane domains in polarized epithelia. *J Cell Biol* **141:**917-927.

Yamato O, Matsunaga S, Takata K, Uetsuka K, Satoh H, Shoda T, Baba Y, Yasoshima A, Kato K, Takahashi K, Yamasaki M, Nakayama H, Doi K, Maede Y, and Ogawa H (2004) GM2-gangliosidosis variant 0 (Sandhoff-like disease) in a family of Japanese domestic cats. *Vet Rec* **155:**739-744.

Yeung T and Grinstein S (2007) Lipid signaling and the modulation of surface charge during phagocytosis. *Immunol Rev* **219:**17-36.

Yue GG, Kwok HF, Lee JK, Jiang L, Wong EC, Gao S, Wong HL, Li L, Chan KM, Leung PC, Fung KP, Zuo Z, and Lau CB (2016) Combined therapy

using bevacizumab and turmeric ethanolic extract (with absorbable curcumin) exhibited beneficial efficacy in colon cancer mice. *Pharmacol Res* **111:**43-57.

Zervas M, Somers KL, Thrall MA, and Walkley SU (2001) Critical role for glycosphingolipids in Niemann-Pick disease type C. *Curr Biol* **11:**1283-1287.

Zhao Y, Ren J, Harlos K, and Stuart DI (2016) Structure of glycosylated NPC1 luminal domain C reveals insights into NPC2 and Ebola virus interactions. *FEBS Lett* **590:**605-612.

Appendix

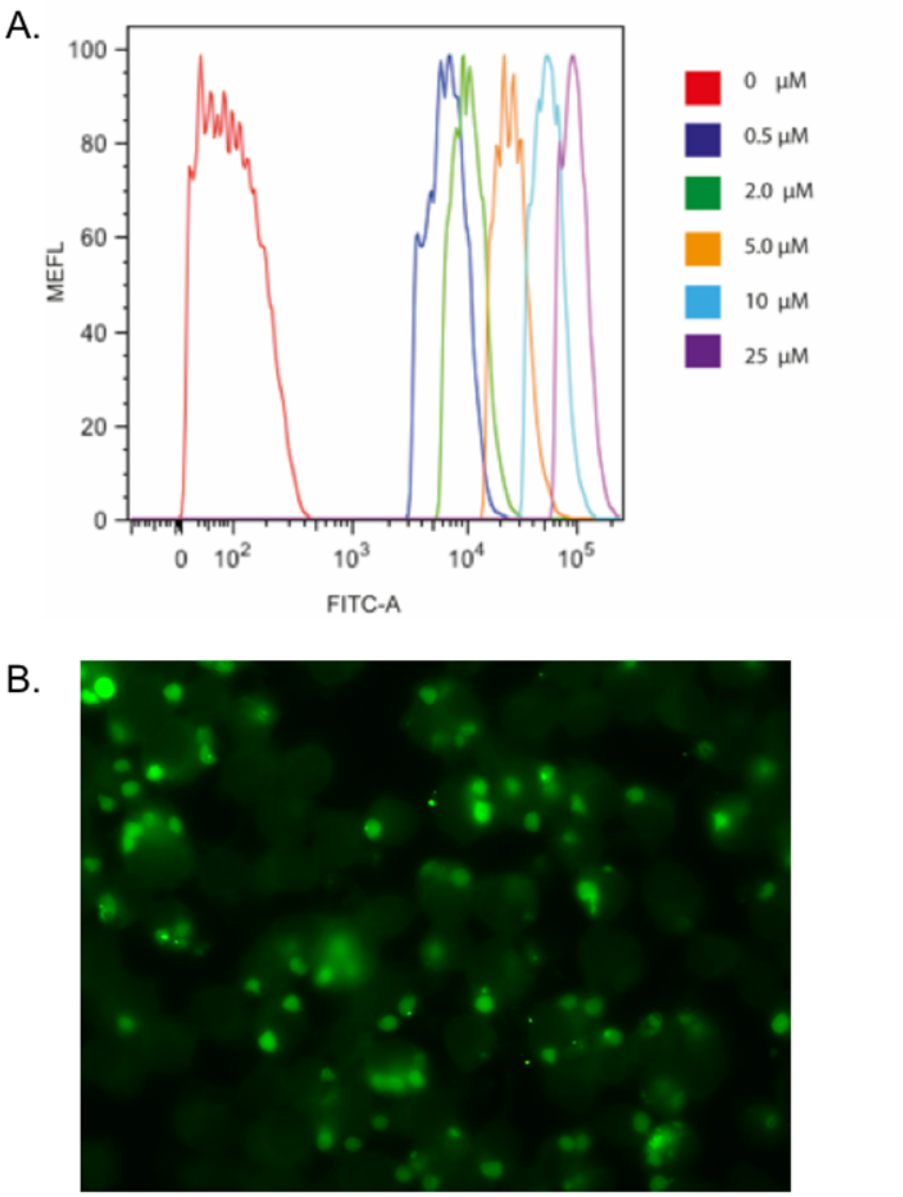


Figure A1: Detection of Celltracker™ Green labelling of sRBC by FACS: (A)FACS histogram showing change in fluorescence of sRBC incubated with various concentrations of cell-tracker green at 37ºC for 60min, 5% CO_2. Fluorescence was measured using the F1- 488 (FITC) channel. Fluorescence was apparent at each concentration. Based on optimal fluorescence, a concentration of 25uM Celltracker™ green was used when labelling sRBC. **(B)** sRBC shown in a control state following 25uM celltracker™ green labelling. sRBC are clearly visible and fluorescently green, 63x.

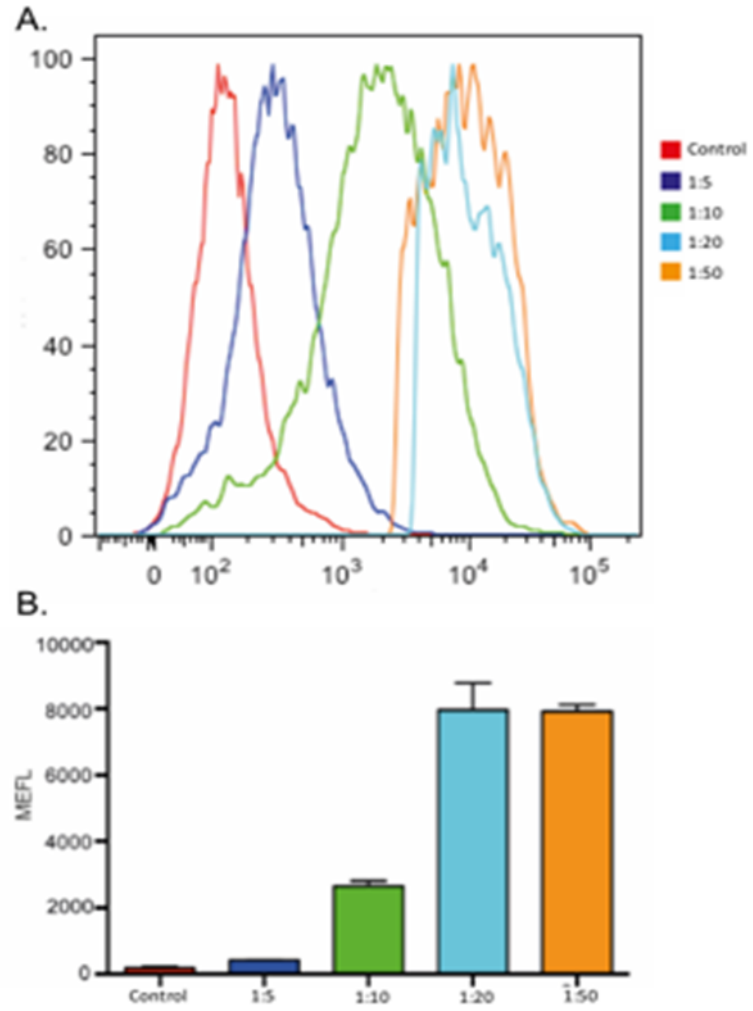


Figure A2. Determination of MΦ:sRBC MOI:
MΦ were overlaid with field of sRBC labeled with 25 μm Celltracker™ green at various MOI to determine optimal fluorescent detection. 1:20 (blue) and 1:50 (orange) MOI gave the highest fluorescent readings by FACS. There was no significant difference between 1:20 and 1:50 therefore an MOI of 1:20 RBC:MΦ was used for experimental analysis.